UNIVERSITY OF MODENA AND REGGIO EMILIA

International Doctoral Program in

CLINICAL AND EXPERIMENTAL MEDICINE (CEM)

Curriculum: Nanomedicine, Medicinal and Pharmaceutical Sciences

Cycle XXXIV

NOVEL ANALYTICAL METHODS FOR THE CHARACTERIZATION OF NATURAL PRODUCTS AS SOURCES OF ACTIVE COMPOUNDS AND THEIR BIOACTIVITY EVALUATION

PhD Candidate:
Lucia Marchetti

Supervisor:
Prof. Davide Bertelli
Co-Supervisor:
Prof. Federica Pellati

PhD program coordinator:
Prof. Giuseppe Biagini

Abstract

Plant extracts mainly consist of complex mixtures of chemically different bioactive compounds also known as secondary metabolites. In most cases the bioactivity of natural products is not ascribable to a single compound, but rather to a multitude of them acting in a synergistic way. In this view, the complete definition of all the phytochemical constituents represents a key point to ensure the efficacy, reliability, and safety in the use of herbal medicines. Even today, quality and authenticity assessment of herbal raw materials is frequently impaired by the lack of validated analytical methods and by the limited availability of certified references. Techniques for the analysis of herbal extracts and nutraceuticals need to be developed and upgraded continuously, since different combinations of ingredients are employed in new formulations. In view of the above, the current PhD project was focused on the development and application of innovative analytical methods for the analysis of plant bioactive secondary metabolites. Particular attention was paid to plants of pharmaceutical (*Cannabis sativa* L., and *Spathodea campanulata* P. Beauv.) and nutraceutical interest (*Morus alba* L., *Aloysia polystachya* Griseb. et Moldenke). Different *in-vitro* assays for the bioactivity evaluation of these plants' extracts were also the object of this PhD thesis. In Chapter 1, the NMR technique was applied for the determination of the main non-psychoactive cannabinoids in fiber-type *Cannabis* female inflorescences. The analytical method was developed and fully validated to show compliance with international requirements. This technique finds application in the monitoring of the plant material, to guarantee a better reproducibility for biological assays, and to ensure the efficacy and safety of *Cannabis*-derived products. As a continuation of this project, the potentialities and drawbacks of separation and non-separation methods for the analysis of cannabinoids were considered and compared. Finally, *C. sativa* non-psychoactive varieties were selected for the preparation of cannabinoids rich extracts to evaluate their antiproliferative activity, by using *in vitro* models. In Chapter 2 the chemical composition of Italian mulberry was investigated, as a source of phytochemicals in the context of new therapeutic approaches for diabetes mellitus. The first aim was to assess the quality of the plant material in comparison to Far Eastern Asia cultivations, where mulberry has been considered as a medicine for the treatment of diabetes for decades. The antiglycative capacity and hypoglycaemic effect of leaf extracts were evaluated on different *in vitro* models, to understand the potentialities of mulberry for the therapy of hyperglycaemia. Finally, the development of novel strategies for delaying the release of mulberry active constituents and enhancing therapeutic results were discussed and intended as the conclusion of this research project. In Chapter 3, the chemical composition of *S. campanulata* was investigated by HPLC-ESI-MS^2, to clarify which are the most active

components responsible for the inhibition of *H. pylori* growth. The aim was also to disclose the mechanisms underlying the biological activity. In Chapter 4, the phenolic composition of *A. polystachya* was investigated by means of three different MS techniques coupled to HPLC. The analytical method was developed and validated for the identification of metabolites, and some phenylpropanoids were detected in this plant for the first time.

Gli estratti ottenuti da piante medicinali sono costituiti per lo più da miscele complesse di composti attivi chimicamente differenti, anche conosciuti come metaboliti secondari. L'attività biologica dei prodotti naturali non è da attribuire a un singolo composto, ma piuttosto alla moltitudine di molecole che agiscono in sinergia tra loro. Per questa ragione la determinazione di tutti i costituenti attivi rappresenta un punto cruciale per assicurare l'efficacia, attendibilità e sicurezza nell'uso dei prodotti medicinali a base di piante. Ancora oggi, il controllo di qualità ed autenticità delle materie prime vegetali è ostacolato dalla mancanza di metodi analitici validati e dalla limitata disponibilità di standard di riferimento. I metodi di analisi per gli estratti vegetali e per i prodotti nutraceutici devono essere costantemente messi a punto ed aggiornati, dal momento che sempre nuove combinazioni di sostanze vengono impiegate in nuove formulazioni. Questo progetto di Dottorato di ricerca si è basato sullo sviluppo e successiva applicazione di metodi innovativi per l'analisi di metaboliti secondari di origine vegetale. Particolare attenzione è stata rivolta all'analisi di piante di interesse farmaceutico (*Cannabis sativa* L., and *Spathodea campanulata* P. Beauv.) e nutraceutico (*Morus alba* L., *Aloysia polystachya* Griseb. et Moldenke). Oggetto di questa dissertazione sono anche i diversi saggi *in-vitro,* messi a punto per valutare l'attività biologica degli estratti in analisi. Nel primo Capitolo, è stata applicata la spettroscopia NMR per la determinazione dei principali cannabinoidi non psicoattivi presenti nelle infiorescenze femminili di *Cannabis* da fibra. Il metodo analitico è stato sviluppato e validato in conformità alle linee guida internazionali. Questa tecnica trova applicazione nel monitoraggio del materiale vegetale di partenza, per garantire una migliore riproducibilità nei test biologici e per assicurare efficacia e sicurezza nell'uso di prodotti farmaceutici derivati. Come proseguimento del lavoro, metodi separativi e non separativi per l'analisi dei cannabinoidi sono stati discussi e messi a confronto per comprenderne potenzialità e svantaggi. Alcune varietà di *C. sativa* sono state selezionate per la preparazione di estratti ricchi in cannabinoidi non psicoattivi, di cui è stata valutata l'attività antiproliferativa su modelli in vitro. Nel secondo Capitolo, è presentato uno studio di caratterizzazione della composizione chimica di varietà di gelso Italiane, quali fonti di principi attivi nel contesto di nuovi approcci terapeutici per il diabete mellito. Questo studio, primo nel

suo genere, prevede di selezionare le cultivar più idonee alla produzione di estratti standardizzati a base di attivi ipoglicemizzanti. Le proprietà antiglicative e antidiabetiche di estratti di foglie di gelso sono state testate e diverse strategie per ritardare il rilascio dei componenti attivi sono state sviluppate al fine di potenziarne le capacità terapeutiche. Nel terzo Capitolo è stata analizzata la composizione chimica di *S. campanulata*, mediante HPLC-ESI-MS^2. L'obiettivo principale è stato quello di individuare i composti responsabili della documentata inibizione di *H. pylori* e fare luce sui meccanismi alla base dell'attività biologica. Nel quarto Capitolo è stata indagata la composizione fenolica di *A. polystachya*, mediante tre differenti tecniche MS accoppiate all'HPLC. Il metodo di analisi è stato sviluppato e validato per l'identificazione dei principali metaboliti, e alcuni di essi sono stati identificati per la prima volta in questa pianta.

TABLE OF CONTENTS

SECTION 3

EVALUATION OF THE ANTIPROLIFERATIVE ACTIVITY OF NON-PSYCHOACTIVE *C. SATIVA* L. EXTRACTS ON HUMAN CANCER CELL LINES

CHAPTER 2

SECTION 1

DETERMINATION OF 1-DEOXYNOJIRIMYCIN (DNJ) IN LEAVES OF ITALIAN OR ITALY-ADAPTED CULTIVARS OF MULBERRY (*MORUS* SP.PL.) BY HPLC-MS

SECTION 2

***IN VITRO* BIOACTIVITY EVALUATION OF MULBERRY LEAF EXTRACTS AS POTENTIAL CANDIDATE FOR THE MANAGEMENT OF DIABETES MELLITUS**

SECTION 3

PREFACE

Since ancient times plants have served mankind as an important source of remedies and medicines. In addition to their nutritional support, a majority of the world population also rely on medicinal plants to meet their health needs [1,2]. Currently we are witnessing a global resurgence in interest and use of plant-based therapies and botanical healthcare products. This evidence in turn has stimulated a greater scientific awareness in exploring and better understanding the pharmacologically active constituents of botanical remedies. It is well known how many natural compounds obtained from plant sources possess biological and pharmacological properties, and even though pharmaceutical companies are failing to invest on developing new drugs at this time, natural products remain an important and viable source of lead compounds in drug discovery programs [3]. According to World Health Organization (WHO) the relevant and widely diffused practice of phytotherapy can be explained considering that in rural areas traditional medicine still represents the primary source of health care for about 60% of the world population [1]. On the other hand, in countries where the healthcare system is well-established, the use of phytotherapy is more reasonably related to historical and cultural influences [2]. At the same time in high-income countries the growing interest in natural products is justified by scientific findings, which demonstrate that they are effective for the prevention of several diseases and for the maintenance of the health condition [1,4]. Modern consumers are showing a greater attention towards alternative medicine, also driven by the erroneous belief that natural products are always safe and might be superior to conventional therapies [4,5]. As a consequence, the use of natural remedies plays a significant role today also in economic terms, given the large market volume of herbal supplements and nutraceutical products [6,7]. However, the major concern in the use of herbal products is represented by the lack of their regulation. According to WHO, 43% of member states do not possess an appropriate regulation on herbal products [1]. These products are widespread and freely available since they are categorized as “dietary supplements” and therefore subjected to less restrictive regulations than drugs in matters of quality control and safety. Nevertheless, dietary supplements require a suitable level of assurance for efficacy and safety in their use, considering their potential side effects and interactions. The huge popularity of herbal ingredients and nutraceuticals has led to an increased scrutiny from consumers, health professionals and regulators about the quality standards and levels of active ingredients in these products. Even though some herbal components and botanical derivatives have been consumed by the population for thousands of years, most of the supplements’ ingredients have not been subject to comprehensive analysis. The great importance of developing novel analytical techniques lies not only in the direct quality control of the starting material, but also in building a solid database

in which analytical data for all products can be easily compared. In addition, from a regulatory point of view, well-established and validated methods will make product monitoring more efficient, and identification of adulterations easier [8]. Even today, quality and authenticity assessment of natural products is frequently impaired by the lack of validated analytical methods and by the limited availability (or excessive cost) of certified reference compounds. The analysis of complex matrices as is often the case of herbal extracts, nutraceuticals, and dietary supplements needs to be developed further, especially since new ingredients are continuously employed. Besides, the development of new formulations represents a challenge from an analytical point of view because existing methods for the analysis of bioactive compounds may not readily be scalable to these innovative products, considering that the effects of the food matrix on the extraction recovery and the stability of the analytes need to be evaluated anew [8]. Moreover, the evaluation of the quality of herb extracts is generally conducted by monitoring only one or two biomarkers or pharmacologically active components. However, plant extracts mainly consist of complex mixtures of chemically different compounds (secondary metabolites). Indeed, in most cases the herbal extract bioactivity is not ascribed to a single compound, but rather it is due to a multitude of them acting in a synergistic way. Botanicals and plant derivatives pose a particular challenge also due to the heterogeneity of secondary plant metabolites. Hence, the development of advanced analytical methods for the qualitative and quantitative analysis of different secondary metabolites in natural products is a crucial point [9]. Several methodologies are available in phytochemical analysis, anyway all can be reduced to two different approaches: the metabolite profiling, based on the study of chemically related compounds involved in specific biosynthetic pathways, and the metabolite fingerprinting, based on the full characterization of samples by comprehensive analysis of metabolites. The most common analytical methods ordinarily include separation and determination of compounds using chromatographic techniques. Although the chromatographic condition and detection techniques may vary, the analysis involves three common steps: extraction, separation, and detection. The inherent complexity and variability of natural extracts represent a challenge for both the separation and the detection of the analytical method. Considering that the majority of bioactive compounds are non-volatile, High-Performance Liquid Chromatography (HPLC) will mostly remain the analytical method of first choice. Nuclear Magnetic Resonance (NMR) spectroscopy is likewise a powerful technique for the identification and quantification of metabolites in plant extracts. In particular, NMR has shown many advantages over other conventional and well-established techniques, because it is non-destructive, unbiased, quantitative, and it does not require separation or derivatization

preparatory steps. Even though NMR is mainly considered a qualitative method, the quantitative application of this technique has been expanding. The main advantages of quantitative NMR (qNMR) are its accuracy, reproducibility, and the ability to simultaneously quantify multiple analytes. Among separative methods, liquid chromatography tandem mass spectrometry (LC/MS-MS) is one of the most sensitive and selective analytical methods. This technique provides information about the molecular weight as well as the structure of the analytes, using the MS/MS (or MS^n) capabilities of the mass analysers. This feature is particularly useful in case of unknown metabolites [8]. Moreover, low detection levels can be overcome by using specific ion transitions, without the need of an intermediate step of concentration of the sample. Separation by reversed phase (RP) HPLC on C_{18} stationary phase is doubtlessly the most widely used technique in this ambit. The chemical and physical properties of the packing in the column are important parameters for the general outcome of the separation performance. As a matter of fact, the HPLC analysis of plant extracts can be time-consuming when conventional fully porous stationary phases are employed. To overcome this issue, significant research effort for the development of novel RP columns has been made [10]. In particular, the fused-core technology represents one of the most recently reported strategies for improving the chromatographic performance in the analysis of complex matrices, including those of natural origin [10]. Although less common, the hydrophilic interaction liquid chromatography (HILIC) is very useful for the analysis of small and polar compounds, providing the strong retention of molecules that are typically unretained under conventional RP conditions. As concerns the choice of the detector, this is usually based on the chemical and physical properties of target analytes. The most common include diode array detection (DAD) and mass spectrometry (MS). HPLC is frequently coupled with DAD for the analysis of secondary metabolites that usually exhibit characteristic UV-Vis spectra. The DAD detector usually provides good linearity and sufficient dynamic range for secondary metabolites in plant extracts and it is widely used also for quantification of individual compounds in the quality control of herbal products [11]. Compared to other detection methods, MS can not only allow the determination of the chemical structure of natural compounds, but it also offers excellent sensitivity. In the ambit of HPLC–MS, many types of mass analysers are available, including the single or triple quadruple, the time-of-flight, and the ion trap. The ion trap is able to provide multiple-stage MS (MS^n) data that may be essential for structural elucidation purposes, thanks to the unique capability of trapping ions for a long time. Currently, tandem mass spectrometry (MS/MS), where two or more mass analysers are coupled together, has been widely applied for structural elucidation and quantitative analysis of natural products; indeed, it allows the

achievement of a better selectivity and sensitivity for quantification. Usually, mass spectrometry data can be acquired in different modes. The most common for natural product analysis are the full scan, the product ion scan and the multiple reaction monitoring (MRM). The latter, firstly uses a quadrupole that targets the ion corresponding to the compound of interest, with subsequent fragmentation of that target ion to produce a range of daughter ions. One (or more) of these fragments can be selected for quantitation purposes. Only compounds that meet both these criteria, *i.e.*, specific parent ions and specific daughter ions corresponding to the mass of the molecule of interest are isolated within the mass spectrometer. By ignoring all other ions that flow into the mass spectrometer the experiment gains sensitivity. Thus, the potential range of LC–MS applications is to a great extent expanded by the combination of different scanning modes.

The above-mentioned analytical techniques were all employed with *ad hoc* optimized methods for the comprehensive analysis of natural products. The current PhD project was focused on the development and application of innovative analytical methods for the multi-component analysis of plant bioactive secondary metabolites. Particular attention was paid to plants of pharmaceutical interest (*Cannabis sativa* L., and *Spathodea campanulata* P. Beauv.) and of nutraceutical interest (*Morus alba* L., and *Aloysia polystachya* Griseb. et Moldenke). Different biological assays for the activity evaluation of the plants' extracts were also the object of this PhD thesis.

LIST OF ABBREVIATIONS

ACN: acetonitrile
AGEs: advanced glycation end products
ALG: alginate
AlpA: adherence-associated lipoprotein A
AlpB: adherence-associated lipoprotein B
Ap: ampicillin
BabA: blood antigen-binding adhesin A
BSA: bovine serum albumin
Ca-ALG: calcium alginate
CagA: cytotoxin-associated protein A
CBC: cannabichromene
CBCA: cannabichromenic acid
CBD: cannabidiol
CBDA: cannabidiolic acid
CBG: cannabigerol
CBGA: cannabigerolic acid
CBN: cannabinol
CCF: concentration conversion factor
$CDCl_3$: deuterated chloroform
CE: capillary electrophoresis
CQA: caffeoylquinic acid
CVs: cultivars
D1-D3: decarboxylated extract
DAD: diode-array detection
DL: drug loading
DM: diabetes mellitus
DMEM: Dulbecco's modified Eagle's medium
DMSO: dimethyl sulfoxide
DNJ: 1-deoxynojirimycin
DW: dry weight
EE: encapsulation efficiency
EtOAc: ethyl acetate
EtOH: ethanol
EXT: mulberry extract
FBS: fetal bovine serum
FCS: fetal calf serum
FDE: freeze-dried extract
G: guluronic acid
GO: glyoxal
HCOOH: formic acid
Hex: n-hexane
HILIC: hydrophilic interaction chromatography

HpaA: *H. pylori* adhesin A
HPLC: high performance liquid chromatography
HopZ: *H. pylori* outer membrane protein
HT29: human colorectal adenocarcinoma cell line
K562: human chronic myelogenous leukaemia
LB: lysogeny broth
LC: liquid chromatography
LOD: limit of detection
LOQ: limit of quantitation
M: mannuronic acid
MAQ: minimum active quantity
ME: methanolic extract
MeOH: methanol
MGO: methylglyoxal
MRM: multiple reaction monitoring
MS: mass spectrometry
MS/MS: tandem mass spectrometry
Na-ALG: sodium alginate
NMR: nuclear magnetic resonance
NOE: nuclear overhauser enhancement
PBMC: peripheral blood mononuclear cell
PBS: sodium phosphate buffer
PDI: polydispersity index
qNMR: quantitative nuclear magnetic resonance
Q-TOF: quadrupole-time of flight
R1-R3: raw extract
SabA: sialic acid-binding adhesin A
SDMs: spray-dry microparticles
SPE: solid phase extraction
TFC: total flavonoid content
TMS: tetramethylsilane
TPC: total phenolic content
TQ: triple-quadrupole
TSP: trimethylsilyl-propionic acid
U87MG: human glioblastoma cell line
VacA: vacuolating cytotoxin A
Δ^9-THCA: tetrahydrocannabinolic acid
Δ^9-THC: tetrahydrocannabinol

CHAPTER 1

In the ambit of plants with pharmaceutical interest, an innovative NMR technique for the quantitative analysis of the main cannabinoids in *Cannabis* female inflorescences was developed and validated, and it is described above in Chapter 1. This study has been published as original research article. In detail, the qualitative and quantitative profiling of the major non-psychoactive cannabinoids was performed by applying both NMR spectroscopy and HPLC coupled with UV/DAD detection. The analytical method optimized in this study was fully validated to show compliance with international requirements. This technique demonstrated the provision of a comprehensive and reliable analysis of natural matrices, which are known to be characterised by a very complex composition. Therefore, it can be applied to ensure a better reproducibility for biological assays, and also to guarantee the efficacy and safety of *C. sativa* derived products to be used in the pharmaceutical or nutraceutical fields. Further, as a continuation of this project, the NMR method was applied for the first time to the quantification of psychoactive cannabinoids, and the potentialities and drawbacks of separation and non-separation methods the were considered and compared. This research has resulted in a recent publication, and it is described in detail in the second section of Chapter 1. Finally, specific non-psychoactive *C. sativa* varieties were selected for the preparation of cannabinoids rich extracts to evaluate their antiproliferative activity, in the context of their application (alone or in combination with cytostatic drugs) in cancer chemotherapy. The assessment of the biological activity of hemp extracts was carried out in collaboration with Dr. Lorenzo Corsi, P.I. of the Pharmacology and Toxicology laboratory of the Department of Life Sciences at the University of Modena and Reggio Emilia. This last study is part of an ongoing project, and the below reported preliminary results are intended as the conclusion of Chapter 1.

In recent years, *Cannabis sativa* L. has been the focus of the attention of the scientific community all over the world, becoming one of the most studied plants. The taxonomy of the plant has always represented a critical issue, due to the huge variability within the same genus [12]. The genus *Cannabis* was initially divided into three species, according both to specific botanical features and to the level of the psychoactive compound Δ^9-tetrahydrocannabinol (Δ^9-THC) and its acidic precursor Δ^9-tetrahydrocannabinolic acid (Δ^9-THCA) in plant female inflorescences. Later, this taxonomic classification has been outgrown in favour of a monotypic one, as a result of the continuous crossbreeding between cannabis species. Therefore, *C. sativa* refers to a plethora of different plants differing in their chemical profile, with particular regard to cannabinoids [13]. In this context, five cannabis chemotypes exist up to date, classified on the basis of the amounts of Δ^9-THC, cannabidiol (CBD), which is actually the main non-psychoactive cannabinoid, and cannabigerol (CBG) in plant female inflorescences. Three are

the predominant chemotypes that can be identified: chemotype I with a Δ^9-THC/CBD ratio >1.0, chemotype II with a Δ^9-THC/CBD ratio close to 1.0 and chemotype III with a Δ^9-THC/CBD ratio <1[13,14]. The taxonomic-based nomenclature, though, is not frequently applied in the cannabis industry, as the plant material is mainly labelled according to its end-use. In this perspective, recreational cannabis, belongs to chemotype I; this plant material is sold illicitly in the black market or in the dark net. Medical cannabis varieties include inflorescences belonging to chemotypes I and II, cultivated under standardized conditions in order to keep a constant level of active compounds and to ensure its usage under medical prescriptions for the treatment of specific pathologies (*i.e.* multiple sclerosis) [15]. Plants belonging to chemotype III can be mentioned as fibre-type cannabis (also known as industrial hemp or hemp); they are usually characterized by a high CBD content and a total Δ^9-THC content below the legal limit of 0.2-0.3%, this value depending on the specific country [15]. The pharmaceutical interest in this plant has been mainly addressed to drug-type *Cannabis*, thanks to its new therapeutic applications [16], while hemp is under-employed in this ambit. However, the number of studies on the characterisation of fibre-type hemp and on the evaluation of the biological potential of non-psychoactive compounds underwent an increase lately [17–19]. The chemistry of *C. sativa* is very complex since it contains over 150 bioactive phytocannabinoids [20]. Indeed, several chemical classes have been identified in the plant, notably terpenes, carbohydrates, fatty acids and their esters, amides, amines, phytosterols, phenolic compounds, and cannabinoids [21]. From a chemical point of view, cannabinoids are meroterpenoids. In fibre-type the most abundant are cannabinoic acids, such as CBDA and CBGA, followed by their decarboxylated forms, namely CBD and CBG. In addition, the primary decomposition product of Δ^9-THC is cannabinol (CBN), which is an oxidized degradant of THC and can be present in small amount in the plant material. Cannabidiol, the most investigated among non-psychoactive compounds, has shown important anti-oxidant and anti-inflammatory activity, in addition to its anticonvulsant, anxiolytic, neuroprotective, and antibiotic properties [22–24]. Cannabidiolic acid has demonstrated antimicrobial and anti-nausea properties, while anti-inflammatory, antimicrobial and analgesic activities have been attributed to CBG [22,25]. Concerning other phenolic compounds, several flavonoids have been identified in *C. sativa*, belonging mainly to flavones and flavonols [24]. Several biological effects have been ascribed to hemp flavonoids, including anti-inflammatory, anti-microbial, neuroprotective, and anti-proliferative activities [21]. In recent years a scientific base for the therapeutic application of cannabinoids for malignant tumours was investigated . Interest in the anticancer properties of cannabinoids was renewed after the discovery of the endocannabinoid

system (ECS), a signalling system comprising the cannabinoid CB1 and CB2 receptors, their intrinsic lipid ligands, endocannabinoids and the associated transporters [26]. Both cannabinoid receptors are G protein-coupled receptors: CB1 are highly distributed in the central nervous system, with low to moderate expression in the periphery, whereas CB2 receptors are high in the immune system, and have a moderate expression in other tissues, including the cardiovascular system, gastro-intestinal tract, liver, adipose tissue, bone, and reproductive system. [26,27] In 1975 Munson *et al*. obtained that Δ^9-THC and CBD were able to inhibit the growth of Lewis lung carcinoma after oral administration in mice [28]. Since then the anti-proliferative and pro-apoptotic effects of several natural and synthetic cannabinoids in cancer cell lines and *in vivo* tumour models were evaluated [29–31]. Moreover, other potential of these compounds including the inhibition of tumour invasion, cell migration and metastasis were disclosed more recently [32]. Since the clinical use of THC and other synthetic agonists of the cannabinoid receptors is limited by their unwanted psychoactive side effects, the interest of the researchers is now oriented to phytocannabinoids, which have no psychoactive effects. In particular, they may be used to modulate the tumour growth and progression in some general types of cancer as breast, lung, colon, and lympho-proliferative malignant diseases.

USE OF ^{13}C-qNMR SPECTROSCOPY FOR THE ANALYSIS OF NON-PSYCHOACTIVE CANNABINOIDS IN FIBRE-TYPE *C. SATIVA* L.

Molecules **2019**, 24(6), 1138; doi:10.3390/molecules24061138

Lucia Marchetti [1,2], Virginia Brighenti [1], Maria Cecilia Rossi [3], Johanna Sperlea [1,4], Federica Pellati [1,*] and Davide Bertelli [1]

[1] Department of Life Sciences, University of Modena and Reggio Emilia, Via G. Campi 103, 41125 Modena, Italy
[2] Doctorate School in Clinical and Experimental Medicine (CEM), University of Modena and Reggio Emilia, 41125 Modena, Italy
[3] Centro Interdipartimentale Grandi Strumenti, University of Modena and Reggio Emilia, Via G. Campi 213/A, 41125 Modena, Italy
[4] Faculty of Agricultural Sciences, Nutritional Sciences, and Environmental Management, Justus-Liebig University of Giessen, Goethestrasse 58, 35390 Giessen, Germany

1. INTRODUCTION

Cannabidiolic acid (CBDA) and cannabigerolic acid (CBGA) are biosynthesized in plants as prenylated aromatic carboxylic acids and their neutral counterparts (CBD and CBG) are generated as a consequence of the spontaneous decarboxylation that can occur either by heat or light for instance during long storage processes [33–35]. This assumption is supported by the fact that almost no neutral cannabinoid can be detected in the fresh plant material [36].

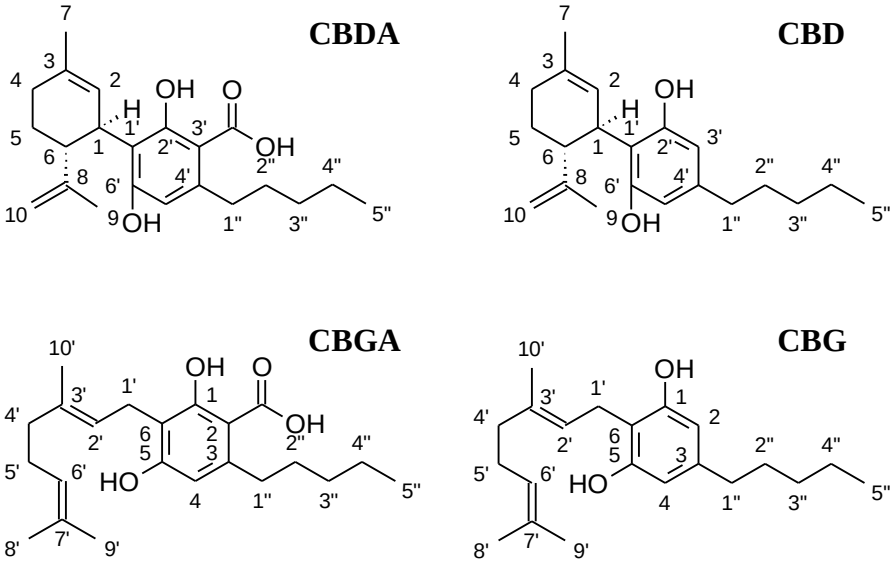

Figure 1. Chemical structures of major non-psychoactive cannabinoids in *C. sativa* L. fibre-type: cannabidiolic acid (CBDA), cannabidiol (CBD), cannabigerolic acid (CBGA) and cannabigerol (CBG).

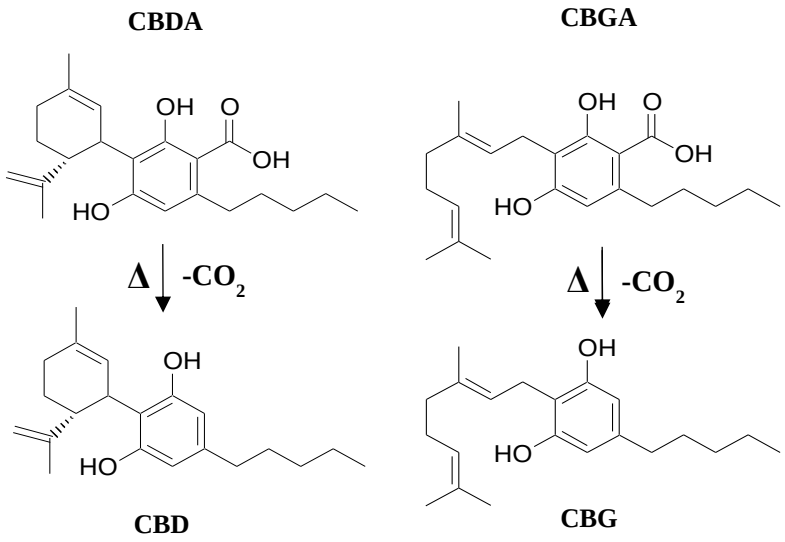

Figure 2. Breakdown products of CBDA and CBGA. The neutral counterparts (CBD, CBG) are generated by spontaneous decarboxylation under the action of heat and light.

In addition to separation techniques involving chromatography, Nuclear Magnetic Resonance (NMR) spectroscopy can be applied to the analysis of the composition of plant extracts, in the structure elucidation of compounds in metabolomics as well as in their quantification [37]. The measuring principle is based on the effect of an external magnetic field on spin possessing atomic nuclei ^{1}H and ^{13}C. Due to changes in the intramolecular magnetic field around an atom, absorption and emission of electromagnetic radiation take place; then, the resonance is detected with a radio receiver. The Fourier transform converts the complex time domain signal emitted by the nuclei into the frequency domain spectrum. Quantitative NMR (qNMR) refers to the application of NMR to determine the concentration of one or more target compounds in solution. The underlying principle is the direct proportional correlation of the area of a signal to the number of nuclides contributing to it. This proportionality depends on pulse excitation, delay time, broad-band decoupling; therefore, constant conditions are necessary [37,38]. Nowadays, there is an increasing interest in the application of qNMR, due to its numerous advantages over chromatographic methods. Indeed, qNMR enables the simultaneous identification and quantification of many, also chemically very different, analytes, in complex mixtures with a reduced time of analysis and a lower solvent usage, if compared with the HPLC technique [39,40].

In the light of all the above, the aim of this study was the development of a reliable ^{13}C-qNMR method for the comprehensive characterisation and determination of the main non-psychoactive cannabinoids (CBD, CBDA, CBG, CBGA) in eight different hemp varieties. The obtained results were compared with those provided by a well-established HPLC method, previously optimized and validated [41,42]. The ^{13}C-qNMR method developed in this study for the first time produced satisfactory results in a competitive time with respect to the most widespread and consolidated technique for cannabinoid analysis (HPLC), thus demonstrating to be suitable for a multi-component analysis of hemp extracts. This technique could also be useful to gain a holistic view of the composition and chemical profile of different hemp varieties and it can be applied for the quality control of both the plant material and its derivatives.

2. EXPERIMENTAL

2.1. Chemicals and solvents

CBD, CBDA, CBG and CBGA standard solutions (1 mg/mL in methanol or acetonitrile) were purchased from Cerilliant. (Round Rock, TX, USA). Deuterated chloroform ($CDCl_3$), tetramethylsilane (TMS) and ethanol analytical grade were from Sigma-Aldrich (Milan, Italy).

2.2. Hemp plant material

Eight samples of fibre-type female inflorescences were analysed in this study, including Antal, Carma, Carmagnola, China, Codimono, Fibrante, Futura and Santhica. These samples (about 100–500 g of dry material each), belonging to different breeding lines, were cultivated under the same agronomic conditions and they were kindly provided by the research centre CREA-CIN (Rovigo, Italy). Each sample was certified for a content of Δ^9-THC below 0.2% (w/w). All the samples considered in this study were approved for commercial use by the European Union.

2.3. Sample preparation

Hemp inflorescences were manually separated from twigs and seeds. After this procedure, the samples were stored at +4.0 °C until analysis. Cannabinoids were extracted from hemp inflorescences by means of dynamic maceration, as previously described in detail [41]. A weighed amount of each sample (1 g) was extracted with 20 mL of absolute EtOH at room temperature for 15 min, under magnetic stirring. The solution was then paper filtered, and the residue was extracted with the same procedure twice more with 20 and 10 mL of same solvent, respectively. The filtrates were then combined and adjusted to 50 mL with EtOH in a volumetric flask. The extraction procedure was repeated twice for each sample. To prepare NMR tubes, the extracts were evaporated under vacuum at 30 °C and the residue was dissolved in 1 mL of $CDCl_3$ (0.03% TMS); finally, 600 μL of this solution were transferred to a WILMAD® NMR tube, 5 mm, Ultra-Imperial grade, 7 in. L, 528-PP (Sigma-Aldrich, Milan, Italy).

2.4. NMR spectroscopy and spectra acquisition procedure

To characterize samples ^{1}H-NMR, ^{13}C-NMR, two-dimensional ^{1}H-^{13}C Heteronuclear Multiple-Bond Correlation (HMBC) and ^{1}H-^{13}C Heteronuclear Single Quantum Coherence (HSQC) spectra were acquired with a Bruker FT-NMR Avance III HD 600 MHz spectrometer (Bruker Biospin GmbH Rheinstetten, Karlsruhe, Germany). All the experiments were performed at 300 K and non-spinning. The assignments for the major compounds were carried out by using standard compounds and by comparison of ^{1}H-NMR and ^{13}C-NMR spectra with literature data. ^{1}H-NMR (*i.e.*, 1D NOESY) experiments were acquired by using the Bruker sequence "noesygppr1d" for residual $CDCl_3$ pre-saturation; the acquisition parameters were as follows: time domain (number of data points), 64 K; dummy scans, 0; number of scans, 128; acquisition time, 3.41 s; delay time, 8 s; spectral width, 16 ppm (9615 Hz), fid resolution 0.2935 Hz; digitization mode, baseopt. Total acquisition time was 24 min and 26 s. ^{13}C-qNMR

quantification experiments were performed by using a 1D inverse gated decoupling sequence to avoid NOE during relaxation (Bruker sequence: "zgpg_pisp_f2.fas"). The acquisition parameters were as follows: time domain (number of data points), 64 K; dummy scans, 10; number of scans, 256; acquisition time, 1 s; delay time, 10 s; spectral width, 220 ppm (33333 Hz); fid resolution, 1.017 Hz; digitization mode, baseopt; the proton decoupling power, 0 db. Total acquisition time was 47 min. The acquisition parameters for the HMBC experiments (Bruker sequence "hmbcetgpl3nd" with three-fold low-pass J-filter to suppress one-bond-correlations) were as follows: time domain, 4 K in the acquisition or direct HMBC dimension F2 (^{1}H) and 256 in indirect HMBC dimension F1 (^{13}C); dummy scans, 16; number of scans, 8; acquisition time, 0.310 s; delay time, 1.5 s; delay time for evolution of long range couplings, 62.5 μs; spectral width, 11 ppm (6602 Hz) in F2 (^{1}H) and 210 ppm (31692 Hz in F1) (^{13}C); fid resolution, 3.22 Hz (F2) 247.60 Hz (F1); digitization mode, baseopt. J-coupling for one-bond correlations suppression: 1J (XH) Min 120 Hz, 1J (XH) Max 170 Hz; J (XH) long range, 8 Hz. Total acquisition time was 1 h and 5 min. The acquisition parameters for the HSQC experiments (Bruker sequence "hsqcedetgpsp.3") were as follows: time domain, 2 K in the acquisition or direct HSQC dimension F2 (^{1}H) and 256 in indirect HSQC dimension F1 (^{13}C); dummy scans, 16; number of scans, 8; acquisition time, 0.156 s, delay time, 2 s; spectral width, 11 ppm (6602 Hz) in F2 (^{1}H) and 210 ppm (31693 Hz in F1) (^{13}C); fid resolution, 6.45 Hz (F2) 247.60 Hz (F1); digitization mode, baseopt. J-coupling for one-bond correlation selection 1J (XH) 145 Hz. Total acquisition time was 1 h and 15 min. After the sample introduction into the probe, at least 5 min were waited to achieve the thermal equilibrium. Afterwards, the magnetic field was locked, the probe head was tuned and matched and, finally, the sample was shimmed. To assure the highest reproducibility, all these procedures were automatically executed. The correct 90° pulse was calibrated for protonic and bi-dimensional spectra with the Bruker AU program "pulsecal", and the receiver gain was set.

2.5.^{13}C-qNMR procedure

Quantitative NMR was performed by using the Concentration Conversion Factor (CCF) method, implemented in Mnova® 12.0 (Mestrelab Research, S.L., Santiago de Compostela, Spain) software. A CBD standard solution (1 mg/mL) was used as the external reference compound. The CCF provided by this analysis was verified and corrected by using a commercial standard of 40% dioxane in benzene-d_6 (Bruker Biospin GmbH Rheinstetten, Karlsruhe, Germany). This solution is normally used for ^{13}C sensitivity test; in our case, the signal at 66.69 ppm (corresponding to the four equivalent carbons) was used for the

quantification. In order to determine the correct delay time (D_1), T_1 was measured for both dioxane and the standard compounds, when possible. In the case of acidic compounds, the T_1 of the signals related to the presence of carboxylic groups was directly estimated in the sample richest in CBDA and CBGA. For T_1 determination, the Bruker Sequence "T_1IR" was employed. The following parameters were applied: a list of 8 increasing delay times (from 0.2 to 20 s); delay time, 20 s; number of scans, 32; total acquisition time, 2 h. A D_1 time equal to 10 sec ($5*T_1$) was set to ensure the nuclei complete relaxation during acquisition. Moreover, only signals presenting a signal to noise ratio (S/N) $\geq$ 50 were used for quantification. An exponential window function, with a line broadening (lb) equal to 0.3, was selected for spectra transformation. Each spectrum was calibrated according to TMS signal and then an automatic zero order phase and base line correction were applied, before peak integration. The quantification tool of Mnova requires a multiplet analysis for the integration; therefore, after the initial spectra processing, a manual multiplet analysis was performed and the peak area of signals belonging to the target compounds were compared to the area of those generated by the CBD standard solution, whose spectrum was acquired under the same conditions. The results were then corrected with the correction factor obtained from the dioxane standard solution. The resonances suitable for quantification are marked with an asterisk in Table 1. In general, more than one signal should be integrated for each compound. In the case of CBD and CBDA, eight carbons having the required characteristics were chosen and they were used to calculate the average concentration of related compounds. For CBG and CBGA, six resonances were selected. In addition, both CBDA and CBGA showed three well resolved peaks, in the region ranging from 160 to 180 ppm, related to the presence of the carboxylic group on the aromatic ring, which were also used for quantification (marked with a double asterisk in Table 2). All the acquisitions were performed in triplicate.

2.6. HPLC analysis

The HPLC analysis was intended to verify ^{13}C-qNMR results and it was carried out by using the previously validated method [33,41,42].

2.7. qNMR method validation

Since that the validation procedure for the extraction and HPLC analysis of hemp extracts has already been discussed [33,41,42], in the present work the attention was focused on the ^{13}C-qNMR method. Linearity was investigated by analyzing both standard solutions at different

concentrations (from 2 to 100 mM) and a sample prepared with different dilution factors. Linearity was evaluated by calculating the CCF of the selected signals for quantitative analysis in the above-mentioned samples and verifying its constancy inside the concentration range. Precision was assessed by analyzing the same extract five times for three different days. The LOD for the target compounds (CBD, CBDA, CBG and CBGA) was determined by gradually diluting a sample containing measurable amounts of the four molecules, until a S/N ratio equal to 3 was reached. Since only signals with a S/N ratio > 50 were considered for quantification, the LOQ value was calculated by using the area of a signal with a S/N equal to 49.

3. RESULTS AND DISCUSSION

3.1. NMR spectroscopic data of extracts from hemp inflorescences

Typical ^{1}H, ^{13}C, HSQC and HMBC spectra of a Santhica extract are shown in Figures 3-5.

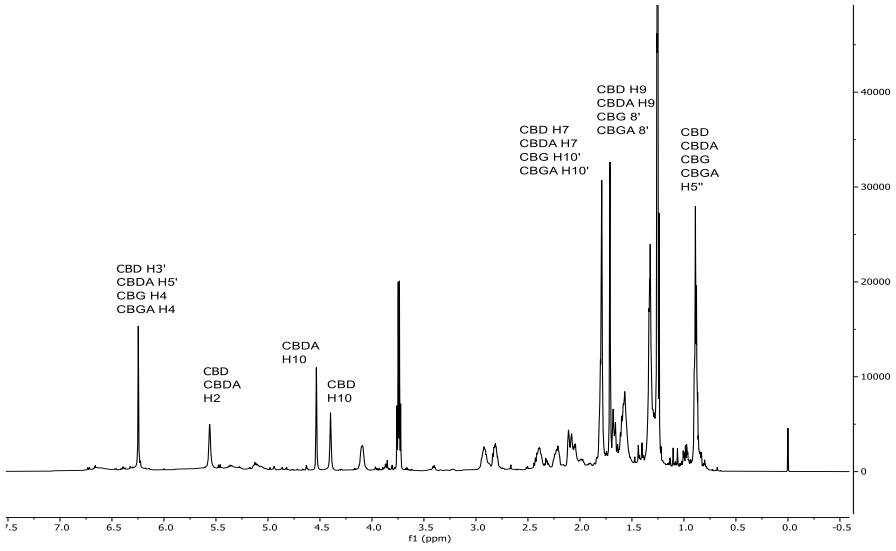

Figure 3. Typical ^{1}H spectrum of a hemp ethanolic extract.

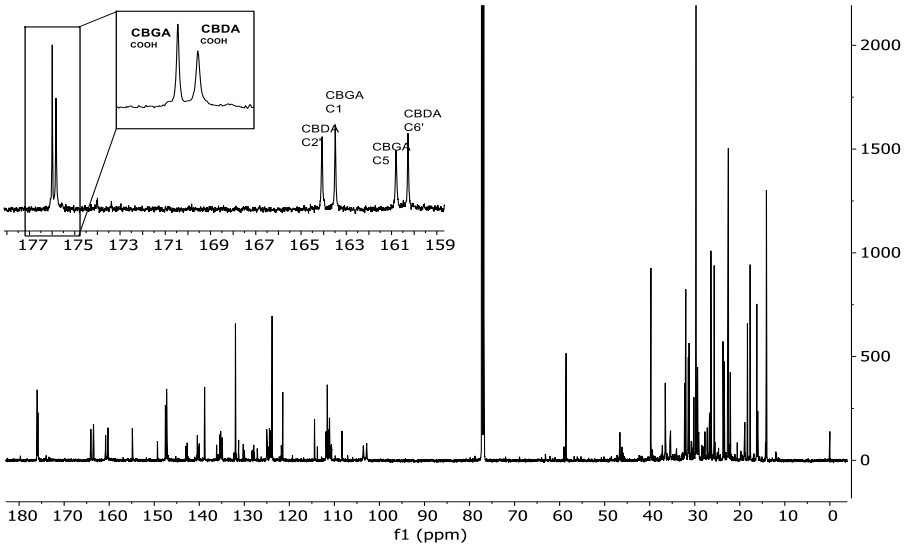

Figure 4. Typical ^{13}C spectrum of a hemp ethanolic extract; the enlarged region shows the high spectral resolution.

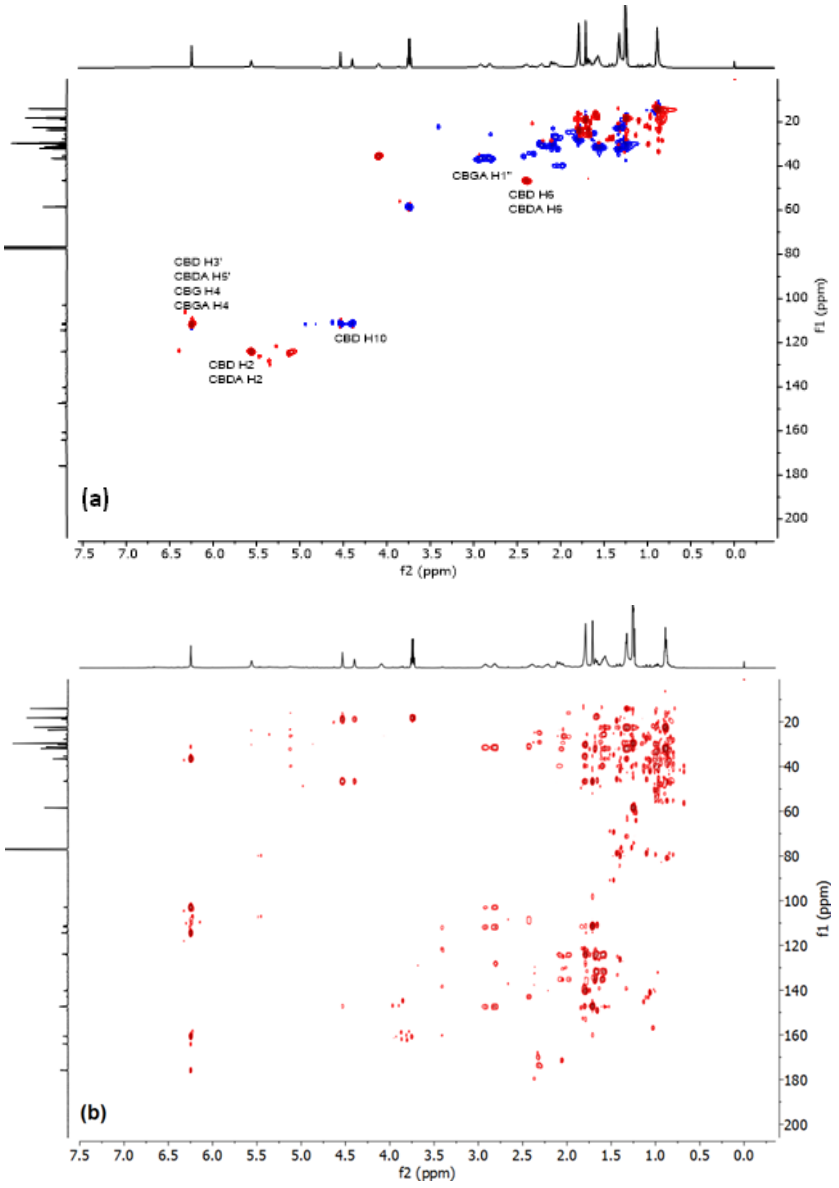

Figure 5. Typical HSQC (a) and HMBC (b) spectra of a hemp ethanolic extract.

The spectra of samples and standard compounds were compared, resulting in the assignments for CBD, CBG, CBDA and CBGA. The chemical shifts in deuterated chloroform for ^{1}H and ^{13}C are shown in Table 1-2, expressed as ppm related to tetramethylsilane (TMS).

Table 1. $^{1}H^{a}$ assignments for hemp cannabinoids in $CDCl_3$

	CBD	**CBDA**	**CBG**	**CBGA**
1	3.86 (1H,m, 11.8 Hz)	3.88 (1H,m, 11.0 Hz)	-	-
2	5.55 (1H,s)	5.55 (1H,s)	6.0 (1H,s)	-
4	2.10 (1H,m); 2.20 (1H,m)	2.10 (1H,m); 2.20 (1H,m)	6.24 (1H,s)	6.23 (1H,s)
5	1.84 (2H,q, 3.0 Hz)	1.86 (2H,q, 3.0 Hz)	-	-
6	2.40 (1H,m)	2.40 (1H,m)	-	-
7	1.79 (3H,s)	1.79 (3H,s)	-	-
9	1.66 (3H,s)	1.72 (3H,s)	-	-
10	4.40 (2H,m)	4.54 (2H,m)	-	-
1’	-	-	1.33 (2H,d, 7.0 Hz)	1.79 (2H,d, 7.4 Hz)
2’	-	-	5.27 (1H,t, 7.0 Hz)	5.27 (1H,t, 7.0 Hz)
3’	6.26 (1H,brs)	-	-	-
4’	-	-	2.04 (2H,t, 6.6 Hz)	2.04 (2H,t, 6.6 Hz)
5’	6.16 (1H,brs)	6.26 (1H,s)	2.07 (2H,q, 6.5 Hz)	2.07 (2H,q, 6.5 Hz)
6’	-	-	5.56 (1H,m)	5.05 (1H,t, 6.6 Hz)
8’	-	-	1.68 (1H,s)	1.67 (3H,s)
9’	-	-	1.58 (1H,s)	1.58 (3H,s)
10’	-	-	1.79 (3H,s)	1.80 (3H,s)
1’’	2.42 (2H,t, 7.5 Hz)	2.42 (2H,t, 7.5 Hz)	2.44 (2H,t, 7.5 Hz)	2.88 (2H,t, 7.6 Hz)
2’’	1.57 (2H,m)	1.58 (2H,m)	1.54 (2H,m)	2.10 (2H,m)
3’’	1.30 (2H,m)	1.33 (2H,m)	1.56 (2H,m)	1.32 (2H,m)
4’’	1.31 (2H,m)	1.34 (2H,m)	1.57 (2H,m)	1.32 (2H,m)
5’’	0.89 (3H,t, 6.8 Hz)	0.90 (3H,t, 6.8 Hz)	0.88 (3H,t, 6.9 Hz)	0.89 (3H,t, 6.9 Hz)

[a] The number of protons, multiplicity and coupling constants are shown in brackets.

Table 2. ^{13}C assignments for hemp cannabinoids in $CDCl_3$

	CBD		CBDA		CBG		CBGA	
	^{13}C	**T_1 (s)**	**^{13}C**	**T_1 (s)**	**^{13}C**	**T_1 (s)**	**^{13}C**	**T_1 (s)**
1	37.0*	1.32	36.7*	1.51	154.9	-	163.5**	2.65
2	124.3*	1.20	124.0*	1.35	108.3	-	103.6	-
3	139.9	5.52	140.3	-	142.7	-	147.5	-
4	31.5	2.10	31.3	-	108.3	-	111.8	-
5	28.4	0.97	27.8	-	154.9	-	160.8**	2.81
6	46.2*	1.90	46.6*	1.91	110.7	6.66	111.1	-
7	23.4*	1.41	23.7*	1.61	-	-	-	-
8	149.9	5.52	147.2	-	-	-	-	-
9	20.3	2.67	18.9	-	-	-	-	-
10	110.8*	0.96	111.3*	1.10	-	-	-	-
1’	113.8	8.08	114.4	-	22.5*	1.35	25.7*	1.54
2’	156.0	-	164.1**	2.5	121.8*	1.89	121.5*	1.92
3’	108.3	-	103.1	-	140.2	6.02	138.8	-
4’	142.9	-	147.2	-	39.7	3.00	39.7	-
5’	108.3	-	111.7	-	26.3	1.02	26.4	-
6’	153.9	-	160.1**	2.7	123.8	2.05	123.8	-
7’	-	-	-	-	132.0	5.50	131.7	-
8’	-	-	-	-	23.4	2.68	23.4	-
9’	-	-	-	-	17.6	1.03	17.8	-
10’	-	-	-	-	16.0*	1.23	16.2*	1.40
1’’	35.5*	1.95	35.4*	1.95	35.6*	1.23	36.3*	1.25
2’’	30.4*	1.12	29.7*	1.12	30.8*	1.06	30.2*	1.10
3’’	30.7*	1.47	30.2*	1.47	31.5*	1.50	31.4*	1.52
4’’	22.5	3.82	22.5	3.88	22.5	3.90	22.5	3.92
5’’	14.1	3.19	14.1	3.23	14.1	3.20	14.1	3.36
-COOH	-	-	175.3**	3.1	-	-	176.0**	3.11

*Signals with T_1<2 s used for quantification.
**Signal with T_1>2 s used for quantification.
T_1 was measured, when possible, by using standard compounds.

As shown in Figure 3, the protonic spectrum presents a huge number of overlapped peaks, thus requiring an extensive use of deconvolution for signal integration, which can introduce some accuracy issues. To overcome this problem, in this work ^{13}C-qNMR was evaluated for the first time for the determination of cannabinoids in hemp extracts. As shown in Figure 4 and Table 2, carbon signals are better resolved and easier to deal with for quantitative purpose. In this context, in these experimental conditions evident signal doubling, due to conformational equilibria, and line broadening did not occur. All the signals used for CBD and CBG quantification showed a measured average half width of 1.25 Hz (maximum 1.5 Hz). CBDA and CBGA signals were slightly broader; in this case, the average half width was 3.3 Hz (maximum 4 Hz). This line broadening effect did not invalidate or affect the quantification of

these compounds, considering that the differences between qNMR and HPLC data are limited and not significant (Table 3).

On the other hand, it is well known that ^{13}C-qNMR presents some complexities, which often makes the use of this technique quite problematic. In particular, the major issues related to ^{13}C-qNMR are:

1. low sensitivity, due to the lower ^{13}C isotopic abundance (1.1 %) in comparison to ^{1}H;
2. carbons typically have long T_1 relaxation time; in this way, signals could not reach their full intensity;
3. the ^{13}C signal intensity is affected by the Nuclear Overhauser Enhancement (NOE) effect, that depends on ^{13}C type (from primary to quaternary).

In order to reduce the impact of these issues, the following measures were applied. As regards the sensitivity problem, it was possible to acquire spectra of concentrated hemp extracts, without disregarding the spectrum quality in terms of resolution, intensity and resonance shifting, due to the matrix effect. To overcome the issue related to ^{13}C long relaxation time, T_1 for each carbon of standard compounds was tentatively measured. Some of the nuclei did not provide results in an acceptable time, due to the molecule structure or to the low amount of standard available (CBDA and CBGA). For this reason, signals with T_1<2 s were initially selected for quantification (marked with an asterisk in Table 2). Furthermore, some characteristic signals with T_1>2 s were also tentatively used for the two acidic compounds (marked with double asterisk in Table 2). Finally, a pulse delay (D_1) equal to 10 sec (5*T_1) was used. This parameter allowed us to obtain the full relaxation in an acceptable time, thus making possible to perform the analysis in a competitive time (47 min) with respect to the most common HPLC technique. The last question was solved by lowering to zero the proton decoupling power.

3.2. ^{13}C-qNMR method validation

The Concentration Conversion Factor (CCF), obtained from the analysis of standards and used by the software to calculate the concentration of compounds in samples, was measured in the range of expected concentrations, by diluting a CBD standard solution. The CCF value was constant (0.71605±0.00004) in all the considered concentration ranges, thus assuring a good

linearity (r^2 = 0.9998). The method proposed here provided also a good intra- and inter-day precision, with percentage relative standard deviation (%RSD) values of 0.8 and 1.5%, respectively. As regards the limit of detection (LOD), in these experimental conditions the lowest concentrations which presented clearly distinguishable signals from the spectral background were 0.6, 0.5, 0.6 and 0.5 mM for CBD, CBDA, CBG and CBGA, respectively, corresponding to LOD values of 188, 180, 190 and 180 μg/mL in the NMR tube. The lowest quantification limits (LOQ), by applying the below mentioned S/N restriction, corresponded to 2.11, 2.15, 2.10 and 2.18 mM for CBD, CBDA, CBG and CBGA, respectively, with relative LOQ values of 660, 746, 664 and 746 μg/mL in the NMR tube.

3.3. Quantitative analysis of hemp inflorescences

Quantitative results of hemp inflorescences obtained by ^{13}C-qNMR are shown in Table 3, compared to those obtained by HPLC [41,42]. Data are expressed as mean (mg/g) ± standard deviation (SD), dry weight. These values correspond to the overall means of three replicates for all the considered signals for each compound. The results provided by ^{13}C-qNMR and HPLC are comparable, without meaningful differences. It should also be considered that the signals tentatively used for CBDA and CBGA with T_1>2 s (marked with double asterisk in Table 2) provided very similar quantitative results as well as those with the lower relaxing times, thus demonstrating the method ruggedness. In particular, ^{13}C-qNMR seems to slightly underestimate the CBD and CBG content with respect to HPLC, since this situation occurs for every cultivar. The mean recovered amounts of CBD and CBDA were significantly higher respect those of CBG and CBGA; this finding is supported by other studies, in which the measured concentrations for these cannabinoids were undetectable or very low [8,30]. In most samples (Antal, Carmagnola, China, Fibrante, Futura and Santhica), the acidic compounds were more concentrated with respect to their neutral counterparts, demonstrating that the extraction method is able to limit the decarboxylation process. Codimono was the cultivar which provided the highest content of CBD, while Futura was the one with the highest amount of CBDA. As concerns CBG, only one hemp variety (Santhica) showed a concentration over the LOQ value. CBGA was determined instead for Antal, Carmagnola, Futura and Santhica, these latter two varieties being the richest ones.

Table 3. qNMR and HPLC data (mg/g) of cannabinoids in hemp inflorescences.

	CBD		CBDA		CBG		CBGA	
	qNMR	**HPLC***	**qNMR**	**HPLC***	**qNMR**	**HPLC**	**qNMR**	**HPLC**
Antal	2.2±0.2	2.4±0.1	15.7±0.5	15.5±0.7	<LOQ[b]	0.3[a]	1.2±0.2	0.6[a]
Carma	5.8±0.4	6.0±0.3	<LOQ[b]	2.2±0.1	<LOQ[b]	0.5±0.1	<LOQ[b]	0.4[a]
Carmagnola	3.0±0.4	3.3±0.3	17.3±0.6	16.7±1.2	<LOQ[b]	0.1[a]	1.2±0.1	0.7±0.1
China	8.0±0.5	8.4±0.1	18.3±0.7	17.2±0.8	<LOQ[b]	0.2±0.1	<LOQ[b]	0.5±0.1
Codimono	9.3±0.6	9.8±0.3	1.1±0.2	2.9±0.3	<LOQ[b]	0.1[a]	<LOQ[b]	< LOQ[d]
Fibrante	6.6±0.5	7.9±0.5	14.7±0.3	14.5±1.1	<LOQ[b]	0.2[a]	<LOQ[b]	0.4[a]
Futura	2.8±0.2	3.3±0.1	34.0±0.6	33.8±0.3	<LOQ[b]	<LOQ[c]	1.7±0.3	1.3±0.1
Santhica	2.1±0.1	2.3±0.2	18.7±0.8	17.3±2.4	1.2±0.1	1.4 [a]	9.4±0.4	9.9±0.2

[a] SD < 0.05. [b]LOQ values are shown in paragraph 3.2. [c]CBG LOQ 1.8 μg/mL [33,41]. [d]CBGA LOQ 2.5 μg/mL [33,41].

4. Conclusions

The ^{13}C-qNMR method here proposed for the quantification of non-psychoactive cannabinoids in hemp provided reliable results in comparison to the most commonly and consolidated HPLC technique. The validation confirmed the ruggedness of this qNMR approach, which was found to be precise and sufficiently sensitive. In conclusion, this ^{13}C-qNMR method is suitable and advantageous for a multi-component analysis of cannabinoids in hemp extracts. This technique could be useful to gain a holistic view of the composition and chemical profile of different hemp varieties and it could be applied in the quality control of both the plant material and its derivatives.

SEPARATION AND NON-SEPARATION METHODS FOR THE ANALYSIS OF CANNABINOIDS IN *CANNABIS SATIVA* L.

Journal of Pharmaceutical and Biomedical Analysis, **2021**, 206; doi:10.1016/j.jpba.2021.114346

Virginia Brighenti [1], Lucia Marchetti [1,2], Lisa Anceschi [1,2], Michele Protti [3], Patrizia Verri [4], Federica Pollastro [5], Laura Mercolini [3], Davide Bertelli [1], Chiara Zanardi [6], Federica Pellati [1,*]

[1] Department of Life Sciences (DSV), University of Modena and Reggio Emilia, Via G. Campi 103, 41125, Modena, Italy
[2] Clinical and Experimental Medicine (CEM) PhD Program, University of Modena and Reggio Emilia, Via G. Campi 287, 41125 Modena, Italy
[3] Department of Pharmacy and Biotechnology (FaBiT), Alma Mater Studiorum University of Bologna, Via Belmeloro 6, 40126 Bologna, Italy
[4] Department of Biomedical, Metabolic and Neural Sciences, University of Modena and Reggio Emilia, Via del Pozzo 71, 41124 Modena, Italy
[5] Department of Pharmaceutical Sciences, University of Eastern Piedmont, Largo Donegani 2, 28100 Novara, Italy
[6] Department of Chemical and Geological Sciences (DSCG), University of Modena and Reggio Emilia, Via G. Campi 103, 41125, Modena, Italy

1. INTRODUCTION

Reliable, sensitive, and fast methods for the determination of the cannabinoid profiles in *Cannabis* plant material is a pivotal issue to ensure quality and safety in use. Most of laboratories all over the world apply HPLC coupled with diode-array detection (UV/DAD) and/or mass spectrometry (MS) detection as the analytical technique of choice for the determination of cannabinoids in the plant material, as it they are both well established and robust [43,44]. On the other hand, the increasing need of faster and eco-friendly methodologies has opened the doors to the application of more modern analytical approaches, based on non-separation procedures, including NMR [41]. The main advantages are related to the reduced amount of solvent required for the analysis and the simultaneous acquisition of the quali- and quantitative data of the target analytes.

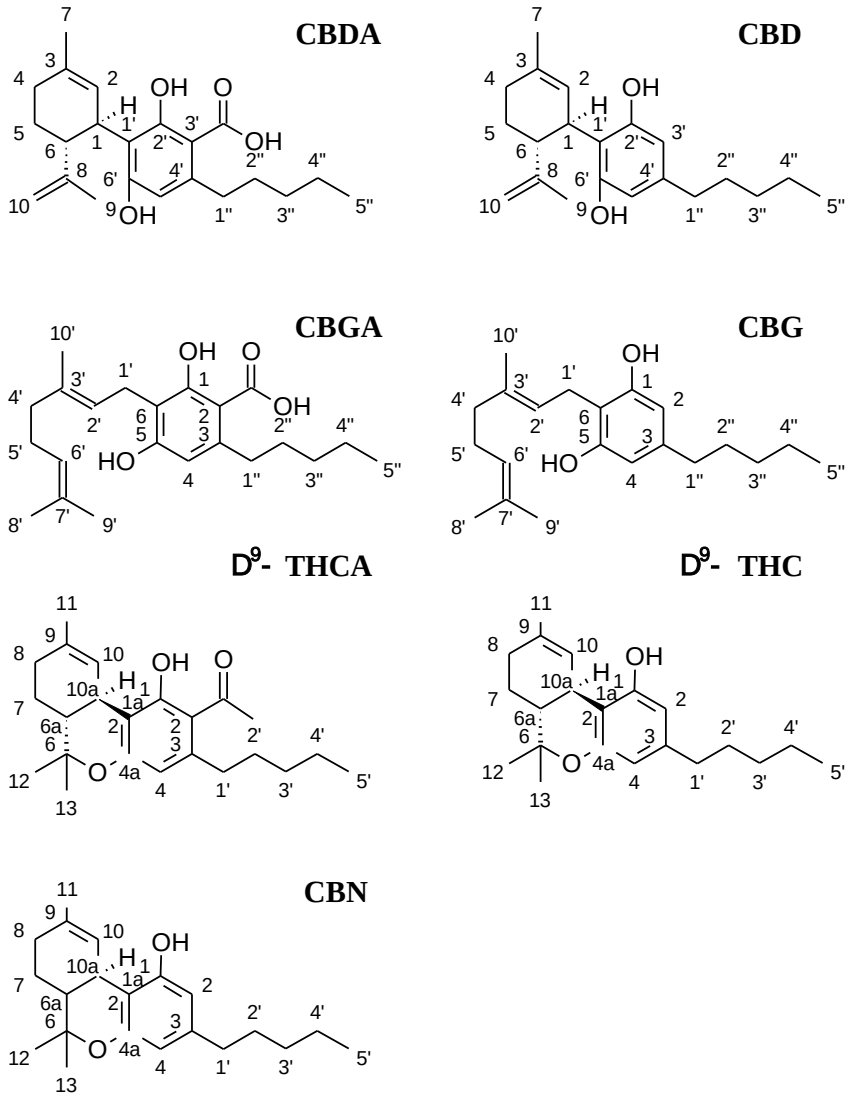

Figure 1. Chemical structures of target cannabinoids.

In the light of all the above, the present study aims at the comparison of the efficiency of different analytical methods for the study of the main cannabinoids in different samples of cannabis inflorescences, belonging to fibre-type, recreational and medical varieties. In particular, a separation method, based on HPLC coupled with UV/DAD detection, and a non-separation method, based on ^{13}C-qNMR, were compared. In brief, the extraction procedure of cannabinoids applied was the same cited above and it was based on a dynamic maceration at room temperature with ethanol (EtOH) as the extraction solvent [33,41]. The previously mentioned analytical methods were then applied to the quantitative analysis of cannabinoids in *Cannabis* samples belonging to different varieties. ^{13}C-qNMR was applied to chemotype discrimination of *C. sativa* varieties here for the first time. The quantitative data obtained by applying the two analytical methods were finally compared, together with the validation parameters monitored for each technique.

2. EXPERIMENTAL

2.1. Chemicals and solvents

Standard solutions of CBDA, CBD, CBGA, CBG, Δ^9-THCA, Δ^9-THC and CBN (1 mg/mL either in acetonitrile or methanol) were purchased from Cerilliant (Round Rock, TX, USA). Deuterated chloroform ($CDCl_3$ 99.8% atom % D), tetramethylsilane (TMS), acetonitrile (ACN), formic acid (HCOOH) and EtOH analytical grade were from Sigma-Aldrich (Milan, Italy).

2.2. Plant material

Fibre-type *C. sativa* female inflorescences (indicated in the text as F1-F8, respectively) were analysed in this study. Samples F1-F7 were kindly provided by Assocanapa s.r.l. (Carmagnola (TO), Italy), while sample F8 was purchased from Materia Medica Processing (Siena, Italy). All the fibre-type samples considered in this study belong to hemp varieties approved for commercial use by the European Union. Eight samples of *Cannabis light* inflorescences were purchased from IperHemp (Pomezia, Rome, Italy), and they were indicated in the text as L1-L8. Eight recreational samples (indicated in the text as R1-R8) were available at the Toxicology Laboratory of the Forensic Institute of the Department of Biomedical, Metabolic and Neurosciences of the University of Modena and Reggio Emilia, while inflorescences belonging to medical cannabis varieties (namely M1-3) were available in a local pharmacy. The plant

material was stored at +4.0 °C to prevent both degradation and decarboxylation of acidic compounds during the storage.

2.3. Sample preparation for HPLC analysis

A portion of 0.25 g of *C. sativa* inflorescences, previously deprived of seeds and twigs and properly grinded, were weighed and added with 10 mL of EtOH [33,41]. The extraction of the target compounds was performed by dynamic maceration at room temperature for 15 min. The extract was then paper-filtered, and the residue was extracted twice more following the same procedure by adding 10 and 5 mL of EtOH, respectively. The filtrates of the three extractions were then combined and brought to the final volume of 25 mL with the extraction solvent. The extracts were diluted 1:5 v/v with the mobile phase prior HPLC-UV/DAD analysis. Extracts were filtered through a 0.45 μm PTFE filter into a HPLC vial prior the injection into the chromatographic system. Ethanolic extracts from recreational cannabis were prepared and analysed at the Toxicology Laboratory of the Forensic Institute of the Department of Biomedical, Metabolic and Neurosciences of the University of Modena and Reggio Emilia. Samples belonging to medical cannabis were extracted in a local pharmacy on medical prescription requests, and the analyses were carried out at the Toxicology Laboratory of the Forensic Institute of the Department of Biomedical, Metabolic and Neurosciences of the University of Modena and Reggio Emilia. The extraction procedure was carried out in duplicate for each sample. The EtOH extracts obtained from the plant material were immediately submitted to HPLC-UV/DAD analysis, in order to avoid any possible alteration of the composition, due to prolonged storage.

2.4. Sample preparation for qNMR analysis

In order to prepare concentrated crude extracts, a weighed amount of 1 g of grinded *C. sativa* inflorescences was extracted at room temperature with 20 mL of EtOH for 15 min. The solution was filtered, and the residue was extracted twice more with 20 and 10 mL of the same solvent. The filtrates were then combined in a volumetric flask and adjusted to 50 mL. Extracts were evaporated under vacuum at 30 °C, and the residue was dissolved in 1 mL of $CDCl_3$ (0.03% TMS). TMS was used as the internal standard for chemical shift referencing. Each sample was extracted twice and further analysed.

2.5. HPLC-UV/DAD analysis

HPLC analyses were performed on an Agilent Technologies (Waldbronn, Germany) modular model 1260 Infinity II system, consisting of a vacuum degasser, a quaternary pump, a manual injector and a diode array detector (DAD). The chromatograms were recorded using an Agilent OpenLab CDS ChemStation Edition (Rev. C.01.10). The analysis of cannabinoids in cannabis extracts was carried out on an Ascentis Express C_{18} column (150 × 3.0 mm I.D., 2.7 μm, Supelco, Bellefonte, PA, USA) [33,41]. The mobile phase was composed of 0.1% HCOOH (v/v) in both (A) water and (B) ACN. The gradient elution was as follows: 0–13 min 60% B, 13–17 min from 60 to 80% B, 17–22 min from 80 to 90% B, which was kept for 8 min. The post-running time and the flow rate were set at 10 min and 0.4 mL/min, respectively. Three μL of each extract were injected into the HPLC system for the analysis. Chromatograms were acquired at the wavelengths of 210 and 220 nm for the analysis of neutral (Δ^9-THC, CBD, CBG and CBN) and acidic cannabinoids (Δ^9-THCA, CBDA and CBGA), respectively. Three injections were performed for each sample.

2.6. ^{13}C-qNMR spectroscopy

^{13}C-NMR spectra were acquired with a Bruker FT-NMR Avance III HD 600 MHz spectrometer (Bruker Biospin GmbH Rheinstetten, Karlsruhe, Germany). The experiments were performed at 298.0 K, non-spinning. Assignment of resonances in sample spectra was achieved by comparison of pure compounds with the literature. Relaxation time (T_1) for all the carbon nuclei used in the quantitative analysis was measured, thus ensuring every signal reaches its full intensity without being underestimated. This measurement was performed by means of the Bruker sequence "t1ir", implemented in Topspin™ 3.5 (Bruker Biospin GmbH, Rheinstetten, Germany). For this experiment, a list of 8 increasing delay times (from 0.2 to 20 s) were selected. Other acquisition parameters were set as follows: delay time, 20 s; number of scans, 32; total acquisition time, 2 h. An adequate delay time (D1=10 s) was finally set for the sample spectrum acquisitions. Carbon spectrum was acquired by using a one-dimensional inverse gated decoupling sequence to avoid Nuclear Overhauser Enhancement (NOE) during relaxation (Bruker sequence: "zgpg_pisp_f2.fas"). The acquisition parameters were as follows: time domain (number of data points), 64 K; dummy scans, 10; number of scans, 256; acquisition time, 1 s; delay time, 10 s; spectral width, 220 ppm (33333 Hz); fid resolution, 1.017 Hz; digitization mode, baseopt. To use this sequence as inverse gated the proton decoupling power (PLW13) during recycle delay and experiment time was set to 0 db. The total acquisition time

was 47 min. After the introduction of the sample inside the probe, five min were waited to achieve the thermal equilibrium. Then, the magnetic field was locked, the probe head was automatically tuned and matched, and the homogeneity of the static magnetic field was adjusted through the gradient shimming. The correct 90° pulse was determined and finally the receiver gain was adjusted to maximize the signal-to-noise ratio. Quantitative analysis was performed using Mnova® 14.2 (Mestrelab Research, S.L., Santiago de Compostela, Spain) by means of the Concentration Conversion Factor (CCF) method. The underlying principle is that the area of a multiplet (and its absolute integral) is proportional to the chemical species that gave rise to it, and inversely related to the number of nuclides for that multiplet. Therefore, CCF is a proportionality constant allowing to convert the integral/nuclides ratio into a concentration, and it only needs to be determined once for an experiment, maintaining its applicability to all the species in the same chemical environment. In this study, a CBD standard solution (1 mg/mL) was used as the external reference compound, and its spectrum was recorded under the same conditions. For the initial processing each spectrum was properly phased, with an automatic zero order phase correction, then the chemical shifts were referenced against the TMS signal. An exponential window function with a line broadening (lb) equal to 0.3 Hz was used for spectrum transformation. Finally, the baseline correction was performed with a Bernstein polynomials of order 3 function. For the peak integration, a manual multiplet analysis was carried out, excluding potential extraneous signals from calculation. Resonances of the target compounds (CBDA, CBD, CBGA, CBG, Δ^9-THCA, Δ^9-THC and CBN) were compared to those generated by CBD external reference, with a calculated CCF equal to 0.72680, thus converted into corresponding concentrations.

2.7. Method validation

Both the analytical method above described, were submitted to validation according to the ICH guidelines [45]. Linearity, sensitivity, and precision of the analytical methods were evaluated. Linearity was evaluated by means of external standard calibration for the HPLC-UV/DAD method. The stock standard solution of each compound was prepared by accurately diluting the respective certified reference solution (1.0 mg/mL either in MeOH or ACN) with the initial mobile phase (60:40 ACN:H_2O, both containing 0.1% of HCOOH). The external standard calibration curve was generated by using five data points, covering the following concentration ranges: 5-100 μg/mL for CBDA, CBGA, CBD and CBG; 5-40 μg/mL for Δ^9-THC and CBN. Aliquots of 3 μL per each standard solution were used for HPLC analysis. Injections were performed in triplicate for each concentration level. The amount of cannabinoids in *C. sativa*

extracts was determined by using the calibration curves of the standard compounds having the same chromophore. The linearity of ^{13C}-qNMR method was assessed by analysing solutions of the external reference CBD at five different concentrations from 2 to 100 mM, consistent with the working range of the method. The Concentration Conversion Factor (CCF) used by the software to calculate the concentration of compounds in samples was constant in the selected range. The limit of detection (LOD) and the limit of quantification (LOQ) for reference compounds were experimentally determined by analysis of serial dilutions of a standard solution to reach a signal-to noise (S/N) ratio of 3 and 10, respectively. The precision of the methods here proposed was determined by multiple measurements on the same sample within one and three different days. The accuracy of the analytical methods was evaluated by using the recovery test. This involved the addition of a known quantity of standard compound to half the weight of a sample to reach 100% test concentration. The fortified samples were then extracted and analysed with the proposed methods.

3. RESULTS AND DISCUSSION

3.1. Quantitative analysis of cannabinoids

Figure 2 shows representative chromatograms of *C. sativa* extracts belonging to different varieties. Quantitative data for target cannabinoids are shown in Table 1.

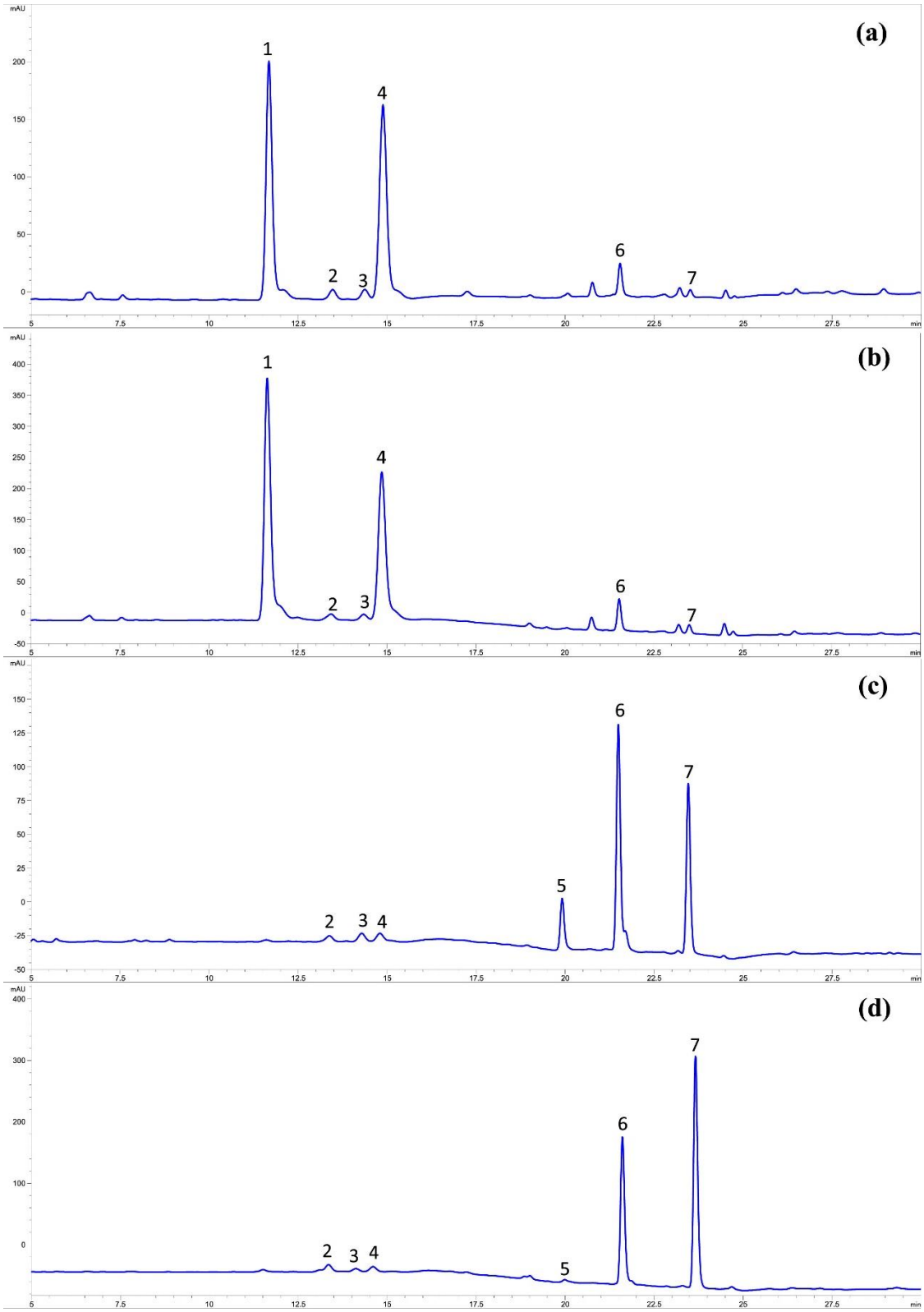

Figure 2. HPLC-UV/DAD chromatograms of EtOH extracts from a representative sample of (a) fibre-type, (b) light, (c) recreational-type and (d) drug-type *Cannabis sativa* L., recorded at 210 nm. Peak identification: (1) CBDA, (2) CBGA, (3) CBG, (4) CBD, (5) CBN, (6) Δ^9-THC, (7) Δ^9-THCA.

Table 1. Quantitative data of target cannabinoids in *Cannabis sativa* L. varieties by means of HPLC-UV/DAD and ^{13}C-qNMR methods.

Sample	CBDA		CBD		CBGA		CBG		Δ^9-THCA		Δ^9-THC		CBN	
	HPLC	qNMR	HPLC	qNMR	HPLC	qNMR	HPLC	qNMR	HPLC	qNMR	HPLC	qNMR	HPLC	qNMR
F1	32.6±2.1	21.7±1.9	8.9±0.7	6.5±0.4	<LOQ	<LOQ	<LOQ	<LOQ	<LOQ	<LOQ	<LOQ	<LOQ	<LOQ	<LOQ
F2	47.1±0.3	36.0±1.6	17.1±0.7	14.2±0.9	4.3±0.2	1.5±0.2	<LOQ	<LOQ	<LOQ	<LOQ	1.8±0.1	0.8±0.2	<LOQ	<LOQ
F3	20.3±1.6	19.8±3.0	19.5±2.0	23.1±4.1	<LOQ	<LOQ	<LOQ	<LOQ	<LOQ	<LOQ	1.6±0.1	1.0[a]	<LOQ	<LOQ
F4	9.4±0.1	9.1±0.2	8.5±0.3	8.4±0.4	<LOQ	<LOQ	<LOQ	<LOQ	<LOQ	<LOQ	<LOQ	<LOQ	<LOQ	<LOQ
F5	13.4±1.4	10.6±0.5	3.5±0.2	3.1±0.2	<LOQ	<LOQ	<LOQ	<LOQ	<LOQ	<LOQ	<LOQ	<LOQ	<LOQ	<LOQ
F6	31.2±2.2	29.7±5.0	11.8±0.4	13.8±2.1	<LOQ	<LOQ	<LOQ	<LOQ	<LOQ	<LOQ	2.6±0.2	<LOQ	<LOQ	<LOQ
F7	22.7±0.7	21.9±1.5	16.9±1.3	17.8±0.5	<LOQ	<LOQ	<LOQ	<LOQ	<LOQ	<LOQ	2.2±0.4	<LOQ	<LOQ	<LOQ
F8	25.8±4.0	23.1±0.7	18.5±2.6	20.9±7.5	<LOQ	<LOQ	<LOQ	<LOQ	<LOQ	<LOQ	1.8±0.1	1.1±0.3	<LOQ	<LOQ
L1	109.0±2.2	81.4±3.1	24.5±0.7	23.3±0.9	<LOQ	<LOQ	<LOQ	<LOQ	1.7±0.1	1.3±0.1	3.1±0.2	2.0±0.1	<LOQ	<LOQ
L2	56.7±1.6	47.7±2.7	19.7±0.7	20.6±0.2	<LOQ	<LOQ	<LOQ	<LOQ	<LOQ	<LOQ	2.1±0.1	1.6±0.1	<LOQ	<LOQ
L3	66.5±1.0	50.6±3.8	20.3±0.9	19.2±0.9	<LOQ	<LOQ	<LOQ	<LOQ	<LOQ	<LOQ	2.6±0.1	1.8±0.2	<LOQ	<LOQ
L4	37.3±1.6	32.1±1.8	24.9±0.5	24.2±2.0	<LOQ	<LOQ	<LOQ	<LOQ	<LOQ	<LOQ	2.1±0.2	1.5±0.2	<LOQ	<LOQ
L5	104.8±3.5	75.0±7.4	26.9±0.9	24.1±1.8	1.9±0.1	<LOQ	<LOQ	<LOQ	2.2±0.1	1.8±0.2	3.4±0.2	1.9±0.1	<LOQ	<LOQ
L6	90.9±0.4	64.1±3.5	28.0±0.5	27.0±2.2	<LOQ	<LOQ	<LOQ	<LOQ	<LOQ	<LOQ	3.3[a]	2.0±0.2	<LOQ	<LOQ
L7	62.1±2.9	54.5±4.5	6.0±0.2	6.4±0.3	<LOQ	<LOQ	<LOQ	<LOQ	1.9±0.2	1.4±0.1	<LOQ	<LOQ	<LOQ	<LOQ
L8	53.9±1.5	44.4±1.4	17.8±0.4	19.3±1.2	<LOQ	<LOQ	<LOQ	<LOQ	<LOQ	<LOQ	<LOQ	<LOQ	<LOQ	<LOQ
R1	3.7±0.2	<LOQ	< LOQ	<LOQ	3.9±0.1	<LOQ	<LOQ	<LOQ	113.2±2.5	115.5±1.7	16.5±1.8	18.5±3.0	<LOQ	<LOQ
R2	< LOQ	<LOQ	3.9±0.1	<LOQ	<LOQ	<LOQ	5.1[a]	4.6±0.4	34.5±10.5	32.4±0.7	29.4±2.2	27.4±1.7	10.5±2.2	10.7±2.8
R3	< LOQ	<LOQ	<LOQ	<LOQ	<LOQ	<LOQ	<LOQ	<LOQ	17.4±2.4	16.4±0.6	0.5[a]	<LOQ	<LOQ	<LOQ
R4	< LOQ	<LOQ	<LOQ	<LOQ	<LOQ	<LOQ	<LOQ	<LOQ	36.1±2.4	34.0±2.5	<LOQ	<LOQ	<LOQ	<LOQ
R5	< LOQ	<LOQ	<LOQ	<LOQ	<LOQ	<LOQ	<LOQ	<LOQ	172.2±5.7	160.9±0.5	30.8±0.8	30.4±0.8	<LOQ	<LOQ
R6	< LOQ	<LOQ	<LOQ	<LOQ	<LOQ	<LOQ	<LOQ	<LOQ	188.9±0.6	186.7±11.6	6.3±0.5	6.3±0.2	<LOQ	<LOQ
R7	< LOQ	<LOQ	<LOQ	<LOQ	<LOQ	<LOQ	<LOQ	<LOQ	100.5±3.1	107.1±1.6	13.0±1.1	12.4±0.2	<LOQ	<LOQ
R8	< LOQ	<LOQ	<LOQ	<LOQ	<LOQ	<LOQ	<LOQ	<LOQ	173.9±11.3	169.6±2.4	5.2±0.6	4.8±0.1	<LOQ	<LOQ
M1	49.9 ±2.6	34.8±5.9	9.2±0.5	6.3±2.0	<LOQ	<LOQ	<LOQ	<LOQ	<LOQ	0.9±0.2	<LOQ	0.5±0.2	<LOQ	<LOQ
M2	44.7±9.6	25.2±1.1	51.8±6.5	36.8±3.0	<LOQ	<LOQ	<LOQ	<LOQ	4.7±1.3	<LOQ	53.6±8.8	31.7±1.9	4.5±0.7	<LOQ
M3	<LOQ	<LOQ	< LOD	<LOQ	<LOQ	<LOQ	<LOQ	<LOQ	181.4±16.5	109.3±2.4	40.6±1.6	26.4±0.8	3.3±0.2	<LOQ

Data are expressed as mg/g ± SD (n = 6). Experimental conditions as in Sections 2.5 and 2.6.

[a] SD < 0.05

As previously reported in the literature, fibre-type and *Cannabis light* samples have a high content in CBDA and CBD [33,41,44]. Recreational type samples have a high amount of Δ^9-THCA, followed by Δ^9-THC. Medical-type samples have either a high content in CBDA/CBD or Δ^9-THCA/Δ^9-THC or a medium level amount in both psychoactive and non-psychoactive cannabinoids. As regards NMR, peaks of structurally related compounds are difficult to be resolved using ^{1}H NMR due to the wide spectral overlay [46,47]. Indeed, the protonic spectrum presents a huge number of overlapped peaks, thus requiring an extensive use of deconvolution for signal integration, which can introduce some accuracy issues. Since ^{13}C spectral window is 20-fold greater than ^{1}H, providing much greater chemical shift dispersion, deconvolution is not usually necessary to obtain accurate carbon peak integrations. On the other hand, ^{13}C-NMR also suffers from complications, due to low natural isotope abundance, carbon long relaxation time and NOE effect. In this respect, concentrated *C. sativa* extracts were prepared to overcome low ^{13}C sensitivity and spectra were acquired under conditions that facilitate carbons with short relaxation times. Instead, some nuclei with long T_1 (>> 2 sec), which did not provide results in an acceptable time, were excluded from calculation. Finally, the NOE effect, namely the transfer of spin polarization from one nuclear spin population to another via cross-relaxation which could affect the real intensity of the resonance, was avoided by zeroing the proton decoupling power. The efficiency and solid performance of qNMR spectroscopy has been previously applied to some hemp samples [21], while a systematic analysis of the most representative cannabis chemotypes (including recreational and medical-type varieties) using this technique was carried out here for the first time. The chemical shifts of the major cannabinoids identified in the samples are shown in Table 2, expressed as ppm related to TMS. Figure 3 shows representative NMR spectra of fibre-type, recreational and medical varieties cannabis samples. The dotted line highlights the aromatic area, which is actually the most informative one.

Table 1: ^{13}C assignments for cannabinoids in $CDCl_3$.

	CBDA	CBD	CBGA	CBG		THCA	THC	CBN
1	36.6	37.0	25.7	22.5	1	164.57	154.74	154.67
2	124.0	124.3	121.5	121.8	1a	109.22	109.93	110.80
3	140.3	139.9	138.8	140.2	2	102.00	107.97	108.00
4	31.3	31.5	39.7	39.7	3	146.83	142.82	144.55
5	27.8	28.4	26.4	26.3	4	112.48	110.02	110.80
6	46.6	46.2	123.8	123.8	4a	159.51	154.09	155.45
7	23.7	23.4	16.2	16.0	6	78.44	77.50	77.70
8	147.2	149.9	131.7	132.0	6a	45.62	45.81	136.88
9	18.9	20.3	23.4	23.4	7	25.04	25.03	122.64
10	111.3	110.8	17.8	17.6	8	29.6	31.18	127.52
1’	114.4	113.8	111.1	110.7	9	133.79	134.38	136.91
2’	164.1	156.0	163.5	154.9	10	123.68	123.74	127.59
3’	103.1	108.3	103.6	108.3	10a	33.48	33.58	107.8
4’	147.2	142.9	147.5	142.7	11	23.38	23.37	21.54
5’	111.7	108.3	111.8	108.3	12	27.39	27.57	29.71
6’	160.1	153.9	160.8	154.9	13	19.39	19.28	29.67
1’’	35.4	35.5	36.5	35.6	1’	36.50	35.49	35.62
2’’	29.7	30.4	30.2	30.8	2’	31.33	30.67	30.47
3’’	30.2	30.7	31.4	31.5	3’	32.04	31.53	31.94
4’’	22.5	22.5	22.5	22.5	4’	22.65	22.56	22.55
5’’	14.1	14.1	14.1	14.1	5’	14.13	14.02	14.02
-COOH	175.3	-	176.0	-	-COOH	178.0	-	-

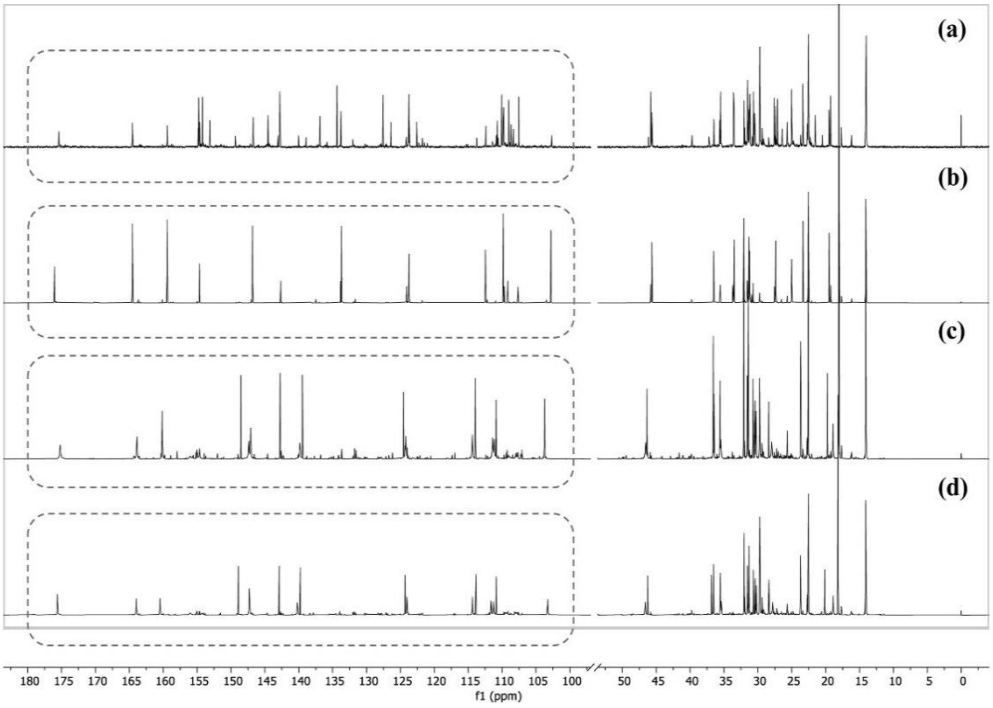

Figure 3. ^{13}C NMR spectra of EtOH extracts obtained from a representative sample of (a) fibre-type, (b) light, (c) recreational-type and (d) drug-type *Cannabis sativa* L. The dashed area is related to cannabinoid signals in the aromatic area.

In general, a good agreement was observed within the two methods in terms of quantitative data of target cannabinoids, thus demonstrating to be both reliable tools for the determination of active compounds in cannabis extracts. Indeed, by comparing results provided by the two methods a high degree of agreement was confirmed by the *t*-student test. By focusing on the main analytes present in the different cannabis varieties analysed in this work (*i.e.*, cannabinoic acids and their neutral counterparts), statistically significant differences ($P < 0.05$) in the content of CBDA and CBD were observed for some samples belonging to fibre-type (F1 and F2), *Cannabis light* (L1, L2, L5 and L7) and medical-type (M1 and M2). As for Δ^9-THCA and Δ^9-THC, statistically significant differences ($P < 0.05$) in their amounts were found only for *Cannabis light* L1 and drug-type M2 and M3 samples. In regard to validation data, the results obtained using HPLC-UV/DAD were comparable to those found in the literature for the same analytical techniques [43,44]. Considering linearity, the HPLC method showed good linearity for the compounds used as cannabinoid standards over the concentration range tested, with r^2 values in the range 0.996-1.000. The LOD and LOQ values were in the range 0.4-1.2 and 1.4-3.8 μg/mL using the UV/DAD detector. The method showed also a good intra- and inter-day precision, with percentage relative standard deviation (%RSD) values related to both retention time and peak area below 0.8 and 6.1%, respectively. For ^{13}C-qNMR, least squares method was used to create a regression line with a correlation coefficient (r^2) equal to 0.9998, thus assuring a good linearity. A good intra- and inter-day precision related to peak areas was observed, with RSD equal to 0.8 and 1.5%, respectively. The lowest concentrations with clearly distinguishable signals from the spectral background fell within the range 0.4-0.8 mM for target cannabinoids, corresponding to LOD values of 2.3-5.7 μg/mL. The LOQ values were found to be in the range 7.7-18.9 μg/mL. As for accuracy, the percentage recovery values, obtained by comparing the results from samples and fortified samples, were found to be higher than 80% for both methods and they can be considered satisfactory.

4. Conclusions

In the present study, two different analytical methods, including both chromatographic and spectroscopic ones, were applied to the quali- and quantitative analysis of cannabinoids in cannabis inflorescences. ^{13}C-qNMR was successfully applied to quantitative analysis of main cannabinoids in different cannabis varieties, including fibre-type, recreational and medical ones, providing consistent results with those obtained by means of the HPLC method, thus highlighting its potential in this field of application, in particular for chemotype discrimination. Overall, it is possible to conclude that NMR spectroscopy represents a promising tool for a

reliable determination of cannabinoids in the plant material and its derived products. Even if this latter technique is not conventional and much diffused in laboratory practice as HPLC, nowadays there is an increasing interest in the application of qNMR, due to its peculiar advantages over chromatographic methods. Indeed, qNMR enables the simultaneous identification and quantification of many analytes, also chemically very different, in complex mixtures with a much lower solvent usage compared with HPLC, which is also a benefit from a sustainable perspective.

EVALUATION OF THE ANTIPROLIFERATIVE ACTIVITY OF NON-PSYCHOACTIVE *C. SATIVA* L. EXTRACTS ON HUMAN CANCER CELL LINES

The experimental work reported in this section has been published as part of the original research article in *Phytotherapy Research*: L., Anceschi, A., Codeluppi, V., Brighenti, R., Tassinari, V., Taglioli, L., Marchetti, L., Roncati, A., Alessandrini, L., Corsi, F., Pellati, (2021) "Chemical characterization of non-psychoactive *Cannabis sativa* L. extracts: *in vitro* antiproliferative activity and induction of apoptosis in chronic myelogenous leukemia cancer cells". Since the candidate's contribution to this paper did not fulfil all the requirements for its inclusion in the thesis as a stand-alone section, only data collected and analysed by the candidate have been reported above.

1. INTRODUCTION

Cancer is a multifactorial disease encompassing a combination of factors, such as genetic susceptibility, exposure to carcinogens, random gene mutations and chronic inflammation. Recently in two Prospective Urban and Rural Epidemiologic (PURE) studies it has been reported that, whereas the first cause of death in the world is still due to cardiovascular disease, in high-income countries (HIC), such as some western countries, cancer is the leading cause of death [48]. If the trend reported in the study is confirmed, cancer could be the first cause of death throughout the world in a couple of decades. These data are of a great importance, and they deserve a very close consideration in both medicinal chemistry and pharmacology ambits. Indeed, it seems paradoxical that in the HIC, where the anticancer treatments are both available and outstanding, the situation is so dramatic. Due to the intrinsic cancer molecular features, the cure of the disease is still far from being achieved, although the great progress in the research and the latest anticancer-drug discoveries. So, it becomes fundamental to investigate every possible new path leading to an improvement in current care. In this context, many reports have been focused on the antiproliferative potential of cannabinoids, showing a promising ability of these compounds to inhibit the progression of various cancer lines [49]. In recent years a conspicuous number of preclinical research have described the activity of cannabinoids as possible anticancer agents [27,50], acting through several molecular mechanisms, such as induction of apoptosis, inhibition of angiogenesis and metastatic processes [51]. Cannabinoids have proven to increase the apoptotic response in leukaemia, supporting the overall concept that these compounds, and in particular CBD, can be valid therapeutic agents [52]. The activity of CBD appears to be mediated by the interaction with G protein-coupled receptor 55 (GPR55) and the transient receptor potential cation channel subfamily V member 1 (TRPV1) [53], but not with the classical cannabinoid receptors CB1 and CB2 [54,55]. CBD can also directly target mitochondria and perturbs calcium homeostasis in acute lymphoblastic leukaemia [56]. CBD is the main compound present in non-psychoactive or fiber-type *Cannabis sativa* L., commonly known as hemp, which differs from recreational and medicinal chemotypes for its cannabinoid profile [57,58]. Indeed, hemp is a rich source of non-psychoactive cannabinoids (CBDA and CBD), as opposed to recreational and medicinal *Cannabis* varieties, which are characterized by a remarkable high content of Δ^9-THC, together with its acidic precursor Δ^9-THCA, as well as cannabinolic acid (CBNA) and cannabinol (CBN), the last two being the oxidized products of Δ^9-THCA and Δ^9-THC, respectively [57–59]. Other cannabinoids can be also found in hemp, though in much lower content, including cannabigerolic acid (CBGA), cannabigerol (CBG), cannabichromenic acid (CBCA) and cannabichromene (CBC) [58,59].

Even if medical *Cannabis* and its psychoactive peculiar compound Δ^9-THC remain the main object of research work, scientific studies devoted to unravelling the biological potential of hemp and non-psychoactive cannabinoids have recently increased in number [60–63]. As the exploration of natural therapeutics continues to expand, non-psychoactive cannabinoids represent a powerful source for complementary therapeutics of cancer diseases [64]. As a result of their antiproliferative properties, in the appropriate context they could be also applied as standalone cancer treatments. In this ambit, the aim of this work was to evaluate the antiproliferative activity of standardized extracts obtained from hemp inflorescences belonging to different varieties against human cancer cells of different embryological origin. In this context, the importance of the use of a phytocomplex in therapy should be considered. Indeed, the presence of different compounds in plant extracts often allows a better management and control of possible side effects.

2. EXPERIMENTAL

2.1. Chemicals and solvents

Stock methanolic solutions (1.0 mg/mL) of Δ^9-tetrahydrocannabinol (Δ^9-THC), cannabidiol (CBD), cannabigerol (CBG) and cannabinol (CBN) and stock acetonitrile solutions (1.0 mg/mL) of Δ^9-tetrahydrocannabinolic acid (Δ^9-THCA), cannabidiolic acid (CBDA) and cannabigerolic acid (CBGA) were purchased from Cerilliant Corporation (Round Rock, TX, USA). Δ^9-THC, CBD, CBG and CBN stock solutions were stable for 3 months when stored at −20 °C, while Δ^9-THCA, CBDA and CBGA solutions were stored at −80 °C. Acetonitrile (ACN), absolute ethanol (EtOH), methanol (MeOH), formic acid (HCOOH), dimethyl sulfoxide (DMSO), 10000 UI penicillin - 10 mg/mL streptomycin association and cell counting kit-8 (CCK-8) were purchased from Sigma Aldrich s.r.l. (Milan, Italy). Water was purified by using a Milli-Q Plus185 system from Millipore (Milford, MA, USA). Dulbecco's Modified Eagle's Medium (DMEM) was purchased from PAN Biotech (Aidenbach, Germany). Roswell Park Memorial Institute (RPMI) media were from EuroClone s.p.a. (Milan, Italy). BioWhittaker fetal bovine serum (FBS) was acquired from Lonza Bioscience (Basel, Switzerland). L-Glutamine was from Invitrogen s.r.l. (San Giuliano Milanese, MI, Italy).

2.2. Hemp plant material

Hemp plant material was kindly provided by the research centre CREA-CIN (Rovigo, Italy). In particular, female inflorescences from three different hemp varieties (Carmagnola, Santhica and Bernabeo) were chosen as the starting material for the preparation of the extracts, given their

high content of non-psychoactive cannabinoids [33]. Three additional extracts, obtained from the same plant material previously submitted to a decarboxylation process, were also prepared in order to obtain the conversion of cannabinoic acids into their neutral counterparts. Extracts obtained from raw hemp inflorescences are referred in the text as R1 (Carmagnola), R2 (Santhica) and R3 (Bernabeo), while extracts obtained from decarboxylated hemp inflorescences as D1 (Carmagnola), D2 (Santhica) and D3 (Bernabeo).

2.3. Preparation of raw hemp extracts

For each hemp variety, 50 g of grounded hemp inflorescences were added with an initial aliquot of 300 mL EtOH and then submitted to dynamic maceration at room temperature for 15 min. The extract was then paper filtered, and the residue was extracted with the same procedure thrice with additional 200 mL of the extraction solvent. The extracts were combined and then brought to dryness under vacuum with a Heidolph Laborota 4000 WB rotary evaporator (Schwabach, Germany). Finally, the extract was placed in a desiccator under vacuum until it reached a constant weight. For R1, R2 and R3 the percentage yield was 7.3%, 5.6% and 6.7% respectively. Approximately 25 mg of the extract were dissolved in 25 mL of the extraction solvent and the solution was injected into the HPLC system after filtration through a 0.45 μm PTFE filter.

2.3.1. Preparation of decarboxylated hemp extracts

A weighed amount of grounded hemp inflorescences (15 g) was placed in an oven at a temperature of 110 °C for 15 min. The temperature was then raised to 120 °C and kept constant for 60 min. The decarboxylated inflorescences were then submitted to dynamic maceration with EtOH, following the same procedure as that described in the previous section. For D1, D2 and D3 the percentage yield was 3.0%, 2.8% and 3.1% respectively. A known amount of the extract (~ 25 mg) was dissolved in 25 mL of EtOH and then filtered through a 0.45 μm PTFE filter, prior the injection into the HPLC system.

2.4. HPLC-UV analysis of hemp extracts

The HPLC-UV analyses of the extracts were performed on an Agilent Technologies (Waldbronn, Germany) modular model 1260 Infinity II system, consisting of a quaternary pump, a manual injector, and a UV variable wavelength detector. Chromatograms were recorded by using an Agilent OpenLab ChemStation (Rev. C.01.10). An Ascentis Express C_{18} column (150 mm × 3.0 mm I.D., 2.7 μm, Supelco, Bellefonte, PA, USA) was used, with a

mobile phase composed of 0.1% HCOOH in both (A) H_2O and (B) ACN. The gradient elution was as follows: 0-13 min 60% B, 13-17 min from 60 to 80% B, 17-22 min from 80 to 90% B, which was kept for 8 min. The post-running time was 15 min. The flow rate was 0.4 mL/min. The sample injection volume was 3 μL. Chromatograms were acquired at 210 nm (for decarboxylated cannabinoids) and at 220 nm (for cannabinoic acids). Calibration curves for target compounds were constructed at five calibration levels by plotting the peak areas of the analytes *vs*. their concentration. Two injections were performed for each sample.

2.5. Preparation of the solutions used in the biological assays

Stock solutions of fibre-type hemp extracts and CBD were prepared by dissolving a known amount of the extract/compound (3 and 100 mg, respectively) in 0.1-1.0 mL of DMSO. The working solutions were obtained by the dilution of the stock solution in the culture medium to reach the desired concentration. The content of DMSO in the working solutions was below 0.5%.

2.6. Cell cultures

Human colorectal adenocarcinoma (HT29) cell line was grown in DMEM medium with high glucose without sodium pyruvate supplemented with 10% FBS, 2 mM L-glutamine, 100 U/mL penicillin and 100 μg/mL streptomycin. Human glioblastoma (U87MG) cell line was grown in DMEM medium with high glucose and with sodium pyruvate supplemented with 10% FBS, 2 mM L-glutamine, 100 U/mL penicillin and 100 μg/mL streptomycin. Human chronic myelogenous leukaemia (K562) cell line was grown in RPMI medium supplemented with 10% FBS, 2 mM L-glutamine, 100 U/mL penicillin and 100 μg/mL streptomycin. All the cell lines were obtained from the American Type Culture Collection (ATCC, Teddington, UK). The cells were cultured in a humidified incubator at 37 °C with 95% humidity and 5% CO_2. All cell lines were used between the 10^{th} and 30^{th} passage.

2.7. Cell viability measurement

Cell viability was assessed after 24, 48 and 72 h of continuous exposure with the different compounds described above. Cell viability of K562, U87MG and HT29 were evaluated by means of the Cell Counting Kit-8 (CCK-8), (Dojindo Laboratories, Kumamoto, Japan). Briefly, the cells were plated on 96-well plates (Euroclone, Milan, Italy) at concentration of 5000 or 10000 cells/cm^2. After exposure to desired concentrations of the different compounds, 10 μl of

CCK-solution was added to each well and incubated for a period of 2 h at 37 °C. The absorption was measured at 450 nm using a multiplate reader multiscan FC (Thermo Scientific, USA). Cell viability was expressed as a percentage of that of the untreated cells referred as control.

2.8. Statistical analysis

Data shown in graphs represent the mean of the three independent experiments, standard deviations (SD) are indicated by error bars. Differences between the treated and control cells were analysed using the GraphPad Prism 8.0 software (GraphPad Software, Inc., San Diego, CA, USA). Statistical comparison was performed by applying one-way analysis of variance (ANOVA) and Dunnett's multiple-comparison test to evaluate difference within control and treatments. Student's *t* test or one-way ANOVA followed by Tukey's Post Hoc test were performed to compare the effects of different treatment groups. Differences were considered statistically significant at $P < 0.05$.

3. RESULTS AND DISCUSSION

3.1. Chemical composition of hemp extracts

The quali-quantitative analysis of *C. sativa* extracts was performed by HPLC-UV. This method has been widely applied and previously validated [33,44,65]. As for extraction, polar solvents, such as EtOH, under dynamic maceration at room temperature have been found to provide the highest extraction efficiency for both cannabinoic acids and decarboxylated cannabinoids [33] therefore, this procedure was applied in this study. Figure 1 shows representative HPLC-UV/DAD overlapped chromatograms of R1 (blue) and D1 (red) extracts at 220 nm. The raw extract R1 was rich in CBDA; the chromatogram also shows minor peaks belonging to CBGA and Δ^9-THCA. As regards the decarboxylated extract D1, the HPLC-UV analysis revealed that the decarboxylation process had successfully occurred.

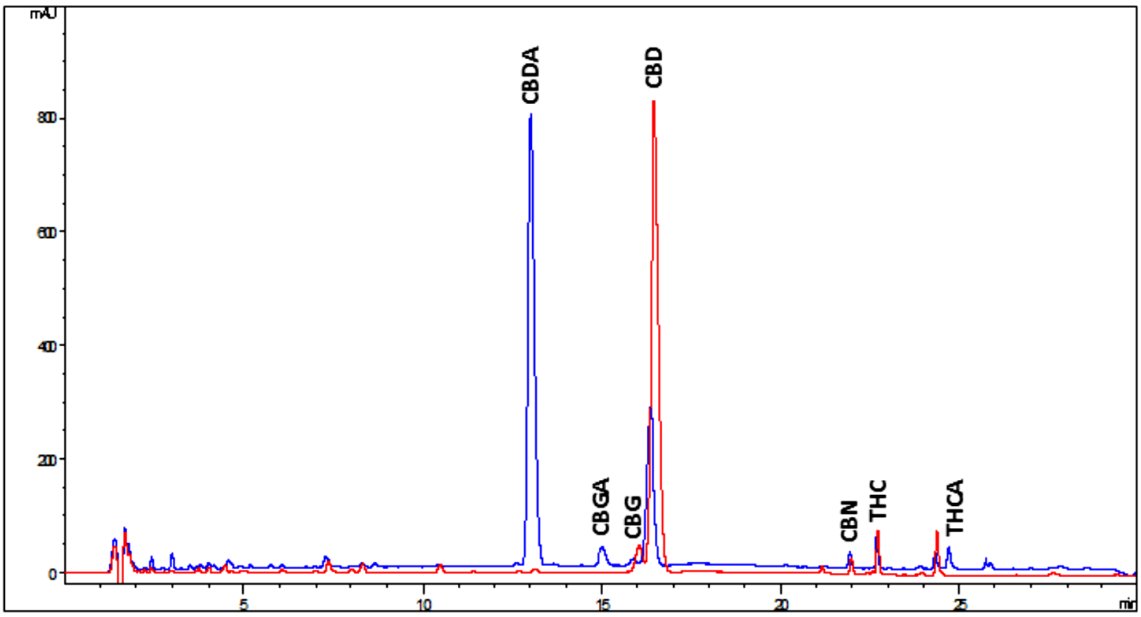

Figure 1. Representative HPLC-UV/DAD overlapped chromatograms of R1 (blue) and D1 (red) extracts at 220 nm. The main neutral and acid cannabinoids are shown, identified on the basis of their retention time.

Table 1 shows the quantitative results obtained from the HPLC-UV analysis of cannabinoids both in the raw (R1-R3) and in decarboxylated (D1-D3) hemp extracts. The quantification of the main cannabinoids in the extracts was achieved by an external calibration with pure analytical standards ($r^2 > 0.998$). The amounts of cannabinoids determined in the extracts from the decarboxylated plant material of the Carmagnola variety (D1) agrees with what has been previously described in the literature [62]. In sample D1, CBD reached up to 92% of total cannabinoids, while the percentage of CBG and Δ^9-THC was 4 and 1% respectively. In sample D2, CBD and CBG correspond to 70% and 27% of total cannabinoids, respectively. In D3, CBD and CBG represented 30 and 68% of total cannabinoids, respectively.

Table 1. Results of the HPLC-UV analysis of cannabinoids in raw (R1-R3) and decarboxylated hemp extracts (D1-D3). Data are expressed as mg/g ± SD.

Peak	Compound	t_R (min)	R1	R2	R3	D1	D2	D3
1	CBDA	11.6	306.4±0.4	86.1±0.4	8.3±0.8	<LOQ	<LOQ	<LOQ
2	CBGA	13.4	15.4±1.4	170.6±0.6	68.1±0.2	<LOQ	<LOQ	<LOQ
3	CBG	14.9	3.9±0.1	109.7±1.1	75.8±0.6	19.7±2.5	48.0±0.5	160.9±1.8
4	CBD	15.4	134.1±2.3	77.2±2.0	57.8±0.8	440.8±5.0	125.8±2.4	70.2±1.1
5	CBN	19.8	8.2±0.4	1.7±0.1	3.2±0.1	6.9±0.3	2.9±0.2	3.5±0.6
6	Δ^9-THC	21.6	<LOQ	<LOQ	<LOQ	5.3±0.1	<LOQ	<LOQ
7	Δ^9-THCA	23.6	11.5±1.5	<LOQ	<LOQ	<LOQ	<LOQ	<LOQ

LOD and LOQ values were in the range 0.4–1.2 and 1.4–3.8 µg/mL, respectively.

3.2. Antiproliferative activity of a CBD-rich hemp extract on human cancer cell lines

The potential ability of the CBD-rich extracts R1 and D1 to interfere with cell viability was assessed at 24 and 48 h on different human cancer cell lines, including the colon carcinoma (HT29), the glioblastoma (U87MG) and the myeloid chronic leukaemia (K562). The first screening was performed with R1 and D1, namely the CBD-type hemp varieties. This choice was based on the recent findings on the antiproliferative activity of CBD against cancer cells [66,67]. In general, the extract which undergone decarboxylation (D1) showed a more pronounced activity on the viability in all the considered cell lines (*P* values are reported in Figure 2). After 24 h of treatment, the R1 extract from raw CBD-type hemp inflorescences did not significantly alter cell viability in U87MG and K562, except for the highest concentration of 100 μg/mL ($P < 0.05$) (Figure 2C, 2E). In the case of HT29, R1 did not decrease the viability at any tested dose (Figure 2A). On the other hand, D1 wherein the CBDA conversion in CBD successfully took place, showed to be much more active in all the tested cell lines. As a matter of fact, D1 induced a significant inhibition of cell viability on K562 starting from the concentration of 20 μg/mL ($P < 0.001$), where 50 μg/mL was the most efficient dose ($P < 0.0001$). In the cases of U87MG and HT29, the cell viability was significantly affected only at the highest dose ($P < 0.0001$) and starting from 50 μg/mL ($P < 0.01$), respectively (Figure 2A, 2C). This effect was even more pronounced after 48 h of treatment for both the extracts in all the cell lines (Figure 2B, 2D, 2F). Interestingly, the non-adherent K562 cell line was the most sensitive to the treatment with R1 and D1 (Figure 2F). In particular, D1 was able to reduce the K562 cell viability by about 50% and 80% at 10 μg/mL and 20 μg/mL concentrations, respectively (Figure 2F). These preliminary findings led us to choose the chronic myelogenous leukaemia (K562) as a suitable model to further characterize the antiproliferative activity of hemp extracts with different phytochemical compositions.

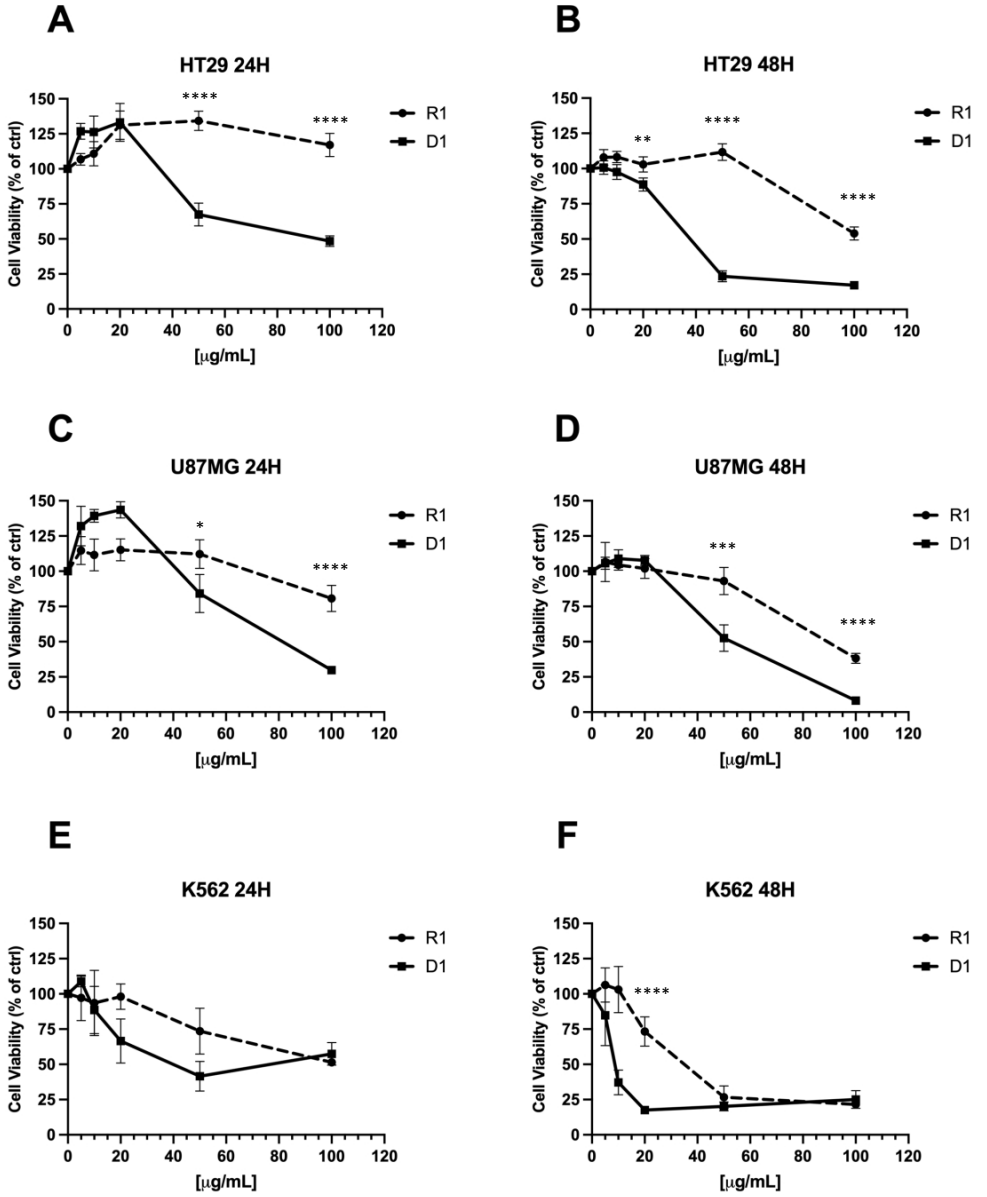

Figure 2. Dose-response curve viability of HT29 (A,B), U87MG (C,D) and K562 (E,F) cells treated for 24-48 h with raw (R1) and decarboxylated (D1) CBD-type hemp extracts (5-100 μg/mL). Data on graphs are shown as mean ± SD (n = 4 per group). A statistical comparison between R1 and D1 treatments was performed by *t*-Student test. Significance levels were defined as: * $P < 0.05$, ** $P < 0.01$, *** $P < 0.001$ and **** $P < 0.0001$.

3.3. Antiproliferative activity of different hemp extracts on K562 cells

Since D1 achieved the best results after 48 h treatment, also D2 and D3 were tested in the same conditions for their ability to modulate the K562 cell viability, having a different cannabinoid profile. As shown in Figure 3, D1 was the most effective in reducing cancer cell growth, with respect to D2 and D3. Indeed, the calculated IC_{50}s were 11.6, 40.9 and 66.7 μg/mL for D1, D2 and D3 respectively.

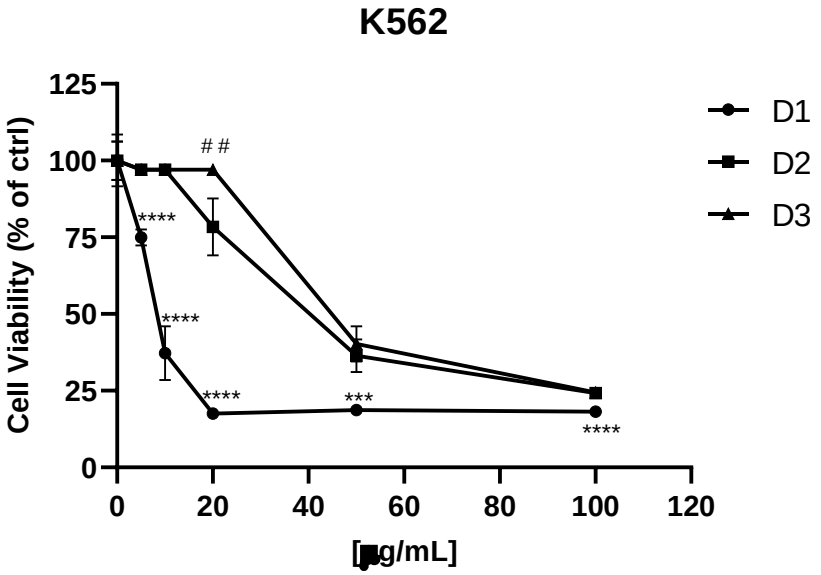

Figure 3. Dose-response curve viability of decarboxylated hemp extracts (D1, D2 and D3) at 5, 10, 20, 50, 100 μg/mL on K562 cells after 48 h treatment. Data on graphs are shown as mean ± SD (n = 4 per group). A comparison within D1, D2, and D3 treatments was performed by one-way ANOVA followed by Tukey's Post Hoc test. Statistical significance levels were defined as: *** $P < 0.001$ and **** $P < 0.0001$ D1 vs. D2 and D3; ## $P < 0.01$ D2 vs. D3.

To exclude an undesired cytotoxic effect on non-cancer cells, the activity of D1 was assessed on human peripheral blood mononuclear cells (PBMC). To be on the safe side, D1 was tested at far higher concentrations (50 and 100 μg/mL) than the IC_{50} previously found on K562 cells (11.6 μg/mL). As shown in Figure 4, D1 did not affect the PBMC viability of after 24-48 h treatment, indicating that D1 was well tolerated, and its activity do not interfere with viability of normal hematopoietic cells.

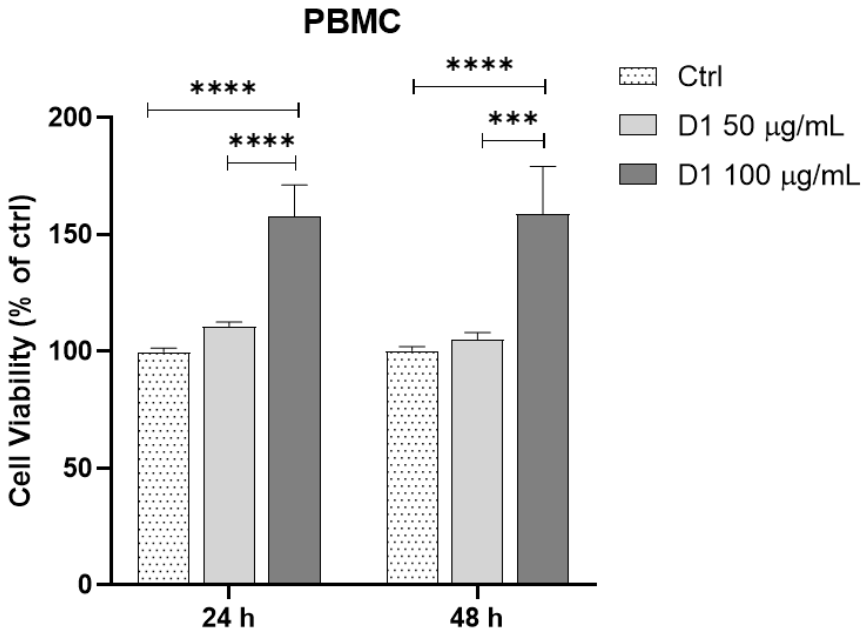

Figure 4. PBMC viability at 24-48h treatment with decarboxylated extract D1 (50 and 100 μg/mL). Data on graphs are shown as mean ± SD (n = 4). A comparison within the Ctrl and two different doses of D1, was performed by one-way ANOVA followed by Tukey's Post Hoc test. Statistical significance levels were defined as: *** $P < 0.001$ and **** $P < 0.0001$.

To clarify the contribution of CBD present in the crude extract, also the activity of the pure compound on K562 cells was assessed. Figure 5 shows the activity of D1 in comparison to that of CBD. The extract D1 was more effective in reducing K562 cells growth (IC_{50}: 11.6 μg/mL, corresponding to 16 μM CBD equivalents) whereas the calculated IC_{50} of CBD was 28 μM. This difference may be due to the complex chemical composition of the extract. Even if CBD is the main component to which the activity of the extract could be ascribed, other minor compounds can work in a synergistic way, enhancing the overall antiproliferative activity of D1.

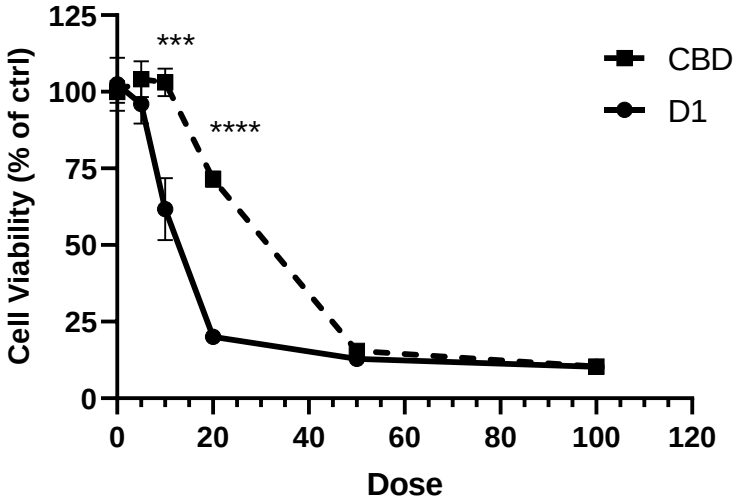

Figure 5. Effect of pure CBD on K562 cells after 48 h, compared with the extract D1. Dose is reported in μg/mL for D1 extract and in μM for CBD. Data on graphs are shown as mean ± SD (n = 4 per group). A comparison between CBD and D1 was performed by *t*-Student test. Statistical significance levels were defined as: *** $P < 0.001$ and **** $P < 0.0001$.

4. Conclusions

The present work was aimed at the characterization of the cannabinoid profile of different hemp varieties, and at the evaluation of their antiproliferative activity. Cancer cell lines of different embryological origin were used as *in vitro* models, among these the chronic myelogenous leukaemia cell line K562 was the most sensitive to the treatment. The decarboxylated extract D1, particularly rich in CBD, was able to reduce by half the viability of K562 cells at a concentration of 11 μg/mL after 48 h. Compared with pure CBD, the extract D1 elicited a higher antiproliferative activity, suggesting a synergistic effect, that may be due to the presence of other minor compounds in the extract. The positive interaction between *C. sativa* components has already been described in literature, thus the combination of cannabinoids appears to have the most potent anti-cancer effect compared to each compound on its own [52,68]. Interestingly, the D1 extract did not affect the viability of PBMCs, indicating a very low level of toxicity *in vitro* at the tested concentration. Definitely, additional research is needed to clarify the mechanisms underlying the biological activity and clinical trials are necessary to validate the here obtained results. In this direction, fundamental research will enable to in-depth understand the interrelationship between the various compounds present in *C. sativa*, the endocannabinoid system and cancer. In conclusion, the present work supports the use of CBD-rich extracts (and CBD) as candidates for eventual therapeutic use in myeloproliferative diseases, either alone or in association with other anticancer agents. This combination may allow for a reduced dosage of each agent required to produce a therapeutic effect, which has the potential to decrease adverse effects experienced by patients from cancer treatments.

CHAPTER 2

The present Chapter is overall focused on the evaluation of mulberry (*Morus alba* L.) leaf extract as source of phytochemicals in the context of new therapeutic approaches for diabetes mellitus. There is an urgent and unmet need for novel lead compounds for diabetes management and the prevention of its complications, which remain the major cause of the disease associated mortality [69]. Medicinal plants represent a rich source of molecules with therapeutic potential, that are of pivotal importance due to their cost-effectiveness and lower side effects, in comparison to reference drugs. Chemicals extracted from plants of the genus *Morus* are emerging as promising candidates in the prevention and treatment of various metabolic disorders, in particular for moderate hyperglycemia and dyslipidemia, which are typical early signs of diabetes [70–72]. The genus *Morus* includes several species, such as *Morus alba*, *M. nigra*, and *M. rubra* with wide distribution in the world. The main constituents are phenols, flavonoids, fatty acids and iminosugars that have shown effective hypoglycaemic, hypolipidemic, antioxidant effects. However, most of the published research on mulberry chemical composition and bioactivity has been carried out only on Asian cultivation. The first section of this Chapter deals with the determination of the main active constituent (1-deoxynojirimycin) in different Italian mulberry cultivars. The aim of the project was to assess the quality of the plant material in comparison to Far Eastern Asia cultivations, where mulberry leaves have been considered as a medicine for the treatment of diabetes for decades. This work represents the first quality reference for Italian mulberry, whereas a strong correlation of environmental factors and plant genetic constitution has been proven. The implications of the harvesting season and thermal treatment of leaf were also the object of the dissertation.

The second section of Chapter 2 focuses on the evaluation of the biological activity of twelve *M. alba* cultivars. In particular, the antiglycative, carbonyl-trapping and hypoglycaemic effects were evaluated on different *in vitro* models. An in-depth investigation of the contribution of different compounds present in the crude extract to the biological effect was performed, to understand the medicinal potentialities of mulberry-based products for the therapy of hyperglycaemia. This work was carried out in collaboration with Prof. Adele Papetti, P.I. of Food Chemistry Laboratory of the Department of Pharmaceutical Chemistry at the University of Pavia. These promising results have fostered us to design and develop an ideal delivery system for mulberry constituents with a view to improve the therapeutical results for the benefit of human health. The development of different strategies for delaying the release of mulberry active constituents and enhance the therapeutic effect will be discussed in the third section of Chapter 2.

DETERMINATION OF 1-DEOXYNOJIRIMYCIN (DNJ) IN LEAVES OF ITALIAN OR ITALY-ADAPTED CULTIVARS OF MULBERRY (*MORUS* SP.PL.) BY HPLC-MS

Plants **2021**, 10, 1553; doi: 10.3390/plants10081553

Lucia Marchetti [1,2], Alessio Saviane [3], Antonella dalla Montà [3], Graziella Paglia [3], Federica Pellati [1], Stefania Benvenuti [1], Davide Bertelli [1,*] and Silvia Cappellozza [3]

[1] Department of Life Sciences, University of Modena and Reggio Emilia, Via G. Campi 103, 41125 Modena, Italy
[2] Doctorate School in Clinical and Experimental Medicine (CEM), University of Modena and Reggio Emilia, 41125 Modena, Italy
[3] Consiglio per la Ricerca in Agricoltura e l'Analisi dell'Economia Agraria (CREA)-Centro per la Ricerca Agricoltura e Ambiente, Laboratorio di Gelsibachicoltura, Via Eulero, 6a, 35143 Padua, Italy

1. INTRODUCTION

Some peculiar characteristics of the third millennium in the Old Continent can be summarized in a few words: increased life expectancy, ageing population, and wide media coverage of health-related topics. Consequently, Europe is a promising market for natural ingredients and companies are continuously launching new natural health products; on the other hand, European consumers are very sensitive to any advertising regarding complementary and alternative medicine. These trends are not expected to change soon so that demand for pharmaceuticals, supplements, and alternative medicine products are forecast to increase in the European market as well as the demand for nutraceuticals. These substances are capable of giving physiological benefits or providing protection against chronic diseases [73]. Among natural products extracted from plants and other sources, iminosugars are analogs of sugars in which an atom of nitrogen replaces the ring oxygen atom. This substitution results in the inhibition of glycosidases and glycosyltransferases, therefore preventing normal carbohydrate metabolism [74]. The compound 1-deoxynojirimycin (DNJ) is one of the most popular iminosugars and was first extracted from mulberry (*Morus* sp.pl.) roots in 1976 [75]. This active ingredient, along with others, interferes with sugar metabolism, and was found at surprisingly high concentrations in the mulberry leaf latex. Indeed, it is involved in the mechanism of defence against insects, as the mulberry leaves are highly toxic for most species of Lepidopterans others than *Bombyx mori* [76]. Even though active ingredients contained in the mulberry leaf are harmful to herbivorous insects, man learnt to use their therapeutic effect from ancient times [77,78]. Furthermore, from the end of the last century DNJ has been widely studied by scientists for its capacity to inhibit α-glucosidase and tumour cell metastasis, reducing postprandial blood glucose and fat accumulation, contrasting aging-related behaviours and HIV progression [79]. Due to its powerful and wide range of possible applications in therapeutics, various efforts have also been carried out to identify the highest-yielding mulberry varieties [71,80–82], the richest branch portions in DNJ leaf content [71,80,83], the optimal harvesting season [84], the influence of the cultivation area and its interaction with the mulberry varieties [84], in addition to the best leaf processing and extraction method [79,80,85]. Furthermore, as mulberry leaves are the only feed of the silkworm *B. Mori,* which is efficient at concentrating the active ingredient in its body tissues, researchers have also been investigating this insect as a precious bio-accumulator [79,86,87]. However, most current research on DNJ has been carried out in Far Eastern Asia (China, India, Korea, Thailand, and Japan), while few data are available on the content of DNJ in the mulberry cultivars (CVs) used in Europe. Therefore, in the current paper, we tried to fill this gap of knowledge with regard to

the European genetic material, by also taking already tested Japanese mulberry CVs, which were grown under European conditions, as a reference. Furthermore, since the correlation among the cultivation area, the genetic material, and the environmental conditions (season of harvesting) has already been proven [84], we repeated the test on different CVs in two subsequent years. The aim was to ascertain whether the difference in the DNJ level, although variable in absolute value along the years, would respect the same ranking, being affected by the plant genetic constitution more than environmental conditions. Another aspect we took into consideration was the treatment of the collected material (leaf) before extraction, which was freezing of fresh samples or drying. In fact, regarding this aspect information is not very exhaustive because it is generally accepted that DNJ is quite resistant to high temperatures [80,88]; but this topic has not been definitely tested. Different methods for the determination of DNJ are available in the literature, and other quantitative techniques are constantly being developed. Regardless, some issues must be considered from an analytical point of view. First, due to the high hydrophilicity and small molecular weight of this compound, the interaction with the stationary phase of conventional reversed phase columns is so weak that DNJ is not retained in the column. Moreover, since the molecule lacks a chromophore, direct UV detection is not suitable like for many other aminoglycosides. Some authors reported pre-column derivatization methods, which, however, involve sample manipulation and ultimately may result in the introduction of impurities or degradation products [88]. On the other hand, derivatization is unnecessary for an HPLC-evaporative light scattering detector (HPLC–ELSD) and HPLC-tandem mass spectrometry (HPLC–MS/MS). Kimura *et al*. successfully used an evaporative light scattering detector (ELSD), which is a universal detector, for relatively non-volatile analytes [89]. The main drawbacks are the poor sensitivity and the long time required to complete the analysis. Hydrophilic interaction chromatography (HILIC), coupled with mass spectrometry, has proven to be a promising technique for DNJ quantitation. In our opinion, this is the most convenient method since it showed the lowest LOD and LOQ and the shortest retention time.

2. EXPERIMENTAL

2.1. Chemicals and solvents

All solvents were analytical grade and purchased from Sigma-Aldrich (Milan, Italy). The reference standard of DNJ (purity ≥ 95.0%) was purchased from Sigma-Aldrich (Milan, Italy). Water was purified by using a Milli-Q Plus185 system from Millipore (Milford, MA, USA).

2.2. Plant material and extraction procedure

Morus sp.pl. (L.) leaves were harvested at different times, (end-May 2017, end-May 2018, and end-July 2018), and were provided by CREA, Research Centre for Agriculture and Environment, laboratory of sericulture (Padua, Italy). This experimental mulberry field preserves a germplasm bank of around 60 *Morus* CVs. The first screening was carried out by considering the more representative CVs of the collection (the varieties of different geographic origin and the same age and pruning type, which were therefore comparable in this study). Within this group, for the subsequent analyses, a more limited number of varieties was explored; these varieties are the most used for sericulture or fruit production in the country, and therefore easily exploitable for pharmaceutical uses too. To ensure the uniformity of the sampling, leaves were collected randomly from at least five different trees per cultivar. A representative sample of about 250 g was labelled in plastic bags and stored according to the chosen treatment method. The content of DNJ was determined in both frozen and dried leaves in order to evaluate the influence of the drying process on the active compound extractability and to assess the potential loss due to thermal degradation. *Morus* leaves were weighed as fresh samples; afterwards, a mild drying process was carried out in an oven at 50 °C until reaching constant weight; then the percentage of humidity was calculated per each sample. Samples were stored at -18 °C and protected from light by storage inside amber glass sealed containers. Then, to prepare the fresh samples, with the aim to prevent any oxidation or degradation process, a representative portion of frozen leaves was ground in an automatic mill with dry ice. Immediately after, two grams of powdered frozen leaves were extracted at room temperature with 20 mL of a water:ethanol (50:50) solution under magnetic stirring. The whole procedure required three consecutive extraction steps of 2 h each. The first extract was centrifuged (RCF 7200 g) for 5 min, the super-natant was collected, paper filtered, and the further two extractions were performed on the residue. The three extracts were combined, and the final volume was adjusted to 100 mL with the same hydroalcoholic solution; the extract was then stored at 4 °C in flasks covered with silver paper until analysis. The extraction procedure was repeated twice for each sample, and it was performed in the same way for dried samples too. Before injection in the UHPLC system, the extracts were filtered by using a 0.22 μm cellulose acetate filter (GVS, Bologna, Italy) into an HPLC vial and properly diluted with acetonitrile.

2.3. HPLC-ESI-MS analysis

The chromatographic method previously developed by Vichasilp *et al*. [90], was herein properly modified and optimized. A Thermo Scientific Dionex Ultimate 3000 UHPLC system equipped with an autosampler, a quaternary pump, and a thermostated column compartment controlled by Chromeleon 7.2 Software (Thermo Scientific, Waltham, MA, USA) was used. The UHPLC system was coupled with a high-resolution QExactive mass spectrometer (Thermo Scientific, Bremen, Germany). The mass spectrometer was calibrated before the analyses. Nitrogen (N2) (purity > 99.99%), obtained from a Zefiro zero 60 LC-MS nitrogen generator (CINEL, Vigonza, Italy), was employed both as the source gas and the collision gas. The capillary temperature was set at 270 °C and the following N2 flows (arbitrary units) were used: sheath gas 40, auxiliary gas 30, and sweep gas 3. The MS/MS parameters were optimized with standard DNJ under positive ion electrospray ionization. A Hydrophilic Interaction Liquid Chromatography column (Cortecs UPLC HILIC, 1.6 μm, 2.1 × 100 mm) was used (Waters, Milford, MA, USA). This kind of column provides strong retention of very polar molecules that are typically unretained under conventional reversed phase conditions. 1-Deoxynojirimycin was eluted with a binary gradient consisting of ammonium formate 20 mM in water (solvent A) and acetonitrile (solvent B). The gradient profile was as follows: 0–10 min, 10% A; 11–16 min, 50% A; 16–27 min, 10% A. The flow rate was adjusted to 0.3 mL/min, and the column temperature was maintained at 30 °C. 1-Deoxynojirimycin was detected by MS/MS with parallel reaction monitoring (PRM) for transition of the parent ion to the product ions. The concentration of DNJ in samples was obtained through the calibration curve built with the pure standard compound. The selected range was 0.31 to 40.9 mM, corresponding to 0.050–6.67 ppm.

2.4. Method validation

The method showed good linearity (r^2 > 0.9995) within the selected range of concentrations. The method was validated in terms of precision and accuracy. Precision was evaluated with the relative standard deviation determined from repeated extract injections and triplicate extractions. Method accuracy was evaluated by recoveries, which were carried out by spiking samples with three different concentrations of standard solutions. Spiking recovery (%) was calculated as: $[(C_2 - C_0)/C_1] \times 100$, where C_2 is the analyte concentration in the final solution after spiking with a known concentration of standard, C_0 is the original analyte concentration in the initial solution, and C1 is the added known concentration of standard. Intra-day precision

was determined by analyzing three replicates of spiked samples, and inter-day precision was determined by running the three replicates of spiked samples on three different days.

2.5. Statistical analysis

Statistical analysis was carried out by using Statistica 6.0 (StatSoft Italia, Vigonza, Italy) and SPSS 13.0 (SPSS Inc., IBM, Segrate, Italy), the significance was established at $P < 0.05$. One-way ANOVA or factorial ANOVA was carried out according to the experimental situation. Factorial ANOVA was used to examine the influence of independent variables (CVs, thermal treatment, harvesting year and their interactions) on the dependent variable DNJ. In addition, Post Hoc analysis based on Tukey's HSD test was performed to evaluate differences among means.

3. RESULTS AND DISCUSSION

The herein used analytical method employs hydrophilic interaction chromatography (HILIC). The hybrid quadrupole-orbitrap mass parameters were optimized under positive ion electrospray ionization. The compound 1-deoxynojirimycin was detected by MS/MS for transition of the parent ion to the product ions. In the reported experimental conditions, retention time of DNJ was 8.57 min, with minimal shifts between samples (Figure 1). The chromatogram of standard DNJ solution (6.67 ppm) is shown in Figure 2.

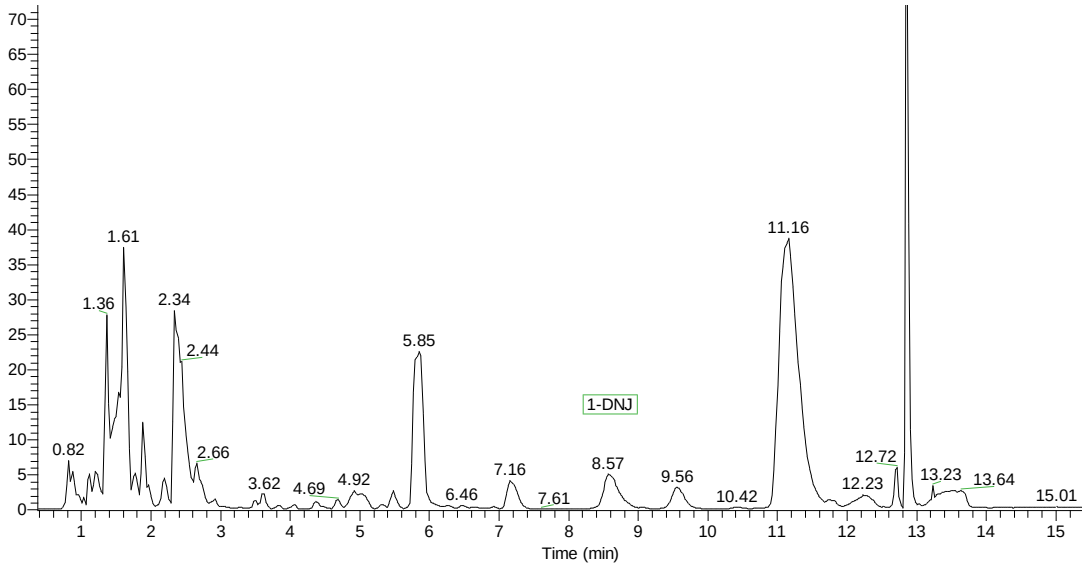

Figure 1. Typical base peak chromatogram of mulberry leaf hydroalcoholic extract.

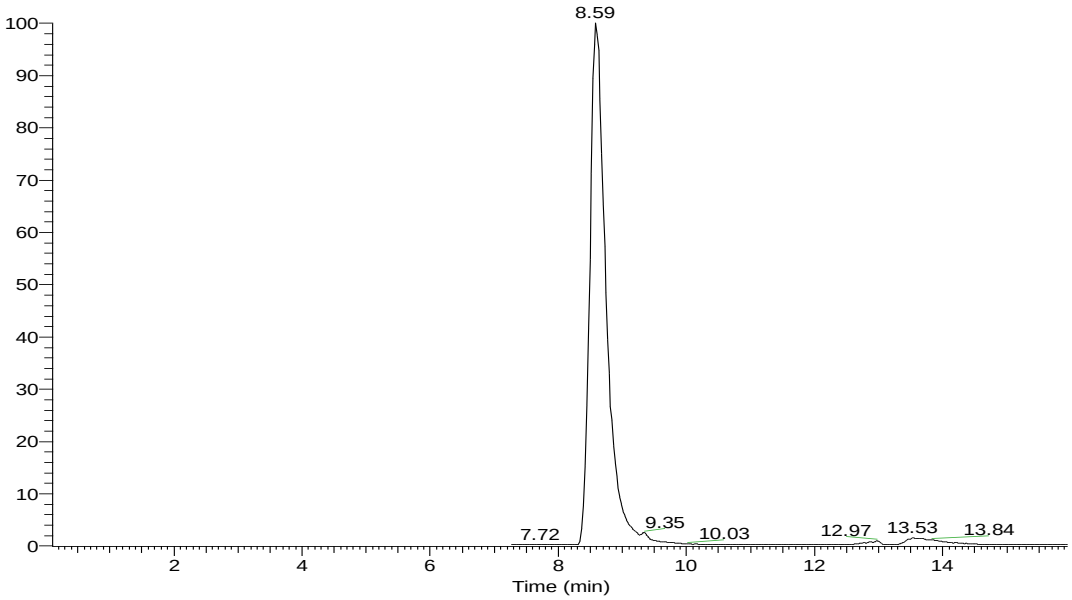

Figure 2. Base peak chromatogram of DNJ standard solution (6.67 ppm).

Figure 3 shows DNJ mass spectrum; an intense molecular ion $[M+H]^+$ *m*/*z* 164.0919 and other fragment ions generated by the consecutive loss of water molecules are present: *m*/*z* 60.0453 (8), 69.0343 (8), 80.0502 (8), 110.0604 (14) $[M+H-3H_2O]^+$, 128.0708 (11) $[M+H-2H_2O]^+$, 146.0812 (33) $[M+H-H_2O]^+$, 164.0919 (100). The integral of the product ion peak (*m*/*z* 146.0811) was used for the quantification. The residual precursor ion and other fragment peaks were used as qualifier ions.

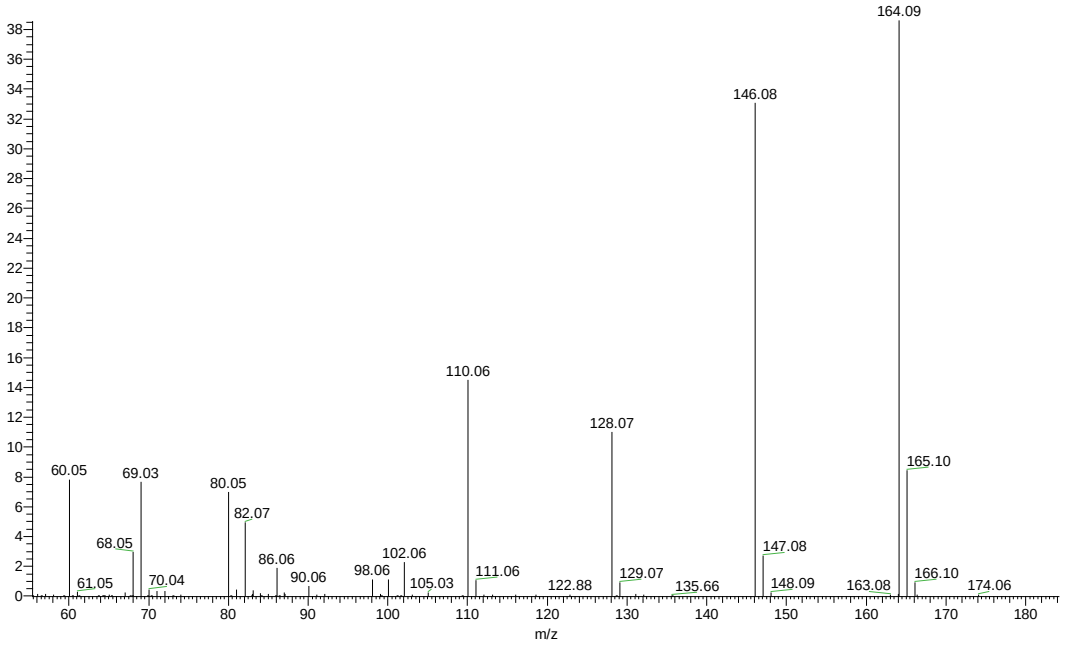

Figure 3. ESI-MS spectrum of DNJ (*m*/*z* 164.09) and its fragments.

Nakagawa *et al*. previously applied HILIC–MS/MS for the simultaneous determination of DNJ and its derivatives. In this case, the selective detection of DNJ was achieved by monitoring the transition *m*/*z* 164 to 69 $[M+H-95]^+$ [91], thus indicating that MRM was adaptable for the HILIC–MS/MS analysis of iminosugars in general. During recent decades, HILIC has proven to be an efficient strategy for the analysis of highly polar compounds, including sugars and peptides. Moreover, the presence of amino groups is prone to the elongation of retention time [92]. Under the herein optimized conditions, DNJ was clearly detected at an acceptable retention time. Data in Tables 1–3 are expressed as the overall mean of two sample replicates, each analyzed twice, ± SD. Data were obtained from the analysis of dried leaves and are expressed as DNJ mg/g dry weight (DW). The content of DNJ was determined in both fresh frozen and dried leaves to evaluate the influence of the drying process (50 °C) on the active compound extractability, and to assess the potential loss due to thermal degradation. Indeed, we tried to assess if the preservation of the mulberry leaf (freezing or drying) is influent on the extractable DNJ content. With this aim, a representative portion of frozen leaves was ground in an automatic mill and extracted with ethanol 50%. The same procedure was repeated on dried leaves. Therefore, data reported in Table 1 are shown in comparison with the DNJ content obtained from fresh leaves and then corrected by the value of humidity related to the specific cultivar. Table 1 shows the DNJ contents of 31 CVs from different *Morus* species, harvested at the end of May 2017. The purpose of the current research was to screen among the most spread varieties largely represented in Italy (country taken as an example of the Mediterranean area) and used for sericulture or fruit production, to enlarge the chance of exploiting the already existing mulberry fields for the pharmaceutical industry. The relative percentages of humidity ranged from 52.9 (Egyptienne, *M. alba* L.) to 74.4% (Nervosa, *M. alba* L.). Two-way ANOVA was carried out by taking into consideration two main factors (thermal treatment and CVs) and their interaction. The statistical analysis confirmed a significant difference in the DNJ content among the different CVs at $P < 0.05$, and a better DNJ yield in the fresh-frozen samples in comparison to the dried ones at $P < 0.05$. The average DNJ loss in dried samples was 12.8%. Only in two cases (Chirtut and Illinois) an increase in the iminosugar content was observed. This slight variation in the DNJ content might be attributable to random sampling or to an analytical error; however, it is worthy of noting that it occurred in the only two varieties belonging to species other than *M. alba*. Therefore, it might be due to a different leaf morphology (hairs, waxes, thickness) or physiology (enzymatic reactions). The interaction between the two factors (cultivar and thermal treatment) was also significant. The Post Hoc

Tukey's test following ANOVA analysis of the different CVs demonstrated that a great variation was present in the genetic material.

Table 1. DNJ content of 31 CVs from five *Morus* species. Data are expressed as mg/g DW ± SD. Content in dry samples is shown in comparison with fresh samples corrected by the relative humidity.

***Morus* CVs**	**End-May 2017**		
	Humidity (%)	**Fresh Samples (mg/g DW) [a]**	**Dry Samples (mg/g of DW) [a]**
Aobanezumi (*M. alba* L.)	69.4	0.55±0.02 ^{m,n}	0.44±0.06 ^{z}
Cattaneo female (*M. alba* L.)	66.3	0.66±0.02 ^{m,n}	0.59±0.03 ^{z,v}
Cattaneo male (*M. alba* L.)	70.5	1.87±0.02 ^{g,h,i}	1.50±0.03 ^{o,p,q}
Egyptienne (*M. alba* L.)	52.9	1.78±0.04 ^{g,h,i}	1.66±0.08 ^{o,n}
Florio (*M. alba* L.)	70.7	0.74±0.02 ^{n,m}	0.55±0.02 ^{v,z}
Giazzola (*M. alba* L.)	67.7	1.33±0.05 ^{i,l}	1.20±0.05 ^{s,t}
Kayriounezumigaeshi (*M. alba* L.)	68.1	1.99±0.04 ^{g,h}	1.86±0.08 ^{l,m}
Limoncina (*M. alba* L.)	64.2	1.01±0.02 ^{l,m}	0.93±0.05 ^{u}
Morettiana (*M. alba* L.)	72.5	1.36±0.02 ^{i,l}	1.26±0.04 ^{r,s}
Nervosa (*M. alba* L.)	74.4	1.70±0.04 ^{h,i}	1.62±0.06 ^{n,o,p}
Pendula (*M. alba* L.)	72.6	1.49±0.05 ^{h,i,l}	1.43±0.04 ^{q,r}
Pyramidalis (*M. alba* L.)	70.2	2.19±0.06 ^{g}	2.07±0.08 ^{i}
Spain Black fruit (*M. alba* L.)	70.3	1.81±0.02 ^{g,h,i}	1.76±0.07 ^{m,n}
Ukraina (*M. alba* L.)	70.5	2.99±0.03 ^{f}	2.94±0.06 ^{f}
Filippine (*M. alba* L.)	65.9	2.26±0.11 ^{n}	2.22±0.11 ^{h}
Kokosou 21 (*M. alba* L.)	70.4	3.17±0.10 ^{f}	2.50±0.04 ^{g}
Restelli (*M. alba* L.)	72.3	4.56±0.11 ^{d}	3.45±0.05 ^{e}
Gorgeous (*M. alba* L.)	70.6	5.65±0.01 ^{c}	4.24±0.01 ^{d}
Queensland black (*M. alba* L.)	64.4	3.56±0.11 ^{f,e}	2.96±0.02 ^{f}
Romana lhou (*M. alba* L.)	70.7	8.55±0.05 ^{b}	6.86±0.22 ^{b}
Wildtype (*M. nigra* L.)	71.9	5.99±0.02 ^{c}	4.46±0.04 ^{c}
Chirtut (*M. nigra* L.)	55.2	0.56±0.06 ^{m,n}	0.66±0.03 ^{v}
Date-Akagi (*M. alba* L.)	68.7	1.61±0.09 ^{h,i}	1.45±0.21 ^{p,q}
Akagi (*M. alba* L.)	61.2	1.57±0.10 ^{h,i}	1.22±0.03 ^{s}
Illinois everbearing (*M. rubra* L.)	59.8	1.74±0.03 ^{g,h,i}	1.96±0.02 ^{i,l}
Muki (*M. alba* L.)	69.5	5.66±0.04^{c}	4.49±0.03 ^{c}
Korin (*M. alba* L.)	72.2	9.55±0.04 ^{a}	7.07±0.14 ^{a}
Miura (*M. alba* L.)	70.7	4.98±0.10 ^{d}	4.32±0.03 $^{c.d}$
Platanoide (*M. alba* L.)	69.0	3.14±0.11 ^{f}	2.57±0.02 ^{g}
Sinuense *(M. alba* L.)	67.5	1.44±0.09 ^{h,i,l}	1.04±0.01 ^{u,t}
Nagazaki (*M. alba* L.)	70.2	3.75±0.11 ^{e}	2.94±0.02 ^{f}

[a] Means followed by distinct letters in the same column statistically differ according to Tukey's Post Hoc test ($P < 0.05$). Homogeneous subsets are indicated by the same letter. Two-way factorial ANOVA: Cultivar $F_{30, 186} = 1392$, $P < 0.05$. Treatment $F_{1, 186} = 597$, $P < 0.05$. Cultivar*Treatment $F_{30, 186} = 34$, $P < 0.05$.

Table 1 reports CVs and their species; the genus *Morus* shows a very complex and uncertain taxonomy because of its broad geographical distribution, long domestication history, morphological plasticity, and documented inter-species hybridization [93]; according to Nepal and Ferguson [94] it comprises 10–13 species, but Zeng *et al*., recently identified eight species only: *M. alba*, *M. nigra*, *M. notabilis*, *M. serrata*, *M. celtidifolia*, *M. insignis*, *M. rubra*, and *M. mesozygia*, based on the technique of internal transcribed spacer-based phylogeny [95]. Therefore, according to this classification, CVs reported in Table 1 all belong to *M. alba*, except for Hicks fancy (*M. rubra*) for the sample of *M. nigra* wild accession, which does not belong to any selected cultivar, and for the *M. nigra* cultivar Chirtut. It is quite clear that the variation in the DNJ content is as broad among CVs belonging to the same species as it is among different species. Since the drying procedure was undertaken at 50 °C, far below the degradation limit temperature, the hypothetical heat-due deterioration of the compound determined in dried leaves seems unlikely. The explanation for the phenomenon is likely simple: in fact, we should take into account the worsening of the compound extractability according to the reduction of the water content, a condition that occurs with the loss of moisture during desiccation [96]. However, it should also be considered that low temperatures (below 50 °C) allow time for enzymatic conversions and respiratory losses, whereas high temperatures (above 80 °C) can cause thermochemical degradation [97]. Therefore, it is worth exploring the difference between short thermal treatments at higher temperatures and longer thermal treatments at lower temperatures to analyze how the duration of the desiccation process affects the DNJ stability in the leaf, especially in the first drying phase, when the water content is still considerable. Furthermore, an interaction between the two factors (thermal treatment and CVs) was demonstrated ($P < 0.05$). This interaction was found to be particularly significant for Restelli (*M. alba* L.), Gorgeous (*M. alba* L.), Romana lhou (*M. alba* L.) Wildtype (*M. nigra* L.), and Korin (*M. alba* L.). In these cases, the DNJ decrease in dry leaves was remarkable. The morphology of the leaf surface, the wax content, the thickness of the leaf blade and leaf hairs can otherwise affect the drying process, determining different efficiencies in the preservation of the compound. Hu *et al*. previously investigated the content of DNJ in mature leaves from 132 *Morus* CVs belonging to nine Chinese species; among them, *M. alba* was the most represented. The mean content found by the authors ranged from 0.13 to 1.47 mg/g DW [98]; these data are slightly lower with respect to the results herein discovered, in which the concentration of DNJ ranged from 0.44 mg/g (Aobanezumi) to 7.07 mg/g (Korin). In addition, comparing the values for Kayriounezumigaeshi and Aobanezumi, recovered under our conditions with the ones shown by Kimura *et al*. [80], we can observe a higher DNJ level for

Kayriounezumigaeshi, but a lower level for Aobanezumi, in May harvests of both years. This fact highlights that the cultivar adaptation to different climatic situations can greatly affect the DNJ content in leaf samples. Table 2 reports the DNJ content found in 14 *M. alba* CVs, relative to the two harvests of 2018. The mean humidity percentages recovered were 66.2±5.8 and 64.9±6.4 in May 2018 and July 2018, respectively. The slight diminution in water in the leaf is a marker of the advancement of leaf maturation; young leaves are richer in water, but their content in nutrients is still low. Pendula was the richest in DNJ both at the end-May and the end-July 2018 harvests. As is well known and extensively outlined in the literature, weather conditions and harvest time play a key role in the abundance of active substances in *Morus* sp. pl. [98,99]. Typically, iminosugar levels start increasing in April, and then the concentration gradually decreases until September, with the maximum around June and July [99]. This study was a first test aimed at investigating the seasonal fluctuation of the DNJ content in leaves even in the Mediterranean area and on local (Italian) varieties, which were compared to Japanese varieties, already considered by other authors.

Table 2. DNJ content of 14 *M. alba* cultivars harvested in 2018. Data are expressed as mg/g DW ± SD.

M. alba CVs	End-May 2018		End-July 2018	
	Humidity (%)	Dry Samples (mg/g DW) [a]	Humidity (%)	Dry Samples (mg/g DW) [a]
Aobanezumi	67.0	0.38±0.02 [l]	65.3	0.77±0.02 [h,i]
Cattaneo female	65.2	0.84±0.02 [b]	64.0	3.88±0.05 [c]
Cattaneo male	69.4	0.74±0.03 [c]	69.0	2.60±0.03 [f]
Egyptienne	62.2	0.42±0.02 [l]	59.2	0.74±0.02 [h,i]
Florio	52.0	0.36±0.01 [l]	50.3	0.88±0.02 [h]
Giazzola	68.2	0.53±0.02 [i]	-	-
Kayriounezumigaeshi	66.1	0.97±0.03 [a]	65.3	3.48±0.05 [d]
Limoncina	59.2	0.42±0.02 [l]	58.8	0.44±0.02 [l]
Morettiana	74.1	0.74±0.04 [c]	73.3	2.75±0.09 [e]
Nervosa	66.0	0.92±0.03 [a]	65.2	5.01±0.08 [b]
Pendula	70.2	0.99±0.05 [a]	68.9	5.48±0.10 [a]
Pyramidalis	69.3	0.63±0.05 [d]	68.4	2.20±0.05 [g]
Spain Black Fruit	74.4	0.97±0.03 [a]	74.0	2.13±0.05 [g]
Ukraina	63.8	0.53±0.02 [i]	62.1	0.65±0.02 [i]

[a] Mean values followed by distinct letters in the same column statistically differ according to Tukey's Post Hoc test ($P < 0.05$). Two-way factorial ANOVA: Cultivar $F_{13, 123} = 2294$, $P < 0.05$. Season $F_{2, 123} = 6512$, $P < 0.05$. Cultivar*Season $F_{25, 123} = 1663$, $P < 0.05$.
The sample Giazzola relative to the end-July 2018 harvest is missing due to the inability to collect leaves.

This trend was also observed for data reported in Table 2. In fact, the mean content of DNJ was 0.68±0.23 mg/g and 2.39±1.69 mg/g in the end-May 2018 and the end-July 2018 harvest, respectively. Hence, the mean DNJ content increased more than threefold, starting from May to July. The two-way ANOVA performed considering simultaneously all the CVs and the two seasons assessed the significance of differences between the two seasons and among CVs ($P <$

0.05). The Post Hoc test identified various homogeneous subsets of CVs (same superscript letters in columns). Factorial ANOVA also highlighted a significant interaction ($P < 0.05$) between seasons and CVs. Different factors can contribute to this mulberry plants' response to the different seasons. First of all, the amount of the average monthly radiation, which, under the conditions of the North-Eastern part of Italy, increases from May to July; the total radiation received by the canopy of mulberry plants might have a direct effect on photosynthesis and, therefore, on the iminosugars synthesis. The same trend is recorded for the average daily temperature, which is also important for plant metabolism. Furthermore, DNJ synthesis by plants might be the defense reaction to the attack of insect populations (increasing their density with subsequent generations in summer), as this iminosugar shows remarkable biological activity against herbivorous predators, by inhibiting intestinal α-glucosidase [100]. Our findings are not conclusive: in fact, the difference in the DNJ-1 content in the leaves of the Italian CVs (Cattaneo female and male, Florio, Giazzola, Limoncina, Morettiana, Nervosa, Pendula, Pyramidalis, Spain Black Fruit) should have been tested in the two different seasons both in 2017 and 2018, while data are available for 2018 only. However, our one-year data collection agrees with those of other authors [80,101,102]. In addition, in the end-July 2018 harvest, Morettiana was selected and analyzed both in the form of apical leaves and branch mature leaves to study the distribution of the constituent in the different parts of the plant. The cultivar Morettiana was specifically chosen because this is one of the most representative and widespread Italian CVs. The DNJ content was equal to 7.34±0.42 in the younger leaves, while the amount in mature leaves was 2.75±0.09 mg/g DW (Figure 4).

Figure 4. DNJ content by leaf-maturity type in cultivar Morettiana.

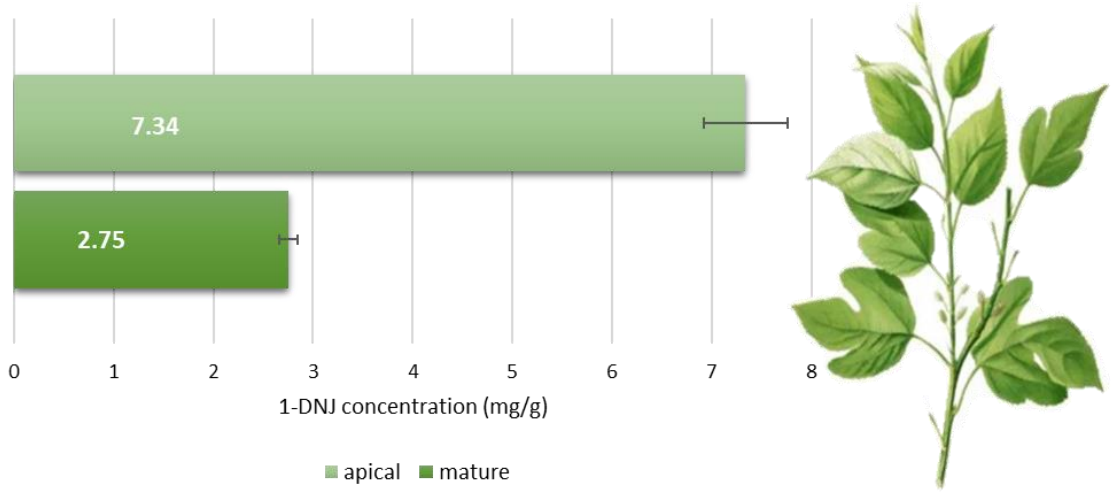

These data are consistent with those previously reported by Hu *et al*. [98], establishing that apical younger leaves usually contain higher DNJ than mature ones. This fact is strengthened by the major enzymatic activity discovered in young leaves that is responsible for the imination of glucose, the initial step in DNJ biosynthesis [82,103]. In Table 3, data from 2017 and 2018 spring harvests are shown in comparison. Two-way ANOVA showed a significant effect for the two main factors CVs ($P < 0.05$) and year ($P < 0.05$), and a significant interaction among factors, demonstrating the importance of annual variation in DNJ content which could be influenced by annual climatic fluctuations. In particular, the amount of DNJ recorded in the mulberry leaf samples at the end of May 2017 was almost double in comparison to the amount in those collected at the end of May 2018. The climatic conditions in the Padua province (North-Eastern Italy) where the experiment was carried out were very different in the two years; May 2018 was rainier (81.8 mm) than May 2017 (79 mm)[104].

Table 3. DNJ content of *M. alba* CVs in 2017 and 2018 samplings.

	End-May 2017		End-May 2018	
***M. alba* CVs**	**Humidity (%)**	**Dry Samples (mg/g DW) [a]**	**Humidity (%)**	**Dry Samples (mg/g DW) [a]**
Aobanezumi	69.4	0.44 ± 0.06 [i]	67.0	0.38 ± 0.02 [f]
Cattaneo Female	66.3	0.59 ± 0.03 [h]	65.2	0.84 ± 0.02 [b]
Cattaneo Male	70.5	1.50 ± 0.03 [e]	69.4	0.74 ± 0.03 [c]
Egyptienne	52.9	1.66 ± 0.08 [d]	62.2	0.42 ± 0.02 [f]
Florio	70.7	0.55 ± 0.02 [h,i]	52.0	0.36 ± 0.01 [f]
Giazzola	67.7	1.20 ± 0.05 [f]	68.2	0.53 ± 0.02 [e]
Kayriounezumigaeshi	68.1	1.86 ± 0.08 [c]	66.1	0.97 ± 0.03 [a]
Limoncina	64.2	0.93 ± 0.05 [g]	59.2	0.42 ± 0.02 [f]
Morettiana	72.5	1.26 ± 0.04 [f]	74.1	0.74 ± 0.04 [c]
Nervosa	74.4	1.62 ± 0.06 [d,e]	66.0	0.92 ± 0.03 [a]
Pendula	72.6	1.43 ± 0.04 [e]	70.2	0.99 ± 0.05 [a]
Pyramidalis	70.2	2.07 ± 0.08 [b]	69.3	0.63 ± 0.05 [d]
Spain Black Fruit	70.3	1.76 ± 0.07 [c,d]	74.4	0.97 ± 0.03 [a]
Ukraina	70.5	2.94 ± 0.06 [a]	63.8	0.53 ± 0.02 [e]

[a] Means followed by distinct letters in the same column statistically differ according to Tukey's Post Hoc test ($P < 0.05$). Two-way factorial ANOVA: Cultivar $F_{13, 84} = 593$, $P < 0.05$. Year $F_{1, 84} = 7615$, $P < 0.05$. Cultivar*Year $F_{13, 84} = 428$, $P < 0.05$.

Furthermore, as it is possible to observe in Table 4, the average daily accumulated energy (calculated at the ground level on the horizontal surface) was 5.16 kWh/m^2/day (18.57 MJ/m^2/day) in May 2018, while it was 5.70 kW /m^2/day (20.52 MJ/m^2/day) in May 2017 [104]. It can be assumed that higher solar radiation (recorded in 2017) produced increased photosynthetic activity and DNJ biosynthesis. In addition, due to the humid conditions and high average temperature (2018), fungal attacks spread on the mulberry plants, affecting the leaf surface, and by extension the photosynthetic capacity. The methodology used to produce these meteorology and solar radiation data are available online [105].

Table 4. Climatic conditions recorded in May 2017 and 2018 in Padua (Italy)

Year	Average radiation (kWh/ m^2/day)	Monthly total rainfall (mm)	Average temperature (°C)
2017	5.70	79 mm	18.6
2018	5.16	81.8 mm	19.4

The results of the recovery and precision studies are shown in Table 5. This method showed a good intra- and inter-day precision, with percentage relative standard deviation (%RSD) values between 2 and 8%. The recovery obtained from spiked samples was in the range 96-106%, in good agreement with international acceptance criteria [106].

Table 5. Precision and recovery percentage obtained with spiked samples.

DNJ	Intra-day *n* = 3						
(µg/mL)	1	2	3	Mean	SD	RSD (%)	Recovery (%)
0.06	0.056	0.058	0.064	0.059	0.004	7.02	98.89
0.60	0.630	0.550	0.570	0.583	0.042	7.14	97.22
6.00	5.980	6.720	6.400	6.367	0.371	5.83	106.11
	Inter-day *n* = 3						
	1	2	3	Mean	SD	RSD (%)	Recovery (%)
0.06	0.062	0.058	0.054	0.058	0.004	6.90	96.67
0.60	0.570	0.620	0.580	0.590	0.026	4.48	98.33
6.00	6.120	5.940	6.200	6.087	0.133	2.19	101.44

4. Conclusions

In conclusion, this work aimed at the quantification of the DNJ in leaves of different mulberry CVs grown in Italy, and at clarifying seasonal fluctuations with a view to determine a rational harvesting time. To the best of our knowledge, this is the first analytical determination of DNJ carried out on Italian crops. This study could be used as a reference to assess the quality of Italian plant material in comparison to cultivations carried out in Far Eastern Asia. Based on our data, we can conclude that the best harvesting time is in the middle of summer, and that apical young leaves are much richer in DNJ than the older located at the base of the shoot. However, with regard to the cultivar selection to maximize DNJ yield, agronomical tests in subsequent years and under different cultivation conditions are recommended. Indeed, the interactions with the weather conditions are determinant for the DNJ leaf content, which, in turn, depends on the physiological status of the tree and its photosynthetic capacity. Furthermore, the drying procedure should be optimized for industrial use before upscaling the crop for pharmaceutical exploitation to avoid the loss of important compounds as well as thermal inactivation during leaf desiccation.

IN VITRO BIOACTIVITY EVALUATION OF MULBERRY LEAF EXTRACTS AS POTENTIAL CANDIDATE FOR THE MANAGEMENT OF DIABETES MELLITUS

The present section of Chapter 2 includes the manuscript entitled "*In vitro* bioactivity evaluation of mulberry leaf extracts as potential candidate for the management of diabetes mellitus". This is an original research article that has been recently submitted to the journal *Food & Function*, and is currently under review.

1. INTRODUCTION

Diabetes mellitus (DM) is a complex metabolic disorder, causing around 5 million deaths per year, and accounting for 14.5% of all-cause mortality worldwide. According to the World Health Organization (WHO), over 460 million adults suffered from diabetes in 2019, and the incidence of this disease is rapidly increasing [107]. Even worse is the fact that DM prevalence has been dramatically rising in low- and middle-income countries where the weaknesses of health care systems are a serious problem [107]. Type 2 diabetes (T2DM or adult-onset) results from the body's insensitivity to insulin and it is the most prevalent disease in many modern societies, becoming a serious public health threat worldwide. Symptoms of type 1 and 2 diabetes may be similar but are often less marked in the second. For this reason, T2DM may be diagnosed many years after onset, when complications have already arisen. Hyperglycemia is the main effect of uncontrolled diabetes, and over time leads to serious damage to many of the body's systems, especially nerves and blood vessels. Indeed, the most common diabetic complications result from macrovascular and microvascular damage, endangering heart, brain, kidneys, peripheral nerves, feet, and eyes [108]. Long-term hyperglycemic state promotes the formation of covalent adducts between reducing sugars and proteins (albumin, fibrinogen, and collagen) through a non-enzymatic process known as glycation. Protein glycation and generation of advanced glycation end products (AGEs) play a crucial role in the initiation and progression of DM. AGEs are formed through a series of reactions involving highly reactive carbonyl intermediates (glyoxal and methylglyoxal) and Amadori products, which in turn promote the formation of additional AGEs at a faster rate than reducing sugars. AGEs cause damage to cells and tissues by cross-linking with proteins, lipids, and nucleic acids, and interacting with plasma membrane localized receptors for AGEs (RAGE) [109]. This interaction activates cellular inflammatory response pathways which ultimately lead to diabetic complications. Experimental studies have shown that the administration of compounds capable of interfering with AGEs (directly or indirectly) produces beneficial effects in various diabetic complications. The currently available therapy of T2DM involves the use of oral hypoglycaemic drugs [110]. Most of them are not well tolerated, and the most common side effects include liver disease, fluid retention and weight gain (thiazolidindiones, sulfonylureas), hypoglycaemia and headache (biguanides). Moreover, nausea, diarrhea, and bloating are typical side effects of biguanides, sulfonylureas and α-glucosidase inhibitors, due to the intestinal fermentation of undigested polysaccharides. Living with T2DM is an expensive condition for both patients and the healthcare system. Direct costs include medical supplies, hospital care and medications; indirect costs as well include absenteeism and reduced

productivity for the employed population. According to the American Diabetes Association, the total estimated cost of diagnosed diabetes in 2017 was $327 billion in the U.S. (American Diabetes Association, 2018). With these numbers, it is not surprising that the cost of this condition continues to be of great concern. There is an increasing need for new options to treat diabetes at its early stage, especially T2DM, due to an ineffective control of its long-term evolution in patients. For the same reasons, herbal remedies have been recently reassessed as a potential treatment owing to their safety, low cost, and effectiveness especially in the case of pre-diabetes or borderline diabetes. In this condition, blood sugar levels are higher than normal but not yet high enough to be diagnosed as DM. Today we are witnessing a global resurgence in interest and use of plant-based therapies and botanical health care products. This evidence in turn has stimulated a greater scientific awareness in exploring and better understanding the pharmacologically active constituents of botanical remedies. The diffused practice of phytotherapy can be explained considering that in rural areas traditional medicine still represents the primary source of health care, while in developed countries the growing interest in natural products is justified by scientific findings, which demonstrate that they are effective for the prevention of several diseases, and for the maintenance of the health condition. In recent years, great attention has been paid by the scientific community to the beneficial effects of phytochemicals on T2DM. Modern research revealed that plants belonging to the genus *Morus* contain phenols, flavonoids, iminosugars and alkaloids that have shown effective hypoglycemic, hypolipidemic, antioxidant, anti-aging, and neuroprotective effects [71,111,112]. Specifically, the bioactive compound 1-deoxynojirimycin (DNJ) was first isolated from mulberry roots in 1976, and it was found to interfere with the metabolism of sugars [75]. As a matter of fact, DNJ is a D-glucose analogue, in which an atom of nitrogen replaces the ring oxygen atom. This substitution results in the effective inhibition of glycosidases and glycosyltransferases, thus preventing normal carbohydrate metabolism. Indeed, α-amylases catalyze the hydrolysis of α-1,4-glucosidic linkages of amylose, and α-glucosidases the further digestion of terminal α-1,4-glucosidic linkages in the small intestinal brush border. Hence, the inhibition of these enzymes limits the rate of glucose release in the small intestine and allows to suppress postprandial hyperglycemia. Most of the current research on mulberry chemical composition and bioactivity has been carried out on Asian cultivation, while few data are available on plants grown in Europe. Indeed, mulberry leaves and fruits in the form of infusion are traditionally used in Far East Asian countries to control hyperglycemia and treat DM. In the current work we tried to fill this gap of knowledge, since a strong correlation among the chemical composition, the plant genetics and the environmental

conditions of the cultivation area has already been proven [113–115]. To achieve this result, twelve different Italian or Italy-adapted mulberry cultivars were selected, and the chemical composition was in-depth investigated by HPLC-MS. The antiglycative capacity at different levels of the protein glycation cascade and the hypoglycemic effect of leaf extracts were evaluated on different in vitro models. The objective was to clarify the existing relationship between different classes of compounds underlying the biological activity. Ultimately, these results may lay the basis for new knowledge and assist in the development of nutraceuticals for the management of T2DM early stage.

2. EXPERIMENTAL

2.1. Chemicals and solvents

Acetonitrile, ethanol, methanol, formic acid, and ammonium formate HPLC grade were purchased from Merck Life Science S.R.L., (Milan, Italy). Caffeic acid, protocatechuic acid, *p*-coumaric acid, quercetin, gallic acid, and kaempferol analytical standards (purity grade > 98%), DNJ reference standard (purity ≥ 95.0%), aluminium chloride, Folin-Ciocâlteu reagent, type I-A porcine pancreatic α-amylase saline suspension (EC 3.2.1.1), type I yeast α-glucosidase from *Saccharomyces cerevisiae* lyophilized powder (EC 3.2.1.20), *p*-nitrophenyl-alpha-d-glucopyranoside (*p*-NPG, purity grade > 99%), starch, acarbose (purity grade > 95%), sodium potassium tartrate tetrahydrate, dinitrosalicylic acid (DNS, purity grade 98%), nitrotetrazolium blue chloride (NBT), D-(+)-glucose (GLU, purity grade > 98%), bovine serum albumin (BSA, purity grade > 98%), glyoxal (GO, 40% aqueous solution), methylglyoxal (MGO, 40% aqueous solution), aminoguanidine hydrochloride (AG, purity grade > 98%), sodium dihydrogen phosphate monohydrate, disodium hydrogen phosphate monohydrate, sodium hydroxide, sodium carbonate, sodium chloride, sodium azide (purity grade 99.5%), 5-methylquinoxaline (5-MQ, purity grade > 98%), and *o*-phenyldiamine (OPD, purity grade > 99.5%) were purchased from Merck Life Science S.R.L., (Milan, Italy). Water was purified by using a Milli-Q Plus185 system from Millipore (Milford, MA, USA).

2.2. Plant material and extraction procedure Trap-MS^n analysis

Morus alba (L.) leaves from twelve varieties were provided by CREA – Research Centre for Agriculture and Environment, laboratory of sericulture (Padova, Italy). Leaves were collected from different trees per each cultivar to ensure the highest uniformity of the sampling. *Morus* leaves have undergone a mild drying process in oven at 50 °C, until reaching constant weight.

Leaves were minced and grinded, and samples were stored at -20 °C in amber glass bottles. The extraction procedure was performed by dynamic maceration under magnetic stirring. Two g of each sample were extracted with 100 mL 50% (v/v) ethyl alcohol at room temperature. The procedure required three consecutive extraction steps of 2 h each, the first and the second with 40 mL, and the last with 20 mL. The first extract was centrifuged (RCF 7200 g) for 5 min, supernatant was collected, paper filtered, and the further two extractions were performed on the residue. The supernatants obtained from all extractions were combined in a volumetric flask and diluted to 100 mL with 50% (v/v) hydroalcoholic solution. This procedure has been previously optimized and validated for the DNJ extraction from mulberry leaf to achieve the best yield [111]. The extraction was repeated twice for each sample. Ethanol was evaporated under vacuum at 50 °C, and the remaining aqueous suspension was freeze-dried (Heraeus Lyovac GT2, Leybold GmbH, Cologne, Germany) to obtain a stable solid product (FDE). Prior to HPLC analysis, FDEs were dissolved in 50% (v/v) ethanol (1 mg/mL), solutions were filtered by 0.22 μm cellulose acetate filter (GVS, Bologna, Italy), and properly diluted with acetonitrile before the injection. HPLC analyses were performed in triplicate.

2.3. HPLC-Ion Trap-MS^n analysis

For the identification of phytochemicals in mulberry leaf extracts, ion trap mass spectrometry was used. The chromatographic system consisted of a 6310 IonTrap (Agilent Technologies Inc., Waldbronn, Germany) equipped with an Agilent 1200 Series LC with binary pump, electrospray interface (ESI) and the ion trap mass spectrometer. Data Analysis Ion Trap Control version 4.0 (Agilent Technologies, Inc.) was used for data acquisition and processing. The chromatography was performed on a Supelco Ascentis Express C18 (10 cm × 2.1 mm i.d., 2.7 mm), at a flow rate of 0.3 mL/min. The eluents were (A) 0.1% formic acid in water and (B) acetonitrile. Temperature was set at 25 °C and separation was achieved with the following gradient: 0-7.5 min, 5% isocratic B; 7.5–30 min, 65% isocratic B; 30–34.90 min, 95% isocratic B; 35 min 5% isocratic B. Five minutes of post time run were necessary for column equilibration, during which no MS data were recorded. The injection volume was 10 mL. The capillary voltage was set at 3500 V, the desolvating temperature was 350 °C. Nitrogen was used as a drying (flow rate 8 L/min) and nebulising gas (pressure 25 psi). The mass spectrometer operated in positive and negative full-scan mode in the scan range 50–800 Da.

2.4. Determination of DNJ by HPLC-ESI-TQ-MS analysis

For the quantification of DNJ, samples were analysed by an Agilent 6400 Series Triple Quadrupole. The LC system was equipped with a binary pump, an autosampler, an on-line degasser and a thermostated column compartment (Agilent, Waldbronn, Germany). MassHunter version B.05.00 (Agilent Technologies, Inc.) was used for data acquisition and processing. The detection was performed using the ESI source operating in positive mode. The capillary voltage was set at 3500 V. The drying gas temperature was 300 °C; nitrogen was used as a drying (flow rate 9 L/min) and nebulising gas (pressure 28 psi). A hydrophilic interaction liquid chromatography was performed on a HILIC Cortecs UPLC column (1.6 μm, 2.1 × 100 mm). 1-Deoxynojirimycin was eluted with a binary gradient consisting of 20 mM ammonium formate in water (A) and acetonitrile (B). The gradient profile was as follows: 0–10 min, 18% A; 11–16 min, 50% A; 16–27 min, 18% A. The flow rate was adjusted to 0.3 mL/min, and the column temperature was maintained at 25 °C. 1-Deoxynojirimycin was detected by multiple reaction monitoring (MRM) for transition of the parent ion (*m/z* 164.09) to the product ions (*m/z* 146.08, 128.07, 110.06). The quantification of DNJ in samples was obtained by external standard method; the calibration curve was built analysing six concentrations of the reference compound in the range 0.005–0.5 mg/mL. Within this interval, a linear relationship was observed, providing a linear regression coefficient (r^2) of 0.9941.

2.5. Determination of total polyphenols and total flavonoids content

The total phenolic content (TPC) was determined using the colorimetric assay based on Folin-Ciocâlteu reagent (FCR), previously reported by Ainsworth and Gillespie (2007) [116]. Briefly, 100 μL FDEs water solution (5 mg/mL) were incubated with 2.5 mL FCR, then 2 mL sodium carbonate (Na_2CO_3) saturated solution were added. After 1 h of incubation at room temperature, absorbance was read at 765 nm (UVmini-1240, Shimadzu Europe, Milano, Italy). A sample of only extract and water was used as blank. The TPC was determined from the equation of the regression curve of gallic acid (y = 0.0009x – 0.0294; r^2 = 0.9998) and expressed as mg of gallic acid equivalents for g of dry leaf (mg GAE/g DW). The total flavonoid content (TFC) was determined according to the aluminium chloride method [117]. Briefly, 100 mL of sample was mixed with 1.9 mL water and 2.0 mL $AlCl_3$ (2% w/v). The reaction mixture was incubated at 25 °C for 30 min, the absorbance was read at 420 nm. The results were extrapolated from the quercetin calibration curve (y = 1.3836x + 0.0091; r^2 = 0.9997) and expressed as mg of

quercetin equivalents per g of dry leaf (mg QE/g DW). The reported values are the means of three independent experiments.

2.6. Evaluation of hypoglycemic activity

The *M. alba* cultivars were tested to evaluate their inhibitory potential against α-amylase and α-glucosidase, the two main digestive enzymes involved in postprandial hyperglycaemia modulation. Freeze-dried extracts were dissolved in sodium phosphate buffer (PBS) at different concentrations (ranging from 0.1 to 20 mg/mL). Data were expressed as the means ± standard deviation (SD) of three independent experiments for each tested concentration.

2.6.1. α-Amylase inhibitory activity

The α-amylase inhibitory assay was performed following the method reported by Milella *et al.* with some modifications [118]. Briefly, 200 mL porcine pancreatic α-amylase (1.3 U/mL in 100 mM PBS, containing 6.7 mM sodium chloride, pH 6.8) were preincubated with 200 mL of each sample in test tubes at 37 °C for 10 min. Then, 200 mL of 0.4% starch (w/v boiled and suspended in 100 mM PBS, pH 6.8) were added. The mixture was incubated for 10 min at 37 °C. Finally, 600 mL DNS reagent (consisting of 20 mL 96 mM DNS, 8 mL 5.3 M sodium potassium tartrate tetrahydrate in 2 M NaOH and 12 mL distilled water) were added. After, the tubes were placed in a boiling water bath for 7 min to stop the reaction, then cooled and diluted 1:10 with distilled water. Absorbance was read at 540 nm (UVmini-1240, Shimadzu Europe, Milano, Italy). The absorbances of samples were also registered in absence of the enzyme solution (sample blank) to remove the background signals. Samples made of only starch and enzyme solution were used as negative control, while acarbose and DNJ as positive controls. The results are expressed as α-amylase inhibition percentage and were calculated by the following formula:

$$\text{Inhibition rate (\%)} = \left(1 - \frac{\text{Abs}_{sample} - \text{Abs}_{background}}{\text{Abs}_{\ negative\ control}}\right) \times 100$$

2.6.2. α-Glucosidase inhibitory activity

The α-glucosidase inhibitory assay was performed following the method reported by Spínola *et al.* with some modifications [119]. Briefly, 100 mL yeast α-glucosidase (0.35 U/mL in 100 mM PBS, pH 6.8) were preincubated with 50 mL of each sample in test tubes at 37 °C for 10 min.

Then, 100 mL *p*-NPG (1.5 mM) solution were added. The mixture was incubated for 20 min at 37 °C in the dark. Finally, 1 mL Na_2CO_3 solution (1 M) was added to the mixture to stop the reaction. Absorbance was read at 400 nm (UVmini-1240, Shimadzu Europe, Milano, Italy). The absorbances of samples were also registered in absence of the enzyme solution (sample blank) to remove the background signals. Samples made of only *p*-NPG and enzyme solution were used as negative control, while acarbose and pure DNJ as positive controls. The results are expressed as α-glucosidase inhibition percentage and were calculated by the following formula:

$$\text{Inhibition rate (\%)} = \left(1 - \frac{\text{Abs}_{sample} - \text{Abs}_{background}}{\text{Abs}_{\ negative\ control}}\right) \times 100$$

2.7. Inhibition of Amadori products (fructosamine) formation assay

The nitroblue tetrazolium (NBT) reductive assay was used to measure the Amadori products [120,121]. An aliquot of 0.5 mL of glycated material, consisting of BSA and GLU incubated in presence or absence of samples for 14 days, was mixed with 2.0 mL NBT reagent (0.3 mM) in sodium carbonate buffer (0.1 M, pH 10.35). The mixture was incubated at room temperature for 20 min. Fructosamine present in the systems reduced NBT to tetrazinolyl radical forming monoformazano (MF^+), a coloured compound that can be measured spectrophotometrically (Spectrophotometer Perkin Elmer Lamda25). The capacity of samples to inhibit fructosamine formation was evaluated by measuring monoformazano (530 nm) as follows:

$$\text{Inhibition rate (\%)} = \left(1 - \frac{\text{Abs}_{\ glycated\ system\ (BSA,GLU,inhibitor)} - \text{Abs}_{\ background\ (BSA,inhibitor)}}{Abs_{\ glycated\ system\ (BSA,GLU)} - \text{Abs}_{\ background\ (BSA)}}\right) \times 100$$

The reported values are the means of three independent experiments, each performed in duplicate.

2.8. Evaluation of antiglycative capacity

The antiglycative properties of *M. alba* extracts were evaluated by the bovine serum albumin (BSA) – methylglyoxal (MGO) assay, as previously described by Mesìas *et al*. [122,123] Freeze-dried extracts (1, 2.5, and 5 mg dry matter /mL reaction mixture) were dissolved in distilled water, while BSA (35 mg/mL) and MGO (0.4 mg/mL) were dissolved in phosphate buffer (PBS, 0.1 M, pH 7.4) containing 0.02% (w/v) of sodium azide (to ensure aseptic conditions). The final reaction mixture containing 500 mL BSA solution and 1 mL MGO

solution was incubated at 37 °C in presence of 375 mL of extract sample or phosphate buffer (blank). The system containing BSA-MGO was incubated for 7 days, with analytical determination at 1, 4, and 7 days. Samples dissolved in phosphate buffer were incubated for the same time as for the reaction mixtures in order to measure their intrinsic fluorescence (background). The fluorescence intensity of incubation mixture without sample was recorded as negative control. Pentosidine-like (λ_{exc} 335 nm; λ_{em} 440 nm) and argpyrimidine-like (λ_{exc} 370 nm; λ_{em} 440 nm) AGE fluorescence was monitored (Spectrofluorometer Perkin Elmer L550B). The percentage inhibition of AGEs formation was calculated at each incubation time as follows:

$$\text{Inhibition rate (\%)} = \left(1 - \frac{\text{Fluorescence intensity}_{sample} - \text{Fluorescence intensity}_{background}}{\text{Fluorescence intensity }_{negative\ control}}\right) \times 100$$

The reported values are the means of two independent experiments, each performed in triplicate.

2.9. Methylglyoxal and glyoxal trapping capacity

Methylglyoxal (MGO) and glyoxal (GO) trapping capacity was evaluated according to the method proposed by Mesías *et al*. with slight modifications [120,123]. Briefly, an aliquot of 100 µL MGO or GO (5.2 mM in 100 mM PBS, pH 7.4) was added to 50 µL 5-MQ (6.1 mM in 50% v/v methanol) as the internal standard, and to 100 µL sample solution (1, 2.5, and 5 mg dry matter/mL) or PBS (control). The reaction mixture was diluted to 1 mL with PBS and incubated at 37 °C for 6, 24, and 48 h. After the addition of 200 µL OPD (10.8 mg/mL in PBS), the mixtures were derivatized at 37 °C for 30 min and the residual MGO and GO were quantified as quinoxaline derivatives by HPLC-DAD. The analyses were performed using a Gemini C18 analytical column (150 × 2.0 mm i.d., 5 µm, Phenomenex, Torrance, CA) with a Hypersil Gold C18 guard column (10 × 2.1 mm i.d.,5 µm, Phenomenex, Torrance, CA). The flow rate was 0.3 mL/min and the injection volume 5 µL. The elution was carried out in isocratic mode using as the mobile phase a solvent mixture consisting of 0.5% acetic acid aqueous solution and methanol, 50/50, v/v. Chromatograms were recorded at 315 nm. Unreacted MGO or GO concentrations were calculated from the ratio between quinoxaline or 2-methylquinoxaline (2-MQ) obtained by the conversion of MGO and GO, respectively, and the internal standard. The percentage of MGO and GO trapped was calculated as follows:

$$\text{MGO or GO decrease } (\%) = \left(\frac{\text{MGO or GO}_{\text{control sample}} - \text{MGO or GO}_{\text{sample}}}{\text{MGO or GO}_{control\ sample}}\right) \times 100$$

The reported values are the means of two independent experiments, each performed in triplicate.

2.10. Statistical analysis

All the analyses were performed in triplicate, data are expressed as the mean ± SD. Shapiro-Wilk test was used to confirm that all the values were normally distributed. Student's t-test and one-way analysis of variance (ANOVA) were used to evaluate the statistical significance of differences between controls and within cultivars respectively. The *P* level was set at 0.05. Dunnett's multiple comparison post-hoc test was used to assess whether the positive control was significantly different from the tested cultivars in inhibition assays. Tukey's post-hoc test was performed to evaluate differences among cultivars for TPC, TFC, DNJ content, and inhibitory capacity. Pearson correlation test was used to determine if a relationship between DNJ, TPC, TFC in samples and the measured biological activity was present. All the analyses were performed using Statistica 6 (StatSoft Italia, Vigonza, Italy) and GraphPad Prism 8.4.3 (GraphPad Software, San Diego, CA).

3. RESULTS AND DISCUSSION

3.1 Identification of phytochemicals

For the identification of phytochemicals in mulberry leaf extracts, ion trap mass spectrometry was used. Based on the accurate mass of the molecular ions, retention time, and MS fragmentation patterns, 30 compounds were tentatively identified in the different *M. alba* varieties. The typical base peak chromatogram is shown in Figure 1.

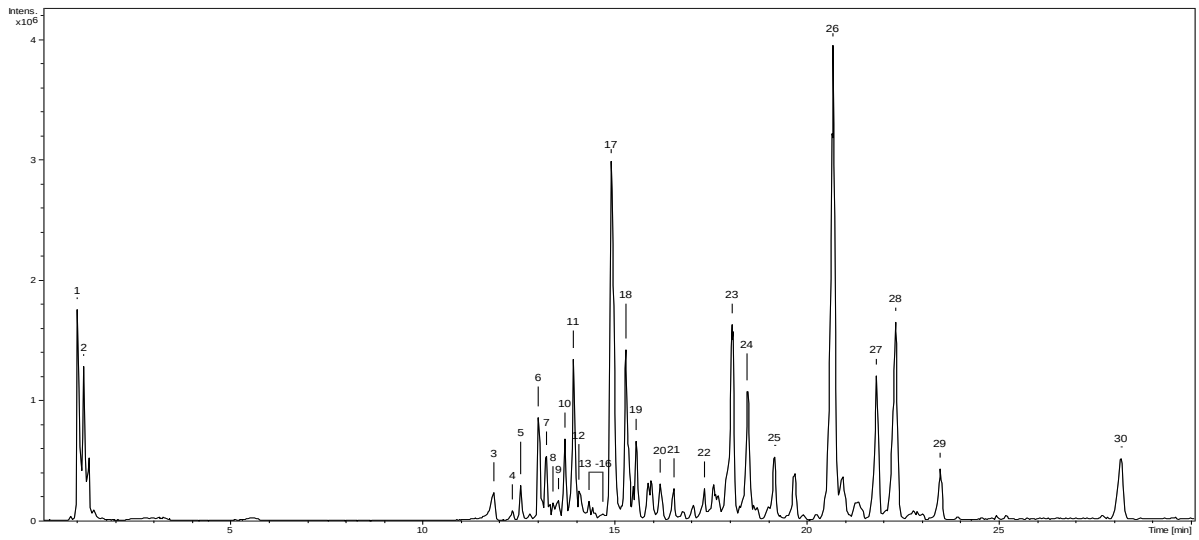

Figure 1. HPLC-ESI-MS base peak chromatogram of Cattaneo female, acquired in negative ionization mode

Table 1. HPLC-MS and MS^n data of the identified compounds in *Morus alba* leaves extracts

	Rt (min)	Putative Identification	Molecular Formula	Precursor ion (m/z)	Molecular ion	Fragment ions	Polarity	References
1	1.50	Quinic acid	$C_7H_{12}O_6$	191.17	$[M-H]^-$	173.00/171.00/126.93/85.10	negative	[124]
2	1.55	Caffeic acid-3-*O*-glucoside	$C_{15}H_{18}O_9$	341.30	$[M-H]^-$	179.10	negative	
3	11.69	Protocatechuic acid-glucoside	$C_{13}H_{15}O_9$	315.25	$[M-H]^-$	152.85/108.94	negative	[124,125]
4	12.80	1,3-di-*O*-caffeoylquinic acid	$C_{25}H_{24}O_{12}$	515.10	$[M-H]^-$	353.02/191.17/179.10/173.00	negative	
5	12.96	*p*-Coumaric acid-4-*O*-glucoside	$C_{15}H_{18}O_8$	325.34	$[M-H]^-$	267.00/219.00/163.06/119.01	negative	
6	13.00	3-*O*-caffeoylquinic acid (Chlorogenic acid)	$C_{16}H_{18}O_9$	353.21	$[M-H]^-$	190.90/179.10/126.93	negative	[124–127]
7	13.40	Quercetin-3-*O*-(6"-*O*-malonylglucoside)	$C_{24}H_{22}O_{15}$	551.47	$[M+H]^+$	303.19	positive	[128,129]
8	13.41	Quercetin 3-*O*-rutinoside (Rutin)	$C_{27}H_{30}O_{16}$	611.46	$[M+H]^+$	465.24/303.19	positive	[125–130]
9	13.49	Quercetin-3-*O*-glucoside (Isoquercitrin)	$C_{21}H_{20}O_{12}$	463.20	$[M-H]^-$	300.90/300.00/270.90	negative	[125–127,130]
				465.38	$[M+H]^+$	303.19	positive	[125,126,130]
10	13.51	*p*-Coumaroylquinic acid	$C_{16}H_{18}O_8$	337.21	$[M-H]^-$	190.90/173.00/126.93/85.10	negative	[126,128]
11	13.60	Kaempferol-3-*O*-rutinoside	$C_{27}H_{30}O_{15}$	593.31	$[M-H]^-$	284.93/254.95/226.90	negative	[124,129]
				595.31	$[M+H]^+$	449.36/287.29	positive	[124,129]
12	13.70	Kaempferol-3-*O*-glucoside (Astragalin)	$C_{21}H_{20}O_{11}$	447.09	$[M-H]^-$	327.10/284.93/254.95/226.90	negative	[124,125]
				449.36	$[M+H]^+$	287.17	positive	[124,125]
13	13.90	Kaempferol-3-(6"-*O*-acetylglucoside)	$C_{23}H_{22}O_{12}$	489.10	$[M-H]^-$	327.10/284.93/254.95/226.90	negative	[126,130]
14	13.91	Kaempferol-3-(6-*O*-malonylglucoside)	$C_{24}H_{22}O_{14}$	533.40	$[M-H]^-$	447.10/284.93/254.95/226.90	negative	[126]
				535.34	$[M+H]^+$	287.21	positive	[126]
15	14.30	Resveratrol	$C_{14}H_{12}O_3$	227.24	$[M-H]^-$	183.00/164.99	negative	[131–133]
16	14.35	Resveratrol-3-*O*-glucoside	$C_{20}H_{22}O_8$	389.16	$[M-H]^-$	227.24/183.00/164.99	negative	[125,132]
17	14.90	Trihydroxy-octadecadienoic acid isomer 1	$C_{18}H_{31}O_5$	327.28	$[M-H]^-$	291.10/229.10/210.96/200.90/170.97	negative	[124]
18	15.30	Trihydroxy-octadecenoic acid	$C_{18}H_{33}O_5$	329.30	$[M-H]^-$	310.99/293.11/228.927/211.00/170.96	negative	[124]
19	17.10	Linolenic acid hydroperoxide isomer 1	$C_{18}H_{29}O_4$	309.27	$[M-H]^-$	291.10/170.99	negative	[124]
20	17.40	Linolenic acid hydroperoxide isomer 2	$C_{18}H_{29}O_4$	309.27	$[M-H]^-$	291.10/170.99	negative	[124]
21	17.9	Linolenic acid hydroperoxide isomer 3	$C_{18}H_{29}O_4$	309.27	$[M-H]^-$	291.10/170.99	negative	[124]
22	18.42	Linolenic acid hydroperoxide isomer 4	$C_{18}H_{29}O_4$	309.27	$[M-H]^-$	291.10/273.12/247.00/229.10/170.99/137.03	negative	[124]
23	19.30	Linolenic acid hydroperoxide isomer 5	$C_{18}H_{29}O_4$	309.45	$[M-H]^-$	290.98/247.05/170.95	negative	[124]
24	20.66	Hydroxy-octadecatrienoic acid isomer	$C_{18}H_{29}O_3$	293.23	$[M-H]^-$	275.03/231.10/171.02	negative	[124]
23	18.51	Gingerglycolipid A	$C_{33}H_{56}O_{14}$	675.44	$[M-H]^-$	415.09/397.05/277.40	negative	[124]
26	21.80	Hydroperoxy-octadecatrienoic acid isomer	$C_{18}H_{27}O_3$	291.26	$[M-H]^-$	273.04/246.95/185.01/125.05/121.22	negative	[124]
27	22.30	Hydroxy-octadecadienoic acid	$C_{18}H_{31}O_3$	295.27	$[M-H]^-$	277.09/170.95	negative	[124]
28	23.40	Oxo-octadecadienoic acid	$C_{18}H_{31}O_3$	293.34	$[M-H]^-$	196.92/184.96	negative	[124]
29	29.00	Linolenic acid	$C_{18}H_{30}O_2$	277.42	$[M-H]^-$	258.85/233.03/59.01	negative	[124,134,135]
30	30.41	Linoleic acid	$C_{18}H_{32}O_2$	279.38	$[M-H]^-$	261.11/234.99/59.01	negative	[124,134,135]

The tentatively identified compounds belonged to different chemical classes (phenols, phenolic acids, flavonoids, stilbenes, and fatty acids), and are listed in Table 1. Among flavonoids, the most abundant were kaempferol, quercetin, and their glycosides, as previously described by other authors [88,112,124,127–130]. As regards phenols, caffeic acid-3-*O*-glucoside (*m/z* 341.30) and 1,3-di-*O*-caffeoylquinic acid (*m/z* 515.10) were tentatively identified here for the first time. In the case of the first compound (**2**), the loss of the glycosyl moiety (162 Da) resulted in the daughter ion *m/z* 179.10 (caffeic acid). In the latter (**4**), the sequential loss of the two caffeoyl moieties (162 Da) led to the formation of the molecular ion of quinic acid (*m/z* 191.17). Among the six structural isomers of di-caffeoylquinic acid (di-CQA), the observed fragmentation pattern is consistent with the 1,3-diCQA isomer, for this reason the others were excluded [136]. The caffeoyl moiety loss $[M-162]^-$ was observed for 3-*O*-caffeoylquinic acid (**6**), *i.e.*, chlorogenic acid (*m/z* 353.21). The isomer 3-CQA was tentatively chosen among the others (1-CQA, 4-CQA, 5-CQA) as the most probable, due to the presence of the intense fragment at *m/z* 179.10 (MS^2). The typical fragmentation was previously reported by Clifford and co-workers [136]. All the other compounds were largely studied and previously reported by other authors (Table 1) for the genus *Morus* from plants of different geographical origin. In particular, different flavonoids glucosides *e.g.*, quercetin-3-*O*-(6"-malonylglucoside), rutin, isoquercitrin, kaempferol-3-*O*-rutinoside, astragalin, kaempferol-3-(6"-*O*-acetylglucoside), and kaempferol-3-(6-*O*-malonylglucoside) were here identified in the extracts. All quercetin glucosides gave the deprotonated aglycone fragment at *m*/z 300.90 in negative ion mode, as shown in Table 1. This aglycone was also confirmed by the MS^2 spectrum, indeed the characteristic product ion at *m*/*z* 270.90 led to the aglycone identification as quercetin. Compound **7** gave the $[M+H]^+$ at *m*/*z* 551.47 in positive ionization mode. The MS^2 spectrum highlighted the presence of one fragment at *m*/*z* 303.19 $[M+H–248]^+$, corresponding to the loss of a hexosyl (162 Da) and the malonyl (86 Da) moieties linked at the same position of the aglycone quercetin. This molecule was tentatively identified as quercetin-3-*O*-(6"-*O*-malonylglucoside). Compound **8** gave the $[M+H]^+$ at *m*/*z* 611.46. The MS^2 spectrum highlighted the presence of one fragment at *m*/*z* 303.19, corresponding to the loss of (162+146 Da), indicating a hexose and a deoxyhexose linked at the same position of the aglycone. The glycosylation site of 3-OH was determined by the intensity of $[M+H–308]^{+\bullet}$ higher than that of $[M+H–308]^+$. Thus, this compound was tentatively identified as quercetin-3-*O*-rutinoside (rutin). Compound **9** produced a deprotonated ion at *m*/*z* 463.20. In analysis of the MS^2 spectrum, two high intensity fragments at *m*/*z* 300.90 $[M–H–162]^-$ and 300.00 $[M–H–162]^{-\bullet}$ were observed. Ions at *m*/*z* 300.90 suggested the loss of a hexose unit. The glycosylation

site of 3-OH was determined by the intensity of $[M–H–162]^{-\bullet}$ higher than that of $[M–H–162]^{-}$. The same compound (*rt* 13.49) gave in positive ion mode the fragmentation $[M+H-162]^{+}$, giving rise to the protonated product ion *m/z* 303.19, thus indicating the loss of a glucose unit. All the identified kaempferol derivatives (**11-14**) showed the deprotonated aglycone fragment at *m/z* 284.93, as shown in Table 1. The aglycone was further confirmed by MS^2 spectrum giving the characteristic product ions at *m/z* 254.93 and 226.90, typical of kaempferol which led to its identification. Compound **11** gave the $[M-H]^-$ at *m/z* 593.31. The MS^2 spectrum highlighted the loss of 308 Da ($[M-H-308]^-$), indicating a hexose (162 Da) and a deoxyhexose (146 Da) linked at the same position of the aglycone. In positive ion mode, the sequential loss of the deoxyhexosyl and hexosyl units from the parent ion 595.31 led to the formation of two product ion peaks at *m/z* 449.36 and 287.29. This compound was tentatively identified as kaempferol-3-*O*-rutinoside. Compound **12** exhibited the molecular ion peaks at *m/z* 447.09 and 449.36 in negative and positive ion mode, respectively. The loss of the glucosyl moiety (162 Da) resulted in the formation of the two product ions highest peaks, respectively at *m/z* 284.93 and 287.17. For this reason, compound **12** was putatively identified as kaempferol 3-*O*-glucoside (astragalin). Compound **13** (*m/z* 489.10) produced a daughter ion at 284.93, by losing an acetylglucose moiety $[M-H-204]^-$, indicating the presence of a kaempferol skeleton. It was identified as kaempferol 3-(6"-*O*-acetylglucoside). The same fragmentation was observed for compound **14,** which was tentatively assigned to kaempferol 3-(6”-*O*-malonylglucoside). The $[M–H]^-$ ion at *m/z* 533.40 in the negative mode, yielded fragment ions corresponding to kaempferol glucoside (*m/z* 447) after the loss of the malonyl moiety (86 Da), and finally to kaempferol after losing the hexosyl moiety (162 Da). Compounds **1** and **10** were putatively identified as quinic (*m/z* 191.17) acid *p*-coumaroylquinic acid (*m/z* 337.21), respectively. For quinic acid, the loss of water (and protons) [M-H-18]- led to the formation of the parent ions *m/z* 173.00 (and 171.00). Further, the subsequent loss of carbon dioxide (44 Da) originated the product *m/z* 126.93. For compound **10,** the loss of 146 Da $[M-H-146]^-$ suggested the presence of a *p*-coumaroyl moiety linked to the quinic acid residue. Compound **3** (*m/z* 315.25) exhibited an intense product ion peak at *m/z* 152.85 by the loss of a glucosyl moiety $[M-H-162]^-$, this molecule was tentatively assigned as protocatechuic acid glucoside. The second fragment in the MS^2 spectrum (*m/z* 108.94) could be produced by loss of carbon dioxide (44 Da) from the aglycone protocatechuic acid. Compound **5** (*m/z* 325.34) showed an intense peak at *m/z* 163.06, which could be due to the cleavage of the glucose unit (162 Da) $[M-H-162]^-$. The product ion at *m/z* 163.06 produced a fragment *m/z* 119.01 in MS^2 spectrum, for possible loss of carbon dioxide (44 Da) from *p*-coumaric acid. Compound **5** was tentatively identified as *p*-coumaric

acid-4-*O*-glucoside based on the characteristic fragmentation pattern, and the accurate mass reported in the literature (163.0561)[137]. Among stilbenes compounds **15** and **16** were tentatively identified as resveratrol and resveratrol 3-*O*-glucoside, respectively. For resveratrol, the proposed fragmentation is due to the loss of carbon dioxide (44 Da) and one molecule of water (18 Da) from the molecular ion $[M-H]^-$ with *m/z* at 227.24, generating the two daughter ions at *m/z* 183.00 and 164.99. Compound **16** presented the same fragmentation pattern as **15,** but with the prior loss of an hexoside unit, thus it was putatively assigned to resveratrol 3-*O*-glucoside, which was already found in *Morus* genus [124,131–133]. Compounds **17**-**18**, **24** and **26**-**28** were all previously detected by HPLC-MS in mulberry species, and were here putatively identified as oleic acid (9-octadecenoic acid) derivatives by means of the typical ion fragmentation [124,134]. Compounds **29** and **30**, with *m/z* 277.42 and 279.38 were respectively identified as linolenic acid and linoleic acid. For both the unsaturated fatty acids, the loss of carboxyl group through the cleavage of carbon dioxide (44 Da) produced the intense fragment at *m/z* 233.03 and 234.99. In the second part of the chromatogram many different oxidized fatty acids were detected and tentatively assigned (**19**-**23**); their presence has already been reported in previous studies [124,126]. All these compounds showed the molecular ion in negative mode at *m/z* 309.27 and they shared the same fragments. Fatty acids peroxidation commonly involves a reaction between unsaturated lipids and oxygen. This kind of reaction may be the product of enzymes or even non-enzymatic. Non-enzymatic lipid oxidation may be due to free radical oxidation or be mediated by singlet oxygen. Singlet oxygen can react with any of the double bonds present in unsaturated fatty acid, such as ω 3,6,9 in linolenic acid, to form hydroperoxide isomers [138]. Compound **25** was tentatively proposed as gingerglycolipid A**,** which is the glycosylmonoacylglycerol of linolenic acid, and its fragmentation has already been reported in the literature [124,139]. Caffeic acid, protocatechuic acid, *p*-coumaric acid, quercetin, and kaempferol standard compounds were used for the aglycones identification.

3.2. HPLC-ESI-TQ-MS method validation

The analytical method for the determination of DNJ has been validated in terms of precision and accuracy. Precision (intra- and inter-day) was evaluated as repeatability at three concentration levels of DNJ (0.05, 0.20, and 0.50 μg/mL) by performing replicate injections (n = 6), and it was expressed as the relative standard deviation of concentration measurements. Injections were performed on the same day and over three different days. Accuracy was evaluated by recovery method, carried out by spiking samples with three different concentrations of standard solutions. Results are shown in Table 2.

Table 2. Recovery percentage and precision data obtained with spiked samples.

Intra–day (n = 6)		
DNJ Nominal concentration (mg/mL)	**RSD (%)**	**Recovery (%)**
0.05	4.16	99.33
0.20	4.08	101.00
0.50	2.85	101.33
Inter–day (n = 6)		
DNJ Nominal concentration (mg/mL)	**RSD (%)**	**Recovery (%)**
0.05	6.60	102.67
0.20	4.15	101.00
0.50	1.69	100.17

The highest RSD was 6.60% and the recoveries ranged from 99.33 to 102.67. These data confirmed that the present method for the DNJ extraction from leaf and its quantification has a satisfactory accuracy, precision, and reproducibility. Limit of detection (LOD) and limit of quantitation (LOQ) for the analyte were calculated as signal-to-noise ratio 3:1 and 10:1 respectively. The calculated LOD and LOQ were 0.19 and 0.62 ng/mL, respectively.

3.3.Determination of DNJ by HPLC-ESI-TQ-MS

Although different methods for the determination of DNJ were available in the literature, HILIC coupled with mass spectrometry has proven to be one of the most convenient for both shortest time of analysis and highest sensitivity [90,91,111]. Due to the very high hydrophilicity and small molecular weight of the molecule, the interaction with the stationary phase of conventional RP columns is too weak for the effective retainment of DNJ. Multiple reaction monitoring is commonly applied in HPLC-MS for the analysis of plant secondary metabolites, owing to the fact that target molecules can be sensitively selected in the first stage, and no other peaks are present in the final chromatogram. For the quantification of DNJ, the transitions of the parent ion (*m/z* 164.09) to the product ions (*m/z* 146.08, 128.07, 110.06) for subsequent losses of water molecules (18 Da) were monitored in positive ion mode. In our experimental conditions DNJ retention time was 4.45 min. The amount of DNJ in FDEs was in the range of 0.47±0.07 to 1.33±0.11 mg/g, as shown in Table 3. The derived amount of DNJ in leaves was in line with those reported by other authors, even if slightly below the average [140–142]. In earlier studies it has been shown that DNJ content widely varied among cultivars, and that it was significantly affected by the leaf position in the range: shoots > young leaves > mature leaves. Typically, the higher amount of DNJ was found in later summer season and at higher latitudes [142]. In our case, mature leaves were harvested in May, this factor could have

negatively impacted the content of the compound. Ideally, varieties of mulberry with higher DNJ levels should be preferred for their use as natural functional products, in any case also the amounts of polyphenols and flavonoids should be considered. Indeed, polyphenols may provide additional health benefits, which are linked to their recognized antioxidant, antidiabetic, and hypolipidemic properties [119,125,127].

3.4. Total polyphenols and total flavonoids contents

Phenols and flavonoids play an important role in a variety of pharmacological activities, notably antioxidant, anti-inflammatory, and antimutagenic [115]. For this reason, the determination of TPC and TFC in mulberry leaves was of major importance. Phenolic rich extracts have already demonstrated a quite good inhibitory activity against digestive enzymes, however showing sometimes contradictory results [143]. This heterogenous and conflicting results available in the literature may be due to the specific chemical composition of the herbal or fruit extract, thus indicating that not all phenolics combinations were equally effective for the enzyme inhibition. The results of the TPC and TFC are presented in Table 3 and varied from 2.10±0.44 to 9.61±0.33 and from 0.15±0.05 to 1.46±0.07 mg/g DW, respectively. These amounts are lower than those found in plants originating from eastern China and Korea [127,144], but in good agreement with those found by Polumackanycz in commercial samples of mulberry [145]. Cattaneo female and male, Egyptienne and Ukraina showed the highest TPC and TFCs. A huge variability in the phenolic and flavonoid profiles among *Morus* cultivars has already been reported in the literature, and the effect of the plant variety was often more relevant than the region of origin [84,127]. As it was previously demonstrated, TPC and TFC were highly susceptible to light exposure, temperature, precipitation amounts of the planting area, and harvesting time. Since all the sample employed in this study were harvested in the same period and originated from the same geographical area, the most likely explanation relied on the differences of the plants' genetic constitution.

Table 3. Contents of polyphenols (TPC), flavonoids (TFC) and DNJ in Italian mulberry CVs.

Morus alba cultivar	DNJ mg/g FDE	DNJ mg/g leaf DW	TPC GAE mg/g leaf DW	TFC QE mg/g leaf DW
Cattaneo f.	0.48±0.03^{a}	0.08±0.02^{a}	7.17±0.07^{d}	0.92±0.10^{fg}
Cattaneo m.	0.54±0.12^{ace}	0.09±0.02^{a}	5.57±0.65^{c}	0.81±0.07^{eg}
Egyptienne	0.92±0.08^{de}	0.22±0.03^{bde}	9.61±0.33^{e}	1.46±0.07^{h}
Giazzola	0.89±0.12^{bd}	0.10±0.03^{a}	4.22±0.43^{b}	0.24±0.08^{ab}
Kayriounezumigaeshi	0.51±0.17^{ab}	0.23±0.02^{cde}	2.18±0.19^{a}	0.38±0.11^{ac}
Limoncina	0.49±0.17^{a}	0.15±0.04^{abc}	4.47±0.02^{bc}	0.15±0.05^{a}
Morettiana	1.31±0.08^{ef}	0.16±0.05^{ae}	4.68±0.18^{bc}	0.41±0.18^{a}
Nervosa	1.33±0.11^{f}	0.11±0.05^{a}	4.77±0.54^{bc}	0.45±0.13^{ad}
Pendula	0.94±0.18^{df}	0.15±0.03^{ad}	4.82±0.7^{bc}	0.70±0.23^{cdef}
Pyramidalis	0.98±0.24^{df}	0.12±0.03^{ab}	2.10±0.44^{a}	0.51±0.11^{abe}
Spain	0.47±0.07^{a}	0.08±0.02^{a}	3.99±0.34^{b}	0.22±0.02^{a}
Ukraina	0.91±0.09^{cd}	0.07±0.03^{a}	8.71±0.17^{e}	1.29±0.12^{h}

Means followed by distinct letters in the same column statistically differ according to Tukey's test ($P < 0.05$). Homogeneous subsets are indicated by the same letter.

3.5. α-Amylase inhibitory activity

As regards α-amylase, a dose-dependent activity was observed for all the tested cultivars, with a maximum inhibition around 40 or 50% for the highest tested dose (20 mg/mL) in our experimental conditions (Figure 2).

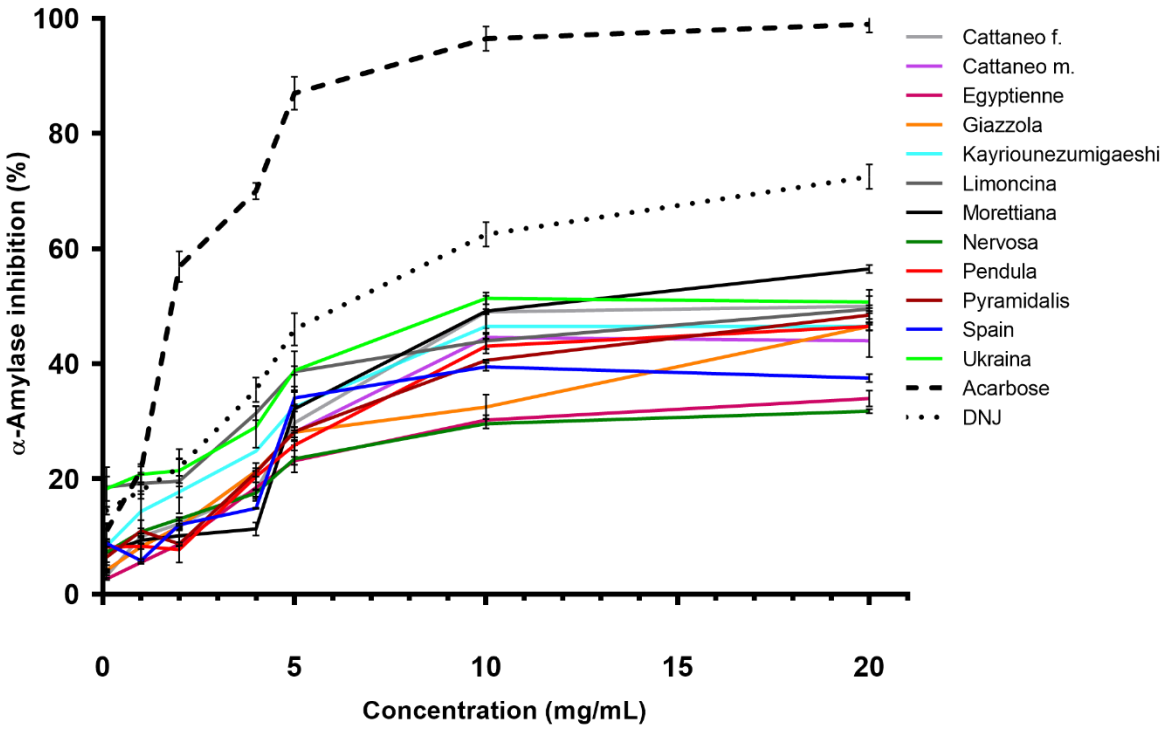

Figure 2. Percentage inhibition of α-amylase by *Morus alba* leaf extracts, DNJ, and acarbose (reference standard).

For this reason, the estimation of IC_{50} was not possible in most cases. Morettiana and Ukraina showed the most effective inhibition (56.55±0.71% and 50.70±1.06%, respectively) when tested at the highest concentration. Minor differences among samples were observed for the other concentration levels. Conversely, both acarbose and DNJ efficiently inhibited this enzyme, with related IC_{50} equal to 2.22±1.25 and 5.22±1.29 mg/mL, respectively. The IC_{50} value of acarbose was 100-fold higher than that obtained by Spìnola *et al*., while the IC_{50} value of DNJ resulted lower than that reported by Qiao and co-workers [119,146]. These differences might be due to the different type and origin of the enzymes, and to variable ratios within inhibitors, enzyme units, and substrate. One-way ANOVA with Tukey's multiple comparison test highlighted significant differences between acarbose and DNJ ($P < 0.01$). Previous studies underlined that rutin, ellagitannins, and cyanidin glycosides were the most effective natural compounds in inhibiting α-amylase [119,147,148]. Even if rutin was detected in all the samples (Table 4), no positive effect was observed on α-amylase inhibition in our study. It must be considered that the overall outcome likely derived from different components of the crude extract acting together, rather than from one single compound. As it was pointed out, the inhibitory effect of polyphenols seems to rely on non-covalent interactions with the enzyme, mainly associated to non-competitive type inhibitions [149]. As a result, glycosylation, conjugation site or class of the glycosyl moieties have direct implications on the inhibitory effect over carbohydrate-hydrolyzing enzymes. Flavonoids may exert different effects (synergistic, additive or antagonistic) depending on these characteristics [119,148]. As it was pointed out by other authors, the glycosylation of hydroxyl group on flavonoids undermined the inhibition of α-amylases and α-glucosidases. In particular, quercetin and its monoglycosides (quercitrin and hyperin) showed stronger inhibitory activity against α-amylase than the polyglycoside form (rutin) [150]. The same evidence was also observed for kaempferol, whose inhibitory effect was significantly higher than those reported for its glycoside forms [150]. The HPLC-MS analysis revealed the presence of flavonoids largely in their glycosylated forms in the extracts, this fact could explain the poor inhibitory activity on amylase, which occurred in our experimental conditions.

Table 4: Compounds identified by HPLC-MS and their distribution in the leaf extracts of *Morus alba* CVs.

	***Morus alba* CVs**	**Cattaneo f.**	**Cattaneo m.**	**Egyptienne**	**Giazzola**	**Kayriounezumigaeshi**	**Limoncina**	**Morettiana**	**Nervosa**	**Pendula**	**Pyramidalis**	**Spain**	**Ukraina**
1	Quinic acid	+++	++	+++	+++	++	+++	++	+++	++	++	+	+++
2	Caffeic acid-3-*O*-glucoside	++	++	++	+	++	+	+	+++	+++	+	+	++
3	Protocatechuic acid-glucoside	+	+	+	+	+	+	++	++	+	+	+	+
4	1,3-di-*O*-caffeoylquinic acid	+	+	+++	++	+	++	+	++	+++	+++	+	+++
5	*p*-Coumaric acid-4-*O*-glucoside	+	++	++	+	++	++	+	+	++	++		++
6	3-O-caffeoylquinic acid	++	++	+++	++	+	++	+	++	+++	+++	+	+++
7	Quercetin-3-*O*-(6"-*O*-malonylglucoside)	+	+++	++	+	+++	+	+	++	++	+	++	+
8	Quercetin 3-*O*-rutinoside	+	++	+++	+	++	++	++	+++	++	++	++	+++
9	Quercetin-3-*O*-glucoside	+	++	+++	++	++	++	++	+++	++	+	++	++
10	*p*-Coumaroylquinic acid	+	++	++	+	+	+	+	++	++	+	+	+
11	Kaempferol-3-*O*-rutinoside	+++	+++	+++	++	++	+	++	+++	++	+	++	+
12	Kaempferol 3-*O*-glucoside	+	++	++	++	+++	+	++	+++	++	+	++	+++
13	Kaempferol 3-(6"-*O*-acetylglucoside)	+	++	++	++	++	+	+	++	++	+	+	++
14	Kaempferol 3-(6-*O*-malonylglucoside)	+	+	+	+	+	+	+	++	+	+	+	+
15	Resveratrol	+	++	++	+	+	++	+	+++	++	++	+	++
16	Resveratrol 3-*O*-glucoside	+	+	++	+	+	+	+	+	++	+	+	+
17	Trihydroxy-octadecadienoic acid isomer 1	+++	++	++	+++	++	+++	+++	+++	++	+	++	++
18	Trihydroxy-octadecenoic acid	+++	++	++	++	++	+	++	++	++	+	++	+
19	Linolenic acid hydroperoxide isomer 1	+++	+	++	++	++	++	++	+	++	+	++	+++
20	Linolenic acid hydroperoxide isomer 2	+	+	+	+		++	+	+	+		+	++
21	Linolenic acid hydroperoxide isomer 3	+	+	+		+	++	++	+	++	++	+	++
22	Linolenic acid hydroperoxide isomer 4	+	++	++		+	++	++	++	++	++	++	++
23	Linolenic acid hydroperoxide isomer 5	+++	+	+	+	+	+	+	++	++	+	+	+
24	Hydroxy-octadecatrienoic acid isomer	+++	++	+++	++	++	+++	+	+++	++	++	++	++
25	Gingerglycolipid A	++	+	+	+	+		+	+	++	+	+	+
26	Hydroperoxy-octadecatrienoic acid isomer	+++	++	+	++	+	+++	+	++	++	++	+	++
27	Hydroxy-octadecadienoic acid	++	+++	++	+	+	++	+++	+++	+++	++	++	++
28	Oxo-octadecadienoic acid	+++	++	+	+	++	+	+++	+	+++	++	+	++
29	Linolenic acid	++	++	+++	+++	++	++	+++	+	+++	+++	+++	++
30	Linoleic acid	++	++	+++	+++	+++	++	+++	++	++	++	++	+++

3.6. α-Glucosidase inhibitory activity

Concerning α-glucosidase, DNJ showed an effective inhibition, even stronger than the reference compound acarbose, with related IC_{50} of 0.24±0.29 and 0.86±0.25 mg/mL, respectively (Figure 3).

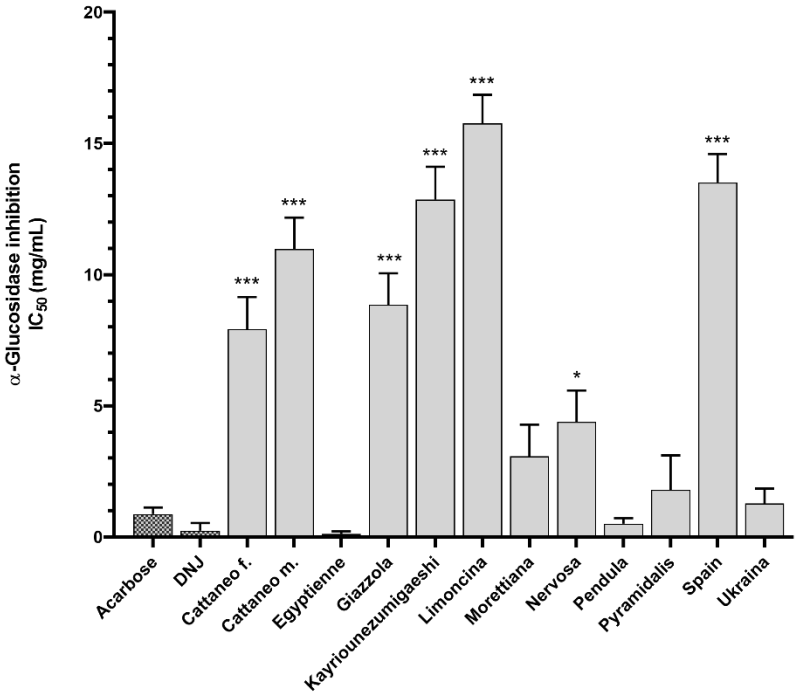

Figure 3. *In vitro* inhibitory activities (IC_{50}) of *Morus alba* leaf extracts, DNJ, and acarbose (reference standard) towards α-glucosidase. A comparison within groups was performed by one-way ANOVA followed by Tukey's Post Hoc test. Statistical significance levels were defined as: * $P < 0.05$, ** $P < 0.01$, *** $P < 0.001$ and **** $P < 0.0001$.

One-way ANOVA and Tukey's Post Hoc test showed no significant difference between DNJ and acarbose ($P < 0.05$). These data are in accordance with those reported by Spìnola *et al*., who also observed a higher selectivity for both these compounds towards the mammalian enzyme, with respect to the here employed yeast type. This discrepancy may be ascribed to structural differences in the catalytic site of the two enzyme isoforms [119]. As concerns the plant extracts, remarkable differences were observed among the cultivars ($P < 0.05$). Egyptienne, Morettiana, Pendula, Pyramidalis, and Ukraina showed the lowest IC_{50} values, corresponding to 0.12±0.09, 3.07±1.20, 0.50±0.21, 1.79±1.31 and 1.27±0.56 mg/mL, respectively. A strong correlation ($r = 0.7548$, $r^2 = 0.5697$, $P = 0.005$) between DNJ content and α-glucosidase inhibition was registered. Conversely, no significant relations were observed between TPC or TFC and glucosidase inhibition, according to Pearson correlation test (data not shown). Interestingly, *Morus* extracts with the highest DNJ level (Morettiana and Nervosa) did not show the most effective inhibition. On the other hand, Egyptienne being characterized by

high amount of DNJ (0.92±0.08 mg/g) along with high TPC and TFC was the most active. The same tendency was observed also for Pendula and Ukraina. This evidence may be explained by assuming a synergistic effect of phenols, flavonoids, and DNJ, playing together a key role for the enzyme inhibition. Combinations of polyphenols and active compounds frequently exhibited synergistic effects, having a higher biological activity than the sum of the individual ones. Previous studies demonstrated that α-glucosidase was susceptible to inhibition by many phenols and flavonoids, including quercetin, kaempferol, rutin, and CQA, which were all identified in the extracts [151]. In particular, 3-CQA (also known as chlorogenic acid), has proven to exert a great inhibition against this enzyme [119,152,153]. The highest amounts of CQA and its derivative 1,3-diCQA were detected in Egyptienne, Pendula, Pyramidalis, and Ukraina by HPLC-MS^n analysis (Table 4). The presence of CQA could enhance the activity of DNJ, confirming the synergy between phytochemicals and explaining the stronger inhibitory efficacy of Egyptienne, with respect to the reference drug acarbose and DNJ alone. A semi-quantitative approach based on the evaluation of the peak areas for the same compound was used to perform a comparison within different cultivars. To be on the safe side, the experimental conditions (extractive method and the LC-MS parameters) were standardized to guarantee the same response factor for each analyte in the HPLC-MS experiments. Disregarding the actual concentration of each phenolic acid and flavonoid, this semi-quantitative comparison was used as a support for the following discussion of the biological activities exerted by the different cultivars. Data reported in Table 4 are to be intended as purely qualitative assessment of the chemical composition of the extracts, whereas the specific determination of flavonoids and phenols was outside the scope of this work.

3.7. Evaluation of antiglycative and MGO/GO trapping capacities

The effect of *Morus* leaf extracts on the early stage of non-enzymatic glycation of protein was monitored by the fructosamine inhibition assay. Fructosamine is an Amadori product generated by the rearrangement of Schiff's bases. These in turn originate from the reaction between the carbonyl groups of monosaccharides and the amino groups of proteins by rearrangements, condensation, or oxidative modifications [120]. In this work, the formation of fructosamine was investigated under mild reaction conditions in presence of glucose (GLU). All samples were able to reduce the formation of the Amadori products in a dose-dependent manner. Results reported in Figure 4 indicate that at the lowest dose (1 mg/mL) FDEs reduced the fructosamine at least by 20%. Besides, Giazzola, Kayriounezumigaeshi, Limoncina, Pendula, Pyramidalis, and Spain totally prevented its formation at the concentration of 5 mg/mL. No significant

correlation was found between DNJ content and fructosamine reduction, while a negative correlation was found for TPC and TFC. Therefore, the higher amounts of phenols and flavonoids seemed to be not positively related to the observed fructosamine reduction capacity, in our conditions.

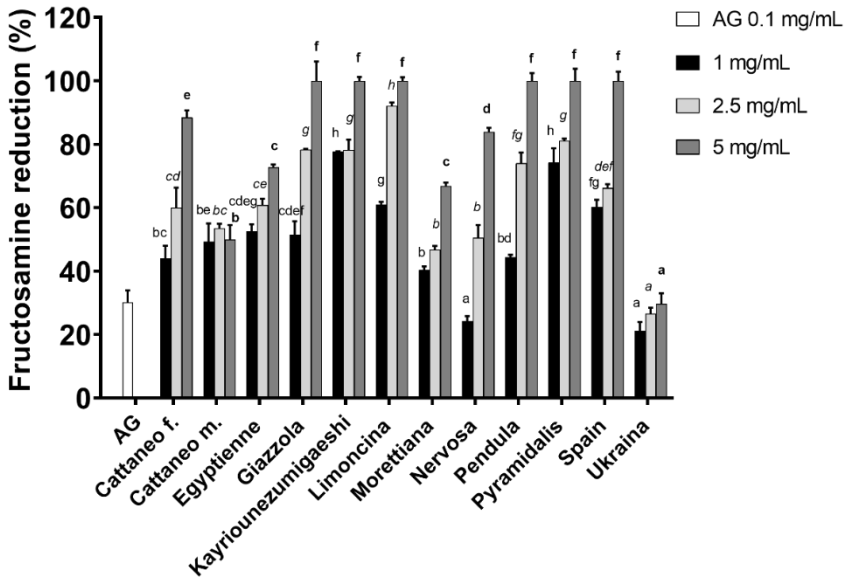

Figure 4. Inhibition of Amadori products formation by *Morus alba* leaf extracts and aminoguanidine (AG, reference standard) in fructosamine assay. One-way ANOVA followed by Tukey's Post Hoc test was used to perform a comparison among CVs within each dose. Different superscript letters indicate significant differences within each group.

Accumulation of AGEs specific fluorescence is considered a general estimation of overall protein glycation damage [123]. Therefore, the antiglycative properties of *Morus* extracts were further investigated by measuring the inhibition of fluorescent AGEs formation, in a glycation model set up using BSA under physiological conditions. The capacity of FDEs (1, 2.5, and 5 mg/mL) to act in the middle stage of protein glycation was evaluated by monitoring the pentosidine- and argpyrimidine-like AGEs formation after 1, 4, and 7 days of incubation. For all the samples a dose-dependent antiglycative activity was observed (Figure 5), and the reduction of BSA glycation at the dose of 5 mg/mL was significantly different with respect to 1 mg/mL for all the CVs ($P < 0.05$). At the lowest tested concentration (1 mg/mL) the most effective reduction of BSA glycation was measured for Cattaneo m., Egyptienne, Nervosa, and Pendula ($P < 0.0001$). No statistically significant correlation among DNJ, TPC and TFC, and reduction of BSA glycation was present (data not shown). At the dose 5 mg/mL, all the extracts were able to completely prevent the AGEs formation, both at the beginning (1 day) and at the end (7 day) of the monitoring period. Aminoguanidine (AG) was used as positive control, due to its documented capacity of inhibiting AGEs formation by reacting with carbonyl groups of reducing sugars and dicarbonyl intermediates [123]. At the concentration of 0.1 mg/mL, AG

reached 79.64±0.63, 74.31±0.94, 72.01±1.70% of inhibition over pentosidine-like AGEs formation at 1, 4, and 7 days, respectively. A less effective reduction ($P < 0.0001$) was exerted on argpyrimidine-like AGEs formation, equal to 53.90±1.43, 53.18±1.32 and 42.94±2.62% at 1, 4 and 7 days of incubation, respectively. Over the period of incubation, a slight progressive decrease of activity was observed both for some FDEs and AG, from 1 till 7 days. In such cases, the best inhibitory capacity was reached within 1 day. In the case of AG, this decrease was significant at $P < 0.001$ between 1 and 7 days of incubation. This peculiar behaviour could be explained considering that the formation of AGEs is a complex process, in which intermediates form and rearrange, through a series of reversible chemical reactions. For this reason, a linear trend over reaction monitoring time is not always present [154].

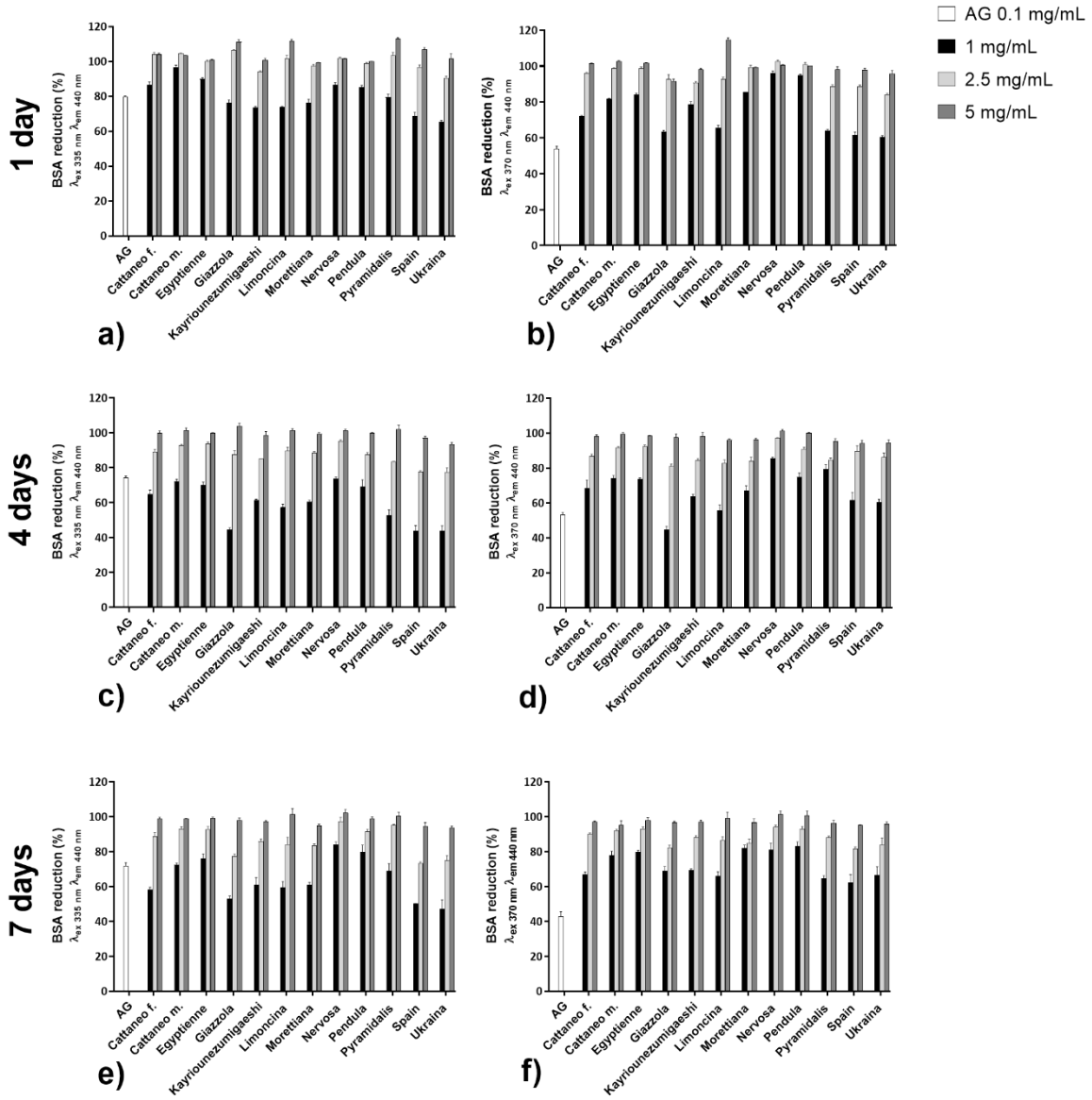

Figure 5. Antiglycative activity of *Morus alba* leaf extracts and aminoguanidine (AG, reference standard) on the formation of pentosidine-like (a, c, e) and argpyrimidine-like (b, d, e) AGEs in BSA-MGO assay. Data shown in graphs are referred to different incubation times (1, 4 and 7 days).

Our promising results on the antiglycative capacity of *Morus* leaf extract are in good agreement with those previously reported by other authors in streptozotocin-induced chronic diabetic rats, which support the use of mulberry-derived products as food supplement or adjunct treatment for DM [72]. In order to gain more insight into the antiglycative potential of *Morus*, the role of dicarbonyl compounds was further investigated in MGO and GO trapping model systems. In this assay the extracts' capacity of acting as direct trapping-agent was monitored at different times (1, 24, 48 h). The results confirm that mulberry extracts exhibited a promising trapping ability against both GO (Figure 6a) and MGO (Figure 6b), which are promoter of the glycation process. Indeed, dicarbonyls have been proven to modify proteins overtime and generate AGEs, which contribute to cellular senescence, aging, and diabetes complications [123].

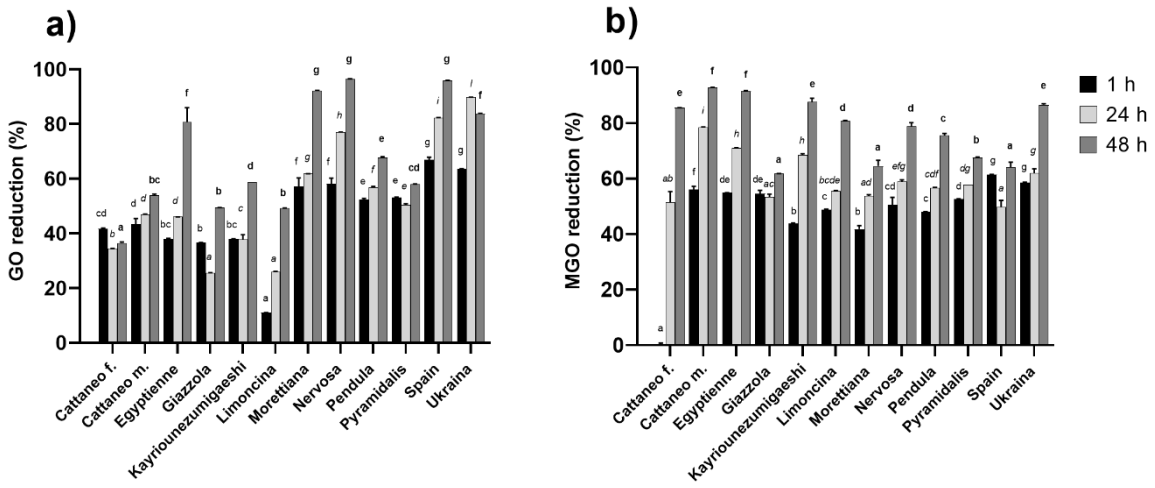

Figure 6. Glyoxal (a) and methylglyoxal (b) trapping capacity of *Morus alba* leaf extracts (5 mg/mL) after incubation (1–48 h). One-way ANOVA followed by Tukey's Post Hoc test was used to perform a comparison among CVs within each monitoring time. Different superscript letters indicate significant differences among CVs, within each monitoring time ($P < 0.05$).

Except for Morettiana, Nervosa and Spain, lower GO scavenging capacity was observed as compared with MGO, especially at 24-48 h of incubation. This evidence, already documented by other authors, may be explained considering that GO is more easily polymerized in aqueous solution, being mainly in the form of a hydrated monomer, dimer, or trimer. The conversion of GO oligomer (or hydrate) to the free form is a limiting factor for its capture by quenchers [155,156]. Afterwards, we tried to establish if a correlation between DNJ, TPC and TFC, and MGO/GO reduction was present (data not shown). Only a weak correlation was found for TPC and MGO reduction (%), with a Pearson's correlation coefficient (r) equal to 0.5345. A moderate positive correlation ($r = 0.5652$) was found for the content of DNJ and GO reduction (%). Conversely, there was a quite strong positive correlation ($r = 0.6519$, $r^2 = 0.4250$, $P = 0.022$) for TFC and MGO reduction (%). Therefore, DNJ may positively impact on GO

reduction, meanwhile flavonoids and phenols on MGO. Many studies confirmed that different polyphenols (caffeic and chlorogenic acid, resveratrol, kaempferol, quercetin, rutin among the others) had antiglycative functions, by reducing the production of dicarbonyl compounds, especially in the early phase of glycation [157]. As regards to phenolic acids, even if the underlying mechanism remains inconclusive, the trapping ability was positively related to the number of hydroxyl groups, which enhanced the reactivity of dicarbonyl compounds by nucleophilic addition [123,155,157]. Therefore, benzoic acids with three (or more) –OH groups have an optimal trapping structure against MGO and GO. Concerning flavonoids, the trapping mechanism was apparently related to the formation of mono- and di- adducts with dicarbonyls at the A ring of the flavonoid skeleton. Moreover, positions 6 and 8 on the A ring were found the major active sites, and are generally intended as the essential structural requirement for trapping MGO and GO [155]. Egyptienne, Morettiana, Nervosa, Spain and Ukraina were the most active CVs against GO (Figure 6a). Likewise, Cattaneo m., Egyptienne, Kayriounezumigaeshi, Nervosa, Ukraina were the most active against MGO (Figure 6b). The qualitative analysis of the chemical composition (Table 4) revealed that quercetin 3-*O*-rutinoside (rutin) was particularly abundant in Egyptienne, Nervosa and Ukraina. The cultivars Cattaneo m., Egyptienne, Kayriounezumigaeshi and Nervosa were rich both in quercetin and kaempferol glucosides. Resveratrol was present in high amount only in sample Nervosa. Concerning phenolic acids, 3-CQA (chlorogenic acid) was abundant in Egyptienne, Pendula, Pyramidalis and Ukraina. Caffeic acid-3-*O*-glucoside was found in quite huge amount in Nervosa and Pendula, and to a lesser extent also in Cattaneo f. and m., Egyptienne, Kayriounezumigaeshi and Ukraina. These results on direct carbonyls trapping are in line with those obtained in the BSA–MGO assay (Figure 5).

4. Conclusions

The here obtained results indicate that the inhibitory effect on digestive enzymes was likely mediated by the contribution of several compounds, namely DNJ, kaempferol, quercetin and chlorogenic acid, present in crude extracts, which could act in a synergistic way. A remarkable inhibitory activity on α-glucosidase was observed for some of the tested Italian *Morus* varieties, being more effective than pure acarbose and DNJ. In addition to the documented hypoglycaemic properties of mulberry, the combined antiglycative and carbonyl trapping capacities may help preventing long-term complications related to AGEs in DM patients. Even if additional research is required to bridge the gap between *in vitro* and clinical data, our results may contribute to new insights for a rational use of mulberry based health products in the

treatment of hyperglycaemia. In conclusion, this study fosters the use of *Morus* leaf phytocomplex to be used alone or in combination with other hypoglycaemic agents for the management of T2DM, allowing the reduction of individual drugs and the related side effects.

STRATEGIES FOR THE SUSTAINED RELEASE OF MULBERRY DNJ TO OBTAIN A PROLONGED HYPOGLYCAEMIC EFFECT

This section is intended as the conclusion of Chapter 2, it contains the candidate's original research work. At present, the collected and analysed data have not been published nor submitted to any journal.

1. INTRODUCTION

Diabetes mellitus (DM) is a complex metabolic disorder, affecting the body's natural regulation of blood glucose level. This condition is characterised by chronic hyperglycaemia and disturbances of carbohydrate and fat metabolism, resulting from inadequate insulin secretion (type 1 DM) or insulin resistance (type 2 DM). This latter is on the rise worldwide, and it is becoming a major health concern according to the WHO, calling for new strategies and cost-effective treatments [107]. Several studies have shown that phytochemicals from natural sources represent a suitable and promising approach for the management of diabetes, especially in the early stage of the disease [158]. In particular, mulberry (*Morus* spp. L.) leaf extract has been traditionally used in Asian countries to treat DM since ancient times [70,78,159]. The well documented inhibition of intestinal α-glycosidases exerted by the mulberry iminosugar 1-deoxynojirimicyn (DNJ) makes it a successful anti-hyperglycaemic agent, by slowing the rate of polysaccharides conversion into sugars [118,160]. Moreover, DNJ was shown to exert several positive systemic effects against hyperglycaemic state. Indeed, it has been proved to down-regulate the expression of glucose transporters and increase the mRNA expression of hepatic enzymes involved in glucose metabolism, accelerating its utilisation and disposal [159]. Finally, DNJ was demonstrated to improve insulin sensitivity and activate fatty acids β-oxidation *in vivo* [70]. In a previous research study, we demonstrated that *Morus* crude leaf extract contains besides DNJ other active constituents (kaempferol, quercetin, and chlorogenic acid) which together exert a potent antiglycative and dicarbonyls trapping activity. For this reason, the extract administration would benefit from the synergy of various components, and the combined effect may help to prevent long-term complications in diabetic patients. Bearing in mind the above-mentioned biological activities, mulberry due to the presence of the active metabolite DNJ can be regarded as one of the most promising functional foods for the management of DM. Unfortunately, DNJ systemic effects are impaired by its short half-life due to the high hydrophilicity and fast renal clearance. As it was previously reported, DNJ is quickly eliminated from the body by renal excretion [161]. For this reason, to reach the therapeutic dose a consistent intake by means of repeated administration is required. On the other hand, drug delivery technology allows to improve the biodistribution of therapeutic agents, enhancing the biological effect. In particular, the encapsulation of the molecules in specific polymers enables to control their release profile by means of the carrier chemical and physical features. The main aim of this work was to prolong the DNJ release by entrapment of mulberry crude extract in alginate (ALG). Among all the possible polymers, ALG was chosen since it is biocompatible and degradable, and it has been largely utilised as additive in foods as well as for drugs

entrapment in the pharmaceutical field [162–165]. Alginate is a generic name assigned to a series of unbranched polyanionic polysaccharides, composed by β-D-mannuronic acid (M) and α-L-guluronic acid (G) units, linked by a 1→4 glycosidic bonds [164]. Different relative ratios of G and M, and chain arrangements depend on the source of extraction of the natural polymer, typically marine brown algae [166]. One of the most convenient ALG features is the capacity to cross-link in water solutions ionotropically, by chelation of divalent cations (Ba^{2+}, Ca^{2+}, Mg^{2+}) from pendant carboxylic moieties. The cross-linking is generated when a divalent cation is coordinated by four guluronate units, thus introducing intermittent binding between the linear ALG chain. This peculiar behaviour is also known as ionic gelation, and it is actually one of the easiest ways for the encapsulation of bioactive agents [163,164]. As a matter of fact, water-soluble drugs are released by delayed diffusion from the cross-linked ALG network. Two different strategies were attempted, the first consisted in the development of Ca-ALG millimetric size particles (Ca-ALG beads), and the second was achieved by spray-drying a solution of Na-ALG and DNJ-rich mulberry extract (EXT) to obtain microparticles (SDMs).
Hence, the production of beads involves the cross-linking of ALG to form a reticulated structure, which was primarily selected to achieve an improved retention of DNJ. The spray-drying was employed as a direct method to encapsulate the active agent into polymeric microspheres, since it is a rapid, scalable, and one-step process. Both approaches were designed to be potentially applied in peroral delivery. To our best knowledge, there are no studies devoted to the formulation of Ca-ALG beads or ALG microparticles containing mulberry extract, as a novel therapeutic approach for hyperglycaemia. The main goal was to design and produce an ideal delivery system to maintain the intestinal DNJ concentration through the administration of the crude extract and prolong its bioactivity *in vivo.* Keeping in view the limited oral bioavailability of DNJ, in this study we monitored the release of the single compound, which is actually the crucial step and may undermine the effectiveness of the treatment. The two here presented techniques are simple and cost-effective. The experimental conditions were set up and optimized to achieve a standardised product. Mean size and distribution, morphology, drug loading, encapsulation efficiency, experimental yield, and release characteristics were determined for the two formulations and will be discussed below.

2. EXPERIMENTAL

2.1. Chemicals and solvents

Acetonitrile and ethanol (HPLC grade), ammonium formate (purity > 99.0%), calcium chloride, disodium hydrogen phosphate monohydrate, deuterium oxide (D_2O), DNJ reference standard (purity ≥ 95.0%), hydrochloric acid, 3-(trimethylsilyl)propionic-2,2,3,3-d_4 acid sodium salt (TSP) were provided by Merck Life Science S.R.L., (Milan, Italy). Sodium alginate (Na-ALG, high G/M ratio) was obtained from Honeywell Fluka (Charlotte, NC, USA). Water was purified by using a Milli-Q Plus185 system from Millipore (Milford, MA, USA).

2.2 Plant material and extraction of mulberry leaves

A mixture of leaves from different *Morus alba* (L.) cultivars was used to obtain a DNJ-rich extract. Mulberry leaves were provided by CREA-Research Centre for Agriculture and Environment, laboratory of sericulture (Padova, Italy). The harvest was made in the middle of the summer, when the DNJ content was higher, as was demonstrated by a previous study conducted by Marchetti and co-workers [167]. Leaves were dried in oven at 50 °C until reaching constant weight, and then ground in an automatic mill. The extraction was performed by dynamic maceration by placing 10 g of leaves with 500 mL 50% (v/v) ethanol at room temperature. The procedure required three consecutive extraction steps of 2 h each, the first and the second with 200 mL, and the last with 100 mL. The first extract was centrifuged for 5 min at 7200 g, paper-filtered, and further two extractions were performed on the residue. *Morus* leaves extracts were combined in a volumetric flask and brought to 500 mL with 50% (v/v) ethanol. The here described DNJ extraction procedure has been previously optimized and validated to achieve the best yield [167]. To obtain a stable solid product to be incorporated in beads, ethanol was evaporated under vacuum at 50 °C, and the remaining aqueous suspension was freeze-dried (Heraeus Lyovac GT2, Leybold GmbH, Cologne, Germany). To determine the DNJ concentration in the freeze-dried extract, it was dissolved in 50% (v/v) ethanol (1 mg/mL), filtered by 0.22 μm cellulose acetate filter (GVS, Bologna, Italy), and properly diluted with acetonitrile before the injection.

2.3. Determination of DNJ by HPLC-ESI-TQ-MS analysis

Samples were analyzed by an Agilent 6400 Series Triple Quadrupole. The LC system was equipped with a binary pump, an autosampler, an on-line degasser, and a thermostated column compartment (Agilent, Waldbronn, Germany). MassHunter (Agilent Technologies, Inc.) was

used for data acquisition and processing. The detection was performed using the ESI source operating in positive mode. The capillary voltage was set at +3500 V. The drying gas temperature was 300 °C; nitrogen was used as a drying (flow rate 9 L/min) and nebulizing gas (pressure 28 psi). A hydrophilic interaction liquid chromatography was performed on a HILIC Cortecs UPLC column (1.6 μm, 2.1 × 100 mm). 1-Deoxynojirimycin was eluted with a binary gradient consisting of 20 mM ammonium formate in water (A) and acetonitrile (B). The gradient profile was as follows: 0–10 min, 18% A; 11–16 min, 50% A; 16–27 min, 18% A. The flow rate was adjusted to 0.3 mL/min, and the column temperature was maintained at 25 °C. HPLC analyses were performed in triplicate. This method has been previously validated for linearity, precision, and accuracy. The method validation results are reported in paragraph "*3.2. HPLC-ESI-TQ-MS method validation"* of the second section of the present thesis Chapter.

2.4. Preparation of Ca-ALG beads

Two different batches of beads (Ca-ALG-2 % and Ca-ALG-3%) were obtained starting from 2 and 3% (w/v) Na-ALG aqueous solution respectively, degassed through an ultrasonic bath (Bandelin electronic GmbH, Berlin, Germany). The Ca-ALG beads were prepared by ionic gelation, according to the method proposed by Iannuccelli *et al.*, with some modifications [168]. To prevent the presence of ethanol in the final product, beads were loaded with freeze-dried extract, wherein the organic solvent has been completely removed. The loaded beads (EXT-Ca-ALG beads) were obtained by dissolving 100 mg of dry EXT into 5 mL of Na-ALG solution. A proper amount of dry EXT was dissolved also into 25 mL of $CaCl_2$ 2% (w/v) solution, to achieve the same concentration of DNJ as for ALG. Briefly, Na-ALG solution was dropped through a silicon tube (inner diameter 2 mm) from a height of 6 cm into $CaCl_2$ solution, under gentle magnetic stirring. The newly formed beads were left for 30 min in contact with the medium under stirring, then were recovered, washed with Milli-Q water, and dried at room temperature for at least 24 h. The occurrence and completed gelation in the inner bead core were checked under visual observation by slicing some of them. Blank beads were prepared in the same manner, without the introduction of the EXT. All the formulations were prepared in triplicate. The yield efficiency of the formulation process was calculated as follows:

$$Yield\ (\%) = \frac{Weight\ of\ the\ obtained\ beads}{(Weight\ of\ NaALG + Weight\ of\ EXT)}$$

2.5. Preparation of ALG microparticles by spray-drying (SDMs)

One hundred mL of 50% ethanolic EXT of mulberry leaves were mixed under gentle magnetic stirring with 100 mL of 2% (w/v) Na-ALG aqueous solution to obtain a final solution at the concentration of 1% of Na-ALG. The solution was degassed through an ultrasonic bath, and then spray-dried (Büchi 190 Mini-Spray Dryer, Büchi Labortechnik, Flawil, Switzerland) with the following operating conditions: inlet temperature, 140 °C; outlet temperature, 65-70 °C; pump flow, 3 mL min^{-1}; spray flow, 600 Nlh^{-1}; aspirator setting, 15; nozzle cap diameter, 0.5 mm. Unloaded SDMs (blank SDMs) were obtained under the same operating conditions starting from a 1% Na-ALG solution in water. All the formulations were prepared in triplicate. The yield efficiency of the formulation process was calculated as follows:

$$Yield\ (\%) = \frac{Weight\ of\ the\ obtained\ SDMs}{(Weight\ of\ NaALG + Weight\ of\ EXT)}$$

The weight of the EXT was calculated by considering the mean weight of the dry EXT obtained from the freeze-drying process.

2.6. Particle size analysis of Ca-ALG beads

The size of blank and loaded beads was obtained by analyzing the images captured by a digital camera. Bead diameters were measured by ImageJ free license software (National Institutes of Health, USA). ImageJ software was calibrated to transform the measure pixels in length units (mm) by measuring a caliper section. The relative frequency distribution of each sample was calculated, and the data were fit with a Gaussian equation on GraphPad Prism 8.4.3 (GraphPad Software, San Diego, CA). Being the diameters normally distributed, the homogeneity of the beads (polydispersity index, PDI) was calculated as follows:

$$PDI = \left(\sigma/_{d}\right)^{2}$$

Where σ and d represent the standard deviation and the mean diameter, respectively.

2.7. Particle size and morphology analysis of SDMs

The particle size of SDMs was determined with a laser diffractometer (Mastersizer hydro 2000 MU, Malvern Panalytical, Malvern, UK) by suspending about 20 mg of SDMs in 25 mL of isopropanol under magnetic stirring. The homogeneity was evaluated by calculating the span factor as follows:

$$Span = \frac{(d^{90} - d^{10})}{d^{50}}$$

Where d^{10}, d^{50}, and d^{90} represented the fine, the median, and the coarse particle fractions, respectively.

The morphological analysis was performed by Environmental Scanning Electron Microscopy (ESEM, Quanta 200, Fei, Hillsboro, Oregon, USA). Before the analysis, SDMs were placed in a desiccator overnight to remove any residual moisture. The loaded and blank SDMs were fixed on aluminum stubs using a double-side carbon type then vacuum coated with gold-palladium in argon atmosphere for 1 min (Sputter Coater Emitech K550, Emitech Ltd., Ashford, Kent, UK).

2.8. DNJ loading and encapsulation efficiency

To determine the amount of encapsulated DNJ in Ca-ALG beads and SDMs, 10 mg of each preparation were placed in 1 mL of 0.2 M HCl solution. After 24 h the suspension was mixed by vortex, diluted with ethanol, and analyzed by HPLC-ESI-TQ-MS, as described in paragraph 2.3. The actual drug loading (DL) and the encapsulation efficiency (EE%) were calculated with the following equations:

$$DL = \frac{Loaded\ DNJ\ (\mu g)}{Particle\ weight\ (mg)}$$

$$EE\ (\%) = \frac{Actual\ DL}{Theoretical\ DL}\ x\ 100$$

2.9. Fourier-transform infrared (FTIR) spectroscopy

The attenuated total reflectance-Fourier transform infrared (ATR-FTIR) spectra of Ca-ALG beads and SDMs (and relative blanks) were obtained using a Spectrum Two equipped with Universal ATR sampling accessory (Perkin Elmer, Milano, Italy). Beads were crushed in mortar to obtain a fine powder. The acquisition spectral range was 4000–450 cm^{-1} with 16 scans, and a resolution of 4 cm^{-1}.

2.10. Nuclear Magnetic Resonance (NMR) relaxometry

The interactions between DNJ and ALG were investigated by proton Nuclear Magnetic Resonance (^{1}H NMR) relaxometry. NMR relaxation measurement has been largely used for the study of molecules interactions and local motions. Two relaxation time constants (T_1 and $T_1\rho$) of DNJ protons were considered for this purpose. After a pulse, the spin-lattice relaxation time

(T_1) is the time constant for regrowth of longitudinal magnetization, namely along the direction of the main magnetic field (z axis). As a result, T_1 basically determines the rate at which a pulse sequence can be repeated. Instead, the spin-lattice in the rotating frame relaxation time ($T_1\rho$) is the time constant for the decay of magnetization along the radio frequency field of an applied spin locking pulse in the rotating frame. The value of $T_1\rho$ is measured by first applying a 90° radio frequency pulse to an equilibrium magnetization vector. A second pulse is then applied, which effectively locks the magnetization vector into the transverse plane (xy). During the spin locking pulse, the magnetization vector decays to its equilibrium value, with a time constant equal to $T_1\rho$. $T_1\rho$ is known to be more sensitive than T_1 to slow molecular fluctuations, typical of *in vivo* processes such as chemical exchange with macromolecules [169–171]. In order to assess whether a sort of interaction existed, the $T_1\rho$ values of DNJ were measured in absence and presence of ALG, in molar ratio 50:1. Afterwards, to gain more insight into the results, specific interaction constants between the ligand (DNJ) at different concentrations and the polymer (ALG) were calculated, according to the method proposed by Di Cocco *et al*.,[172]. In this regard, DNJ-ALG solutions were prepared by adding 1% (w/v) ALG to DNJ solutions in D_2O at different concentrations (4, 5, 10, 15, 20, 25 mM). The association constants (K_a) were determined following the evolution of DNJ relaxation times by increasing its concentration and keeping constant that of ALG. NMR experiments were carried out on a Bruker FT-NMR Avance III HD 600 MHz spectrometer (Bruker Biospin GmbH Rheinstetten, Karlsruhe, Germany), at 298 K and non-spinning. The chemical shift values were expressed in ppm relative to TSP. $T_1\rho$ relaxation times were measured by using the Bruker sequence "t1rho_esgp2d". The acquisition parameters were as follows: time domain (number of data points), 32 K; dummy scans, 4; number of scans, 16; pulse width, 12.03 μs (90°); acquisition time, 2.50 s; delay time, 5 s; spectral width, 11 ppm (6602 Hz), fid resolution 0.40 Hz; digitization mode, baseopt. Total acquisition time was 32 min and 30 s. A total of 14 values for τ from 10 ms to 6 s were employed for the calculation. ^{1}H-NMR experiments for the measurement of T_1 were acquired using the Bruker sequence "t1ir_pr", with presaturation of residual water signal. The acquisition parameters were as follows: time domain (number of data points), 128 K; dummy scans, 0; number of scans, 4; pulse width, 11.84 μs (90°); acquisition time, 4.96 s; delay time, 5 s; spectral width, 22 ppm (13204 Hz), fid resolution 0.2 Hz; digitization mode, baseopt. Total acquisition time was 7 min and 42 s. Spin–lattice relaxation times were measured by inversion-recovery pulse sequence (180° – τ – 90°) and fitted by exponential regression analysis of the recovery curves of longitudinal magnetization components. A total of 8 values for τ from 100 μs to 20 s were employed for the calculation.

2.11. Ca-ALG beads swelling study

The water absorption behaviour of Ca-ALG beads was studied gravimetrically [173]. The pre-weighed beads (approximately 100 mg) were placed in simulated gastric fluid (HCl solution, pH 3) and 0.1 M phosphate buffer saline (PBS, pH 6.8) under sink conditions at 37 °C. The beads were taken out at fixed time intervals and wiped superficially to remove weakly bound surface water, then accurately weighed, and put again in the swelling media. All the experiments were carried out in triplicate. The dynamic weight change (%) of the beads was determined according to the following expression:

$$Weight\ change\ (\%) = \frac{Ws - Wi}{Wi}\ x\ 100$$

Where Ws is the weight of the beads in the swollen state and Wi is the initial weight.

2.12. In vitro release of DNJ

The release of DNJ from the different formulations was investigated in sink conditions in gastrointestinal simulated fluids. Regarding DNJ release from Ca-ALG beads, approximately 40 mg were placed into 4 mL of HCl solution (pH 3) under magnetic stirring at 37 °C, and after 2 h the beads were paper filtered and placed in 4 mL of 0.1 M PBS (pH 6.8), for further 3 h under continuous stirring. With regard to SDMs, an aliquot of 40 mg was placed into a dialysis membrane (cut off 12,000/14,000 Da), and immediately soaked in 10 mL of HCl solution (pH 3.0) under magnetic stirring (100 rpm) at 37±0.5 °C. After 2 h, the dialysis membrane was moved into 10 mL of PBS (pH 6.8) for further 3 h, under stirring at 37±0.5 °C. For both the release studies, sample solutions were withdrawn at fixed time intervals and the initial volume was restored with fresh medium. The solutions were properly diluted with the mobile phase and analyzed by HPLC-ESI-TQ-MS. The experiments were performed in triplicate on different batches.

2.13. Statistical analysis

Significant differences within groups were determined at $P < 0.05$ using Student's t-test and one-way analysis of variance (ANOVA) followed by Tukey's Post Hoc test. All the analyses were accomplished using GraphPad Prism 8.4.3 (GraphPad Software, San Diego, CA).

3. RESULTS AND DISCUSSION

In this work, a novel approach for the sustained release of the mulberry main active constituent was attempted by means of ALG particles. Due to its antidiabetic potential, DNJ has attracted much attention for use as functional food or medical supplement to control postprandial hyperglycaemia, and type 2 DM at its early stage. The main goal was to develop a delivery system able to entrap the compound and retard its release in the gut, where it could directly act as glucosidase inhibitor and reach the circulation to exert systemic effects. Encapsulation of small hydrophilic molecules poses a big challenge and often leads to poor results in terms of entrapment efficiency and undesired release profile. We tried to overcome these issues by using ALG, which besides being well-tolerated and biocompatible may benefit from electrostatic interactions with DNJ, resulting in an improved retention of the compound. Two differently sized drug carriers were designed and developed, and their release characteristics were compared. Millimetric Ca-ALG beads were selected for their low surface area-to-volume ratio, which can reduce the release of small hydrophilic drugs [174]. Conversely, micrometric SDMs were taken into account for their easy production and scalable technology at the industrial level. As a matter of fact, spray-drying technology is rapid, continuous, highly reproducible, and allows the obtainment of a product with low moisture content. The polymer ALG was selected with a high G/M ratio. Indeed, the specific G conformation guarantees a high degree of coordination of bivalent ions, leading to the formation of a more rigid gel. As a consequence, the particles composed of guluronic-rich alginates might result in more effective systems for the controlled diffusion release [175,176].

3.1. Determination of DNJ by HPLC-ESI-TQ-MS analysis

Due to the shortest time of analysis and highest sensitivity HILIC coupled with mass spectrometry (MS) has proven to be one of the most recommended methods for DNJ determination [90,91,167]. The transition of the intense molecular ion (*m/z* 164.09) to the product ions (*m/z* 146.08, 128.07, 110.06) for subsequent losses of water molecules (18 Da), was used for selective DNJ detection. This quantitative approach was based on multiple reaction monitoring (MRM). The quantification of DNJ in samples was obtained by external standard method. The calibration curve was built analyzing six concentrations of the reference compound in the range 0.005–0.5 μg/mL. In our experimental conditions, DNJ retention time was 4.50 min. Figure 1 shows the MRM chromatogram of mulberry leaf ethanolic EXT and the related ESI-MS spectrum.

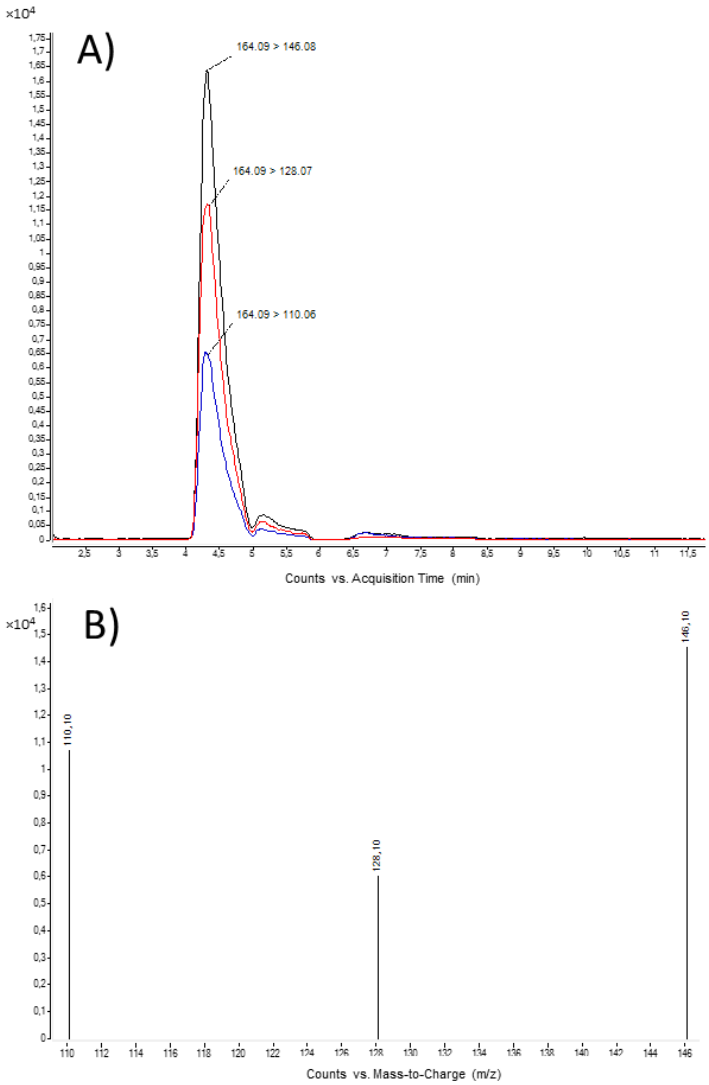

Figure 1. An overlay of MRM transitions monitored for DNJ (A) and the related ESI-MS spectrum (B) from mulberry leaf extract.

The amount of DNJ in the ethanolic EXT was 15.93±0.19 μg/mL, and 1.93±0.04 mg/g in the freeze-dried product. The dry product yield of the freeze-drying process was 4.50±0.52 mg/mL.

3.2. Particle size, morphological analysis, and DNJ content

The particle size and drug content parameters of Ca-ALG beads and SDMs are reported in Table 1. DNJ content is expressed as entrapment efficiency (EE%) and drug loading (DL).

Table 1. Particle size, homogeneity, yield, entrapment efficiency (EE%), and drug loading (DL) of Ca-ALG beads and SDMs.

Formulation	Size	Size distribution		Yield (%)	EE (%)	DL (μg/mg)
		PDI	SPAN			
Blank Ca-ALG-2% beads	1.30±0.19 mm	0.020±0.006	–	72.48±2.01	–	–
EXT-Ca-ALG-2% beads	1.10±0.16 mm	0.020±0.008	–	76.31±1.78	54.0±0.41	0.52±0.02
Blank Ca-ALG-3% beads	1.55±0.15 mm	0.021±0.041	–	88.54±2.58	–	–
EXT-Ca-ALG-3% beads	1.51±0.21 mm	0.010±0.002	–	91.64±1.15	55.2±0.30	0.43±0.04
Blank SDMs	11.18±5.98 μm	–	3.73±0.15	65.05±3.45	–	–
EXT-SDMs	80% 10.55±5.10 μm 20% 52.78±11.28 μm	–	7.80±1.57	66.70±2.51	98.56±3.47	0.63±0.02

Data are expressed as mean ± SD of three independent experiments. PDI, polydispersity index.

Ca-ALG beads had spherical geometry with a diameter ranging from 1.10±0.16 to 1.55±0.15 mm in the dried state. As previously reported, many factors may influence the formation, particle size, and properties of ALG particles obtained by ionotropic gelation. Particle size is positively correlated with ALG concentration, cross-linking time, and needle/tip diameter of the dripping system as well [163,177,178]. Conversely, dimensions are negatively correlated with stirring speed and $CaCl_2$ abundance, due to a more rigid gel network and a greater electrical conductivity in presence of a higher concentration of the cross-linking agent [165,179–181]. A quite good size homogeneity was observed for Ca-ALG beads, as indicated by the PDI values lower than 0.1, which implies a monodisperse population of particles. Both 2 and 3% blank Ca-ALG beads showed a slightly higher mean diameter than their respective loaded formulation. Nonetheless, beads size homogeneity was not significantly affected ($P < 0.05$) by the addition of the extract, maintaining the narrow distribution for both the concentrations (Table 1). No significant difference in size was observed either between 2 and 3% Ca-ALG beads, suggesting that the small variation in ALG concentration did not result in a remarkable increase in dimensions. With a view to achieving the maximum efficiency in DNJ encapsulation, dry EXT was added also in $CaCl_2$ solution in the same proportion as for ALG solution [182]. However, due to the extremely high-water solubility, hydrophilic nature, and low molecular weight, DNJ has shown a quite low EE (%) in the case of beads. A critical loss of compound could be caused by the final washing step to remove the excess of cross-linking agent [163,183]. Furthermore, DNJ might be lost during the drying process, when the water incorporated in the gelled beads was removed, and partially absorbed on filter paper. In the case of Ca-ALG-3% beads, a higher EE% was found ($P < 0.05$) owing to the higher concentration of Na-ALG employed in the

formulation process. Indeed, the increase of ALG concentration provided a greater availability of binding site for Ca^{2+} ions, leading to the formation of a more compact gel membrane with smaller pore size [165]. As a consequence, the leak of DNJ during the formulation process was moderate [184,185]. At the same time, the higher ALG concentration has led to the lowering of DL from 0.52±0.02 to 0.43±0.04 μg/mg, in Ca-ALG-3% and 2% beads, respectively ($P < 0.05$). The morphological analysis confirmed the circularity of the beads and highlighted some differences on the surface structure mainly depending on polymer concentration in the blank formulations. Indeed, the particle surface of blank-Ca-ALG-2% appeared roughed and more fibrous than blank-Ca-ALG-3%. The encapsulation of the EXT seemed to confer a more compact texture (Figure 2).

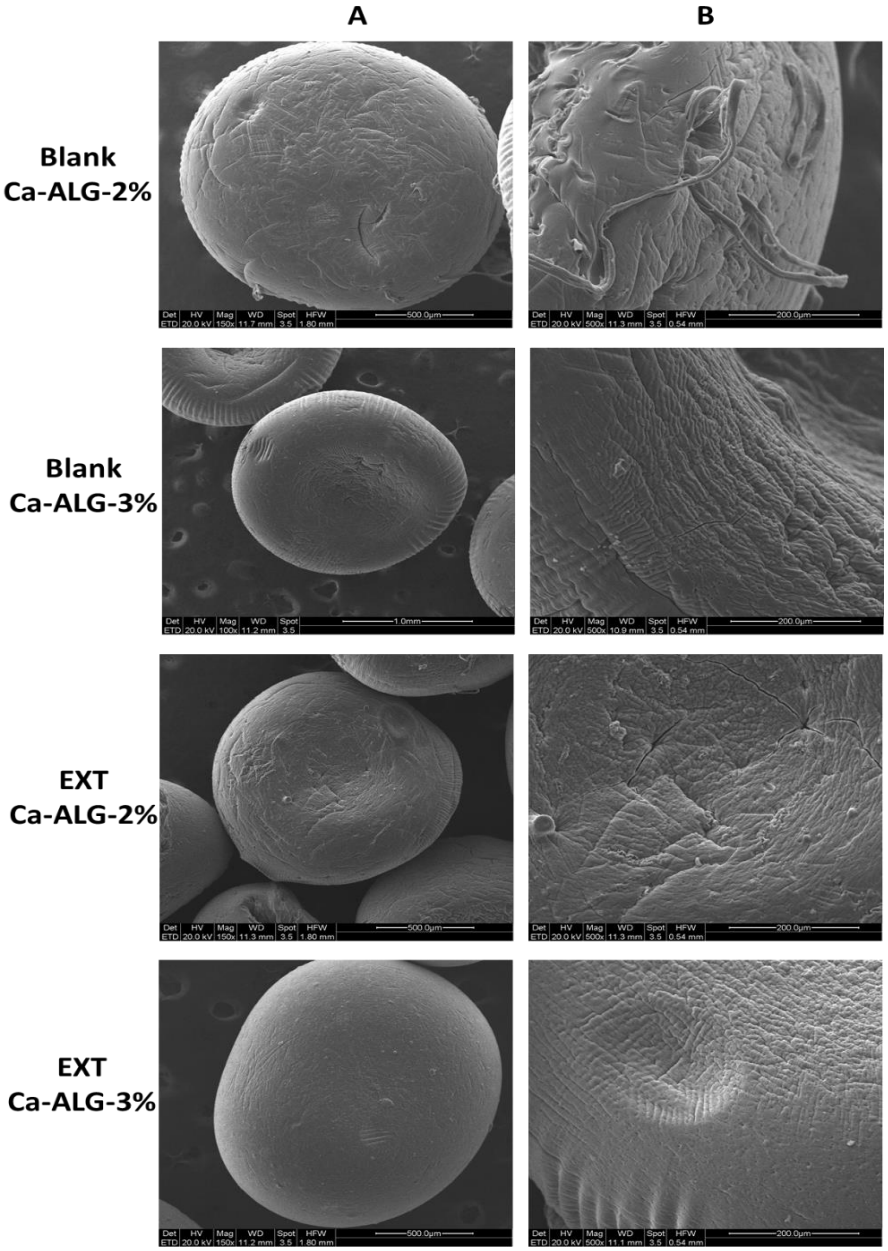

Figure 2. ESEM micrograph of blank and EXT-loaded ALG-beads 2 and 3% at 150x (A) and 500x (B) magnification.

Regarding the SDMs, the yield resulted quite low, around 60%. Indeed, the conventional spray-dryer at laboratory scale has been reported to be not very satisfactory due to the loss of particles onto the walls of the drying chamber and cyclone [186]. The blank SDMs exhibited a monodisperse population with a low span value. Conversely, SDMs showed a bimodal distribution (Table 1), with the smaller size (10.55±5.10 μm) which was the most abundant (approximately 80%). This evidence may be attributable to an increased propensity of particles to form agglomerates in presence of crude EXT, due to natural occurrence of sugars, glycosides, and other sticky components [187,188]. As it was previously pointed out, microparticles incapsulating plant extracts usually tended to establish bridges to connect to each other by absorbing moisture from the environment. Moreover, agglomeration can take place from the collision of particles during drying, which may result in the co-existence of smaller and larger particles [188]. The non-homogeneity of SDMs was also highlighted by the ESEM analysis (Figure 3). Some morphological differences were observed between blank SDMs (Figure 3A) and SDMs (Figure 3B).

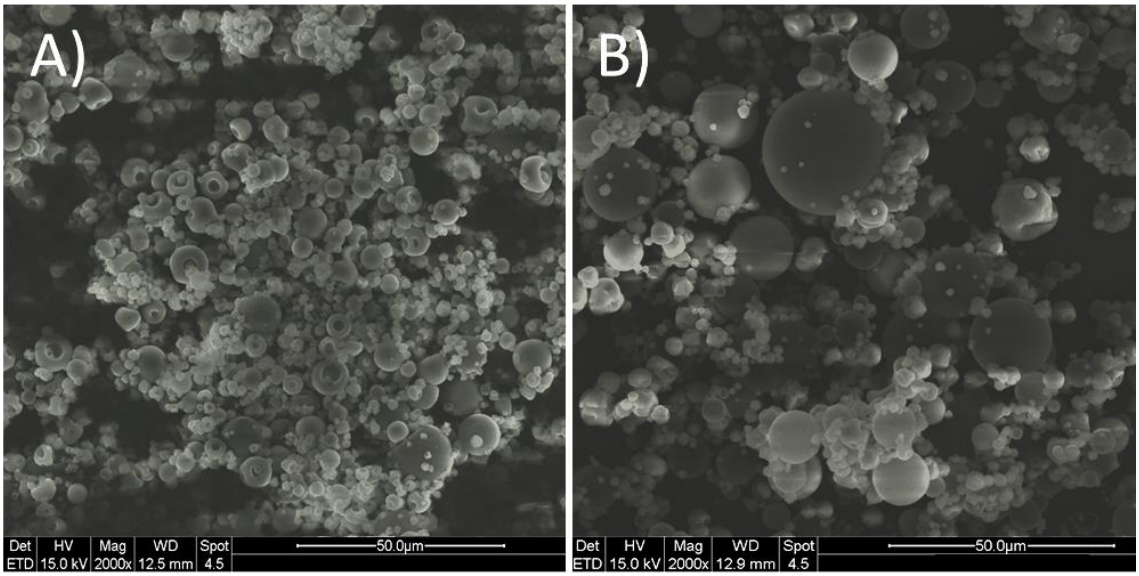

Figure 3. ESEM micrograph of blank SDMs (A) and SDMs (B) at 2000x magnification.

Loaded microparticles (EXT-SDMs) displayed a spherical shape and smooth surface. Conversely, some of the blank SDMs have collapsed or appeared as dimpled spheres. According to the hypothesis proposed by Ameri *et al*., the formation of a polymer film at the external surface of the droplet during the initial drying phase caused by the rapid evaporation of solvent may explain the presence of dimples. The further increase in the concentration of the polymer at the surface could hamper the water diffusion to the periphery of the droplet and cause a build-up of vapour pressure inside the particle. Finally, the burst of the film would result

in dimples or drilled particles [189]. Regarding the encapsulation of DNJ in SDMs, the efficiency was higher than 80%, suggesting that the ratio between polymer and EXT, and the spray-drying parameters were optimal [190]. The DL of SDMs was significantly higher ($P < 0.01$) than beads DL. Notwithstanding SDMs exhibited an EE% two-fold higher (98.55±3.47%), the DL was of the same order of magnitude of those of beads. This fact may be explained given that the preparation of SDMs involved the use of the ethanolic EXT, with a lower total amount of DNJ, which was directly employed, without preliminary concentration by freeze-drying. Therefore, the ratio between DNJ and ALG in SDMs was lower than in Ca-ALG beads.

3.3. Fourier-transform infrared (FTIR) spectroscopy

The ATR-FTIR spectra of mulberry leaf EXT, Ca-ALG beads, SDMs and relative blanks were recorded and are displayed in Figure 4. Since no differences between Ca-ALG-2 and -3% were recorded, only the spectra of Ca-ALG-2% beads were reported. The spectrum of the raw EXT showed several broad peaks, mainly ascribable to functional groups of phenolic acids and flavonoids. Specifically, the spectral bands at 3274, 1038, and 990 cm^{-1} were representative of O−H and C−O stretching of alcohols, while the peaks at 1367 and 1272 cm^{-1} were induced by phenol O−H bends and secondary O−H in-plane bend respectively. Finally, the signals at 1722 and 1580 cm^{-1} were attributable to C=O bond of carboxylic and carbonylic groups of ketones or esters [191,192]. As concerns the unloaded SDMs and the unloaded Ca-ALG beads, the main signals around 3258, 1604, 1412, and 1028 cm^{-1} were induced by stretching vibrations of O−H, C=O (symmetrical and asymmetrical) of carboxylate groups, and C−O−C bond respectively [162]. These spectra resulted similar with slight shifts of about 20 cm^{-1} at lower wavelengths in the case of Ca-ALG beads for the hydroxyl and carbonylic vibrations. The shifts were caused by the interaction of these functional groups with calcium ions [162,193]. The loading of the EXT into both Ca-ALG beads and SDMs did not change the IR spectra of the polymer, and the typical signal bands of the EXT were not detected. This evidence was previously reported by Bagheri *et al*. [162] and corroborates the encapsulation of the EXT successfully took place.

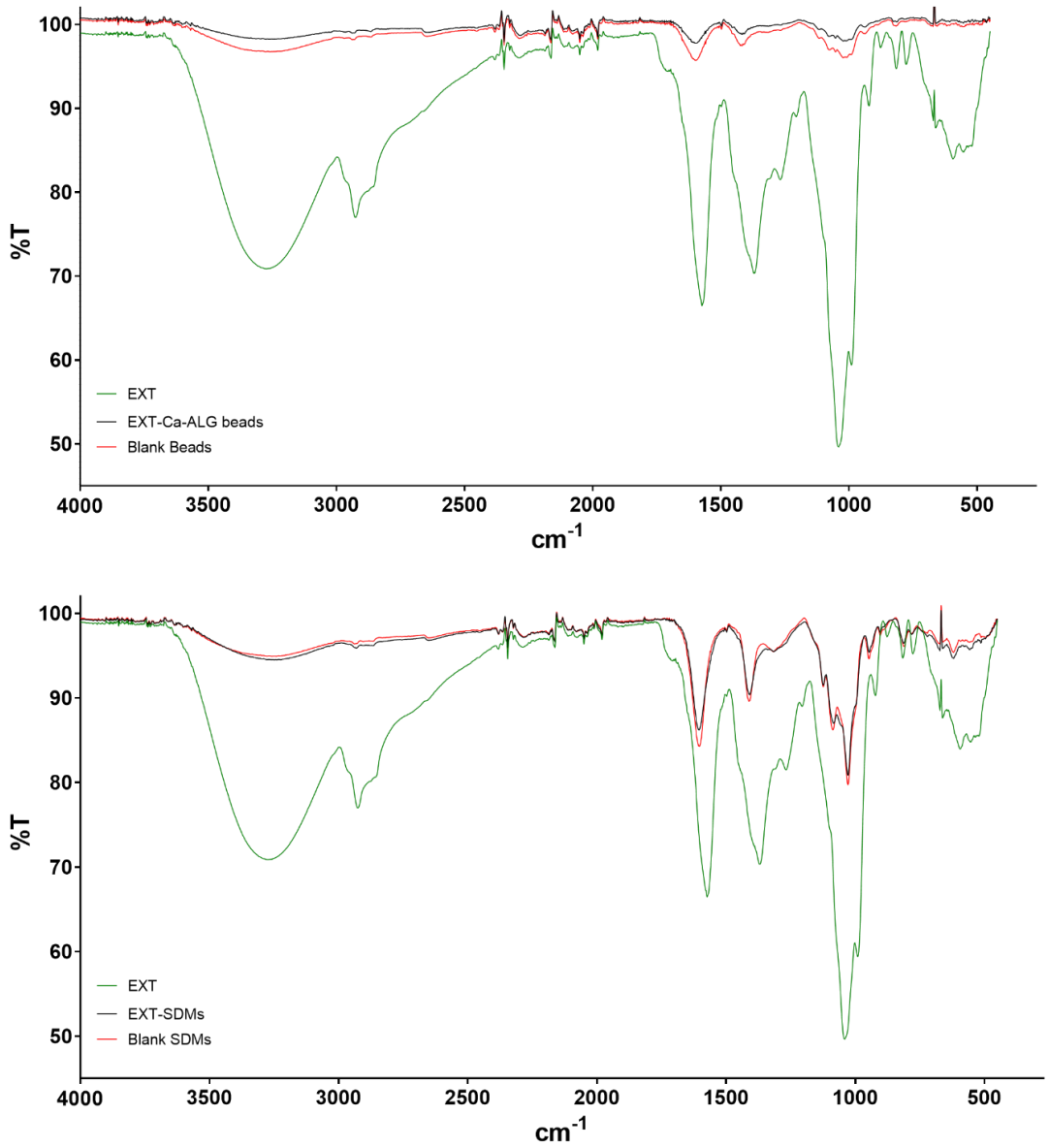

Figure 4. FTIR spectra of mulberry extract (EXT), blank, and EXT loaded Ca-ALG-2% beads (top) and SDMs (bottom).

3.4. Interaction study by NMR relaxometry

This study was carried out to in-depth investigate the nature of the interaction between DNJ and ALG. In particular, the monitoring and measurement of spin–lattice relaxation rates can provide information about ligand mobility in presence or absence of the macromolecule [172,194,195]. ^{1}H NMR chemical shifts, signal multiplicity, and assignments of DNJ are reported below in Figure 5 and Table 2.

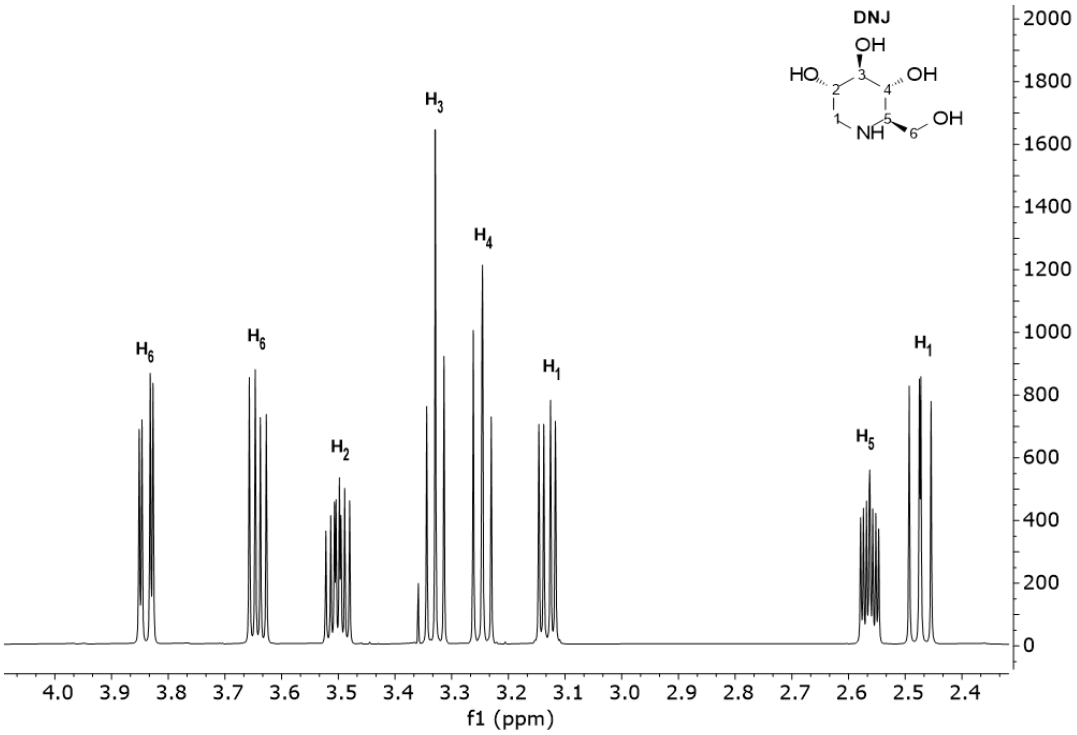

Figure 5: ^{1}H NMR spectrum and assignments of DNJ in deuterium oxide (D_2O). Chemical shifts are related to TSP.

Table 2. ^{1}H NMR assignments, chemical shifts, and signal multiplicity for DNJ in deuterium oxide.

DNJ Assignment	δ (ppm)	Multiplicity	*J* (Hz)
H_1	2.47	dd	10.80, 12.50
H_1	3.13	dd	5.05, 12.36
H_2	3.50	m	–
H_3	3.33	t	9.14
H_4	3.24	t	9.50
H_5	2.56	m	–
H_6	3.64	dd	6.23, 11.64
H_6	3.84	dd	2.90, 11.60

Table 3. Spin–lattice relaxation time in the rotating frame ($T_1\rho$) of DNJ protons in absence and presence of alginate.

DNJ	$T_1\rho$ $_{DNJ}$ (s)	$T_1\rho$ $_{DNJ + ALG}$ (s)	Δ (s)
H_1	0.535	0.440	0.095
H_1	0.663	0.530	0.133
H_2	1.760	1.390	0.370
H_3	1.810	1.430	0.380
H_4	1.801	1.401	0.400
H_5	0.963	0.640	0.323
H_6	0.679	0.548	0.131
H_6	0.680	0.517	0.163

As can be seen from Table 3, the presence of ALG caused a remarkable decrease in the $T_1\rho$ values of DNJ protons, especially for H_2, H_3, H_4 and H_5. This decrease is indicative of the reduction in the mobility of the small molecule [196,197], suggesting the formation of electrostatic interactions, hydrogen bonding or other weak intermolecular forces between DNJ protons and carboxyl groups of ALG. Once established that the interaction occurred, NMR was further employed for the determination of binding constants, according to the method proposed by Di Cocco *et al*., [172].When a ligand (L) interacts with a macromolecule (M) an equilibrium occurs, and it is expressed by the following equation:

$$L + M \rightleftarrows LM$$

If the complex is held together by weak intermolecular forces the equilibrium constant is defined as association constant (K_a) and the product has chemical characteristics which still strongly resemble the unassociated (or free) molecules. K_a can be obtained as:

$$K_a = \frac{[LM]}{[L][M]}$$

Where [L],[M], and [LM] are the molar concentrations of the free ligand, macromolecule and complex, respectively.

Relaxation rate (R) is the reciprocal of T_1, and it is the NMR experimental parameter that best explains the dynamic coupling between L and M. The experimentally determined relaxation rate of the ligand in presence of the macromolecule (R_{obs}) can be expressed as:

$$R_{obs} = p_f R_f + p_b R_b$$

p_f: fraction of the free ligand
p_b: fraction of the associated ligand
R_f: Relaxation rate in the free state
R_b: Relaxation rate in the associated state

Assuming that the fraction of the free ligand is far higher than that of the associated form (p_b <<<1), and taking pb + p_f = 1:

$$\Delta R = R_{obs} - R_f \cong p_b R_b \quad (1)$$

The association constant K_a can be expressed as:

$$K_a = \frac{[LM]}{[L][M]} = \frac{[LM]}{[L]([M_0] - [LM])} \quad (2)$$

$$[LM] = \frac{K_a[L]M_0}{1 + K_a[L]} \quad (3)$$

Where $[M_0]$ is the initial concentration of the macromolecule

Since p_b is the fraction of the associated ligand, then:

$$p_b = \frac{[LM]}{[L] + [LM]} \cong \frac{[LM]}{[L]} \tag{4}$$

Finally, by substitution of (3) in (4) and then in (1), the following equation is obtained:

$$\frac{1}{\Delta R} = \left(\frac{1}{K_a} + [L]\right)\frac{1}{R_b[M_0]} \tag{5}$$

The last equation (5) shows a linear relationship for $1/\Delta R$ and [L]. In practice, T_1 values were measured at different DNJ concentration (4-25 mM) in absence and presence of ALG (1% w/v). Then the difference between the reciprocal of T_1 was calculated (ΔR). The value ($1/\Delta R$) was then plotted versus DNJ concentrations, and a linear regression was obtained for each proton. For $1/\Delta R = 0$, $-1/ K_a$ was extrapolated. Data are reported in Tables 4-5.

Table 4. Spin–lattice relaxation times (T_1) of DNJ protons in absence and presence of ALG.

DNJ (mM)	T_1 H_1 2.47 ppm (s)		T_1 H_1 3.13 ppm (s)		T_1 H_2 3.50 ppm (s)		T_1 H_3 3.33 ppm (s)		T_1 H_4 3.24 ppm (s)		T_1 H_5 2.56 ppm (s)		T_1 H_6 3.64 ppm (s)		T_1 H_6 3.84 ppm (s)	
	DNJ	DNJ + ALG	DNJ	DNJ + ALG	DNJ	DNJ + ALG	DNJ	DNJ + ALG	DNJ	DNJ + ALG	DNJ	DNJ + ALG	DNJ	DNJ + ALG	DNJ	DNJ + ALG
4	0.671	0.545	0.781	0.597	2.422	1.438	2.505	1.934	0.818	0.523	1.468	1.048	0.827	0.618	2.542	1.742
5	0.670	0.538	0.784	0.560	2.382	1.346	2.501	1.837	0.817	0.523	1.469	0.963	0.820	0.592	2.533	1.569
10	0.662	0.559	0.771	0.604	2.337	1.532	2.440	2.036	0.806	0.579	1.432	1.061	0.808	0.630	2.463	1.810
15	0.666	0.580	0.774	0.607	2.347	1.607	2.459	2.075	0.811	0.597	1.435	1.071	0.814	0.637	2.468	1.861
20	0.661	0.584	0.770	0.605	2.324	1.739	2.431	2.124	0.806	0.616	1.422	1.080	0.806	0.650	2.440	1.893
25	0.654	0.584	0.760	0.637	2.212	1.780	2.323	2.090	0.794	0.669	1.403	1.070	0.787	0.695	2.386	1.860

Table 5. Association constants (K_a) of DNJ protons, obtained from the difference of spin-lattice relaxation time (T_1) values in absence and presence of ALG.

	$1/\Delta R$ (s^{-1})							
DNJ (mM)	H_1 2.47 ppm	H_1 3.13 ppm	H_2 3.50 ppm	H_3 3.33 ppm	H_4 3.24 ppm	H_5 2.56 ppm	H_6 3.64 ppm	H_6 3.84 ppm
4	2.900	2.534	3.539	8.485	1.450	3.663	2.445	5.535
5	2.730	1.960	3.095	6.919	1.453	2.796	2.129	4.123
10	3.600	2.789	4.448	12.297	2.056	4.095	2.860	6.827
15	4.492	2.813	5.097	13.288	2.262	4.222	2.929	7.567
20	5.040	2.823	6.900	16.819	2.613	4.491	3.358	8.444
25	5.420	3.936	9.114	20.837	4.260	4.508	5.945	8.437
$-1/K_a$	-17.646	-28.406	-7.098	-8.365	-6.609	-49.466	-9.198	-23.948
K_a	57	35	141	120	151	20	109	42

It is generally accepted that NMR based determinations of K_a are only reliable if in the range 10-10^4 M^{-1} [196]. The here obtained values of K_a were all within the acceptability range and consistent with those from another interaction study between ALG and different amino acids, which closely resemble DNJ from a chemical point of view [172]. The highest interaction constants were obtained for H_6 (109 M^{-1}), H_3 (120 M^{-1}), H_2 (141 M^{-1}), and H_4 (151 M^{-1}). Based on these results we may conclude that a specific interaction involved the above mentioned DNJ protons and ALG, due to the most significant decrease in the observed relaxation times. Data related to T_1 measurements (Table 5) agree also with the $T_1\rho$ values experimentally determined and above reported in Table 3. As a matter of fact, DNJ is a basic iminosugar (pKa 8.06) that might be electrostatically bonded to the carboxylic groups of guluronic and mannuronic acids. This electrostatic interaction may contribute to the stabilization of the EXT loaded particle and achieve the prolonged release of the active compound, regulated by a dynamic equilibrium of dissociation from the polymer.

3.5.Ca-ALG beads swelling study

Since beads are formed by a characteristic crosslinked ALG matrix, in order to use them as oral dosage form, they should be investigated for their swelling behavior in simulated gastric and intestinal fluids. For this reason, the swelling study of Ca-ALG beads was performed under the same conditions as the *in vitro* release. During the swelling study, two distinct mechanisms occurred. The first consisted of the hydration of the hydrophilic groups of ALG [198], as a consequence of the water penetration through the bead surface and the filling of the pores among the polymer chains. The second mechanism was related to the Ca^{2+} exchange with Na^+ ions present in the environment, as was the case of simulated intestinal fluid. The swelling ratio of the beads was heavily dependent on the pH and ionic strength of the solution in which the bead was placed, as is clearly visible in Figure 6. The beads placed in simulated gastric fluid (HCl solution, pH 3) moderately increased the weight (around 40-45%), reaching the maximum swelling in approximately 60 min (Figure 6). All the formulations exhibited more significant swelling rates when placed in simulated intestinal fluid (PBS, pH 6.8). Here, the beads showed an initial water uptake in the first 60 min, then they began to lose weight as a result of the progressive external erosion, probably due to the dissolution of alginate chains induced by ion exchange. The former water uptake was mainly related to the exchange between Na^+ and Ca^{2+} ions bound to external polymannuronate sequences [199]. When Ca^{2+} ions are replaced, the polymer chains undergo a relaxation, leading the beads to swell along with water absorption. The second massive water uptake (from 90-120 min until the end) prevailed over the erosion,

and involved this time the exchange of Na^+ from the medium with Ca^{2+} ions linked with carboxylic groups of the inner polyguluronate units, as previously described by Bajpai and co-workers [199]. In the light of the above, the presence of Na^+ in the environment is responsible to a greater extent for the swelling process and the subsequent degradation of the beads, which actually did not occur during the 120 min exposure to hydrochloric acid solution. The results suggest that the dried beads may swell slightly in the gastric environment and then they possibly undergo a significant water uptake in the upper intestine. This behavior indicates that the beads are stable in the acidic medium, being able to release the entrapped amount of active compound in the gut for a longer duration. One-way ANOVA and Tukey's Post Hoc test highlighted significant differences among all the samples at 180 min in the simulated intestinal fluid ($P < 0.01$). Specifically, the highest swelling degree was obtained for Ca-ALG-3% beads, thus indicating that the concentration of the polymer was positively correlated with an increased relaxation of the ALG chains. On the other hand, in EXT-Ca-ALG beads the overall swelling was significantly reduced ($P < 0.0001$), supporting the hypothesis that the electrostatic interaction between ALG and DNJ may stabilize the structure by hardening polymer chains.

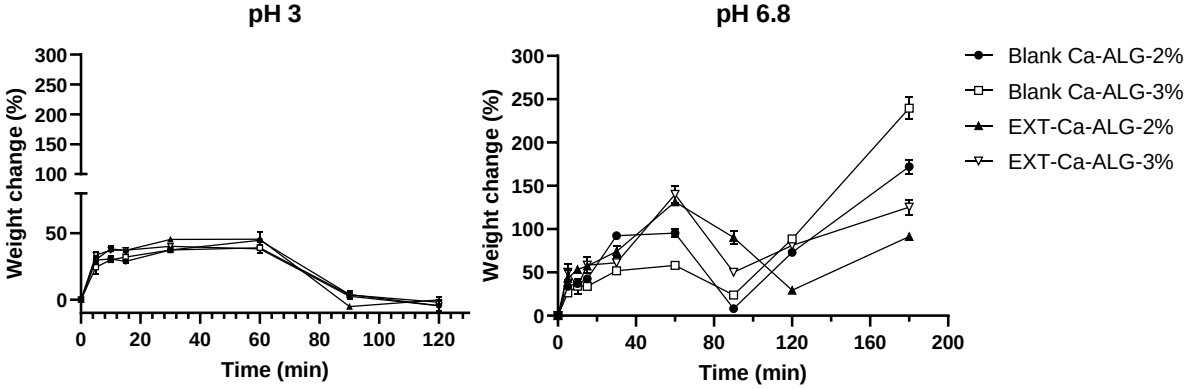

Figure 6. Dynamic uptake of water for blank and EXT loaded Ca-ALG beads, in simulated gastric (pH 3) and intestinal (pH 6.8) fluid. Data are shown as means ± SD of three independent experiments.

3.6. In vitro release of DNJ

The release of DNJ from Ca-ALG beads and SDMs was investigated in gastrointestinal simulated fluids (Figures 7-8). Thus, the release was monitored for 2 h in pH 3 medium, and then in pH 6.8 PBS for further 3 h. The pH of the aqueous media was selected to mimic the post-prandial conditions of the gastrointestinal tract. In the case of Ca-ALG beads, a burst effect was observed in the first 10 min upon contact with gastric fluid, reaching 28.31±3.83 and 36.20±6.02% of the cumulative release for 3% and 2% ALG concentration, respectively. These differences were not significant at $P < 0.05$. The initial release of DNJ from Ca-ALG-3% beads

was slightly faster than Ca-ALG-2% beads, even though higher ALG concentrations have generally been reported to be more effective in retarding drug release [200–202]. This initial rapid release was probably caused by the fast permeation of water among the polymer chains observed during the swelling studies. Thus, the DNJ absorbed onto the outer polymer chains via electrostatic interaction quickly dissolved in the external medium [177]. Subsequently, the DNJ release in acidic conditions was slow and constant extending up to 2 h, which is the approximate residence time in the stomach. Since the swelling of Ca-ALG beads in acidic conditions only occurred to a minor extent, DNJ was likely released by diffusion from the insoluble matrix [203]. Conversely, the DNJ release in the intestinal fluid was expected to be induced by the complex process "swelling-dissolution-erosion" [203]. Indeed, in the intestinal fluid, Ca^{2+} was replaced in exchange for Na^{+} from the environment, and as a result the beads visibly lost their compact shape after 60 min, being readily degraded. This fact is also confirmed by the significant loss of weight recorded during the swelling studies. Interestingly, even though the progressive disintegration and solubilization of the beads occurred, the DNJ concentration did not increase over the 27.27±6.31 and 36.51±6.49% for Ca-ALG-2% and Ca-ALG-3% beads, respectively. Considering that DNJ is an extremely high soluble compound with a small chemical structure, its low free concentration might be explained by the strong interaction with the polymer demonstrated by the NMR studies.

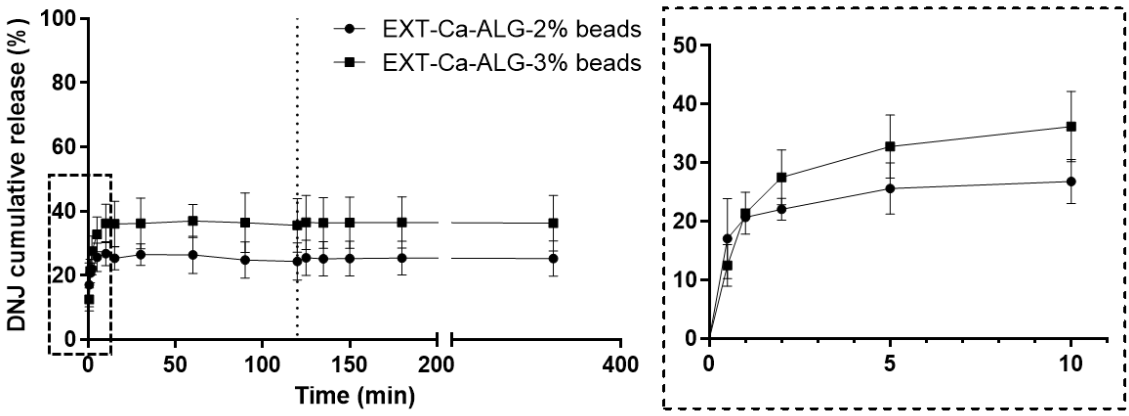

Figure 7. *In vitro* DNJ release from ALG beads in gastric (0-120 min) and intestinal (120-360 min) simulated fluids. Data in graphs are shown as mean ± SD of three independent experiments. The enlargement of the dotted-line area shows the release profile in the first minutes.

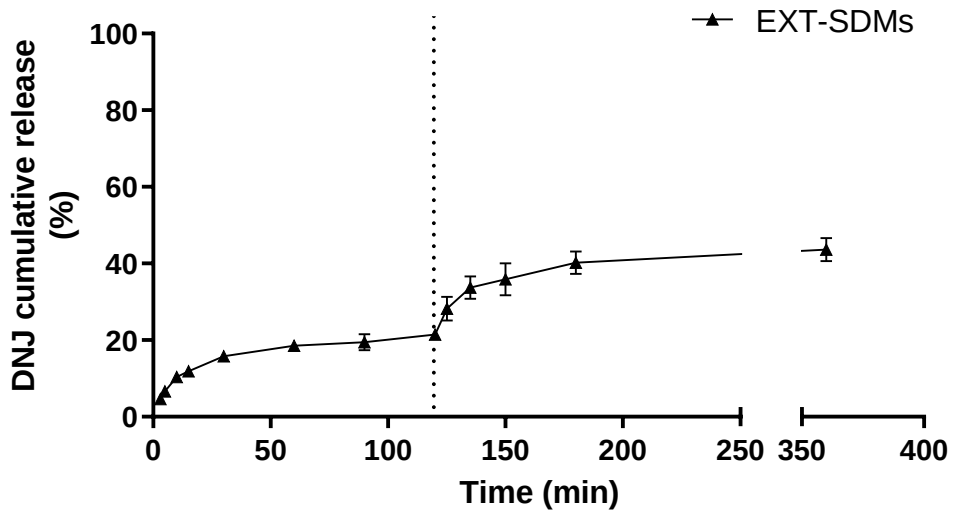

Figure 8. *In vitro* DNJ release from ALG SDMs in gastric (0-120 min) and intestinal (120-360 min) simulated fluids. Data in graphs are shown as mean ± SD of three independent experiments.

In light of the evidence observed during the DNJ release from the beads, the *in vitro* release was performed also for SDMs under the same conditions. In this case, the DNJ release was carried out by using the dialysis bag to avoid the withdrawal of the microparticles from the aqueous media. By comparing the two different profiles in Figure 7 and 8, it was evident that the encapsulation by calcium cross-linking of ALG did not play a central role in delaying the release of the active compound. Ordinarily, the release of drugs from Na-ALG is related to the solubility of the drug and the polymer, the polymer concentration, and the interaction between them [204]. The main factor involved in controlling the DNJ release from SDMs seemed to be the interaction between the polymer and the iminosugar. Furthermore, the pH of the solvents might have played a central role in controlling the release of DNJ. As a matter of fact, depending on the pH, Na-ALG might undergo to structural changes. In acidic conditions (pH < 5) the carboxylic groups are protonated, converting ALG to alginic acid, and leading to the formation of a high viscous solution [205]. During the release experiments at pH 3, the SDMs progressively dissolved in the media creating a viscous gel which caused the molecule to diffuse slowly [206]. The cumulative percentage increased gradually from 4.63±1.45 to 19.46±2.08% in simulated gastric fluid. A faster release profile, likely caused by the DNJ located onto the surface of SDMs, was observed in the initial 30 min of the gastric simulation, reaching then a first plateau until the end (120 min). These results highlighted that the electrostatic interaction between DNJ and ALG was stronger than DNJ salt formation with HCl present in the gastric simulated environment. For this reason, even though DNJ is a high hydrophilic compound, the complete release did not occur. During the subsequent intestinal simulation, a little additional release was observed. The pH transition from 3.0 to 6.8 might have induced the polymer

structure rearrangement with a reduced viscosity leading to a faster release of DNJ in the first 30 minutes of intestinal simulation. When the equilibrium was established again at 150 min, the compound reached a new plateau at approximately 43% of the cumulative release. The uncomplete release of DNJ here observed was in contrast with Gavini and co-workers' results, who evaluated the *in vitro* release of metoclopramide from SDMs [207]. The authors achieved the complete release of the alkaline drug in 3 h (pH 7), even though a possible electrostatic interaction between the ALG and the drug was supposed [207]. Thus, the results of the *in vitro* simulated release suggested that Ca-ALG beads and SDMs could maintain their integrity in the acid and hostile environment of the stomach. Furthermore, the controlled release of DNJ seemed to be mainly governed by the electrostatic interaction between the active compound and the carboxylic groups of ALG. As a consequence, the encapsulation of DNJ into a structured carrier such as the Ca-ALG beads might not be necessary to achieve the goal of a sustained and prolonged release.

4. Conclusions

In the current work, two different strategies for the incorporation of DNJ were developed and fully characterized to prolong the release and improve its therapeutic efficacy. Both carriers demonstrated to successfully delay and control the release of DNJ in the gastrointestinal environment, but the highest encapsulation efficiency was achieved for SDMs. *In vitro* simulation pointed out that the release was governed by the strong electrostatic interaction between the iminosugar and the carboxylic groups of ALG, which was also demonstrated by NMR. The DNJ delivery strategy based on the cross-linking of Na-ALG with $CaCl_2$ to generate Ca-ALG beads showed to be the less convenient option to reach the goal. Indeed, Ca-ALG beads required a higher amount of EXT in the gelling solution to achieve the same loading compared to SDMs. In conclusion, the SDMs formulation resulted being the easiest, most promising, and scalable strategy to deliver the mulberry DNJ, although the product yield might be improved. Based on these findings, the active compound could be released slowly and gradually from the stomach to the intestine, allowing it to persist *in situ* and act over an extended period of time. This evidence would provide a good probability that a large dose of the loaded compound would pass into the bloodstream, ensuring the highest bioavailability and the optimal therapeutic result. This work is of utmost importance to overcome issues related to the poor bioavailability of DNJ as well as other freely soluble drugs, nonetheless further studies are required to bridge the gap between *in vitro* and clinical data.

CHAPTER 3

NEW INSIGHTS INTO BIOACTIVE COMPOUNDS FROM THE MEDICINAL PLANT *SPATHODEA CAMPANULATA* P. BEAUV., AND THEIR ACTIVITY AGAINST *HELICOBACTER PYLORI*

Antibiotics **2020**, 9(5), 258; doi:10.3390/antibiotics9050258

Corinne Raïssa Ngnameko [1,2], Lucia Marchetti [1,3], Barbara Zambelli [4], Antonio Quotadamo [1,3], Davide Roncarati [5], Davide Bertelli [1], Frederic Nico Njayou [2], Stella I. Smith [6], Paul F. Moundipa [2,*], Maria Paola Costi [1] and Federica Pellati [1,*]

[1] Department of Life Sciences, University of Modena and Reggio Emilia, Via G. Campi 103, 41125 Modena, Italy
[2] Department of Biochemistry, Faculty of Science, University of Yaounde I, P. Box 812 Yaounde, Cameroon;
[3] Doctorate School in Clinical and Experimental Medicine (CEM), University of Modena and Reggio Emilia, 41125 Modena, Italy
[4] Department of Pharmacy and Biotechnology, Alma Mater Studiorum University of Bologna, Viale Fanin 44, 40127 Bologna, Italy
[6] Nigerian Institute of Medical Research, PMB 2013, Yaba, Lagos, Nigeria

1. INTRODUCTION

Helicobacter pylori (*H. pylori*) is a Gram-negative bacterium that persistently colonizes the stomach of more than half the human population and its prevalence is significantly higher in the developing countries [208,209] . It causes gastric inflammation, gastric mucosa-associated lymphoid tissue lymphoma, and cancer. Due to its role in cancer, it was listed as a class I carcinogen by the World Health Organization (WHO) in 1994 [210]. Several meta-analyses have pointed out that the mass eradication of *H. pylori* would have beneficial effects, such as reduction in gastric cancer incidence, peptic ulcer development, dyspepsia symptoms, and anemia occurrence. Nonetheless, the efficacy of current treatments remains a major concern. The medical therapy for *H. pylori* still relies on a combination of antibiotics and anti-secretory agents, *e.g.*, proton pump inhibitors (PPIs) [211]. However, several studies have described high resistance to antibiotic treatment [212–214]. Indeed, in 2017 WHO included *H. pylori* in the list of antibiotic resistant bacterium for which the identification and development of new antimicrobial drugs represent a global priority [215]. To grow in the gastric acid medium *H. pylori* takes advantage of the Ni(II)-dependent urease enzyme, which catalyzes the hydrolysis of urea to produce ammonia and carbamate, the latter subsequently decomposes to ammonia and bicarbonate. The effect of this process is the increase of the medium pH, hence making the environment comfortable for *H. pylori* colonization, despite the harsh acidic conditions of the stomach [216,217]. Urease is therefore a target for the development of alternative and specific antibacterial strategies to overcome *H. pylori* gastric infection. *H. pylori* uses adhesins to bind and enter to the gastric mucosa. Adhesins are cell-surface proteins that enable bacterial adherence to cells. *H. pylori* major adhesive factors, which belong to the largest outer membrane protein (OMP) family, include blood group antigen-binding adhesion (BabA), sialic acid-binding adhesion (SabA), *H. pylori* outer membrane protein (HopZ), adherence-associated lipoprotein A and B (AlpA-B), *H. pylori* adhesin A (HpaA) and Lewis^{x}–LPS. *H. pylori* adhesins are considered bacterial virulence factors and they are involved in several processes during the early and chronic phases of the infection. The most studied virulence factors of *H. pylori* are cytotoxin-associated protein A (CagA) and vacuolating cytotoxin A (VacA)[218,219]. CagA is able to initiate in host cells NF-κB, MAPK, and SHP-2/ERK pathways, producing inflammatory factors and pro-inflammatory cytokines (IL-6, IL-8, INF-γ, TNF-α). These substances may cause extensive infection sites and inflammation, leading to gastritis or gastric cancer [218,219]. The capacity to inhibit the growth of this bacterium has been ascribed to a variety of medicinal plants and natural compounds. However, only a few papers have described

the mechanisms of action of natural products against *H. pylori* [220,221]. In general, these mechanisms include urease activity inhibition, anti-adhesion activity, DNA damage, protein synthesis inhibition, and oxidative stress [222,223]. *Spathodea campanulata* P. Beauv. (Bignoniaceae) is a medicinal plant traditionally used in Africa for the prevention and treatment of diseases of the kidney and urinary systems, the skin, the gastrointestinal tract, and inflammation in general [224,225]. Extracts of this plant have been found to be active against proliferative diseases, involving cancer cells and bacteria [226]. More recently, anti-*H. pylori*, anti-adhesive, and growth inhibitory activities of a methylene chloride/methanol extract from the bark of the plant have been described [227]. Data about the chemical characterization of *S. campanulata* are limited. Nevertheless, previous studies undertaken on the stem bark and leaves have shown the presence of phenolic acids, flavonoids, triterpenoids, iridoids, and sterols [228–233]. Consequently, this is the first chemical characterization study of the main compounds present in the extract, fractions and sub-fractions of *S. campanulata* bark using UHPLC-HRMS, which were also evaluated for their anti-*H. pylori*, anti-urease, and anti-adhesins effects.

2. EXPERIMENTAL

2.1. Chemicals and solvents

Analytical grade solvents, HPLC grade solvents and ammonium formate were from Sigma–Aldrich (Milan, Italy). Ultrapure water was obtained from a Millipore water purification system (Merck Life Science, Milan, Italy). Pre-coated aluminum Kieselgel 60 F254 plates (layer thickness 0.2 mm, Merck, Darmstadt, Germany) were used for analytical thin-layer chromatography (TLC).

2.2. Plant material and preparation of the crude extract

The bark from *S. campanulata* was collected in July 2018 in Foumbot (West Region, Cameroon). A sample of the bark was deposited at the HNC-Cameroon National Herbarium, with the voucher number 50085/HNC. The bark used in this study was harvested from at least three different trees, in order to have a representative sample. The plant material was washed with water and dried at room temperature for several weeks. The dried plant material was then powdered using a grinder. The obtained powder was kept at 4 °C until the preparation of the extracts. A portion of 500 g of powdered plant material was soaked in 2 L of solvent solution composed by methylene chloride (DCM)/methanol (MeOH) (1:1, v/v) for 48 h and paper

filtered. The filtrate was dried using a rotary evaporator to obtain the crude extract.

2.3. Fractionation procedure

The crude extract was purified on silica gel by preparative flash column chromatography using in sequence *n*-hexane (Hex), ethyl acetate (EtOAc), and methanol (MeOH). Eight stages of polarity were used: Hex (fraction A), Hex/EtOAc 25% (fraction B), Hex/EtOAc 50% (fraction C), Hex/EtOAc 75% (fraction D), EtOAc (fraction E), and MeOH (fraction F). The fractions were further partitioned using a silica gel column chromatography with an Isolera apparatus (Biotage, Charlotte, NC, USA) with different solvents, according to the result of TLC. In this way, different sub-fractions were collected: SA1 (90% Cyhex/EtOAc) from fraction A, SB1 and SB2 (70% Cyhex/EtOAc and 90% Cyhex/EtOAc, respectively) from fraction B, SC1 and SC2 (95% DCM/MeOH) from fraction C, SD1 and SD2 (20% Cyhex/EtOAc) from fraction D, SE1 and SE3 (50% MeOH/H_2O and 70% MeOH/H_2O, respectively) from fraction E, and SF (80% Cyhex/EtOAc) from fraction F. The solvent was removed from the collected fractions and sub-fractions by using a rotary evaporator.

2.4. Determination of total polyphenols and total flavonoids

For the determination of total polyphenols and total flavonoids, the crude extract and its fractions were dissolved in MeOH at a concentration of 100 µg/mL. The content of total polyphenols was analyzed according to the Folin-Ciocâlteu method, as previously described [234]. Briefly, 50 µL of sample were added to a solution composed of 2.4 mL of distilled water, 200 µL of Folin-Ciocâlteu reagent (2 N), and 500 µL of Na_2CO_3 20%. The reaction mixture was incubated at 25 °C in the dark for 1 h, and the absorbance was read at 765 nm. The total phenolic content was expressed as milligrams of gallic acid equivalents (GAE) per gram of extract, by using a calibration curve built with gallic acid as reference. The total flavonoid content was analyzed according to the aluminum chloride method [234]. Briefly, 50 µL of sample was mixed with 0.95 mL of methanol and 1.0 mL of $AlCl_3$ (2%). The reaction mixture was incubated at 25 °C for 30 min, and the absorbance was read at 420 nm. The results were compared to quercetin calibration curve and the total flavonoids content was expressed as milligrams of quercetin equivalents (QE) per gram of extract.

2.5. UHPLC-HRMS analysis

For the UHPLC-HRMS analysis, 2 mg of each fraction and sub-fraction obtained from the crude plant extract were dissolved in 1.0 mL of acetonitrile (ACN), filtered using a PTFE filter, and vortex mixed for 20 s, spun at 5000 g for 5 min. Then, 5 µL of this solution were injected in duplicate, for the analysis. A Thermo Scientific Dionex Ultimate 3000 UHPLC system equipped with an autosampler, a quaternary pump and a thermostated column compartment controlled by the Chromeleon 7.2 Software (Thermo Scientific, Waltham, MA, USA) was employed for the analysis. The UHPLC system was coupled to a high-resolution Q Exactive mass spectrometer (Thermo Scientific, Bremen, Germany), which was calibrated before the analyses. Nitrogen (N_2) (purity > 99.99%), obtained from a Zefiro zero 60 LC-MS nitrogen generator (CINEL, Vigonza, Italy), was employed both as the source gas and the collision gas. The chromatographic system was hyphenated to the MS with an electrospray ionization (ESI) source, operating both in the positive and in the negative ion modes. The capillary temperature was set at 270 °C and the following N_2 flows (arbitrary units) were used: sheat gas 40, auxiliary gas 30, and sweep gas 3. The capillary voltage was set at −3.5 and +3 kV. The chromatographic separation was performed on an Ascentis Express C_{18} (10 cm × 2.1 mm i.d., 2.7 µm) (Supelco, Bellefonte, PA, USA). The column was kept at 25 °C. The mobile phase was composed of 80% H_2O + 0.1% formic acid (mobile phase A) and 20% ACN (mobile phase B) at 0.3 mL/min. The following gradient was used: from 0.1 to 10.1 min from 20% to 98% B, which was kept constant for 8.8 min, before the reconditioning step, for a total analysis time of 25 min. Both MS and MS^2 spectra were recorded from 100 to 1000 *m/z*, at a resolution of 70,000 and 17,500, respectively. The three most intense ions were selected for MS^2 N_2-promoted collision-induced dissociation (CID) (stepped CE = 20, 28 eV). A precursor active exclusion of 6 s was set. In parallel, the all-ion fragmentation experiment (CE = 28 eV) was scheduled for post-hoc analysis. The mass calibration was performed weekly, both in the negative and in the positive ion modes, to ensure the highest mass accuracy. XCalibur 2.9 (Thermo Scientific, Bremen, Germany) and FreeStyle 1.3 software (Thermo Scientific, San José, CA, USA) were used for UHPLC control and MS data processing, respectively.

2.6. Antimicrobial disk diffusion test

H. pylori strain G27 was obtained from the University of Bologna, Italy. *H. pylori* cells were recovered from glycerol stocks on Brucella broth agar plates, containing 5% fetal calf serum (FCS), added with Dent's antibiotic supplement in an atmosphere of 9% CO_2/91% air,

maintained at 37 °C, and 95% humidity in water-jacketed incubator (Thermo Fisher Scientific, Waltham, MA, USA). All reagents were purchased from Oxoid, United Kingdom. The assay was carried out following the method described by Balouiri *et al*. [235]. *H. pylori* cells were collected from Brucella broth agar plates, suspended in 500 µL of liquid Brucella broth with 5% Dent's antibiotic supplement and subsequently the cell density (OD600) of bacterial suspension was determined. Then, *H. pylori* cells were diluted in melted Brucella broth Soft Agar medium (Brucella broth agar plates containing 0.5% agar) to obtain a final OD600 of 0.07 and 6.5 mL of this suspension was poured into a sterile standard Brucella broth agar plate. After that, 5 mm sterile paper disks were deposited into the agar. A total of 4 µL of the crude extract, fraction B, C, E, and subfractions SA1, SB1, SB2, SC2, SD1, SE3 and SF (10 mg/mL) prepared using DMSO/H_2O (25% v/v) were dropped into the disk. The DMSO/H_2O solution was used as the negative control. Kanamycin (10 µg) was used as the reference antibiotic. The plates were incubated under microaerophilic conditions at 37 °C for 72 h. The products that showed a diameter of inhibition ≥ 8 mm were considered to be active [235]. The active products were serially diluted using sterile DMSO/H_2O (25% v/v) to obtain three decreasing concentrations, which were re-tested in triplicate and the results expressed as a mean diameter of inhibition zone. The minimum active quantity (MAQ) for each extract was determined as the minimum quantity that produced an inhibition zone ≤ 8 mm.

2.7. In-cell urease activity test

Escherichia coli TOP10 cells harboring pGEM-ureOP plasmid were pre-cultured at 37 °C in 1 mL of lysogeny broth (LB), containing 100 µg/mL of ampicillin (Ap). After 16 h, 40 µL of pre-culture were used to inoculate 2 mL of LB medium containing 100 µg/mL of Ap and 10 µg/L of cresol red pH indicator. When OD600 reached 0.7–0.9, 90 µL of each culture was inoculated in 96-well plates with 80 mM urea, with and without 10 µL of different concentrations of either the fractions or the sub-fractions of the plant extract or DMSO. Immediately before running the experiment, 2.5 µL of 10 mM $NiSO_4$ was added to each culture to a final concentration of 250 µM. In each well, 30 µL of mineral oil was added to prevent the medium evaporation during the culture. The color change of cresol red indicator was monitored over time spectrophotometrically in a multi-plate reader, measuring the absorption at 430 and 580 nm.

2.8. Western blot analysis

Three days old cultures of the *H. pylori* G27 strain were harvested into Brucella broth medium supplemented with 10% fetal bovine serum (FBS) to 0.8 OD600. Then, 100 µL of the mixture was added to each well in a 96-well plate. A total of 100 µL of the plant extract at the three concentrations was used. The plates were incubated at 37 °C under microaerophilic conditions for 4 h. After incubation, 200 µL of the mixture was transferred into a microcentrifuge tube and centrifuged at 14,000 rpm for 5 min at 4 °C. The supernatant was discarded, and the pellet was washed with phosphate buffer saline (PBS). Protein in Laemmli loading buffer was separated by 12% sodium dodecyl sulfate poly-acrylamide gel electrophoresis (SDS-PAGE) and electro-transferred into a polyvinylidene difluoride paper (PVDF) blotting membrane (GE Healthcare, Germany). The membranes were blocked with 5% w/v non-fat milk in phosphate buffered saline Tween-20, incubated overnight at 4 °C with primary antibodies (BabA, CagA, HopZ, and HP1043 as the loading control), rinsed, and then incubated for 1 h at 25 °C with horseradish peroxidase-conjugated secondary antibodies. The blots were then developed by using a chemiluminescent method (Sigma, Germany). The densitometric analysis of the protein bands was performed using the ImageJ Software (NIH, USA).

2.9. Statistical analysis

Significant differences within groups were determined at $P < 0.05$ by using two-way ANOVA and Bonferroni's multiple comparisons test. Statistical analysis was performed by using GraphPad Prism 5.0 (GraphPad Software, San Diego, CA). The results were reported as mean ± standard deviation (SD) of three independent experiments.

3. RESULTS AND DISCUSSION

3.1. Chemical composition of S. campanulata fractions and sub-fractions

To identify new anti-*H. pylori* growth inhibitors, we first tested fractions and sub-fractions of bark of *S. campanulata* against the bacterium and then we focused on the urease enzyme and adhesin proteins involved in adhesion to gastric mucosa. After the extraction of the plant material, its fractionation and further sub-fractionation were performed by means of preparative flash column chromatography. Six fractions were obtained, which were further sub-fractioned using silica gel column chromatography to provide 10 sub-fractions. The content of total

polyphenols and total flavonoids in the crude plant extract and in the six fractions is shown in Table 1.

Table 1. Total polyphenols and total flavonoids content in *Spathodea campanulata* crude extract and fractions (A–F).

Total Polyphenols (mg GAE/g) [a]						
Crude extract	**A**	**B**	**C**	**D**	**E**	**F**
51.4 [b]	46.4 ± 0.5	43.0 ± 0.1	53.0 [b]	48.3 [b]	68.8 ± 0.3	56.3 ± 1.1
Total Flavonoids (mg QE/g) [a]						
Crude extract	**A**	**B**	**C**	**D**	**E**	**F**
5.2 ± 0.2	2.8 ± 0.1	1.8 [b]	1.9 [b]	2.0 [b]	7.1 [b]	1.9 ± 0.1

[a] Data of total polyphenols are expressed as mg of gallic acid equivalents (GAE)/g; data of total flavonoids as mg of quercetin equivalents (QE)/g (± SD). [b] SD < 0.05.

Eleven compounds were tentatively identified on the basis of retention times, accurate mass, MS fragmentation data, and by comparison with literature [228–233,236]. The compound 5,7-dihydroxy-4-metilcoumarin was detected in this plant for the first time to our best knowledge, through the mass spectral database mzCloud. The MS and MS/MS data of all the identified compounds are shown in Table 2.

Table 2: Compounds identified in the active fractions and sub-fractions of *S. campanulata* by UHPLC- HRMS

Fraction	Ion mode	Precursor ion	Fragments	Molecular Formula	Tentative Identification	Reference
C	$[M-H]^-$	191.0342	176.0106,148.0155,104.0255	$C_{10}H_8O_4$	5,7-dihydroxy-4-metilcoumarin	
C	$[M-H]^-$	137.0235	105.4586,93.0333	$C_7H_6O_3$	4-hydroxy-benzoic acid	[236]
C	[M-H]-	301.0354	273.0408,245.0457,178.9977, 151.0026	$C_{15}H_{10}O_7$	Quercetin	[229]
C	$[M-H]^-$	285.0405	151.0025,133.0283	$C_{15}H_{10}O_6$	Kaempferol	[231]
C	$[M+H]^+$	139.0391	95.0497,91.0548,67.0550	$C_7H_6O_3$	4-hydroxy-benzoic acid	[236]
C	$[M+H]^+$	193.0498	178.0261,165.0549,150.0312, 133.0285,122.0365	$C_{10}H_8O_4$	5,7-dihydroxy-4-metilcoumarin	
C	$[M+H]^+$	147.0442	103.0547,91.0548,77.0392, 65.0394	$C_9H_6O_2$	Coumarin	[229]
C	$[M+H]^+$	287.0552	269.0440,153.0183,137.0232	$C_{15}H_{10}O_6$	Kaempferol	[231]
C	$[M+H]^+$	111.0445	93.0703,65.0394,55,0551	$C_6H_6O_2$	Catechol	[229]
SC2	$[M-H]^-$	191.0342	176.0106,148.0155,104.0255	$C_{10}H_8O_4$	5,7-dihydroxy-4-metilcoumarin	
SC2	$[M-H]^-$	285.0405	151.0025,133.0283	$C_{15}H_{10}O_6$	Kaempferol	[231]
SC2	$[M+H]^+$	139.0391	95.0497,91.0548,67.0550	$C_7H_6O_3$	4-hydroxy-benzoic acid	[236]
SC2	$[M+H]^+$	287.0552	269.0440,153.0183,137.0232	$C_{15}H_{10}O_6$	Kaempferol	[231]
E	$[M+H]^+$	447.0933	285.0402,151.0027	$C_{21}H_{20}O_{11}$	Kaempferol 3-glucoside	[232]
E	$[M-H]^-$	285.0405	229.2277,151.0029,133.0284	$C_{15}H_{10}O_6$	Kaempferol	[231]
E	$[M-H]^-$	455.3531	411.3633	$C_{30}H_{48}O_3$	Ursolic acid	[228,230]
E	$[M+H]^+$	153.0546	123.0441,95.0132,79.0184	$C_8H_8O_3$	Methyl 4-hydroxybenzoate	[236]
E	$[M+H]^+$	193.0498	178.0258,150.0311,133.0283, 137.0595	$C_{10}H_8O_4$	5,7-dihydroxy-4-metilcoumarin	
E	$[M+H]^+$	449.1078	287.0551	$C_{21}H_{20}O_{11}$	Kaempferol 3-glucoside	[232]
E	$[M+H]^+$	455.3516	437.3415,409.3470,391.3368, 219.1742	$C_{30}H_{46}O_3$	Tomentosolic acid	[228,230]
E	$[M+H]^+$	457.3313	439.3628,411.3253,393.3140, 339.2325, 175.1483	$C_{30}H_{48}O_3$	Ursolic acid	[228,230,231]
E	$[M+H]^+$	429.3725	412.3649,346.2809,317.2466, 303.2307, 89.21592,177.0911, 151.0753,137.0596	$C_{29}H_{48}O_2$	Spathodol	[230,233]
E	$[M+H]^+$	489.3585		$C_{30}H_{48}O_5$	Spathodic acid	[230]
SA1	$[M-H]^-$	455.3531	411.3633	$C_{30}H_{48}O_3$	Ursolic acid	[230]
SB1	$[M-H]^-$	471.3479	427.3579,409.3479	$C_{30}H_{48}O_4$	Alpha-hydroxy ursolic acid	[230]
SB1	$[M-H]^-$	453.3376	409.3776	$C_{30}H_{46}O_3$	Tomentosolic acid	[228,230]
SB1	$[M-H]^-$	455.3531	411.3633	$C_{30}H_{48}O_3$	Ursolic acid	[228,230,231]
SB1	$[M+H]^+$	153.0546	111.0443	$C_8H_8O_3$	Methyl 4-hydroxybenzoate	[236]
SD2	$[M-H]^-$	455.3531	411.3633	$C_{30}H_{48}O_3$	Ursolic acid	[230]
SE1	$[M-H]^-$	447.0933	285.0402,151.0027	$C_{21}H_{20}O_{11}$	Kaempferol 3-glucoside	[232]
SE1	$[M+H]^+$	449.1078	287.0551	$C_{21}H_{20}O_{11}$	Kaempferol 3-glucoside	[232]
SE3	$[M-H]^-$	285.0405	151.0025,133.0283	$C_{15}H_{10}O_6$	Kaempferol	[231]

Table 3. Identified compounds and their distribution in the active fractions and sub-fractions of *Spathodea campanulata.*

Compound	Fraction/Sub-Fraction							
	C	E	SA1	SB1	SC2	SD2	SE1	SE3
4-Hydroxy benzoic acid	+	-	-	-	+	-	-	-
Methyl-4-hydroxybenzoate	-	+	-	+	-	-	-	-
5,7-Dihydroxy-4-metilcoumarin	+	+	-	-	+	-	-	-
Quercetin	+	-	-	-	-	-	-	-
Kaempferol	+	+	-	-	+	-	-	+
Kaempferol 3-*O*-glucoside	-	+	-	-	-	-	+	-
Spathodol	-	+	-	-	-	-	-	-
Spathodic acid	-	+	-	-	-	-	-	-
Tomentosolic acid	-	+	-	+	-	-	-	-
Ursolic acid	-	+	+	+	-	+	-	-
Corosolic acid	-	-	-	+	-	-	-	-

3.2. Inhibitory activity of S. campanulata fractions and sub-fractions against H. pylori

The inhibitory activity on *H. pylori* of all the fractions and sub-fractions is shown in Table 4. The minimum active quantity (MAQ) values ranged from 0.1 mg to 10 mg/mL. The lowest MAQ value of 0.1 mg/mL was obtained with fractions B, C, and E and sub-fractions SA1 and SB1 on *H. pylori*. The measurement of the cellular urease activity was performed in a heterologous *E. coli* bacterial model overexpressing the enzyme, as previously described [237].

Table 4. Mean diameter of inhibition and minimum active quantity (MAQ) values (mg/mL) of *Spathodea campanulata* crude plant extract, active fractions and sub-fractions against *Helicobacter pylori.*

Sample	Concentration			
	0.1 mg/mL	1.0 mg/mL	10.0 mg/mL	MAQ (mg/mL)
Crude extract	ND	8.6 ± 0.8	11.6 ± 0.7	1.0
B	11.3 ± 1.2	11.7 ± 2.1	12.1 ± 1.0	0.1
C	10.0	12.0	16.3 ± 2.5	0.1
E	10.0	11.7 ± 0.6	15.8 ± 0.3	0.1
SA1	9.8 ± 0.4	10.0 ± 1.0	10.7 ± 1.2	0.1
SB1	9.3 ± 0.6	9.7 ± 0.6	10.7 ± 0.6	0.1
SB2	ND	8.7 ± 2.3	11.3 ± 2.5	1.0
SC2	ND	8.0	10.0	1.0
SD1	ND	ND	10.3 ± 0.6	10.0
SE3	ND	ND	13.0 ± 1.0	10.0
SF	ND	9.3 ± 1.2	10.7 ± 0.6	1.0
Kanamycin (2.5 mg/mL)	35.7 ± 0.6	–	–	–

The results indicated that sub-fractions SD2, SE1 and SE3 produced minor urease inhibition (Figure 1), while the sub-fraction SB2 inhibited urease in living bacteria with an IC_{50} value of 3.3 mg/mL (Figure 2). All the other fractions showed either low solubility or limited activity.

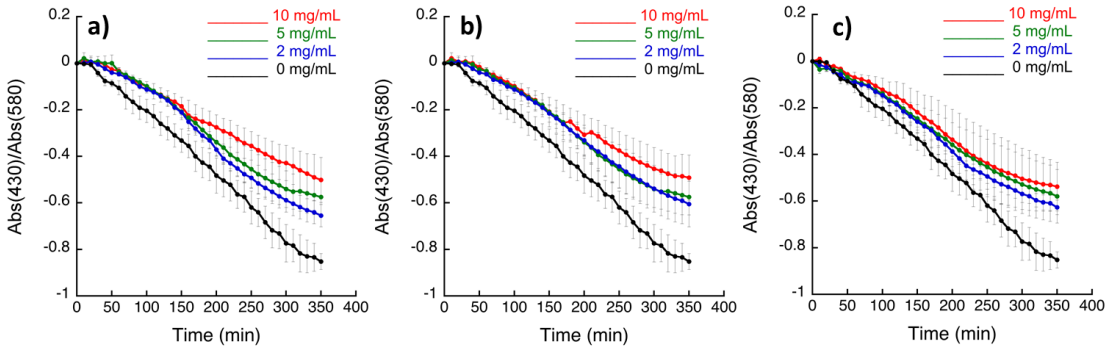

Figure 1. Urease activity of recombinant *E. coli* cells in the presence of 250 µM Ni(II) and of 80 mM urea, measured as a change of pH detected by the cresol red indicator. Increasing concentrations of the sub-fraction was added to the *E. coli* culture before performing the colorimetric assay. Data are shown as mean ± SD of the triplicates. Figure 1a) sub-fraction SD2 (20% Cyhex/EtOAc), b) sub-fraction SE1 (50% MeOH/H2O), and c) sub-fraction SE3 (70% MeOH/H2O).

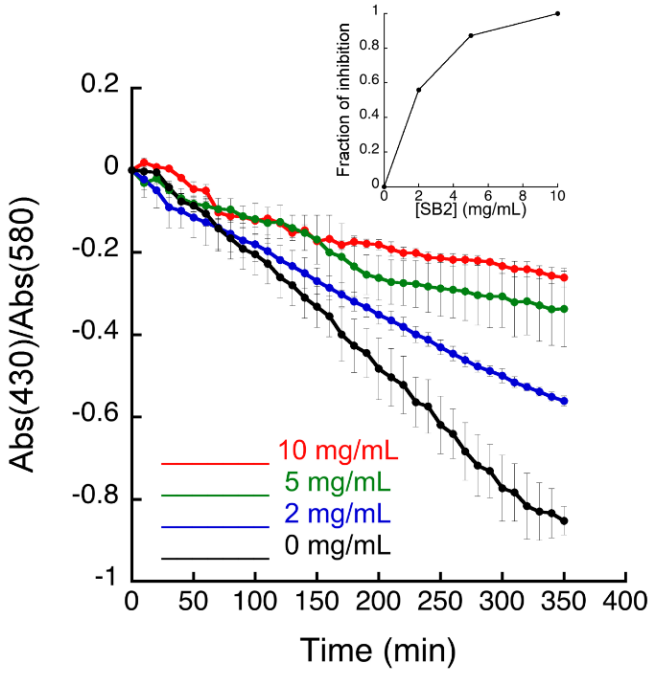

Figure 2. Urease activity of recombinant *E. coli* cells in the presence of 250 µM Ni(II) and of 80 mM urea, measured as a change of pH detected by the cresol red indicator. Increasing concentrations of the sub-fraction SB2 were added to the *E. coli* culture before performing the colorimetric assay. Data are shown as mean ± SD of the triplicates. The insert represents the dose-response plot for the SB2 sub-fraction. Sub-fraction SB2 (90% Cyhex/EtOAc) was obtained from fraction B.

3.3. Effect of S. campanulata fractions and sub-fractions on H. pylori virulence factors

The effect of *S. campanulata* fractions and sub-fractions on the expression of specific *H. pylori* virulence factors, including the two adhesins BabA and HopZ, and the cytotoxin-associated gene A (CagA), was investigated by Western blot. The samples that showed a significant effect in this preliminary assay were further investigated (Figure 3; Figures 4–6).

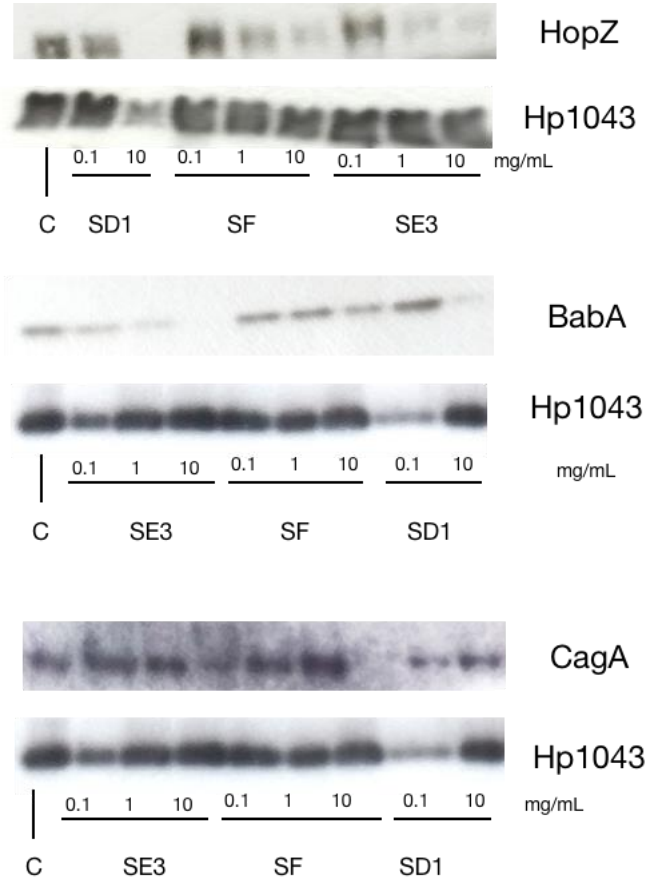

Figure 3. Western blot analysis of *H. pylori* cells, treated with various concentrations of sub-fractions, to quantify the expression levels of HopZ, BabA and CagA proteins. DMSO was used as the control treatment (C), while HP1043 staining was used as the loading control. Sub-fraction SD1 (20% Cyhex/EtOAc), sub-fraction SE3 (70% MeOH/H2O) and sub-fraction SF (80% Cyhex/EtOAc) were from fractions D, E and F, respectively.

HP1043 staining was used as the loading control. Densitometric analysis of blot was performed, and quantification data are reported in the bar chart. Values are expressed as means ± SD of two independent experiments. Specifically, sub-fractions SD1, SE3, and SF were able to inhibit HopZ expression (Figure 4). At the dose of 0.1 mg/mL, all sub-fractions were significantly different one from each other (except for SD1 and SE3) and from control ($P < 0.0001$). For the higher concentrations (1 and 10 mg/mL) all the considered sub-fractions significantly reduced the adhesin expression ($P < 0.0001$). As concerns BabA (Figure 5), only SD1 and SE3 exhibited an effective reduction of the protein expression. At 0.1 and 10 mg/mL, SE3 was significantly

different from control ($P < 0.0001$) and from SD1 and SF ($P < 0.0001$), thus being SE3 the most effective. With regard to CagA expression (Figure 6), at the lowest concentration only sub-fraction SD1 exhibited a significant effect, with respect to the control ($P < 0.0001$). At 10 mg/mL all sub-fractions reduced the expression of the protein ($P < 0.0001$). Sub-fractions SF and SE3 were the most active and were different one from another at $P < 0.001$.

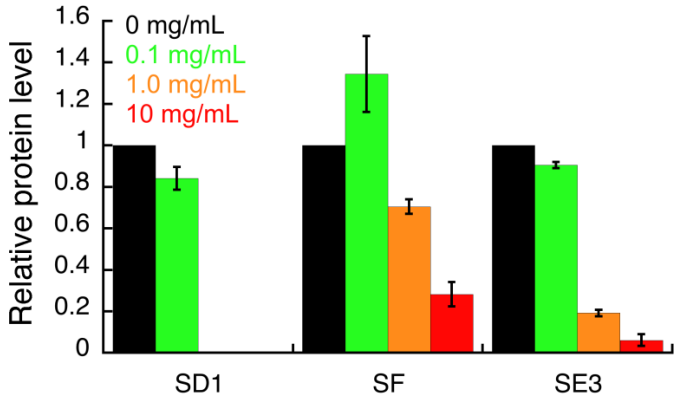

Figure 4. Densitometric analysis of the Western blot images, indicating the effects of *S. campanulata* on *H. pylori* G27 HopZ adhesin expression. *H. pylori* cells were treated with different concentrations of *S. campanulata* sub-fractions for 4 h and protein level of HopZ adhesin was determined by Western blot, using a specific anti-HopZ antibody. Values are expressed as means ± SD of two independent experiments Sub-fraction SD1 (20% Cyhex/EtOAc), sub-fraction SE3 (70% MeOH/H_2O), and sub-fraction SF (80% Cyhex/EtOAc) were from fractions D, E, and F, respectively.

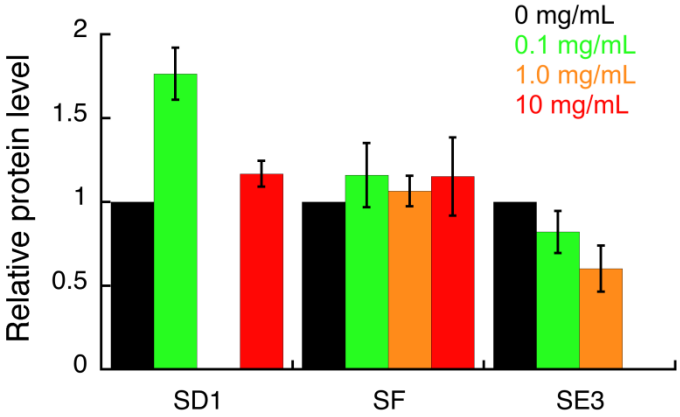

Figure 5. Densitometric analysis of the Western blot images, indicating the effects of *S. campanulata* on *H. pylori* G27 BabA adhesin expression. *H. pylori* cells were treated with different concentrations of *S. campanulata* sub-fractions for 4 h and protein level of BabA adhesin was determined by Western blot, using a specific anti-BabA antibody. Values are expressed as means ± SD of two independent experiments. Sub-fraction SD1 (20% Cyhex/EtOAc), sub-fraction SE3 (70% MeOH/H_2O), and sub-fraction SF (80% Cyhex/EtOAc) were from fractions D, E, and F, respectively.

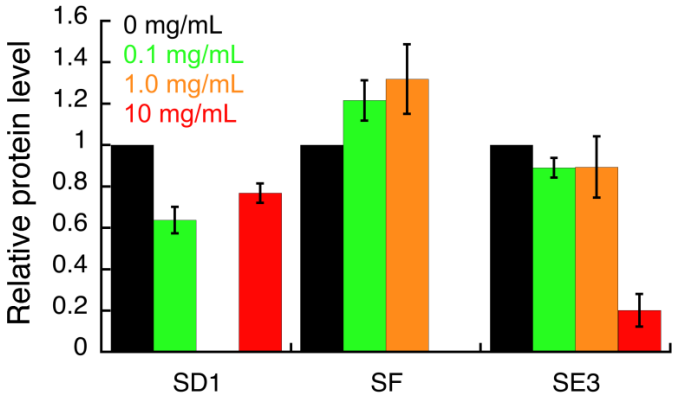

Figure 6. Densitometric analysis of the Western blot images, indicating the effects of *S. campanulata* on *H. pylori* G27 CagA expression. *H. pylori* cells were treated with different concentrations of *S. campanulata* sub-fractions for 4 h and protein level of the virulence factor CagA was determined by Western blot, using a specific anti-CagA antibody. Values are expressed as means ± SD of two independent experiments. Sub-fraction SD1 (20% Cyhex/EtOAc), sub-fraction SE3 (70% MeOH/H_2O), and sub-fraction SF (80% Cyhex/EtOAc) were from fractions D, E, and F, respectively.

The compounds identified in this work by UHPLC-HRMS may be involved in the observed biological activity either by inhibiting urease activity or by modulating the expression of the virulence factors mentioned above. The plant sub-fraction SE3, able to simultaneously modulate the expression of two adhesins (HopZ and BabA) and one cytotoxin (CagA), was obtained from fraction E, which was the richest one in total polyphenols and total flavonoids (Table 1); the flavonol kaempferol was identified in sub-fraction SE3 by UHPLC-HRMS analysis. As for the other two sub-fractions SD1 and SF, their chemical composition was not disclosed by UHPLC-HRMS analysis. Phenolics have general antimicrobial activity and some of them are also active against *H. pylori* [220,238]. Several phytochemicals may act by inhibiting enteric microbial growth, inducing cellular membrane perturbations, interfering with certain metabolic processes, and modulating signal transduction or gene expression pathways [238]. Notably, it has been recently observed that the flavonoid kaempferol, a widely diffused natural flavonol, has an anti-inflammatory effect on *H. pylori*-induced inflammation by suppressing the translocation of CagA and VacA proteins and leading to the downregulation of pro-inflammatory cytokines [239]. Recently, kaempferol has been found to inhibit the in vitro DNA binding activity of the homeostatic stress regulator (HsrA), a protein which plays as a global homeostatic regulator, synchronizing metabolic functions and virulence with availability of nutrients and cell division, also mediating the response to oxidative stress. HsrA represents a novel and effective therapeutic target in *H. pylori* infection [240]. In the present work, the sub-fraction SE3 from *S. campanulata*, which contains kaempferol, was found to simultaneously modulate the expression of the two *H. pylori* adhesins HopZ and BabA and the cytotoxin CagA; in addition, this sub-fraction showed a mild urease inhibition. Regarding the effect of natural compounds on the expression of HopZ, to the best of our knowledge no information is available

in the literature. N-phenylpropenoyl-L-amino acids (NPAs) has been identified as polyphenol/amino acid conjugates in the seeds of theobroma cacao as well as in a variety of herbal drugs; they have been described for their inhibitors of *H. pylori* BabA outer membrane protein [241]. As for CagA, in addition to kaempferol, binding interactions between this virulence factor and natural compounds have been investigated by molecular docking and four hit compounds have been identified, including one phytosterol, one chalcone, and two carotenoids [242]. Due to the reduced number of natural compounds able either to inhibit urease enzymatic activity or to modulate the expression of *H. pylori* virulence factors, the research in this field deserves a great attention in the medicinal chemistry field, in order to develop the identified hit kaempferol, alone or in combination with known drugs. This outcome agrees with a recent study [240], where kaempferol has exhibited a potent bactericidal activity against *H. pylori*, with an MBC value from 28 to 56 µM, the latter in resistant strains. However, the wide group of intracellular targets and the high number of natural compounds potentially effective as therapeutic agents against *H. pylori* which are present in this plant extract require further evidence to better understand the role of these substances using *in vivo* models, as previously described in the literature for kaempferol isolated from *Polygonum tinctorium* [243].

4. Conclusions

It can be assumed from this study that natural compounds present in *S. campanulata* bark extract could be effective as potential therapeutic agents against *H. pylori*, by inhibiting urease activity and some virulence factors and by modulating the expression of the adhesins BabA and HopZ and the cytotoxin CagA. These results suggest that enriched extracts from this plant could be useful for the treatment of *H. pylori* mediated gastric diseases, and they could be used synergistically with antibiotics in conventional therapy. The flavonol kaempferol, identified by UHPLC-HRMS has to be further assessed as a new hit for its potential therapeutic activity against *H. pylori* infection.

CHAPTER 4

IDENTIFICATION AND DETERMINATION OF PHENYLPROPANOID GLYCOSIDES OF *ALOYSIA POLYSTACHYA* (GRISEB. ET MOLDENKE) BY HPLC-MS

Journal of Pharmaceutical and Biomedical Analysis **2019**, 166, 364–370

Lucia Marchetti [1,2], Federica Pellati [1], Riccardo Graziosi [1], Virginia Brighenti [1], Diego Pinetti [3], Davide Bertelli [1,*]

[1] Department of Life Sciences, University of Modena and Reggio Emilia, Via G. Campi 103, 41125 Modena, Italy
[2] Doctorate School in Clinical and Experimental Medicine (CEM), University of Modena and Reggio Emilia, 41125 Modena, Italy
[3] Centro Interdipartimentale Grandi Strumenti, University of Modena and Reggio Emilia, Via G. Campi 213/A, 41125 Modena, Italy

1. INTRODUCTION

The Verbenaceae family comprises over 100 genera and about 2000 species of wide geographical distribution, which includes tropical, subtropical and temperate regions [244]. This family includes aromatic species used since ancient times in ethnobotany as beverages, food, seasoning and remedies in traditional medicine. *Aloysia citriodora* Palau, also commonly known as "cedron" or "lemon verbena" and *Lippia turbinata* Griseb., known as "poleo", are the two predominant species, and are used in the forms of leaf infusions or decoctions, typically for the treatment of gastrointestinal disorders [244]. Lemon verbena dietary supplementation has been found to induce beneficial effects on colonic damage, inflammation, and oxidative stress related diseases. *Aloysia polystachya* (Griseb. et Moldenke) is largely distributed in South America, particularly in Paraguay and in the northern Argentina, where is also commonly known as "Burrito" or "Té-burro" [245]. Here, the plant leaves are usually assumed in accordance with the local usages in daily life as beverage [246–249]. Few data on the chemical composition of *Aloysia polystachya* (Griseb. et Moldenke) are available in the literature. In 2011, Consolini *et al*. evaluated the pharmacological basis of Aloysia polystachya decoction in the popular use, as well as the correlation with chemical composition [250]. Phenolic compounds characterization in vegetable matrix can be very difficult, due to bonds to different sugar moieties, or conjugation giving rise to complex structures. Nowadays, UV spectroscopy is the main used technique for the quantification of polyphenols, through its simplicity and low cost. Furthermore, for the determination of different structural groups present in phenolic compounds, common assays are even employed. However, spectrophotometric assays only give an estimation of the total phenolic content; they do not separate nor give quantitative measurement of individual compounds. Among separative techniques capillary electrophoresis (CE) is suitable for the separation and quantification of compounds with limited molecular weight [251]. It is a versatile analytical tool for the routine determination of phenolic compounds in different matrices due to its high separation efficiency, high resolution power, short time of analysis and low consumption of sample and reagents. On the other hand, CE is characterized by a low sensitivity, in terms of analyte concentration, and poor reproducibility, compared to chromatographic techniques [252]. Gas chromatography (GC) is a widely employed technique with a great separation capacity, high sensitivity, and selectivity especially when combined with mass spectrometry (MS). Nevertheless, the preparation of samples for GC analysis is quite laborious, including the derivatisation for low volatile polyphenols. Among all the available methods, high-performance liquid chromatography (HPLC) is the favourite for separation and quantification of polyphenols [253]. Owing to the low detection limit and

sensitivity, HPLC methods present some limitations, especially in the analysis of complex matrices, such as raw plant extracts. Therefore, a prior phase of concentration and purification of active substances from the matrix is a critical step to simplify the chromatogram, and to reliably identify and quantify the phenolic compounds. Hence, the coupling of HPLC with MS can highly enhance the sensitivity of the method. Even if data about chemical composition are limited, the leaves of *Aloysia* spp. mainly contain flavonoids and phenolic acids, but also phenylpropanoid glycosides: widely distributed water-soluble compounds [254]. Among phenylpropanoids, verbascoside is the most represented in *Aloysia* spp. [254,255]. This molecule is characterized by a caffeic acid bound to β-(D)-glucopyranoside through ester link and a 4,5-hydroxyphenylethanol bounded by glycosidic links to the glucose, and a rhamnose unit (Table 1).

Table 1. Chemical structures of the phenylpropanoid glycosides identified in ME of the *Aloysia polystachya* (Griseb. et Moldenke) leaves.

Structure	Assignment	Compound	R_1	R_2	R_3
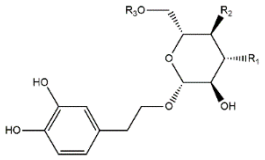	Verbascoside	(1)	Rhamnose	Caffeic acid	H
	Isoverbascoside	(2)	Rhamnose	OH	Caffeic acid
	Forsythoside A	(3)	OH	Caffeic acid	Rhamnose
	Leucosceptoside A	(5)	Rhamnose	Ferulic acid	H
	Plantainoside C	(6)	Rhamnose	OH	Ferulic acid
	Purpureaside D	(7)	OH	Ferulic acid	Rhamnose
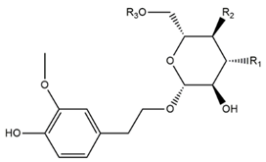	Martynoside	(9)	Rhamnose	Ferulic acid	H
	Isomartynoside	(10)	Rhamnose	OH	Ferulic acid

Among others, verbascoside has exhibited a wide range of biological activities, including antioxidant and free radical scavenging which are the most representative properties [256,257]. In addition, the antitumoral [258], antimicrobial [259], anti-inflammatory [260] and wound healing properties have been previously described [261]. Besides verbascoside and its positional isomers (isoverbascoside and forsythoside A), other phenylpropanoids were identified in verbenaceae: leucosceptoside and its isomers (plantainoside C and purpureaside D), martynoside and its isomers (isomartynoside and another unknown isomer) [257]. All these molecules are structurally very similar. Data about the chemical characterization of *Aloysia*

polystachya (Griseb. et Moldenke) are few in the literature and to the best of our knowledge, no study has been performed at present on isomartynoside. In this work the qualitative characterization and determination by HPLC-MS of the phenylpropanoid glycosides fraction purified by Solid Phase Extraction (SPE) were performed. To achieve this purpose, three different MS techniques have been coupled to HPLC: ion trap tandem mass spectrometry (Ion Trap LC/MS), quadrupole-time of flight high resolution mass spectrometry (Q-TOF HRMS) and triple-quadrupole (TQ LC/MS). The ion trap LC/MS analyses were performed to support structure elucidation, based on *m/z* values of the detected ions. LC/Q-TOF HRMS analysis allowed to obtain the accurate mass measurements, providing the most probable molecular formula which is useful to confirm the identity of the compounds in the extract. Finally, quantitative analysis was assessed by TQ.

2. EXPERIMENTAL

2.1. Chemicals and solvents

All solvents (HPLC-MS grade) were purchased from Sigma-Aldrich (Milan, Italy). The reference standard of verbascoside (purity 86.87%) was purchased from HWI ANALYTIK GmbH (Rülzheim, Germany). Water was purified by using a Milli-Q Plus185 system from Millipore (Milford, MA, USA).

2.2. Samples and extraction procedure

The leaves of *Aloysia polystachya* (Griseb. et Moldenke) were collected in Paraguay. A representative sample of herbal material was dried at room temperature and then protected from light and humidity until the analysis. Ten different aliquots of the bulk material were analysed. For each aliquot the powdered leaves (1 g) were defatted with 10 mL of hexane and successively with 10 mL of chloroform for 15 min, under magnetic stirring. The whole extraction procedure required 5 consecutive extraction steps, each lasting 30 minutes. The first was carried out with 20 mL of absolute methanol, others with 10 mL. The extracts were centrifuged (RCF 7200 g) for 10 min. Supernatant was collected, filtered, and stored at 4 °C until analysis. Infusion and decoction of the leaves were also prepared (leaves:water ratio 3% w/v). The infusion was obtained by pouring ultrapure boiling water on powdered leaves in a closed vessel and left for 10 minutes under stirring. The decoction involved the use of ultrapure water at room temperature, then increased until boiling point and left at 100 °C for 10 minutes. Infusion and decoction were paper filtered and stored until the analysis.

2.3. Solid phase extraction (SPE) and purification

The methanolic extract (ME) was purified on a C18 Solid-Phase cartridge (Discovery DSC-18, 6 mL tubes, 500 mg sorbent, Supelco, Bellefonte, PA, USA), according to the method described by De Marco *et al*. opportunely modified [262]. One mL of ME was evaporated under nitrogen flow at room temperature and the residue was dissolved in 1 mL of ultrapure water. The solution was immediately adsorbed onto a C18 cartridge, previously activated with 5 mL of absolute methanol, followed by 5 mL of water. Aqueous methanol solutions at different concentration, between 10 and 100% v/v of MeOH, were tested to find the best elution condition for phenylpropanoids. The flow rate was adjusted at 0.5 mL/min. Considering the results obtained from different methanol solutions, the cartridge was first washed with 10 mL of methanol:water, 20:80 (v/v) to remove the more hydrophilic compounds, then the elution of phenylpropanoid glycosides was achieved under atmospheric pressure by using 15 mL of methanol:water, 50:50 (v/v) solution. Finally, the SPE extract was filtered through a 0.22 μm filter and injected into the HPLC system.

2.4. Identification of phenylpropanoid glycosides by Ion Trap LC/MS

The chromatographic system consisted of a 6310A Ion Trap LC-MS^n (Agilent Technologies Inc., Waldbronn, Germany) equipped with an Agilent 1200 Series LC with binary pump, electrospray interface (ESI) and the ion trap mass spectrometer. Data Analysis 4.0 (Agilent Technologies, Inc.) was used for data acquisition and processing. The chromatography was performed on a Supelco Ascentis Express C18 10 cm x 2.1 mm i.d., 2.7 μm p.s., at a flow rate of 0.2 mL/min. The eluents were: (A) 0.1% formic acid in water, and (B) 0.1% formic acid in acetonitrile. Separations were achieved at 30 °C with the following gradient: 1% B isocratic for 1 min, 10-35% B in 20 min, 35–100% B in 8 min, 100% B isocratic for 10 min, 10% B in 3 min. A delay of 2 min was necessary for column equilibration, during which no MS data were recorded. The injection volume was 10 μl. The capillary voltage was set to -3500 V, the desolvating temperature was 350 °C. Nitrogen was used as a drying (flow rate 8 L/min) and nebulising gas (pressure 25 psi). The mass spectrometer operated in negative full-scan mode in the scan range 100–800 Da. Target mass and the ion charge control were set to 600 Da and 25000 Da respectively [263].

2.5. LC/Q-TOF HRMS analysis

The Agilent 1200 Series LC was coupled to a 6520 Accurate-Mass Q-TOF mass spectrometer (Agilent Technologies Inc., Waldbronn, Germany) equipped with an ESI interface. To achieve the most reproducible results, the same chromatographic and ionization conditions as for the Ion Trap LC/MS analysis were set and same parameters were used. The HPLC system was coupled to a Q-TOF mass spectrometer, equipped with an ESI interface. The capillary voltage was set to -3500 V, the drying gas temperature was 350 °C; nitrogen was used as a drying (flow rate 8 L/min) and nebulising gas (pressure 25 psi). The mass spectrometer operated in negative mode in the scan range 100–800 Da. The accurate mass data of the molecular ions were processed through the MassHunter Workstation Software, and an accuracy threshold of 10 ppm was selected.

2.6. HPLC-ESI-TQ MS analysis

Samples were analysed by Agilent technologies HPLC series 1200 and MS-TQ mass spectrometer 6410. The detection was performed using the ESI source operating in negative ion multiple reaction monitoring mode (MRM). The capillary voltage was set to -4000 V. The drying gas temperature was 350 °C; nitrogen was used as a drying (flow rate 9 L/min) and nebulising gas (pressure 25 psi). Chromatographic conditions were the same as reported before. Standard stock solution for quantification was prepared by dissolving verbascoside standard in HPLC grade methanol at the concentration of 5 mg/mL and properly diluted to obtain working solutions. The concentrations of individual standards measured in three-fold serial injections were 0.1, 0.5, 1.25, 2.5, 5.0 µg/mL. Over this interval a linear relationship was observed. Due to the inability to find on the market the appropriate standards, we verified the possibility to employ the same verbascoside calibration curve to tentatively quantify all the related compounds.

2.7. Method validation

For the method validation, the following validation parameters were considered: linearity, limit of detection (LOD), limit of quantification (LOQ), precision, and accuracy. Linearity was determined by means of external standard calibration. Verbascoside stock standard solution was gradually diluted to five data points in the working range 0.1-5.0 µg/mL, and the linear fitting was evaluated through the correlation coefficient (r^2).

LOD and LOQ were calculated according to IUPAC guidelines as:

$$\mathrm{LOD} = \mathrm{BLANK} + 3\mathrm{SD} \times \mathrm{BLANK}$$

$$\mathrm{LOQ} = \mathrm{BLANK} + 10\mathrm{SD} \times \mathrm{BLANK}$$

Precision was evaluated using 10 independent replicates of a sample, analysed within one and three different days. Precision values are expressed as CV%. Accuracy was evaluated measuring the recovery obtained from a sample spiked with 1 mg of verbascoside pure standard.

3. RESULTS AND DISCUSSION

From spectrometric analyses of *Aloysia polystachya* (Griseb. et Moldenke) ME, it was possible to identify three different groups of structural isomers with *m/z* of 623, 637, 651, respectively. In Figure 1, are shown the MRM reconstructed chromatograms for the groups of isomers, and the peaks were identified with numbers (**1-11**) according to the elution order.

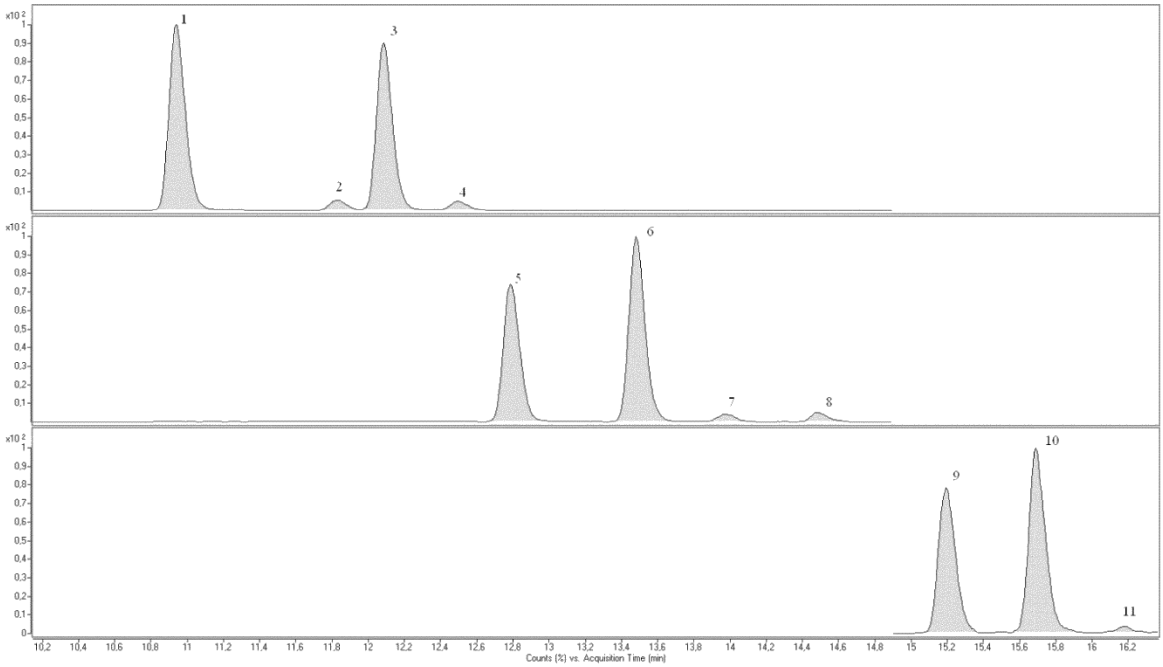

Figure 1. MRM reconstructed chromatograms for the three groups of isomers.

The compounds were identified by the interpretation of their ESI-MS and ESI-MS^2 spectra and by LC/Q-TOF HRMS exact mass determination for molecular ions and fragments. These analyses presented, for all the considered ions, errors below the established threshold (10 ppm). The obtained experimental results were finally compared to data present in the literature [263–265] confirming the compound identification obtained by MS^2 experiments. The main peak was identified as verbascoside (**1**), besides were identified three verbascoside isomers, which showed the same MS^2 profile. Compound **2**, corresponded to isoverbascoside and compound **3**

was designated as forsythoside A, owing to its occurrence in natural products containing verbascoside [266]. The MS^2 analyses produced fragments at *m/z* 461 and 315, resulting from the loss of the caffeoyl moiety $[M-H-162]^-$ and the successive loss of rhamnose $[M-H-146]^-$, respectively, according to the fragmentation pathway shown in Figure 2. This is consistent with the observed fragmentation pattern of isoverbascoside and forsythoside A given in the literature [265].

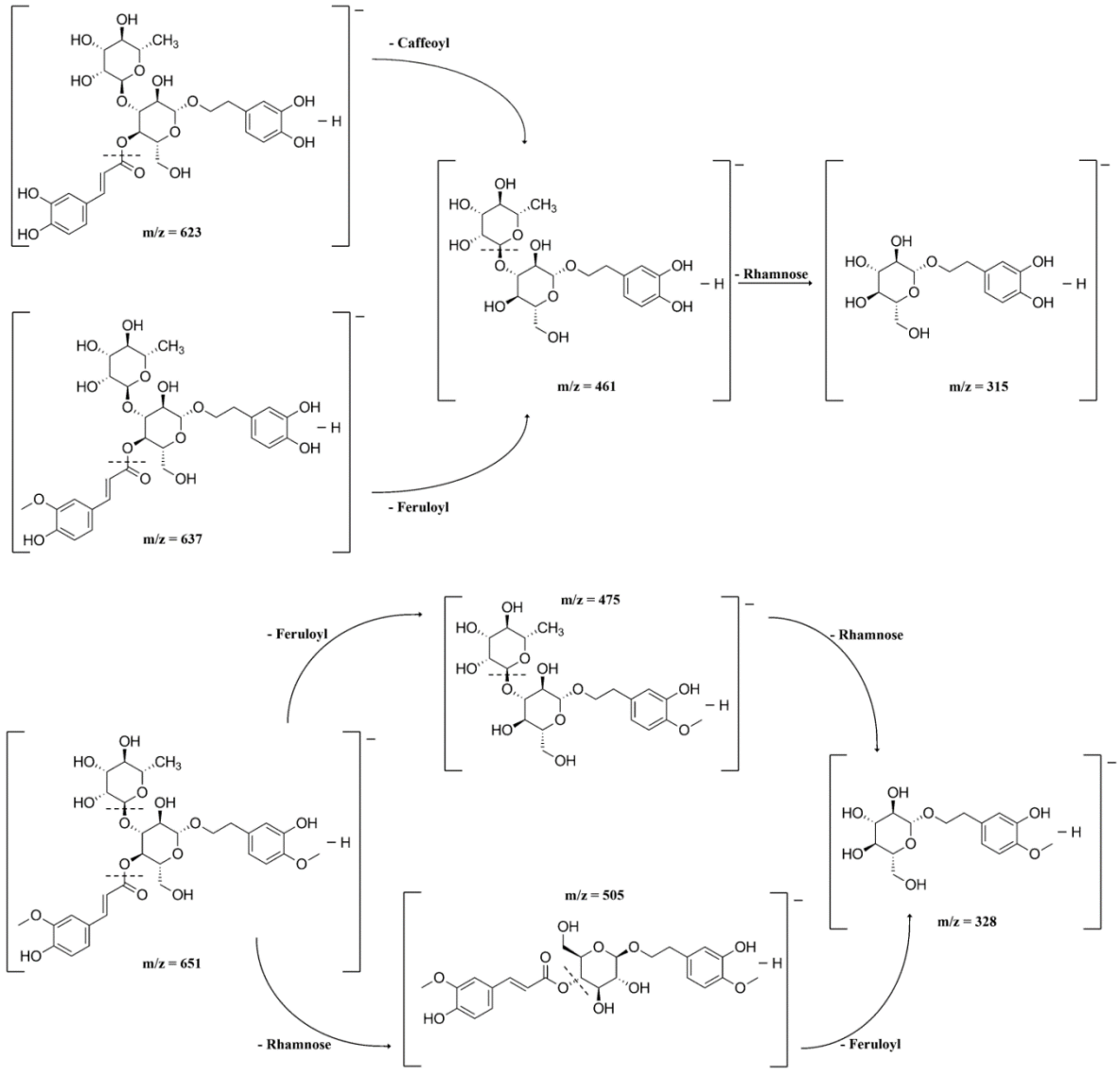

Figure 2. Proposed fragmentation pathway for verbascoside (**1**), leucosceptoside A (**5**), and martynoside (**9**).

Another probable verbascoside isomer was found (**4**) that showed the same fragmentation, but it could not be conclusively identified. The two most probable candidates were isoforsithoside or cis-verbascoside. Compound **5**, leucosceptoside A, showed an ion at *m/z* 637 in the full MS ($[M-H]^-$) spectrum. In the MS^2 experiment, characteristic ions at *m/z* 461, and *m/z* 315 were observed, due to the loss of the feruloyl unit $[M-H-176]^-$, and rhamnose $[M-H-146]^-$,

respectively (Figure 2). Compounds **6**, **7** and **8** corresponded to leucosceptoside A isomers, which showed the same MS^2 profile. The first two compounds were tentatively identified as plantainoside C and purpureaside D respectively, taking also into account the molecular formula provided, the presence of the feruloyl unit and rhamnose in the structure and the natural occurrence in herbal products [267,268]. Conversely, it was not possible the identification of the third compound (**8**). Compound **9**, martynoside, exhibited the characteristic phenylethanoid glycoside fragmentation pattern, being characterized by the loss of rhamnose moiety $[M-H-146]^-$ at *m/z* 505, the feruloyl unit $[M-H-176]^-$ at *m/z* 475, and water at *m/z* 457. Another fragmentation ion peak was observed at *m/z* 328, due to the loss of feruloyl unit $[M-H-176]^-$ and rhamnose moiety $[M-H-146]^-$ from the deprotonated molecular ions at *m/z* 505 and 475, respectively. The proposed fragmentation pathway is shown in Figure 2. Compound **10** and **11** corresponded to martynoside isomers, which presented the same MS^2 profile. Compound **10** was tentatively identified as isomartynoside due to the presence of the feruloyl unit and rhamnose in the structure, the molecular formula and the well-documented occurrence in natural products [269,270]. These results were confirmed by HRMS analysis. Table 2 summarises the results of the mass spectrometric analyses, all measured *m/z* values showed errors below 10 ppm.

Table 2. Results of HPLC-ESI-TQ MS analysis for each proposed compound (1-9)

Peak	t_R (min)	*m/z* calculated	*m/z* (Q-TOF HRMS)	Error (ppm)	Molecular formula	MS^2 fragments	Proposed compound
1	11.0	623.1981	623.1985	4	$C_{29}H_{36}O_{15}$	461, 315	Verbascoside (**1**)
2	11.8	623.1981	623.1988	7	$C_{29}H_{36}O_{15}$	461, 315	Isoverbascoside (**2**)
3	12.1	623.1981	623.1991	10	$C_{29}H_{36}O_{15}$	461, 315	Forsythoside A (**3**)
4	12.5	623.1981	623.1991	10	$C_{29}H_{36}O_{15}$	461, 315	**1** isomer (unknown)
5	12.8	637.2138	637.2130	8	$C_{30}H_{38}O_{15}$	461, 315	Leucosceptoside A (**5**)
6	13.5	637.2138	637.2147	9	$C_{30}H_{38}O_{15}$	461, 315	Plantainoside C (**6**)
7	13.9	637.2138	637.2129	9	$C_{30}H_{38}O_{15}$	461, 315	Purpureaside D (**7**)
8	14.5	637.2138	637.2129	9	$C_{30}H_{38}O_{15}$	461, 315	**5** isomer (unknown)
9	15.2	651.2294	651.2294	6	$C_{31}H_{40}O_{15}$	505, 475, 457, 328	Martynoside (**9**)
10	15.7	651.2294	651.2298	4	$C_{31}H_{40}O_{15}$	475, 457	Isomartynoside (**10**)
11	16.2	651.2294	651.2286	8	$C_{31}H_{40}O_{15}$	475, 457	**9** isomer (unknown)

As regard the quantitative analysis, verbascoside was directly determined using its calibration curve. Since the detected compounds (**1-11**) belonged to three groups of homologs (verbascoside and its isomers; forsythoside and its isomers; martynoside and its isomers) which all presented the same fragmentation pattern it may be assumed that they have a similar ionization efficiency, which is not significantly affected by mobile phase composition. As a matter of fact, this value increased less than 7.0% in organic solvent during the elution of

compounds. For this reason, the overall determination of the analytes was attempted by only using the verbascoside calibration curve.

As concerns the method validation, it showed good linearity in the tested concentration range (r^2 = 0.9983). A good intra- and inter-day precision were also observed, with CV% equal to 3.7 and 9.1%, respectively. The percentage recovery was found to be higher than 98%, hence all the validation parameters can be considered satisfactory.

Table 3. Validation parameters of the method for determination of phenylpropanoid glycosides in *Aloysia polystachya*.

Method validation parameters	
r^2	0.9983
LOD	58 ng/mL
LOQ	64 ng/mL
Precision (intra-day, n=10)	3.7 CV%
Precision (inter-day, n=10)	9.1 CV%
Recovery	98.0%

Quantitative results for ME, infusion, and decoction of *Aloysia polystachya* leaves are reported in Table 4.

Table 4. Quantitative results of verbascoside, leucosceptoside A, martynoside and their isomers.

	Compound	Extract (mg/g)	Infusion (mg/100 mL)	Decoction (mg/100 mL)
1	Verbascoside	3.60±0.15	3.63±0.11	0.95±0.22
2	Isoverbascoside	0.25±0.01	0.45±0.08	< LOD
3	Forsythoside A	2.06±0.07	0.20±0.01	< LOD
4	Unknown	< LOQ	< LOQ	< LOD
5	Leucosceptoside A	0.13±0.01	0.19±0.007	< LOQ
6	Plantainoside C	0.15±0.01	0.14±0.01	< LOD
7	Purpureaside D	0.08±0.001	0.08±0.04	< LOD
8	Unknown	< LOQ	< LOQ	< LOD
9	Martynoside	0.12±0.01	0.08±0.009	< LOD
10	Isomartynoside	0.12±0.02	< LOQ	< LOD
11	Unknown	< LOQ	< LOQ	< LOD

The obtained results indicate that the mass spectrometric detection with different analysers, which include Ion Trap and Q-TOF, could be a useful tool in the qualitative characterization of the phenylpropanoid glycosides of *Aloysia polystachya* leaves extract. To our knowledge, the compounds forsythoside A, plantainoside C, purpureaside D, martynoside and its two isomers were described here for the first time in *Aloysia polystachya* (Griseb. et Moldenke). Among the tested extraction procedures, highest amounts were obtained for ME, whereas in the case of decoction, all concentrations except for verbascoside were lower than LOQ. Comparing the result obtained from 3% (w/v) infusion with those from methanolic extraction, the recovery of

extractable verbascoside was 33.6%, this percentage decreased even further in the case of decoction (8.8%). For leucosceptoside A the infusion recovery is only of 3.2%, while this compound resulted less concentrated than LOD in the case of decoction. Also for martynoside a similar trend has been observed. It can be assumed that this class of compounds is very sensitive to air and temperature exposure and, for this reason, the intake of phenylpropanoids by means of leaves decoction would be significantly lower with respect to other forms. In the ME, verbascoside and forsythoside A were the most abundant compounds, while martynoside was the lowest. Even though data about *Aloysia polystachya* chemical composition are limited, verbascoside, leucosceptoside A and martynoside were previously determined in *Clerodendrum phlomidis* L. roots (Lamiaceae) and *Verbena officinalis* L. leaves (Verbenaceae) by other authors using HPTLC and HPLC-UV techniques [271]. Comparing results provided by the HPLC-MS method here described with the few available in literature, similar contents of verbascoside were obtained, while other principal compounds seem to be more abundant in roots of Clerodendrum than in leaves of Aloysia. Verbascoside content in *Verbena officinalis* L. ranged from 1.58 to 4.45 mg/g of dry weight depending on seasonal variation [272], while in *Clerodendrum phlomidis* L. the contents of leucosceptoside A and martynoside ranged from 3.2 to 4.5 mg/g and 4.0 to 5.4 mg/g of dry matter, respectively [271].

4. Conclusions

In this work an efficient HPLC-MS method was developed, optimized, and validated for the identification of the main compounds present in *Aloysia polystachya* leaves. This analytical approach that combines different mass analysers provided a good separation of the different classes of phenylpropanoids and gave accurate results; further validation criteria were in the acceptable limits. To the best of our knowledge, forsythoside A, plantainoside C, purpureaside D, martynoside and its two isomers were herein described for the first time in this plant. These findings could be helpful for the evaluation of the quality of the herbal material, with a view to obtain a standardised product for the extraction of bioactive compounds to be used as functional supplementation or nutraceuticals products.

GENERAL CONCLUSIONS

The global diffusion of nutraceuticals and plant-based products has rapidly increased in recent years. One of the factors that has positively affected the market of these products, is that nutraceuticals have no strict regulations to control them, and they often are erroneously advertised under the claim of being always safe, or effective as a drug substitute. The COVID-19 ongoing pandemic, has additionally shifted consumer preferences towards natural, health-boosting products, contributing to a massive increase in demand for products claiming to prevent various health disorders. This market growth has created new challenges for both the industry and governmental authorities from a regulatory, and an analytical point of view. For this reason, the main scope of this PhD thesis was to create new knowledge in the field of extraction, purification and determination of the bioactive constituents present in plants of pharmaceutical and nutraceutical interest (*Cannabis sativa* L., *Spathodea campanulata* P. Beauv., *Morus alba* L., *Aloysia polystachya* Griseb. et Moldenke). The analytical methods here developed and applied for this purpose cover a pivotal role in the long path from the herbal material to the final product. First, in the quality monitoring of the herbal starting material, second, to guarantee a better reproducibility in biological assays and finally to ensure the safety for consumer use. The results here disclosed demonstrate the great importance of developing updated and efficient analytical methods for the characterization of plant bioactive secondary metabolites, together with the establishment of high-yielding and environmentally sustainable extraction procedures. Several advanced analytical techniques, including HPLC methods coupled with UV/DAD or MS detectors and non-separation techniques (NMR), were optimised, and validated, then applied to the qualitative and quantitative analysis of plant bioactive secondary metabolites. The combination of different techniques was useful for the identification of phenylpropanoids in *A. polystachya* for the first time, and to disclose the composition of *S. campanulata*, in order to clarify which were the most active components responsible for the inhibition of *H. pylori* growth. Different bioassays were performed as well, to evaluate the therapeutic potential of these natural extracts, to promote their rational use in the treatment or prevention of health disorders, and to facilitate the validation of health claims. In particular, the antiproliferative activity of non-psychoactive *C. sativa* L. was evaluated on human cancer cell lines, and these results support the use of CBD-rich extracts as candidates for therapeutic use in myeloproliferative diseases. Particular attention was paid to promote the use of Italian mulberry as a source of phytochemicals in the context of new therapeutic approaches for diabetes mellitus. The antiglycative capacity and hypoglycaemic effect of leaf extracts were evaluated on different *in vitro* models, showing great potentialities for the therapy of hyperglycaemia. These promising results have fostered us to develop an ideal oral dosage

form for the delivery of mulberry constituents, with the aim to improve the therapeutical results for the benefit of human health.

References

1. *WHO Traditional Medicine Strategy 2013-2024*; World Health Organization: Geneva, 2013; ISBN 978-92-4-150609-0.
2. Jonas, W.B.; Eisenberg, D.; Hufford, D.; Crawford, C. The Evolution of Complementary and Alternative Medicine (CAM) in the USA over the Last 20 Years. *Forsch. Komplementarmedizin 2006* 2013, *20*, 65–72, doi:10.1159/000348284.
3. Che, C.-T.; Zhang, H. Plant Natural Products for Human Health. *Int. J. Mol. Sci.* 2019, *20*, doi:10.3390/ijms20040830.
4. Ekor, M. The Growing Use of Herbal Medicines: Issues Relating to Adverse Reactions and Challenges in Monitoring Safety. *Front. Pharmacol.* 2014, *4*, doi:10.3389/fphar.2013.00177.
5. Süntar, I. Importance of Ethnopharmacological Studies in Drug Discovery: Role of Medicinal Plants. *Phytochem. Rev.* 2020, *19*, 1199–1209, doi:10.1007/s11101-019-09629-9.
6. Hahn, A. Pflanzliche Drogen im Spannungsfeld zwischen Nahrungsergänzungsmitteln und Arzneimitteln. *Z. Für Phytother.* 2008, *29*, 262–270, doi:10.1055/s-0028-1124028.
7. Colombo, M.L. Botanicals Authentication in Food, Food Supplements and Herbal Medicinal Products. *Plant Biosyst. - Int. J. Deal. Asp. Plant Biol.* 2016, *150*, 22–26, doi:10.1080/11263504.2014.984009.
8. Schieber, A.; Lopes-Lutz, D. 4.40 - Analytical Methods – Functional Foods and Dietary Supplements. In *Comprehensive Biotechnology (Second Edition)*; Moo-Young, M., Ed.; Academic Press: Burlington, 2011; 487–499 ISBN 978-0-08-088504-9.
9. Kumar, A.; Kumar, S.; Thomas, T.D.; Ramchiary, N.; Swamy, M.K.; Ahmad, I. Linking Omics Approaches to Medicinal Plants and Human Health. In *Natural Bio-active Compounds: Volume 3: Biotechnology, Bioengineering, and Molecular Approaches*; Akhtar, M.S., Swamy, M.K., Eds.; Springer: Singapore, 2019; 31–57 ISBN 9789811374388.
10. Kirkland, J.J.; Schuster, S.A.; Johnson, W.L.; Boyes, B.E. Fused-Core Particle Technology in High-Performance Liquid Chromatography: An Overview. *J. Pharm. Anal.* 2013, *3*, 303–312, doi:10.1016/j.jpha.2013.02.005.
11. Karioti, A.; Giocaliere, E.; Guccione, C.; Pieraccini, G.; Gallo, E.; Vannacci, A.; Bilia, A.R. Combined HPLC-DAD–MS, HPLC–MSn and NMR Spectroscopy for Quality Control of Plant Extracts: The Case of a Commercial Blend Sold as Dietary Supplement. *J. Pharm. Biomed. Anal.* 2014, *88*, 7–15, doi:10.1016/j.jpba.2013.07.040.
12. Suman, C.; Hemant, L.; Mahmoud A., ElSohly *Cannabis Sativa L.- Botany and Biotechnology*; Springer International Publishing AG: Cham, Switzerland, 2017; ISBN 978-3-319-54563-9.
13. Hurgobin, B.; Tamiru-Oli, M.; Welling, M.T.; Doblin, M.S.; Bacic, A.; Whelan, J.; Lewsey, M.G. Recent Advances in Cannabis Sativa Genomics Research. *New Phytol.* 2021, *230*, 73–89, doi:10.1111/nph.17140.
14. McPartland, J.M.; Guy, G.W. Models of Cannabis Taxonomy, Cultural Bias, and Conflicts between Scientific and Vernacular Names. *Bot. Rev.* 2017, *83*, 327–381, doi:10.1007/s12229-017-9187-0.
15. Dei Cas, M.; Casagni, E.; Saccardo, A.; Arnoldi, S.; Young, C.; Scotti, S.; Vieira de Manicor, E.; Gambaro, V.; Roda, G. The Italian Panorama of Cannabis Light Preparation: Determination of Cannabinoids by LC-UV. *Forensic Sci. Int.* 2020, *307*, 110113, doi:10.1016/j.forsciint.2019.110113.
16. Cascio, M.G.; Pertwee, R.G.; Marini, P. The Pharmacology and Therapeutic Potential of Plant Cannabinoids. In *Cannabis sativa L. - Botany and Biotechnology*; Chandra, S., Lata, H., ElSohly, M.A., Eds.; Springer International Publishing: Cham, 2017; 207–225 ISBN 978-3-319-54564-6.
17. Ferrante, C.; Recinella, L.; Ronci, M.; Menghini, L.; Brunetti, L.; Chiavaroli, A.; Leone, S.; Di Iorio, L.; Carradori, S.; Tirillini, B.; et al. Multiple Pharmacognostic Characterization on Hemp Commercial Cultivars: Focus on Inflorescence Water Extract Activity. *Food Chem. Toxicol.* 2019, *125*, 452–461, doi:10.1016/j.fct.2019.01.035.
18. Lopez, H.L.; Cesareo, K.R.; Raub, B.; Kedia, A.W.; Sandrock, J.E.; Kerksick, C.M.; Ziegenfuss, T.N. Effects of Hemp Extract on Markers of Wellness, Stress Resilience, Recovery and Clinical

Biomarkers of Safety in Overweight, But Otherwise Healthy Subjects. *J. Diet. Suppl.* 2020, *17*, 561–586, doi:10.1080/19390211.2020.1765941.
19. Todorova, J.; Lazarov, L.I.; Petrova, M.; Tzintzarov, A.; Ugrinova, I. The Antitumor Activity of Cannabidiol on Lung Cancer Cell Lines A549 and H1299: The Role of Apoptosis. *Biotechnol. Biotechnol. Equip.* 2021, *35*, 873–879, doi:10.1080/13102818.2021.1915870.
20. Appendino, G.; Taglialatela-Scafati, O. Cannabinoids: Chemistry and Medicine. In *Natural Products*; Springer Berlin Heidelberg: Berlin, Heidelberg, 2013; 3415–3435.
21. Andre, C.M.; Hausman, J.-F.; Guerriero, G. Cannabis Sativa: The Plant of the Thousand and One Molecules. *Front. Plant Sci.* 2016, *7*, 19, doi:10.3389/fpls.2016.00019.
22. Alexander, S.P.H. Therapeutic Potential of Cannabis-Related Drugs. *Prog. Neuropsychopharmacol. Biol. Psychiatry* 2016, *64*, 157–166, doi:10.1016/j.pnpbp.2015.07.001.
23. Campos, A.C.; Fogaça, M.V.; Sonego, A.B.; Guimarães, F.S. Cannabidiol, Neuroprotection and Neuropsychiatric Disorders. *Pharmacol. Res.* 2016, *112*, 119–127, doi:10.1016/j.phrs.2016.01.033.
24. Pollastro, F.; Minassi, A.; Fresu, L.G. Cannabis Phenolics and Their Bioactivities. *Curr. Med. Chem.* 2018, *25*, 1160–1185, doi:10.2174/0929867324666170810164636.
25. Izzo, A.A.; Borrelli, F.; Capasso, R.; Marzo, V.D.; Mechoulam, R. Non-Psychotropic Plant Cannabinoids: New Therapeutic Opportunities from an Ancient Herb. *Trends Pharmacol. Sci.* 2009, *30*, 515–527, doi:10.1016/j.tips.2009.07.006.
26. Lu, H.-C.; Mackie, K. An Introduction to the Endogenous Cannabinoid System. *Biol. Psychiatry* 2016, *79*, 516–525, doi:10.1016/j.biopsych.2015.07.028.
27. Zhelyazkova, M.; Kirilov, B.; Momekov, G. The Pharmacological Basis for Application of Cannabidiol in Cancer Chemotherapy. *Pharmacia* 2020, *67(4)*, 239–252, doi:10.3897/pharmacia.67.e51304.
28. Munson, A.E.; Harris, L.S.; Friedman, M.A.; Dewey, W.L.; Carchman, R.A. Antineoplastic Activity of Cannabinoids2. *JNCI J. Natl. Cancer Inst.* 1975, *55*, 597–602, doi:10.1093/jnci/55.3.597.
29. Galve-Roperh, I.; Sánchez, C.; Cortés, M.L.; del Pulgar, T.G.; Izquierdo, M.; Guzmán, M. Anti-Tumoral Action of Cannabinoids: Involvement of Sustained Ceramide Accumulation and Extracellular Signal-Regulated Kinase Activation. *Nat. Med.* 2000, *6*, 313–319, doi:10.1038/73171.
30. Casanova, M.L.; Blázquez, C.; Martínez-Palacio, J.; Villanueva, C.; Fernández-Aceñero, M.J.; Huffman, J.W.; Jorcano, J.L.; Guzmán, M. Inhibition of Skin Tumor Growth and Angiogenesis in Vivo by Activation of Cannabinoid Receptors. *J. Clin. Invest.* 2003, *111*, 43–50, doi:10.1172/JCI16116.
31. Blázquez, C.; González-Feria, L.; Álvarez, L.; Haro, A.; Casanova, M.L.; Guzmán, M. Cannabinoids Inhibit the Vascular Endothelial Growth Factor Pathway in Gliomas. *Cancer Res.* 2004, *64*, 5617–5623, doi:10.1158/0008-5472.CAN-03-3927.
32. Freimuth, N.; Ramer, R.; Hinz, B. Antitumorigenic Effects of Cannabinoids beyond Apoptosis. *J. Pharmacol. Exp. Ther.* 2010, *332*, 336–344, doi:10.1124/jpet.109.157735.
33. Brighenti, V.; Pellati, F.; Steinbach, M.; Maran, D.; Benvenuti, S. Development of a New Extraction Technique and HPLC Method for the Analysis of Non-Psychoactive Cannabinoids in Fibre-Type Cannabis Sativa L. (Hemp). *J. Pharm. Biomed. Anal.* 2017, *143*, 228–236, doi:10.1016/J.JPBA.2017.05.049.
34. Happyana, N.; Kayser, O. Monitoring Metabolite Profiles of Cannabis Sativa L. Trichomes during Flowering Period Using 1H NMR-Based Metabolomics and Real-Time PCR. *Planta Med.* 2016, *82*, 1217–1223, doi:10.1055/s-0042-108058.
35. Flores-Sanchez, I.J.; Verpoorte, R. PKS Activities and Biosynthesis of Cannabinoids and Flavonoids in Cannabis Sativa L. Plants. *Plant Cell Physiol.* 2008, *49*, 1767–1782, doi:10.1093/pcp/pcn150.
36. Aizpurua-Olaizola, O.; Omar, J.; Navarro, P.; Olivares, M.; Etxebarria, N.; Usobiaga, A. Identification and Quantification of Cannabinoids in Cannabis Sativa L. Plants by High Performance Liquid Chromatography-Mass Spectrometry. *Anal. Bioanal. Chem.* 2014, *406*, 7549–7560, doi:10.1007/s00216-014-8177-x.

37. Chauthe, S.K.; Sharma, R.J.; Aqil, F.; Gupta, R.C.; Singh, I.P. Quantitative NMR: An Applicable Method for Quantitative Analysis of Medicinal Plant Extracts and Herbal Products. *Phytochem. Anal.* 2012, *23*, 689–696, doi:10.1002/pca.2375.
38. Molyneux, R.J.; Wong, Y.-I. Nuclear Magnetic Resonance Spectroscopic Determination of .Alpha.- and .Beta.-Acid Homolog Composition in Hops. *J. Agric. Food Chem.* 1975, *23*, 1201–1204, doi:10.1021/jf60202a012.
39. Pauli, G.F.; Chen, S.-N.; Simmler, C.; Lankin, D.C.; Gödecke, T.; Jaki, B.U.; Friesen, J.B.; McAlpine, J.B.; Napolitano, J.G. Importance of Purity Evaluation and the Potential of Quantitative ^{1}H NMR as a Purity Assay. *J. Med. Chem.* 2014, *57*, 9220–9231, doi:10.1021/jm500734a.
40. Bertelli, D.; Brighenti, V.; Marchetti, L.; Reik, A.; Pellati, F. Nuclear Magnetic Resonance and High-Performance Liquid Chromatography Techniques for the Characterization of Bioactive Compounds from Humulus Lupulus L. (Hop). *Anal. Bioanal. Chem.* 2018, *410*, 3521–3531, doi:10.1007/s00216-018-0851-y.
41. Pellati, F.; Brighenti, V.; Sperlea, J.; Marchetti, L.; Bertelli, D.; Benvenuti, S.; Pellati, F.; Brighenti, V.; Sperlea, J.; Marchetti, L.; et al. New Methods for the Comprehensive Analysis of Bioactive Compounds in Cannabis Sativa L. (Hemp). *Molecules* 2018, *23*, 2639, doi:10.3390/molecules23102639.
42. Protti, M.; Brighenti, V.; Battaglia, M.R.; Anceschi, L.; Pellati, F.; Mercolini, L. Cannabinoids from Cannabis Sativa L.: A New Tool Based on HPLC− DAD−MS/MS for a Rational Use in Medicinal Chemistry, doi:10.1021/acsmedchemlett.8b00571.
43. Citti, C.; Braghiroli, D.; Vandelli, M.A.; Cannazza, G. Pharmaceutical and Biomedical Analysis of Cannabinoids: A Critical Review. *J. Pharm. Biomed. Anal.* 2018, *147*, 565–579, doi:10.1016/j.jpba.2017.06.003.
44. Brighenti, V.; Protti, M.; Anceschi, L.; Zanardi, C.; Mercolini, L.; Pellati, F. Emerging Challenges in the Extraction, Analysis and Bioanalysis of Cannabidiol and Related Compounds. *J. Pharm. Biomed. Anal.* 2021, *192*, 113633, doi:10.1016/j.jpba.2020.113633.
45. International Conference on Harmonisation of Technical Requirements for Registration of Pharmaceuticals for Human Use - Validation of Analytical Procedures: Text and Methodology Q2(R1) 2005.
46. Araneda, J.F.; Chu, T.; Leclerc, M.C.; Riegel, S.D.; Spingarn, N. Quantitative Analysis of Cannabinoids Using Benchtop NMR Instruments. *Anal. Methods* 2020, *12*, 4853–4857, doi:10.1039/D0AY01511C.
47. Marchetti, L.; Pellati, F.; Benvenuti, S.; Bertelli, D. Use of 1H NMR to Detect the Percentage of Pure Fruit Juices in Blends. *Molecules* 2019, *24*, doi:10.3390/molecules24142592.
48. Dagenais, G.R.; Leong, D.P.; Rangarajan, S.; Lanas, F.; Lopez-Jaramillo, P.; Gupta, R.; Diaz, R.; Avezum, A.; Oliveira, G.B.F.; Wielgosz, A.; et al. Variations in Common Diseases, Hospital Admissions, and Deaths in Middle-Aged Adults in 21 Countries from Five Continents (PURE): A Prospective Cohort Study. *The Lancet* 2020, *395*, 785–794, doi:10.1016/S0140-6736(19)32007-0.
49. Hinz, B.; Ramer, R. Anti-Tumour Actions of Cannabinoids. *Br. J. Pharmacol.* 2019, *176*, 1384–1394, doi:10.1111/bph.14426.
50. Javid, F.A.; Phillips, R.M.; Afshinjavid, S.; Verde, R.; Ligresti, A. Cannabinoid Pharmacology in Cancer Research: A New Hope for Cancer Patients? *Eur. J. Pharmacol.* 2016, *775*, 1–14, doi:10.1016/j.ejphar.2016.02.010.
51. Śledziński, P.; Zeyland, J.; Słomski, R.; Nowak, A. The Current State and Future Perspectives of Cannabinoids in Cancer Biology. *Cancer Med.* 2018, *7*, 765–775, doi:10.1002/cam4.1312.
52. Scott, K.A.; Dalgleish, A.G.; Liu, W.M. Anticancer Effects of Phytocannabinoids Used with Chemotherapy in Leukaemia Cells Can Be Improved by Altering the Sequence of Their Administration. *Int. J. Oncol.* 2017, *51*, 369–377, doi:10.3892/ijo.2017.4022.
53. Muller, C.; Morales, P.; Reggio, P.H. Cannabinoid Ligands Targeting TRP Channels. *Front. Mol. Neurosci.* 2019, *11*, 487, doi:10.3389/fnmol.2018.00487.
54. Moreno, E.; Cavic, M.; Krivokuca, A.; Casadó, V.; Canela, E. The Endocannabinoid System as a Target in Cancer Diseases: Are We There Yet? *Front. Pharmacol.* 2019, *10*, 339, doi:10.3389/fphar.2019.00339.

55. Pellati, F.; Brighenti, V.; Sperlea, J.; Marchetti, L.; Bertelli, D.; Benvenuti, S. New Methods for the Comprehensive Analysis of Bioactive Compounds in Cannabis Sativa L. (Hemp). *Molecules* 2018, *23*, 2639, doi:10.3390/molecules23102639.
56. Olivas-Aguirre, M.; Torres-López, L.; Valle-Reyes, J.S.; Hernández-Cruz, A.; Pottosin, I.; Dobrovinskaya, O. Cannabidiol Directly Targets Mitochondria and Disturbs Calcium Homeostasis in Acute Lymphoblastic Leukemia. *Cell Death Dis.* 2019, *10*, 1–19, doi:10.1038/s41419-019-2024-0.
57. Aliferis, K.A.; Bernard-Perron, D. Cannabinomics: Application of Metabolomics in Cannabis (Cannabis Sativa L.) Research and Development. *Front. Plant Sci.* 2020, *11*, 554, doi:10.3389/fpls.2020.00554.
58. Bonini, S.A.; Premoli, M.; Tambaro, S.; Kumar, A.; Maccarinelli, G.; Memo, M.; Mastinu, A. Cannabis Sativa: A Comprehensive Ethnopharmacological Review of a Medicinal Plant with a Long History. *J. Ethnopharmacol.* 2018, *227*, 300–315, doi:10.1016/j.jep.2018.09.004.
59. Appendino, G.; Chianese, G.; Taglialatela-Scafati, O. Cannabinoids: Occurrence and Medicinal Chemistry. *Curr. Med. Chem.* 2011, *18*, 1085–1099, doi:10.2174/092986711794940888.
60. Alves, P.; Amaral, C.; Teixeira, N.; Correia-da-Silva, G. Cannabis Sativa: Much More beyond Δ9-Tetrahydrocannabinol. *Pharmacol. Res.* 2020, *157*, 104822, doi:10.1016/j.phrs.2020.104822.
61. Atalay, S.; Jarocka-Karpowicz, I.; Skrzydlewska, E. Antioxidative and Anti-Inflammatory Properties of Cannabidiol. *Antioxidants* 2020, *9*, 21, doi:10.3390/antiox9010021.
62. Corsi, L.; Pellati, F.; Brighenti, V.; Plessi, N.; Benvenuti, S. Chemical Composition and In Vitro Neuroprotective Activity of Fibre-Type Cannabis Sativa L. (Hemp). *Curr. Bioact. Compd.* 2019, *15*, 201–210.
63. Iseppi, R.; Brighenti, V.; Licata, M.; Lambertini, A.; Sabia, C.; Messi, P.; Pellati, F.; Benvenuti, S. Chemical Characterization and Evaluation of the Antibacterial Activity of Essential Oils from Fibre-Type Cannabis Sativa L. (Hemp). *Molecules* 2019, *24*, 2302, doi:10.3390/molecules24122302.
64. Luca Roncati, M.V.; Luca Roncati, M.V. Immunohistochemical expression of cannabinoid receptors in women's cancers: what's new? *Eur. J. Gynaecol. Oncol.* 2021, *42*, 193–195, doi:10.31083/j.ejgo.2021.02.5463.
65. Protti, M.; Brighenti, V.; Battaglia, M.R.; Anceschi, L.; Pellati, F.; Mercolini, L. Cannabinoids from Cannabis Sativa L.: A New Tool Based on HPLC–DAD–MS/MS for a Rational Use in Medicinal Chemistry. *ACS Med. Chem. Lett.* 2019, *10*, 539–544, doi:10.1021/acsmedchemlett.8b00571.
66. Petrovici, A.R.; Simionescu, N.; Sandu, A.I.; Paraschiv, V.; Silion, M.; Pinteala, M. New Insights on Hemp Oil Enriched in Cannabidiol: Decarboxylation, Antioxidant Properties and In Vitro Anticancer Effect. *Antioxidants* 2021, *10*, 738, doi:10.3390/antiox10050738.
67. Wang, F.; Multhoff, G. Repurposing Cannabidiol as a Potential Drug Candidate for Anti-Tumor Therapies. *Biomolecules* 2021, *11*, 582, doi:10.3390/biom11040582.
68. Marcu, J.P.; Christian, R.T.; Lau, D.; Zielinski, A.J.; Horowitz, M.P.; Lee, J.; Pakdel, A.; Allison, J.; Limbad, C.; Moore, D.H.; et al. Cannabidiol Enhances the Inhibitory Effects of Delta9-Tetrahydrocannabinol on Human Glioblastoma Cell Proliferation and Survival. *Mol. Cancer Ther.* 2010, *9*, 180–189, doi:10.1158/1535-7163.MCT-09-0407.
69. Vrijhoef, H.J.; De Belvis, A.G.; de la Calle, M.I.; De Sabata, S.; Kownatka, D.; Guldemond, N.A.; Montante, S.; Pelizzola, D.; Rehfeld, C.; Saraheimo, M. Global Report on Diabetes. *Eurohealth* 2017, *23*, 1–88.
70. Thakur, K.; Zhang, Y.-Y.; Mocan, A.; Zhang, F.; Zhang, J.-G.; Wei, Z.-J. 1-Deoxynojirimycin, Its Potential for Management of Non-Communicable Metabolic Diseases. *Trends Food Sci. Technol.* 2019, *89*, 88–99, doi:10.1016/j.tifs.2019.05.010.
71. Song, W.; Wang, H.-J.; Bucheli, P.; Zhang, P.-F.; Wei, D.-Z.; Lu, Y.-H. Phytochemical Profiles of Different Mulberry (*Morus* Sp.) Species from China. *J. Agric. Food Chem.* 2009, *57*, 9133–9140, doi:10.1021/jf9022228.
72. Naowaboot, J.; Pannangpetch, P.; Kukongviriyapan, V.; Kongyingyoes, B.; kukongviriyapan, U. Antihyperglycemic, Antioxidant and Antiglycation Activities of Mulberry Leaf Extract in Streptozotocin-Induced Chronic Diabetic Rats. *Plant Foods Hum. Nutr.* 2009, *64*, 116–121, doi:10.1007/s11130-009-0112-5.

73. Nasri, H.; Baradaran, A.; Shirzad, H.; Rafieian-Kopaei, M. New Concepts in Nutraceuticals as Alternative for Pharmaceuticals. *Int. J. Prev. Med.* 2014, *5*, 1487–1499.
74. Zamoner, L.O.B.; Aragão-Leoneti, V.; Carvalho, I. Iminosugars: Effects of Stereochemistry, Ring Size, and N-Substituents on Glucosidase Activities. *Pharmaceuticals* 2019, *12*, doi:10.3390/ph12030108.
75. Yagi, M. The Structure of Moranoline, a Piperidine Alkaloid from Morus Species. *Nippon Nogei Kagaku Kaishi* 1976, *50*, 571–572.
76. Konno, K.; Ono, H.; Nakamura, M.; Tateishi, K.; Hirayama, C.; Tamura, Y.; Hattori, M.; Koyama, A.; Kohno, K. Mulberry Latex Rich in Antidiabetic Sugar-Mimic Alkaloids Forces Dieting on Caterpillars. *Proc. Natl. Acad. Sci. U. S. A.* 2006, *103*, 1337–1341, doi:10.1073/pnas.0506944103.
77. Lemus, I.; García, R.; Delvillar, E.; Knop, G. Hypoglycaemic Activity of Four Plants Used in Chilean Popular Medicine. *Phytother. Res.* 1999, *13*, 91–94, doi:10.1002/(SICI)1099-1573(199903)13:2<91::AID-PTR350>3.0.CO;2-8.
78. Wang, Z.; Wang, J.; Chan, P. Treating Type 2 Diabetes Mellitus with Traditional Chinese and Indian Medicinal Herbs. *Evid. Based Complement. Alternat. Med.* 2013, *2013*, 1–17, doi:10.1155/2013/343594.
79. Wang, N.; Zhu, F.; Chen, K. 1-Deoxynojirimycin: Sources, Extraction, Analysis and Biological Functions. *Nat. Prod. Commun.* 2017, *12*, 1934578X1701200934, doi:10.1177/1934578X1701200934.
80. Kimura, T.; Nakagawa, K.; Kubota, H.; Kojima, Y.; Goto, Y.; Yamagishi, K.; Oita, S.; Oikawa, S.; Miyazawa, T. Food-Grade Mulberry Powder Enriched with 1-Deoxynojirimycin Suppresses the Elevation of Postprandial Blood Glucose in Humans. *J. Agric. Food Chem.* 2007, *55*, 5869–5874, doi:10.1021/jf062680g.
81. Yatsunami, K.; Ichida, M.; Onodera, S. The Relationship between 1-Deoxynojirimycin Content and α-Glucosidase Inhibitory Activity in Leaves of 276 Mulberry Cultivars (Morus Spp.) in Kyoto, Japan. *J. Nat. Med.* 2008, *62*, 63–66, doi:10.1007/s11418-007-0185-0.
82. Vichasilp, C.; Nakagawa, K.; Sookwong, P.; Higuchi, O.; Luemunkong, S.; Miyazawa, T. Development of High 1-Deoxynojirimycin (DNJ) Content Mulberry Tea and Use of Response Surface Methodology to Optimize Tea-Making Conditions for Highest DNJ Extraction. *LWT - Food Sci. Technol.* 2012, *45*, 226–232, doi:10.1016/j.lwt.2011.09.008.
83. Esti Wulandari, Y.R.; Prasasty, V.D.; Rio, A.; Geniola, C. Determination of 1-Deoxynojirimycin Content and Phytochemical Profiles from Young and Mature Mulberry Leaves of Morus Spp. *OnLine J. Biol. Sci.* 2019, *19*, 124–131, doi:10.3844/ojbsci.2019.124.131.
84. Hao, J.-Y.; Wan, Y.; Yao, X.-H.; Zhao, W.-G.; Hu, R.-Z.; Chen, C.; Li, L.; Zhang, D.-Y.; Wu, G.-H. Effect of Different Planting Areas on the Chemical Compositions and Hypoglycemic and Antioxidant Activities of Mulberry Leaf Extracts in Southern China. *PLoS ONE* 2018, *13*, doi:10.1371/journal.pone.0198072.
85. Przygoński, K.; Wojtowicz, E. The Optimization of Extraction Process of White Mulberry Leaves and the Characteristic Bioactive Properties Its Powder Extract. *Herba Pol.* 2019, *65*, 12–19, doi:10.2478/hepo-2019-0003.
86. Tomotake, H.; Katagiri, M.; Yamato, M. Silkworm Pupae (Bombyx Mori) Are New Sources of High Quality Protein and Lipid. *J. Nutr. Sci. Vitaminol. (Tokyo)* 2010, *56*, 446–448, doi:10.3177/jnsv.56.446.
87. Tong, T.-T.; Zhao, E.-H.; Gao, H.-L.; Xu, Y.-H.; Zhao, Y.-J.; Fu, G.; Cui, H. Recent Research Advances of 1-Deoxynojirimycin and Its Derivatives. *Zhongguo Zhong Yao Za Zhi Zhongguo Zhongyao Zazhi China J. Chin. Mater. Medica* 2018, *43*, 1990–1997, doi:10.19540/j.cnki.cjcmm.20180125.010.
88. Rodríguez-Sánchez, S.; Hernández-Hernández, O.; Ruiz-Matute, A.I.; Sanz, M.L. A Derivatization Procedure for the Simultaneous Analysis of Iminosugars and Other Low Molecular Weight Carbohydrates by GC–MS in Mulberry (Morus Sp.). *Food Chem.* 2011, *126*, 353–359, doi:10.1016/j.foodchem.2010.10.097.
89. Kimura, T.; Nakagawa, K.; Saito, Y.; Yamagishi, K.; Suzuki, M.; Yamaki, K.; Shinmoto, H.; Miyazawa, T. Determination of 1-Deoxynojirimycin in Mulberry Leaves Using Hydrophilic Interaction Chromatography with Evaporative Light Scattering Detection. *J. Agric. Food Chem.* 2004, *52*, 1415–1418, doi:10.1021/jf0306901.

90. Vichasilp, C.; Nakagawa, K.; Sookwong, P.; Suzuki, Y.; Kimura, F.; Higuchi, O.; Miyazawa, T. Optimization of 1-Deoxynojirimycin Extraction from Mulberry Leaves by Using Response Surface Methodology. *Biosci. Biotechnol. Biochem.* 2009, *73*, 2684–2689, doi:10.1271/bbb.90543.
91. Nakagawa, K.; Ogawa, K.; Higuchi, O.; Kimura, T.; Miyazawa, T.; Hori, M. Determination of Iminosugars in Mulberry Leaves and Silkworms Using Hydrophilic Interaction Chromatography–Tandem Mass Spectrometry. *Anal. Biochem.* 2010, *404*, 217–222, doi:10.1016/j.ab.2010.05.007.
92. Tolstikov, V.V.; Fiehn, O. Analysis of Highly Polar Compounds of Plant Origin: Combination of Hydrophilic Interaction Chromatography and Electrospray Ion Trap Mass Spectrometry. *Anal. Biochem.* 2002, *301*, 298–307, doi:10.1006/abio.2001.5513.
93. Burgess, K.S.; Morgan, M.; Deverno, L.; Husband, B.C. Asymmetrical Introgression between Two Morus Species (M. Alba, M. Rubra) That Differ in Abundance. *Mol. Ecol.* 2005, *14*, 3471–3483, doi:10.1111/j.1365-294X.2005.02670.x.
94. Nepal, M.P.; Ferguson, C.J. Phylogenetics of Morus (Moraceae) Inferred from ITS and TrnL-TrnF Sequence Data. *Syst. Bot.* 2012, *37*, 442–450, doi:10.1600/036364412X635485.
95. Zeng, Q.; Chen, H.; Zhang, C.; Han, M.; Li, T.; Qi, X.; Xiang, Z.; He, N. Definition of Eight Mulberry Species in the Genus Morus by Internal Transcribed Spacer-Based Phylogeny. *PLOS ONE* 2015, *10*, e0135411, doi:10.1371/journal.pone.0135411.
96. Gąsecka, M.; Siwulski, M.; Magdziak, Z.; Budzyńska, S.; Stuper-Szablewska, K.; Niedzielski, P.; Mleczek, M. The Effect of Drying Temperature on Bioactive Compounds and Antioxidant Activity of Leccinum Scabrum (Bull.) Gray and Hericium Erinaceus (Bull.) Pers. *J. Food Sci. Technol.* 2020, *57*, 513–525, doi:10.1007/s13197-019-04081-1.
97. Chlumská, Z.; Janeček, S.; Doležal, J. How to Preserve Plant Samples for Carbohydrate Analysis? Test of Suitable Methods Applicable in Remote Areas. *Folia Geobot.* 2013, *49*, doi:10.1007/s12224-013-9153-5.
98. Hu, X.-Q.; Jiang, L.; Zhang, J.-G.; Deng, W.; Wang, H.-L.; Wei, Z.-J. Quantitative Determination of 1-Deoxynojirimycin in Mulberry Leaves from 132 Varieties. *Ind. Crops Prod.* 2013, *49*, 782–784, doi:10.1016/j.indcrop.2013.06.030.
99. Han, W.; Chen, X.; Yu, H.; Chen, L.; Shen, M. Seasonal Variations of Iminosugars in Mulberry Leaves Detected by Hydrophilic Interaction Chromatography Coupled with Tandem Mass Spectrometry. *Food Chem.* 2018, *251*, 110–114, doi:10.1016/j.foodchem.2018.01.058.
100. Asano, N.; Oseki, K.; Tomioka, E.; Kizu, H.; Matsui, K. N-Containing Sugars from Morus Alba and Their Glycosidase Inhibitory Activities. *Carbohydr. Res.* 1994, *259*, 243–255, doi:10.1016/0008-6215(94)84060-1.
101. Sugiyama, M.; Katsube, T.; Koyama, A.; Itamura, H. Seasonal Changes in Functional Component Contents in Mulberry (*Morus Alba* L.) Leaves. *Hortic. J.* 2017, *86*, 534–542, doi:10.2503/hortj.OKD-053.
102. Nakanishi, H.; Onose, S.; Kitahara, E.; Chumchuen, S.; Takasaki, M.; Konishi, H.; Kanekatsu, R. Effect of Environmental Conditions on the α-Glucosidase Inhibitory Activity of Mulberry Leaves. *Biosci. Biotechnol. Biochem.* 2011, *75*, 2293–2296, doi:10.1271/bbb.110407.
103. Shibano, M.; Fujimoto, Y.; Kushino, K.; Kusano, G.; Baba, K. Biosynthesis of 1-Deoxynojirimycin in Commelina Communis: A Difference between the Microorganisms and Plants. *Phytochemistry* 2004, *65*, 2661–2665, doi:10.1016/j.phytochem.2004.08.013.
104. Prediction of Worldwide Energy Resource Available online: https://power.larc.nasa.gov/data-access-viewer/.
105. Power Data Methodology Available online: https://power.larc.nasa.gov/docs/methodology/.
106. MacDougall, Daniel.; Crummett, W.B.; et al., . Guidelines for Data Acquisition and Data Quality Evaluation in Environmental Chemistry. *Anal. Chem.* 1980, *52*, 2242–2249, doi:10.1021/ac50064a004.
107. Global Report on Diabetes (WHO). 2016, 1–83.
108. Borghetti, G.; von Lewinski, D.; Eaton, D.M.; Sourij, H.; Houser, S.R.; Wallner, M. Diabetic Cardiomyopathy: Current and Future Therapies. Beyond Glycemic Control. *Front. Physiol.* 2018, *9*, 1514, doi:10.3389/fphys.2018.01514.
109. Singh, R.; Shushni, M.; Belkheir, A. Antibacterial and Antioxidant Activities of Mentha Piperita L. *Arab. J. Chem.* 2015, *8*, 322–328.

110. Tran, L.; Zielinski, A.; Roach, A.H.; Jende, J.A.; Householder, A.M.; Cole, E.E.; Atway, S.A.; Amornyard, M.; Accursi, M.L.; Shieh, S.W.; et al. Pharmacologic Treatment of Type 2 Diabetes: Oral Medications. *Ann. Pharmacother.* 2015, *49*, 540–556, doi:10.1177/1060028014558289.
111. Marchetti, L.; Saviane, A.; Montà, A. dalla; Paglia, G.; Pellati, F.; Benvenuti, S.; Bertelli, D.; Cappellozza, S. Determination of 1-Deoxynojirimycin (1-DNJ) in Leaves of Italian or Italy-Adapted Cultivars of Mulberry (Morus Sp.Pl.) by HPLC-MS. *Plants* 2021, *10*, 1553, doi:10.3390/plants10081553.
112. Ji, T.; Li, J.; Su, S.-L.; Zhu, Z.-H.; Guo, S.; Qian, D.-W.; Duan, J.-A. Identification and Determination of the Polyhydroxylated Alkaloids Compounds with α-Glucosidase Inhibitor Activity in Mulberry Leaves of Different Origins. *Molecules* 2016, *21*, 206, doi:10.3390/molecules21020206.
113. Wang, Z.; Tang, C.; Xiao, G.; Dai, F.; Lin, S.; Li, Z.; Luo, G. Comparison of Free and Bound Phenolic Compositions and Antioxidant Activities of Leaves from Different Mulberry Varieties. *BMC Chem.* 2021, *15*, 21, doi:10.1186/s13065-021-00747-0.
114. Yaman, R. Phytochemical Properties of Some Mulberry Genotypes Grown in Malatya Province. *Üzüncü Il Üniversitesi Tarım Bilim. Derg.* 2021, *31*, 348–355, doi:10.29133/yyutbd.785270.
115. Chan, E.W.C.; Wong, S.K.; Tangah, J.; Inoue, T.; Chan, H.T. Phenolic Constituents and Anticancer Properties of Morus Alba (White Mulberry) Leaves. *J. Integr. Med.* 2020, *18*, 189–195, doi:10.1016/j.joim.2020.02.006.
116. Ainsworth, E.A.; Gillespie, K.M. Estimation of Total Phenolic Content and Other Oxidation Substrates in Plant Tissues Using Folin–Ciocalteu Reagent. *Nat. Protoc.* 2007, *2*, 875–877, doi:10.1038/nprot.2007.102.
117. Pękal, A.; Pyrzynska, K. Evaluation of Aluminium Complexation Reaction for Flavonoid Content Assay. *Food Anal. Methods* 2014, *7*, 1776–1782, doi:10.1007/s12161-014-9814-x.
118. Milella, L.; Milazzo, S.; De Leo, M.; Vera Saltos, M.B.; Faraone, I.; Tuccinardi, T.; Lapillo, M.; De Tommasi, N.; Braca, A. α-Glucosidase and α-Amylase Inhibitors from *Arcytophyllum Thymifolium*. *J. Nat. Prod.* 2016, *79*, 2104–2112, doi:10.1021/acs.jnatprod.6b00484.
119. Spínola, V.; Pinto, J.; Castilho, P.C. Hypoglycemic, Anti-Glycation and Antioxidant in Vitro Properties of Two Vaccinium Species from Macaronesia: A Relation to Their Phenolic Composition. *J. Funct. Foods* 2018, *40*, 595–605, doi:10.1016/j.jff.2017.12.002.
120. Maietta, M.; Colombo, R.; Corana, F.; Papetti, A. Cretan Tea (Origanum Dictamnus L.) as a Functional Beverage: An Investigation on Antiglycative and Carbonyl Trapping Activities. *Food Funct.* 2018, *9*, 1545–1556, doi:10.1039/C7FO01930K.
121. Zhang, L.-S.; Wang, X.; Dong, L.-L. Antioxidation and Antiglycation of Polysaccharides from Misgurnus Anguillicaudatus. *Food Chem.* 2011, *124*, 183–187, doi:10.1016/j.foodchem.2010.06.006.
122. Maietta, M.; Colombo, R.; Lavecchia, R.; Sorrenti, M.; Zuorro, A.; Papetti, A. Artichoke (Cynara Cardunculus L. Var. Scolymus) Waste as a Natural Source of Carbonyl Trapping and Antiglycative Agents. *Food Res. Int.* 2017, *100*, 780–790, doi:10.1016/j.foodres.2017.08.007.
123. Mesías, M.; Navarro, M.; Gökmen, V.; Morales, F.J. Antiglycative Effect of Fruit and Vegetable Seed Extracts: Inhibition of AGE Formation and Carbonyl-Trapping Abilities. *J. Sci. Food Agric.* 2013, *93*, 2037–2044, doi:10.1002/jsfa.6012.
124. Nastić, N.; Borrás-Linares, I.; Lozano-Sánchez, J.; Švarc-Gajić, J.; Segura-Carretero, A. Optimization of the Extraction of Phytochemicals from Black Mulberry (Morus Nigra L.) Leaves. *J. Ind. Eng. Chem.* 2018, *68*, 282–292, doi:10.1016/j.jiec.2018.07.055.
125. Jin, Q.; Yang, J.; Ma, L.; Cai, J.; Li, J. Comparison of Polyphenol Profile and Inhibitory Activities Against Oxidation and α-Glucosidase in Mulberry (Genus Morus) Cultivars from China. *J. Food Sci.* 2015, *80*, C2440-2451, doi:10.1111/1750-3841.13099.
126. Sánchez-Salcedo, E.M.; Mena, P.; García-Viguera, C.; Hernández, F.; Martínez, J.J. (Poly)Phenolic Compounds and Antioxidant Activity of White (Morus Alba) and Black (Morus Nigra) Mulberry Leaves: Their Potential for New Products Rich in Phytochemicals. *J. Funct. Foods* 2015, *18*, 1039–1046, doi:10.1016/j.jff.2015.03.053.
127. Zhang, D.-Y.; Wan, Y.; Hao, J.-Y.; Hu, R.-Z.; Chen, C.; Yao, X.-H.; Zhao, W.-G.; Liu, Z.-Y.; Li, L. Evaluation of the Alkaloid, Polyphenols, and Antioxidant Contents of Various Mulberry Cultivars from Different Planting Areas in Eastern China. *Ind. Crops Prod.* 2018, *122*, 298–307, doi:10.1016/j.indcrop.2018.05.065.

128. Katsube, T.; Imawaka, N.; Kawano, Y.; Yamazaki, Y.; Shiwaku, K.; Yamane, Y. Antioxidant Flavonol Glycosides in Mulberry (Morus Alba L.) Leaves Isolated Based on LDL Antioxidant Activity. *Food Chem.* 2006, *97*, 25–31, doi:10.1016/j.foodchem.2005.03.019.
129. Kwon, O.-C.; Ju, W.-T.; Kim, H.-B.; Sung, G.-B.; Kim, Y.-S. UPLC-DAD-QTOF/MS Analysis of Flavonoids from 12 Varieties of Korean Mulberry Fruit. *J. Food Qual.* 2019, *2019*, e1528917, doi:10.1155/2019/1528917.
130. Kim, S.Y.; Gao, J.J.; Lee, W.-C.; Ryu, K.S.; Lee, K.R.; Kim, Y.C. Antioxidative Flavonoids from the Leaves of Morus Alba. *Arch. Pharm. Res.* 1999, *22*, 81–85, doi:10.1007/BF02976442.
131. Shrikanta, A.; Kumar, A.; Govindaswamy, V. Resveratrol Content and Antioxidant Properties of Underutilized Fruits. *J. Food Sci. Technol.* 2015, *52*, 383–390, doi:10.1007/s13197-013-0993-z.
132. Choi, S.W.; Jang, Y.J.; Lee, Y.J.; Leem, H.H.; Kim, E.O. Analysis of Functional Constituents in Mulberry (Morus Alba L.) Twigs by Different Cultivars, Producing Areas, and Heat Processings. *Prev. Nutr. Food Sci.* 2013, *18*, 256–262, doi:10.3746/pnf.2013.18.4.256.
133. Hyun-Bok, K.; Jung-Bong, K.; Sun-Lim, K.; Seong-Hyouk, K.; Young-Seek, S. Quantitative Analysis of Resveratrol in Mulberry Leaves. *Quant. Anal. Resveratrol Mulberry Leaves* 2011, *56*, 23–28, doi:10.7740/KJCS.2011.56.1.023.
134. Ercisli, S.; Orhan, E. Chemical Composition of White (Morus Alba), Red (Morus Rubra) and Black (Morus Nigra) Mulberry Fruits. *Food Chem.* 2007, *103*, 1380–1384, doi:10.1016/j.foodchem.2006.10.054.
135. Sánchez-Salcedo, E.M.; Sendra, E.; Carbonell-Barrachina, Á.A.; Martínez, J.J.; Hernández, F. Fatty Acids Composition of Spanish Black (Morus Nigra L.) and White (Morus Alba L.) Mulberries. *Food Chem.* 2016, *190*, 566–571, doi:10.1016/j.foodchem.2015.06.008.
136. Clifford, M.N.; Knight, S.; Kuhnert, N. Discriminating between the Six Isomers of Dicaffeoylquinic Acid by LC-MS(n). *J. Agric. Food Chem.* 2005, *53*, 3821–3832, doi:10.1021/jf050046h.
137. Bystrom, L.M.; Lewis, B.A.; Brown, D.L.; Rodriguez, E.; Obendorf, R.L. Characterization of Phenolics by LC-UV/Vis, LC-MS/MS and Sugars by GC in Melicoccus Bijugatus Jacq. 'Montgomery' Fruits. *Food Chem.* 2008, *111*, 1017–1024, doi:10.1016/j.foodchem.2008.04.058.
138. Girotti, A.W. Mechanisms of Lipid Peroxidation. *J. Free Radic. Biol. Med.* 1985, *1*, 87–95, doi:10.1016/0748-5514(85)90011-x.
139. Crescenzi, M.A.; D'Urso, G.; Piacente, S.; Montoro, P. LC-ESI/LTQOrbitrap/MS Metabolomic Analysis of Fennel Waste (Foeniculum Vulgare Mill.) as a Byproduct Rich in Bioactive Compounds. 2021, 16.
140. Yu, Y.; Li, H.; Zhang, B.; Wang, J.; Shi, X.; Huang, J.; Yang, J.; Zhang, Y.; Deng, Z. Nutritional and Functional Components of Mulberry Leaves from Different Varieties: Evaluation of Their Potential as Food Materials. *Int. J. Food Prop.* 2018, *21*, 1495–1507, doi:10.1080/10942912.2018.1489833.
141. Yatsunami, K.; Ichida, M.; Onodera, S. The Relationship between 1-Deoxynojirimycin Content and α-Glucosidase Inhibitory Activity in Leaves of 276 Mulberry Cultivars (Morus Spp.) in Kyoto, Japan. *J. Nat. Med.* 2007, *62*, 63–66, doi:10.1007/s11418-007-0185-0.
142. Lou, D.-S.; Zou, F.-M.; Yan, H.; Gui, Z.-Z. Factors Influencing the Biosynthesis of 1-Deoxynojirimycin in Morus Alba L. 2011, *6(13)*, 2998–3006.
143. Martinez-Gonzalez, A.I.; Díaz-Sánchez, Á.G.; de la Rosa, L.A.; Vargas-Requena, C.L.; Bustos-Jaimes, I.; Alvarez-Parrilla, E. Polyphenolic Compounds and Digestive Enzymes: In Vitro Non-Covalent Interactions. *Mol. J. Synth. Chem. Nat. Prod. Chem.* 2017, *22*, 669, doi:10.3390/molecules22040669.
144. Kim, D.-S.; Kang, Y.M.; Jin, W.Y.; Sung, Y.-Y.; Choi, G.; Kim, H.K. Antioxidant Activities and Polyphenol Content of Morus Alba Leaf Extracts Collected from Varying Regions. *Biomed. Rep.* 2014, *2*, 675–680, doi:10.3892/br.2014.294.
145. Polumackanycz, M.; Sledzinski, T.; Goyke, E.; Wesolowski, M.; Viapiana, A. A Comparative Study on the Phenolic Composition and Biological Activities of Morus Alba L. Commercial Samples. *Molecules* 2019, *24*, 3082, doi:10.3390/molecules24173082.
146. Qiao, Y.; Ito, M.; Kimura, T.; Ikeuchi, T.; Takita, T.; Yasukawa, K. Inhibitory Effect of Morus Australis Leaf Extract and Its Component Iminosugars on Intestinal Carbohydrate-Digesting Enzymes. *J. Biosci. Bioeng.* 2021, *132*, 226–233, doi:10.1016/j.jbiosc.2021.05.005.

147. Ferron, L.; Colombo, R.; Mannucci, B.; Papetti, A. A New Italian Purple Corn Variety (Moradyn) Byproduct Extract: Antiglycative and Hypoglycemic In Vitro Activities and Preliminary Bioaccessibility Studies. *Molecules* 2020, *25*, 1958, doi:10.3390/molecules25081958.
148. Di Sotto, A.; Locatelli, M.; Macone, A.; Toniolo, C.; Cesa, S.; Carradori, S.; Eufemi, M.; Mazzanti, G.; Di Giacomo, S. Hypoglycemic, Antiglycation, and Cytoprotective Properties of a Phenol-Rich Extract From Waste Peel of Punica Granatum L. Var. Dente Di Cavallo DC2. *Molecules* 2019, *24*, 3103, doi:10.3390/molecules24173103.
149. Martinez-Gonzalez, A.I.; Díaz-Sánchez, Á.G.; de la Rosa, L.A.; Vargas-Requena, C.L.; Bustos-Jaimes, I.; Alvarez-Parrilla, E. Polyphenolic Compounds and Digestive Enzymes: In Vitro Non-Covalent Interactions. *Mol. J. Synth. Chem. Nat. Prod. Chem.* 2017, *22*, 669, doi:10.3390/molecules22040669.
150. Cao, H.; Chen, X. Structures Required of Flavonoids for Inhibiting Digestive Enzymes. *Anticancer Agents Med. Chem.* 2012, *12*, 929–939, doi:10.2174/187152012802650110.
151. Ye, X.-P.; Song, C.-Q.; Yuan, P.; Mao, R.-G. α-Glucosidase and α-Amylase Inhibitory Activity of Common Constituents from Traditional Chinese Medicine Used for Diabetes Mellitus. *Chin. J. Nat. Med.* 2010, *8*, 349–352, doi:10.1016/S1875-5364(10)60041-6.
152. Shi, M.; Loftus, H.; McAinch, A.J.; Su, X.Q. Blueberry as a Source of Bioactive Compounds for the Treatment of Obesity, Type 2 Diabetes and Chronic Inflammation. *J. Funct. Foods* 2017, *30*, 16–29, doi:10.1016/j.jff.2016.12.036.
153. Boath, A.S.; Stewart, D.; McDougall, G.J. Berry Components Inhibit α-Glucosidase in Vitro: Synergies between Acarbose and Polyphenols from Black Currant and Rowanberry. *Food Chem.* 2012, *135*, 929–936, doi:10.1016/j.foodchem.2012.06.065.
154. Singh, V.P.; Bali, A.; Singh, N.; Jaggi, A.S. Advanced Glycation End Products and Diabetic Complications. *Korean J. Physiol. Pharmacol. Off. J. Korean Physiol. Soc. Korean Soc. Pharmacol.* 2014, *18*, 1–14, doi:10.4196/kjpp.2014.18.1.1.
155. Shao, X.; Chen, H.; Zhu, Y.; Sedighi, R.; Ho, C.-T.; Sang, S. Essential Structural Requirements and Additive Effects for Flavonoids to Scavenge Methylglyoxal. *J. Agric. Food Chem.* 2014, *62*, 3202–3210, doi:10.1021/jf500204s.
156. Li, X.; Zheng, T.; Sang, S.; Lv, L. Quercetin Inhibits Advanced Glycation End Product Formation by Trapping Methylglyoxal and Glyoxal. *J. Agric. Food Chem.* 2014, *62*, 12152–12158, doi:10.1021/jf504132x.
157. Navarro, M.; Morales, F.J. In Vitro Investigation on the Antiglycative and Carbonyl Trapping Activities of Hydroxytyrosol. *Eur. Food Res. Technol.* 2016, *242*, 1101–1110, doi:10.1007/s00217-015-2614-8.
158. Naveen, Y.P.; Urooj, A.; Byrappa, K. A Review on Medicinal Plants Evaluated for Anti-Diabetic Potential in Clinical Trials: Present Status and Future Perspective. *J. Herb. Med.* 2021, *28*, 100436, doi:10.1016/j.hermed.2021.100436.
159. Li, Y.-G.; Ji, D.-F.; Zhong, S.; Lin, T.-B.; Lv, Z.-Q.; Hu, G.-Y.; Wang, X. 1-Deoxynojirimycin Inhibits Glucose Absorption and Accelerates Glucose Metabolism in Streptozotocin-Induced Diabetic Mice. *Sci. Rep.* 2013, *3*, 1377, doi:10.1038/srep01377.
160. Yatsunami, K.; Saito, Y.; Fukuda, E.; Onodera, S.; Oshigane, K. α-Glucosidase Inhibitory Activity in Leaves of Some Mulberry Varieties. *Food Sci. Technol. Res.* 2003, *9*, 392–394, doi:10.3136/fstr.9.392.
161. Gao, K.; Zheng, C.; Wang, T.; Zhao, H.; Wang, J.; Wang, Z.; Zhai, X.; Jia, Z.; Chen, J.; Zhou, Y.; et al. 1-Deoxynojirimycin: Occurrence, Extraction, Chemistry, Oral Pharmacokinetics, Biological Activities and In Silico Target Fishing. *Molecules* 2016, *21*, 1600, doi:10.3390/molecules21111600.
162. Bagheri, L.; Madadlou, A.; Yarmand, M.; Mousavi, M.E. Spray-Dried Alginate Microparticles Carrying Caffeine-Loaded and Potentially Bioactive Nanoparticles. *Food Res. Int.* 2014, *Complete*, 1113–1119, doi:10.1016/j.foodres.2014.05.040.
163. Kurozawa, L.E.; Hubinger, M.D. Hydrophilic Food Compounds Encapsulation by Ionic Gelation. *Curr. Opin. Food Sci.* 2017, *15*, 50–55, doi:10.1016/j.cofs.2017.06.004.
164. Sosnik, A. Alginate Particles as Platform for Drug Delivery by the Oral Route: State-of-the-Art. *ISRN Pharm.* 2014, *2014*, 1–17, doi:10.1155/2014/926157.

165. Uyen, N.T.T.; Hamid, Z.A.A.; Tram, N.X.T.; Ahmad, N. Fabrication of Alginate Microspheres for Drug Delivery: A Review. *Int. J. Biol. Macromol.* 2020, *153*, 1035–1046, doi:10.1016/j.ijbiomac.2019.10.233.
166. Łabowska, M.B.; Michalak, I.; Detyna, J. Methods of Extraction, Physicochemical Properties of Alginates and Their Applications in Biomedical Field – a Review. *Open Chem.* 2019, *17*, 738–762, doi:10.1515/chem-2019-0077.
167. Marchetti, L.; Saviane, A.; Paglia, G.; Pellati, F.; Benvenuti, S.; Bertelli, D.; Cappellozza, S. Determination of 1-Deoxynojirimycin (1-DNJ) in Leaves of Italian or Italy-Adapted Cultivars of Mulberry (Morus Sp.Pl.) by HPLC-MS. *Plants* 2021, *10*, 1–13, doi:10.3390/plants10081553.
168. Iannuccelli, V.; Coppi, G.; Cameroni, R. Biodegradable Intraoperative System for Bone Infection Treatment. I. The Drug/Polymer Interaction. *Int. J. Pharm.* 1996, *143*, 195–201, doi:10.1016/S0378-5173(96)04703-5.
169. Kock, F.V.C.; Monaretto, T.; Colnago, L.A. Time-Domain NMR Relaxometry as an Alternative Method for Analysis of Chitosan-Paramagnetic Ion Interactions in Solution. *Int. J. Biol. Macromol.* 2017, *98*, 228–232, doi:10.1016/j.ijbiomac.2017.01.083.
170. Serai, S.D. Basics of Magnetic Resonance Imaging and Quantitative Parameters T1, T2, T2*, T1rho and Diffusion-Weighted Imaging. *Pediatr. Radiol.* 2021, doi:10.1007/s00247-021-05042-7.
171. Fieber, W.; Herrmann, A.; Ouali, L.; Velazco, M.I.; Kreutzer, G.; Klok, H.-A.; Ternat, C.; Plummer, C.J.G.; Månson, J.-A.E.; Sommer, H. NMR Diffusion and Relaxation Studies of the Encapsulation of Fragrances by Amphiphilic Multiarm Star Block Copolymers. *Macromolecules* 2007, *40*, 5372–5378, doi:10.1021/ma070222i.
172. di Cocco, M.E.; Bianchetti, C.; Chiellini, F. 1H NMR Studies of Alginate Interactions with Amino Acids. *J. Bioact. Compat. Polym.* 2003, *18*, 283–296, doi:10.1177/088391103037015.
173. Pasparakis, G.; Bouropoulos, N. Swelling Studies and in Vitro Release of Verapamil from Calcium Alginate and Calcium Alginate–Chitosan Beads. *Int. J. Pharm.* 2006, *323*, 34–42, doi:10.1016/j.ijpharm.2006.05.054.
174. Khorram, M.; Samimi, M.; Samimi, A.; Moghadam, H. Electrospray Preparation of Propranolol-Loaded Alginate Beads: Effect of Matrix Reinforcement on Loading and Release Profile. *J. Appl. Polym. Sci.* 2015, *132*, doi:10.1002/app.41334.
175. Østberg, T.; Vesterhus, L.; Graffner, C. Calcium Alginate Matrices for Oral Multiple Unit Administration. II: Effect of Process and Formulation Factors on Matrix Properties. 1993, doi:10.1016/0378-5173(93)90138-6.
176. Takka, F.A., S. Calcium Alginate Microparticles for Oral Administration: II Effect of Form Ulation Factors on Drug Release and Drug Entrapment Efficiency. *J. Microencapsul.* 1999, *16*, 291–301, doi:10.1080/026520499289022.
177. Li, Q.; Li, X.; Zhao, C. Strategies to Obtain Encapsulation and Controlled Release of Small Hydrophilic Molecules. *Front. Bioeng. Biotechnol.* 2020, *8*, 437, doi:10.3389/fbioe.2020.00437.
178. Jeong, C.; Kim, S.; Lee, C.; Cho, S.; Kim, S.-B. Changes in the Physical Properties of Calcium Alginate Gel Beads under a Wide Range of Gelation Temperature Conditions. *Foods* 2020, *9*, 180, doi:10.3390/foods9020180.
179. Lin, S.-F.; Chen, Y.-C.; Chen, R.-N.; Chen, L.-C.; Ho, H.-O.; Tsung, Y.-H.; Sheu, M.-T.; Liu, D.-Z. Improving the Stability of Astaxanthin by Microencapsulation in Calcium Alginate Beads. *PLOS ONE* 2016, *11*, e0153685, doi:10.1371/journal.pone.0153685.
180. Cho, A.R.; Chun, Y.G.; Kim, B.K.; Park, D.J. Preparation of Alginate–CaCl2 Microspheres as Resveratrol Carriers. *J. Mater. Sci.* 2014, *49*, 4612–4619, doi:10.1007/s10853-014-8163-x.
181. Jain, D.; Verma, K.; Verma, S.; Shukla, S. Formulation and in Vitro Characterization of Alginate Microspheres Loaded with Diloxanide Furoate for Colon- Specific Drug Delivery. *Asian J. Pharm.* 2010, *4*, 199, doi:10.4103/0973-8398.76742.
182. Wang, S.-B.; Chen, A.-Z.; Weng, L.-J.; Chen, M.-Y.; Xie, X.-L. Effect of Drug-Loading Methods on Drug Load, Encapsulation Efficiency and Release Properties of Alginate/Poly-L-Arginine/Chitosan Ternary Complex Microcapsules. *Macromol. Biosci.* 2004, *4*, 27–30, doi:10.1002/mabi.200300043.
183. Vichasilp, C.; Nakagawa, K.; Sookwong, P.; Higuchi, O.; Kimura, F.; Miyazawa, T. A Novel Gelatin Crosslinking Method Retards Release of Mulberry 1-Deoxynojirimycin Providing a

Prolonged Hypoglycaemic Effect. *Food Chem.* 2012, *134*, 1823–1830, doi:10.1016/j.foodchem.2012.03.086.
184. Essifi, K.; Lakrat, M.; Berraaouan, D.; Fauconnier, M.-L.; El Bachiri, A.; Tahani, A. Optimization of Gallic Acid Encapsulation in Calcium Alginate Microbeads Using Box-Behnken Experimental Design. *Polym. Bull.* 2021, *78*, 5789–5814, doi:10.1007/s00289-020-03397-9.
185. Essifi, K.; Brahmi, M.; Berraaouan, D.; Ed-Daoui, A.; El Bachiri, A.; Fauconnier, M.-L.; Tahani, A. Influence of Sodium Alginate Concentration on Microcapsules Properties Foreseeing the Protection and Controlled Release of Bioactive Substances. *J. Chem.* 2021, *2021*, e5531479, doi:10.1155/2021/5531479.
186. Sosnik, A.; Seremeta, K.P. Advantages and Challenges of the Spray-Drying Technology for the Production of Pure Drug Particles and Drug-Loaded Polymeric Carriers. *Adv. Colloid Interface Sci.* 2015, *223*, 40–54, doi:10.1016/j.cis.2015.05.003.
187. Esposito, T.; Mencherini, T.; Del Gaudio, P.; Auriemma, G.; Franceschelli, S.; Picerno, P.; Aquino, R.P.; Sansone, F. Design and Development of Spray-Dried Microsystems to Improve Technological and Functional Properties of Bioactive Compounds from Hazelnut Shells. *Molecules* 2020, *25*, 1273, doi:10.3390/molecules25061273.
188. Lourenço, S.C.; Moldão-Martins, M.; Alves, V.D. Microencapsulation of Pineapple Peel Extract by Spray Drying Using Maltodextrin, Inulin, and Arabic Gum as Wall Matrices. *Foods* 2020, *9*, 718, doi:10.3390/foods9060718.
189. Ameri, M.; Maa, Y.-F. Spray Drying of Biopharmaceuticals: Stability and Process Considerations. *Dry. Technol.* 2006, *24*, 763–768, doi:10.1080/03602550600685275.
190. Piñón-Balderrama, C.I.; Leyva-Porras, C.; Terán-Figueroa, Y.; Espinosa-Solís, V.; Álvarez-Salas, C.; Saavedra-Leos, M.Z. Encapsulation of Active Ingredients in Food Industry by Spray-Drying and Nano Spray-Drying Technologies. *Processes* 2020, *8*, 889, doi:10.3390/pr8080889.
191. Das, D.; Ghosh, R.; Mandal, P. Biogenic Synthesis of Silver Nanoparticles Using S1 Genotype of Morus Alba Leaf Extract: Characterization, Antimicrobial and Antioxidant Potential Assessment. *SN Appl. Sci.* 2019, *1*, 498, doi:10.1007/s42452-019-0527-z.
192. Coates, J. Interpretation of Infrared Spectra, A Practical Approach. In *Encyclopedia of Analytical Chemistry*; John Wiley & Sons, Ltd, 2006 ISBN 978-0-470-02731-8.
193. Daemi, H.; Barikani, M. Synthesis and Characterization of Calcium Alginate Nanoparticles, Sodium Homopolymannuronate Salt and Its Calcium Nanoparticles. *Sci. Iran.* 2012, *6*, 2023–2028, doi:10.1016/j.scient.2012.10.005.
194. Mic, M.; Pîrnău, A.; Floare, C.G.; Bogdan, M. Study of the Binding Affinity between Imatinib and α-1 Glycoprotein Using Nuclear Spin Relaxation and Isothermal Titration Calorimetry. *Int. J. Biol. Macromol.* 2020, *147*, 326–332, doi:10.1016/j.ijbiomac.2020.01.077.
195. Jaski, J.M.; Barão, C.E.; Morais Lião, L.; Silva Pinto, V.; Zanoelo, E.F.; Cardozo-Filho, L. β-Cyclodextrin Complexation of Extracts of Olive Leaves Obtained by Pressurized Liquid Extraction. *Ind. Crops Prod.* 2019, *129*, 662–672, doi:10.1016/j.indcrop.2018.12.045.
196. Fielding, L. Determination of Association Constants (Ka) from Solution NMR Data. *Tetrahedron* 2000, *56*, 6151–6170, doi:10.1016/S0040-4020(00)00492-0.
197. Oku, K.; Watanabe, H.; Kubota, M.; Fukuda, S.; Kurimoto, M.; Tsujisaka, Y.; Komori, M.; Inoue, Y.; Sakurai, M. NMR and Quantum Chemical Study on the OH···π and CH···O Interactions between Trehalose and Unsaturated Fatty Acids: Implication for the Mechanism of Antioxidant Function of Trehalose. *J. Am. Chem. Soc.* 2003, *125*, 12739–12748, doi:10.1021/ja034777e.
198. Hoffman, A.S. Hydrogels for Biomedical Applications. *Adv. Drug Deliv. Rev.* 2002, *54*, 3–12, doi:10.1016/S0169-409X(01)00239-3.
199. Bajpai, S.K.; Sharma, S. Investigation of Swelling/Degradation Behaviour of Alginate Beads Crosslinked with Ca^{2+} and Ba^{2+} Ions. *React. Funct. Polym.* 2004, *59*, 129–140, doi:10.1016/j.reactfunctpolym.2004.01.002.
200. Mandal, S.; Kumar, S.S.; Krishnamoorthy, B.; Basu, S.K. Development and Evaluation of Calcium Alginate Beads Prepared by Sequential and Simultaneous Methods. *Braz. J. Pharm. Sci.* 2010, *46*, 785–793, doi:10.1590/S1984-82502010000400021.
201. Aldawsari, M.F.; Ahmed, M.M.; Fatima, F.; Anwer, Md.K.; Katakam, P.; Khan, A. Development and Characterization of Calcium-Alginate Beads of Apigenin: In Vitro Antitumor, Antibacterial, and Antioxidant Activities. *Mar. Drugs* 2021, *19*, 467, doi:10.3390/md19080467.

202. Pillay, V.; Dangor, C.M.; Govender, T.; Moopanar, K.R.; Hurbans, N. Drug Release Modulation from Cross-Linked Calcium Alginate Microdiscs, 1: Evaluation of the Concentration Dependency of Sodium Alginate on Drug Entrapment Capacity, Morphology, and Dissolution Rate. *Drug Deliv.* 1998, *5*, 25–34, doi:10.3109/10717549809052024.
203. Tønnesen, H.H.; Karlsen, J. Alginate in Drug Delivery Systems. *Drug Dev. Ind. Pharm.* 2002, *28*, 621–630, doi:10.1081/DDC-120003853.
204. Hussein, N.; Omer, H.; Ismael, A.; Albed Alhnan, M.; Elhissi, A.; Ahmed, W. Spray-Dried Alginate Microparticles for Potential Intranasal Delivery of Ropinirole Hydrochloride: Development, Characterization and Histopathological Evaluation. *Pharm. Dev. Technol.* 2020, *25*, 290–299, doi:10.1080/10837450.2019.1567762.
205. Qin, Y. 7 - Seaweed Hydrocolloids as Thickening, Gelling, and Emulsifying Agents in Functional Food Products. In *Bioactive Seaweeds for Food Applications*; Qin, Y., Ed.; Academic Press, 2018; 135–152 ISBN 978-0-12-813312-5.
206. Li, Y.; Wang, C.; Luan, Y.; Liu, W.; Chen, T.; Liu, P.; Liu, Z. Preparation of PH-responsive Cellulose Nanofibril/Sodium Alginate Based Hydrogels for Drug Release. *J. Appl. Polym. Sci.* 2022, *139*, 51647, doi:10.1002/app.51647.
207. Gavini, E.; Rassu, G.; Sanna, V.; Cossu, M.; Giunchedi, P. Mucoadhesive Microspheres for Nasal Administration of an Antiemetic Drug, Metoclopramide: In-Vitro/Ex-Vivo Studies. *J. Pharm. Pharmacol.* 2005, *57*, 287–294, doi:10.1211/0022357055623.
208. Cover, T.L.; Blaser, M.J. Helicobacter Pylori in Health and Disease. *Gastroenterology* 2009, *136*, 1863–1873, doi:10.1053/j.gastro.2009.01.073.
209. Testerman, T.L.; Morris, J. Beyond the Stomach: An Updated View of Helicobacter Pylori Pathogenesis, Diagnosis, and Treatment. *World J. Gastroenterol. WJG* 2014, *20*, 12781–12808, doi:10.3748/wjg.v20.i36.12781.
210. Ferlay, J.; Soerjomataram, I.; Dikshit, R.; Eser, S.; Mathers, C.; Rebelo, M.; Parkin, D.M.; Forman, D.; Bray, F. Cancer Incidence and Mortality Worldwide: Sources, Methods and Major Patterns in GLOBOCAN 2012: Globocan 2012. *Int. J. Cancer* 2015, *136*, E359–E386, doi:10.1002/ijc.29210.
211. Safavi, M.; Shams-Ardakani, M.; Foroumadi, A. Medicinal Plants in the Treatment of Helicobacter Pylori Infections. *Pharm. Biol.* 2015, *53*, 939–960, doi:10.3109/13880209.2014.952837.
212. Al-Eraky, D.M.; Helmy, O.M.; Ragab, Y.M.; Abdul-Khalek, Z.; El-Seidi, E.A.; Ramadan, M.A. Prevalence of CagA and Antimicrobial Sensitivity of H. Pylori Isolates of Patients with Gastric Cancer in Egypt. *Infect. Agent. Cancer* 2018, *13*, 24, doi:10.1186/s13027-018-0198-1.
213. Harrison, U.; Fowora, M.A.; Seriki, A.T.; Loell, E.; Mueller, S.; Ugo-Ijeh, M.; Onyekwere, C.A.; Lesi, O.A.; Otegbayo, J.A.; Akere, A.; et al. Helicobacter Pylori Strains from a Nigerian Cohort Show Divergent Antibiotic Resistance Rates and a Uniform Pathogenicity Profile. *PLOS ONE* 2017, *12*, e0176454, doi:10.1371/journal.pone.0176454.
214. Ndip, R.N.; Takang, A.E.M.; Ojongokpoko, J.E.A.; Luma, H.N.; Malongue, A.; Akoachere, J.-F.T.K.; Ndip, L.M.; MacMillan, M.; Weaver, L.T. Helicobacter Pylori Isolates Recovered from Gastric Biopsies of Patients with Gastro-duodenal Pathologies in Cameroon: Current Status of Antibiogram. *Trop. Med. Int. Health* 2008, *13*, 848–854, doi:10.1111/j.1365-3156.2008.02062.x.
215. *WHO* Global Priority List of Antibiotic-Resistant Bacteria to Guide Research, Discovery, and Development of New Antibiotics, Available online: http://www.who.int/medicines/publications/global-priority-list-antibiotic-resistant-bacteria/en/
216. Konieczna, I.; Żarnowiec, P.; Kwinkowski, M.; Kolesińska, B.; Frączyk, J.; Kamiński, Z.; Kaca, W. Bacterial Urease and Its Role in Long-Lasting Human Diseases. *Curr. Protein Pept. Sci.* 2012, *13*, 789–806, doi:10.2174/138920312804871094.
217. Rutherford, J.C. The Emerging Role of Urease as a General Microbial Virulence Factor. *PLoS Pathog.* 2014, *10*, e1004062, doi:10.1371/journal.ppat.1004062.
218. Hage, N.; Howard, T.; Phillips, C.; Brassington, C.; Overman, R.; Debreczeni, J.; Gellert, P.; Stolnik, S.; Winkler, G.S.; Falcone, F.H. Structural Basis of Lewisb Antigen Binding by the Helicobacter Pylori Adhesin BabA. *Sci. Adv.* 2015, *1*, doi:10.1126/sciadv.1500315.
219. Kalali, B.; Mejías-Luque, R.; Javaheri, A.; Gerhard, M. *H. Pylori* Virulence Factors: Influence on Immune System and Pathology. *Mediators Inflamm.* 2014, *2014*, 1–9, doi:10.1155/2014/426309.

220. Escandón, R.A.; del Campo, M.; López-Solis, R.; Obreque-Slier, E.; Toledo, H. Antibacterial Effect of Kaempferol and (−)-Epicatechin on Helicobacter Pylori. *Eur. Food Res. Technol.* 2016, *242*, 1495–1502, doi:10.1007/s00217-016-2650-z.
221. Hassan, S.T.S.; Žemlička, M. Plant-Derived Urease Inhibitors as Alternative Chemotherapeutic Agents. *Arch. Pharm. (Weinheim)* 2016, *349*, 507–522, doi:10.1002/ardp.201500019.
222. Ghasemian, A.; Fattahi, A.; Mostafavi, S.K.S.; Almarzoqi, A.H.; Memariani, M.; Braiek, O.B.; Yassine, H.M.; Mostafavi, N.S.S.; Ahmed, M.M.; Mirforughi, S.A. Herbal Medicine as an Auspicious Therapeutic Approach for the Eradication of Helicobacter Pylori Infection: A Concise Review. *J. Cell. Physiol.* 2019, *234*, 16847–16860, doi:10.1002/jcp.28363.
223. Wang, Y.-C. Medicinal Plant Activity on Helicobacter Pylori Related Diseases. *World J. Gastroenterol.* 2014, *20*, 10368–10382, doi:10.3748/wjg.v20.i30.10368.
224. Ilodigwe, E.E.; Akah, P.A.; Nworu, C.S. Anticonvulsant Activity of Ethanol Leaf Extract of Spathodea Campanulata P. Beauv (Bignoniaceae). *J. Med. Food* 2010, *13*, 827–833, doi:10.1089/jmf.2009.0144.
225. Ofori-Kwakye, K.; Kwapong, A.A.; Adu, F. Antimicrobial Activity of Extracts and Topical Products of the Stem Bark of Spathodea Campanulata for Wound Healing. *Afr. J. Tradit. Complement. Altern. Med. AJTCAM* 2009, *6*, 168–174, doi:10.4314/ajtcam.v6i2.57089.
226. Teinkela, J.E.M.; Nguedia, J.C.A.; Meyer, F.; Donfack, E.V.; Ndjakou, B.L.; Ngouela, S.; Tsamo, E.; Adiogo, D.; Azebaze, A.G.B.; Wintjens, R. In Vitro Antimicrobial and Anti-Proliferative Activities of Plant Extracts from Spathodea Campanulata, Ficus Bubu, and Carica Papaya. *Pharm. Biol.* 2016, *54*, 1086–1095, doi:10.3109/13880209.2015.1103273.
227. Ngnameko, C.R.; Njayou, F.N.; Fowora, M.; Nemg, F.B.S.; Moundipa Fewou, P.; Smith, S.I. Inhibitory Effect of Medicinal Plants from Cameroon on the Growth and Adhesion of Helicobacter Pylori. *Eur. J. Integr. Med.* 2019, *30*, 100957, doi:10.1016/j.eujim.2019.100957.
228. Amusan, O.O.G.; Adesogan, E.K.; Makinde, J.M. Antimalarial Active Principles of Spathodea Campanulata Stem Bark. *Phytother. Res.* 1996, *10*, 692–693, doi:10.1002/(SICI)1099-1573(199612)10:8<692::AID-PTR928>3.0.CO;2-O.
229. Boniface, P.K.; Singh, M.; Verma, S.; Shukla, A.; Khan, F.; Srivastava, S.K.; Pal, A. RP-HPLC-DAD Method for the Identification of Two Potential Antioxidant Agents Namely Verminoside and 1-O-(E)-Caffeoyl-β-Gentiobiose from Spathodea Campanulata Leaves. *Nat. Prod. Res.* 2015, *29*, 676–680, doi:10.1080/14786419.2014.981538.
230. Heim, S.C.; Guarnier, F.A.; Ferreira, D.T.; Braz-Filho, R.; Cecchini, R.; Cecchini, A.L. Antioxidant Activity of Spathodea Campanulata (Bignoneaceae) Extracts. *Rev. Bras. Plantas Med.* 2012, *14*, 287–292, doi:10.1590/S1516-05722012000200006.
231. Lifongo, L.L.; Simoben, C.V.; Ntie-Kang, F.; Babiaka, S.B.; Judson, P.N. A Bioactivity versus Ethnobotanical Survey of Medicinal Plants from Nigeria, West Africa. *Nat. Prod. Bioprospecting* 2014, *4*, 1–19, doi:10.1007/s13659-014-0005-7.
232. Nazif, N.M. Phytochemical and Antioxidant Activity of Spathodea Campanulata P. Beauvois. Growing in Egypt. *Nat. Prod. Sci.* 2007, *13*, 11–16.
233. Ngouela, S.; Tsamo, E.; Sondengam, B.L.; Connolly, J.D. Spathodol, a New Polyhydroxysterol from the Leaves of Spathodea Campanulata. *J. Nat. Prod.* 1991, *54*, 873–876, doi:10.1021/np50075a023.
234. Ndam Ngoungoure, V.L.; Mfotie Njoya, E.; Ngamli Fewou, S.; Fils Ella, A.; McGaw, L.J.; Moundipa, P.F. Acetylcholinesterase Inhibitory, Anti-Inflammatory and Antioxidant Properties of Some Cameroonian Medicinal Plants Used to Treat Some Neurological Disorders. *Investig. Med. Chem. Pharmacol.* 2019, *2*, 1–13, doi:10.31183/imcp.2019.00033.
235. Balouiri, M.; Sadiki, M.; Ibnsouda, S.K. Methods for in Vitro Evaluating Antimicrobial Activity: A Review. *J. Pharm. Anal.* 2016, *6*, 71–79, doi:10.1016/j.jpha.2015.11.005.
236. Pianaro, A.; Pinto, J.; Trevisan Ferreira, D.; Ishikawa, N.; Braz-Filho, R. Iridoid Glucoside and Antifungal Phenolic Compounds from Spathodea Campanulata Roots. *SEMINA Cienc. Agrar.* 2007, *28*, 251–255.
237. Tarsia, C.; Danielli, A.; Florini, F.; Cinelli, P.; Ciurli, S.; Zambelli, B. Targeting Helicobacter Pylori Urease Activity and Maturation: In-Cell High-Throughput Approach for Drug Discovery. *Biochim. Biophys. Acta BBA - Gen. Subj.* 2018, *1862*, 2245–2253, doi:10.1016/j.bbagen.2018.07.020.

238. Godstime, O.C.; García, A.; Augustina, J.O.; Christopher, E. Mechanisms of Antimicrobial Actions of Phytochemicals against Enteric Pathogens – A Review.; 2014.
239. Yeon, M.J.; Lee, M.H.; Kim, D.H.; Yang, J.Y.; Woo, H.J.; Kwon, H.J.; Moon, C.; Kim, S.-H.; Kim, J.-B. Anti-Inflammatory Effects of Kaempferol on Helicobacter Pylori-Induced Inflammation. *Biosci. Biotechnol. Biochem.* 2019, *83*, 166–173, doi:10.1080/09168451.2018.1528140.
240. González, A.; Salillas, S.; Velázquez-Campoy, A.; Espinosa Angarica, V.; Fillat, M.F.; Sancho, J.; Lanas, Á. Identifying Potential Novel Drugs against Helicobacter Pylori by Targeting the Essential Response Regulator HsrA. *Sci. Rep.* 2019, *9*, 11294, doi:10.1038/s41598-019-47746-9.
241. Niehues, M.; Stark, T.; Keller, D.; Hofmann, T.; Hensel, A. Antiadhesion as a Functional Concept for Prevention of Pathogens: N-Phenylpropenoyl-L-Amino Acid Amides as Inhibitors of the Helicobacter Pylori BabA Outer Membrane Protein. *Mol. Nutr. Food Res.* 2011, *55*, 1104–1117, doi:10.1002/mnfr.201000548.
242. Racha, S.; Wongrattanakamon, P.; Raiwa, A.; Jiranusornkul, S. Discovery of Novel Potent Small Natural Molecules Able to Enhance Attenuation of the Pathobiology of Gastric Cancer-Associated Helicobacter Pylori by Molecular Modeling. *Int. J. Pept. Res. Ther.* 2019, *25*, 881–896, doi:10.1007/s10989-018-9737-2.
243. Kataoka, M.; Hirata, K.; Kunikata, T.; Ushio, S.; Iwaki, K.; Ohashi, K.; Ikeda, M.; Kurimoto, M. Antibacterial Action of Tryptanthrin and Kaempferol, Isolated from the Indigo Plant (Polygonum Tinctorium Lour.), against Helicobacter Pylori-Infected Mongolian Gerbils. *J. Gastroenterol.* 2001, *36*, 5–9, doi:10.1007/s005350170147.
244. Wernert, MF Wagner, ML Gurn, i AA Carballo, MA Ricco, R. Study of Polyphenols in Infusions and Decoctions from Leaves of "Cedron" (Aloysia Citriodora Palau) and "Poleo" (Lippia Turbinata Griseb.)-Verbenaceae. In *Bol Latinoam Caribe Plant Med Aromat*; 2009; 308–311.
245. Botta, S. Las Especies Argentinas Del Genero Aloysia (Verbenaceas). *Darwiniana*, 1979; 67–108.
246. Martìnez Crovetto, R. Plantas Utilizadas En Medicina Popular En El Noroeste de Corrientes. *Ministerio de Cultura y Educacion. Fundacion Miguel Lillo*; 1981; 113–139.
247. Martinez, M.R.; Pochettino, M.L. The "Farmacia Casera" (Household Pharmacy): A Source of Ethnopharmacobotanical Information. *Fitoterapia*, 1992; Vol. 63, 209–216.
248. Filipov, A. Medicinal Plants of the Pilaga of Central Chaco. *J Ethnopharmacol*; 1994;181–193.
249. Alonso J, D.C. Plantas Medicinales Autóctonas de La Argentina. *Literatura of Latin American*; 2005; 88–92.
250. Consolini, A.E.; Berardi, A.; Rosella, M.A.; Volonté, M. Antispasmodic Effects of Aloysia Polystachya and A. Gratissima Tinctures and Extracts Are Due to Non-Competitive Inhibition of Intestinal Contractility Induced by Acethylcholine and Calcium. *Rev. Bras. Farmacogn.* 2011, *21*, 889–900, doi:10.1590/S0102-695X2011005000137.
251. Caridi, D.; Trenerry, V.; Rochfort, S.; Duong, S.; Laugher, D.; Jones, R. Profiling and Quantifying Quercetin Glucosides in Onion (Allium Cepa L.) Varieties Using Capillary Zone Electrophoresis and High Performance Liquid Chromatography. *Food Chem.* 2007, *105*, 691–699, doi:10.1016/j.foodchem.2006.12.063.
252. Liu, Q.; Cai, W.; Shao, X. Determination of Seven Polyphenols in Water by High Performance Liquid Chromatography Combined with Preconcentration. *Talanta* 2008, *77*, 679–683, doi:10.1016/j.talanta.2008.07.011.
253. Timóteo, P.; Karioti, A.; Leitão, S.G.; Vincieri, F.F.; Bilia, A.R. A Validated HPLC Method for the Analysis of Herbal Teas from Three Chemotypes of Brazilian Lippia Alba. *Food Chem.* 2015, *175*, 366–373, doi:10.1016/j.foodchem.2014.11.129.
254. Aguado, M.I.; Nuñez, M.B.; Bela, A.J.; Okulik, N.B.; Bregni, C. Caracterización Fisicoquímica y Actividad Antioxidante de Un Extracto Etanólico de Aloysia Polystachya (Griseb.) Mold. (Verbenaceae). 2013, *44*, 46–51.
255. Sun, Y.; Wang, Y.; Cai, R.; Zhang, H.; Wang, Y. Identification of the Chemical Compositionsof *Verbena Officinalis L* . Extract by High Performance Liquid Chromatography-Photodiode Array-High Resolution Mass Spectrometry. *Chin. J. Chromatogr.* 2017, *35*, 987, doi:10.3724/SP.J.1123.2017.05010.

256. Abderrahim, F.; Estrella, S.; Susín, C.; Arribas, S.M.; González, M.C.; Condezo-Hoyos, L. The Antioxidant Activity and Thermal Stability of Lemon Verbena (Aloysia Triphylla) Infusion. *J. Med. Food* 2011, *14*, 517–527, doi:10.1089/jmf.2010.0102.
257. Quirantes-Piné, R.; Herranz-López, M.; Funes, L.; Borrás-Linares, I.; Micol, V.; Segura-Carretero, A.; Fernández-Gutiérrez, A. Phenylpropanoids and Their Metabolites Are the Major Compounds Responsible for Blood-Cell Protection against Oxidative Stress after Administration of Lippia Citriodora in Rats. *Phytomedicine* 2013, *20*, 1112–1118, doi:10.1016/j.phymed.2013.05.007.
258. Ohno, T.; Inoue, M.; Ogihara, Y.; Saracoglu, I. Antimetastatic Activity of Acteoside, a Phenylethanoid Glycoside. *Biol. Pharm. Bull.* 2002, *25*, 666–668, doi:10.1248/bpb.25.666.
259. Guillermo Avila, J.; de Liverant, J.G.; Martínez, A.; Martínez, G.; Muñoz, J.L.; Arciniegas, A.; Romo de Vivar, A. Mode of Action of Buddleja Cordata Verbascoside against Staphylococcus Aureus. *J. Ethnopharmacol.* 1999, *66*, 75–78, doi:10.1016/S0378-8741(98)00203-7.
260. Hausmann, M.; Obermeier, F.; Paper, D.H.; Balan, K.; Dunger, N.; Menzel, K.; Falk, W.; Schoelmerich, J.; Herfarth, H.; Rogler, G. *In Vivo* Treatment with the Herbal Phenylethanoid Acteoside Ameliorates Intestinal Inflammation in Dextran Sulphate Sodium-Induced Colitis. *Clin. Exp. Immunol.* 2007, *148*, 373–381, doi:10.1111/j.1365-2249.2007.03350.x.
261. Korkina, L.G.; Mikhal'chik, E. V.; Suprun, M. V.; Pastore, S.; Dal Toso, R. Molecular Mechanisms Underlying Wound Healing and Anti-Inflammatory Properties of Naturally Occurring Biotechnologically Produced Phenylpropanoid Glycosides. *Cell Mol Biol* 2007, *53*, 84–91, doi:10.1170/T822.
262. De Marco, E.; Savarese, M.; Paduano, A.; Sacchi, R. Characterization and Fractionation of Phenolic Compounds Extracted from Olive Oil Mill Wastewaters. *Food Chem.* 2007, *104*, 858–867, doi:10.1016/j.foodchem.2006.10.005.
263. Arthur, H.; Joubert, E.; De Beer, D.; Malherbe, C.J.; Witthuhn, R.C. Phenylethanoid Glycosides as Major Antioxidants in Lippia Multiflora Herbal Infusion and Their Stability during Steam Pasteurisation of Plant Material. *Food Chem.* 2011, *127*, 581–588, doi:10.1016/j.foodchem.2011.01.044.
264. Piccinelli, A.L.; De Simone, F.; Passi, S.; Rastrelli, L. Phenolic Constituents and Antioxidant Activity of *Wendita Calysina* Leaves (Burrito), a Folk Paraguayan Tea. *J. Agric. Food Chem.* 2004, *52*, 5863–5868, doi:10.1021/jf040100e.
265. Quirantes-Piné, R.; Funes, L.; Micol, V.; Segura-Carretero, A.; Fernández-Gutiérrez, A. High-Performance Liquid Chromatography with Diode Array Detection Coupled to Electrospray Time-of-Flight and Ion-Trap Tandem Mass Spectrometry to Identify Phenolic Compounds from a Lemon Verbena Extract. *J. Chromatogr. A* 2009, *1216*, 5391–5397, doi:10.1016/j.chroma.2009.05.038.
266. Guo, H.; Liu, A.-H.; Ye, M.; Yang, M.; Guo, D.-A. Characterization of Phenolic Compounds in the Fruits Of Forsythia Suspensa by High-Performance Liquid Chromatography Coupled with Electrospray Ionization Tandem Mass Spectrometry. *Rapid Commun. Mass Spectrom.* 2007, *21*, 715–729, doi:10.1002/rcm.2875.
267. Kırmızıbekmez, H.; Çalış, İ.; Piacente, S.; Pizza, C. Iridoid and Phenylethyl Glycosides From Globularia Sintenisii. *Helv. Chim. Acta* 2004, *87*, 1172–1179, doi:10.1002/hlca.200490107.
268. Jin, Q.; Jin, H.-G.; Shin, J.-E.; Hong, J.-K.; Woo, E.-R. Phenylethanoid Glycosides from Digitalis Purpurea L. *Bull. Korean Chem. Soc.* 2011, *32*, 1721–1724, doi:10.5012/bkcs.2011.32.5.1721.
269. Vo, T.N.; Nguyen, P.L.; Tuong, L.T.; Vo, P.N.; Nguyen, K.P.P.; Nguyen, N.S. Constituents of the Leaves of Pseuderanthemum Carruthersii (Seem.) Guill. Var. Atropurpureum (Bull.) Fosb. *Phytochem. Lett.* 2012, *5*, 673–676, doi:10.1016/j.phytol.2012.07.004.
270. Khodaie, L.; Delazar, A.; Lotfipour, F.; Nazemiyeh, H.; Asnaashari, S.; Moghadam, S.B.; Nahar, L.; Sarker, S.D. Phytochemistry and Bioactivity of Pedicularis Sibthorpii Growing in Iran. *Rev. Bras. Farmacogn.* 2012, *22*, 1268–1275, doi:10.1590/S0102-695X2012005000107.
271. Yadav, A.K.; Gupta, M.M. Quantitative Determination of Bioactive Phenylethanoid Glycosides in Clerodendrum Phlomidis Using HPTLC. *Med. Chem. Res.* 2014, *23*, 1654–1660, doi:10.1007/s00044-013-0738-6.

272. Calvo, M.I.; Crespo, A.; Fernández, M. Seasonal Variations of the Iridoids, Flavonoids and Verbascoside Content from Verbena Officinalis l. *Acta Hortic.* 2000, 169–176, doi:10.17660/ActaHortic.2000.516.20.

ACKNOWLEDGEMENTS

I would like to express my sincere gratitude to my supervisor Prof. Davide Bertelli for the continuous support during these three years of PhD, both from a professional and personal point of view. I am very grateful to him for always being an excellent mentor.

I am truly grateful to my second supervisor, Prof. Federica Pellati, for her support and valuable contributions to my research.

A special gratitude goes to Prof. Lorenzo Corsi, Prof. Adele Papetti and Prof. Valentina Iannuccelli for their noteworthy collaboration to the research projects and their precious guidance and expertise, which was a great source of inspiration.

My sincerest thanks also go to the technical staff, Dr. Maria Cecilia Rossi, Dr. Filippo Genovese and Dr. Diego Pinetti for the precious assistance during the experimental work.